Retrofitting of infilled RC frames using collar jointed masonry

By

Chuanlin Wang

Submitted in accordance with the requirements for the degree of

Doctor of Philosophy

The University of Leeds

School of Civil Engineering

January 2017

The candidate confirms that the work submitted in his own and that appropriate credit has been given where reference has been made to the work of others.

This copy has been supplied on the understanding that it is copyright material and that no quotation from the thesis may be published without proper acknowledgement.

The right of Chuanlin Wang to be identified as Author of this work has been asserted by him in accordance with the Copyright, Designs and Patents Act 1988.

Acknowledge

Abstract

Masonry is a composite material made of masonry units bonded together with mortar. A large number of historical buildings constructed using masonry can be found all over the world. Little or no seismic loading was considered when they were built. Therefore, masonry structures often need to be retrofitted or strengthened. This research proposed a new strengthening approach using a collar-jointed technique. Namely, the approach is implemented by building another masonry wall parallel to the existing single-leaf wall and bonding the two together using a mortar collar joint. Furthermore, collar-jointed masonry wall construction is also a popular construction system in reality. This thesis considers two different types of collar wall strengthening applications: pre- and post-damaged walls. The results found out that the pre-damaged strengthening could improve the lateral resistance by about 50% while the post-damaged retrofitting can only restore the initial strength.

A simplified micro-scale finite element model for fracture in masonry walls was developed. The mortar joints and the brick-mortar interfaces are taken to have zero-thickness. The bricks were modelled as elastic elements while the brick-mortar interfaces were represented using a Mohr-Coulomb failure surface with a tension cut-off and a linear compression cap. One feature of the research was to identify the material parameters for the constitutive model. The material parameters were tuned by minimizing the difference between the experimental and numerical results of a single leaf wall panel. The model was then validated by assigning the parameters to the single-leaf masonry wall as well as to the double-leaf wall to predict its mechanical behaviour. Good agreement with experimental results was found.

Furthermore, masonry is also widely used in the form of infill panels within RC frames. Therefore, the collar-jointed technique has also been extended and applied to the infilled RC frame. The numerical results showed that the

collar-jointed technique could provide some benefits to the composite structure.

Contents

List of figures

List of tables

List of notations

Symbol	Description
A_0	Crosse section
c	Cohesion of brick-mortar interface
C_n	Control the interaction between cap mode and tension mode
C_{nn}	Control the centre of cap mode
C_{ss}	Control the contribution of the shear stress to failure in cap mode
E	Elastic modulus
E_b	Elastic modulus of brick unit
E_c	Elastic modulus of concrete
E_m	Elastic modulus of mortar
E_s	Elastic modulus of steel
F	External force
f_b	Compressive strength of brick unit
f_{tc}	Tensile strength of concrete
f_t	Tensile strength of brick-mortar interface
f_c	Compressive strength of brick-mortar interface
f_m	Compressive strength of mortar
f_{cc}	Compressive strength of concrete
f_{bt}	Tensile strength of brick interface
f_y^1	Yield strength of steel
f_u^2	Ultimate strength of steel
G_f^I	Mode I fracture energy of brick-mortar interface
G_f^{II}	Mode II fracture energy of brick-mortar interface
G_f^c	Compressive fracture energy of brick-mortar interface
G_b	Shear modulus of brick unit
G_m	Shear modulus of mortar joint
G_f^{bt}	Tensile fracture energy of brick interface
G_{fc}^I	Mode I fracture energy of concrete
G_{cc}^{II}	Mode II fracture energy of concrete
h_m	Mortar joint thickness

K_n	Normal stiffness of brick-mortar interface
K_s	Shear stiffness of brick-mortar interface
κ_1	Amount of hardening or softening of tension mode
κ_2	Amount of hardening or softening of shear mode
κ_3	Amount of hardening or softening of compressive mode
k_{bn}	Normal stiffness of brick interface
k_{bs}	Shear stiffness of brick interface
L_0	Initial length
ΔL	Change in length under external loading
v_b	Poisson's ration of brick unit
v_m	Poisson's ration of mortar joint
v_c	Poisson's ration of concrete
v_s	Poisson's ration of steel
σ	Normal stress
σ_1	Normal stress of tension mode
σ_2	Normal stress of shear mode
σ_3	Normal stress of compressive mode
$\bar{\sigma}_1$	Yield stress of tension mode
$\bar{\sigma}_2$	Yield stress of shear mode
$\bar{\sigma}_3$	Yield stress of compressive mode
τ	Shear stress
ε	Strain
Φ	Friction angle
Φ_0	Initial friction angle
Φ_r	Residual friction angle
Ψ	Dilatancy angle

Chapter 1   Introduction

1. 1   Background

Masonry is a composite material made of masonry units and bonded together with or without mortar, which has been used for centuries in building constructions. A large number of historical buildings constructed using masonry can be found all over the world. Load bearing walls, infill panels, pre-stressed masonry cores and low-rise buildings are some examples of its wide spread use. Masonry units usually consist of fired clay or calcium bricks, concrete blocks, adobes and stones. Mortar is normally a mixture of cement, lime, sand and water and masonry is constructed by stacking masonry units on top and next to each other and using mortar to bond them. Though new developments in masonry materials and application has occurred over the last few decades, this concept of building masonry structures has not changed much up until now. By using different combinations of masonry units, mortars and unit bonding patterns, a large number of geometric arrangements and strength characteristics can be obtained. This makes masonry a popular construction material due to the reason that it can meet different requirements easily. Furthermore, as a popular and old construction material, masonry has many inherent characteristics, and the most important one is its simplicity. Other important characteristics are the aesthetics, solidity, durability and low maintenance, versatility, sound absorption and fire protection (Lourenco 1996).

Masonry is widely used in seismic-prone areas, such as masonry structures and masonry-concrete structures. Besides, it is often used in the form of infill panels within reinforced concrete (RC) or steel frames in modern structures. Infills are customarily considered as secondary elements (also referred to as

non-structural elements) to the structure and usually are not considered in the calculations of seismic capacity for simplification (sometimes the mass is considered while the stiffness not). On one hand, it has been indicated from experimental observations and analytical studies that masonry infills may produce some beneficial effects on the response of the building. However, observations from past earthquakes also showed that severe damage and loss of life could occur in infilled frame buildings, which has led to the idea that this type of structure exhibits poor seismic performance (Crisafulli et al. 2005). As such, the performance of masonry infill can be a decisive factor, which may lead to a catastrophic structural failure. Therefore, it is necessary to investigate the influence of the masonry infill on the composite structure. Moreover, there is a large inventory of unreinforced masonry (URM) buildings in the world. Little or no seismic loading was considered when they were built, and they might not be capable of dissipating energy through inelastic deformation during earthquakes (Ehsani et al. 1999). Therefore, with this in mind, masonry structures often need to be retrofitted following earthquake events or strengthened prior to seismic actions in order to ensure that they can perform these important energy absorption and force relieving roles.

In the past decades, the retrofitting or strengthening of masonry wall panels has intrigued researchers' interest and extensive studies have been carried out. The aim of strengthening is to improve the mechanical behaviour of masonry structures, which is usually done before structural damage occurred. However, retrofitting is normally done after the damage in order to restore or improve its initial load carrying capacity.

Over the past decades, researchers have proposed various methods to enhance the seismic behaviour of unreinforced masonry walls. The proposed methods consist of two main groups: (1) conventional approaches and (2) modern approaches. Among the conventional strengthening approaches, ferrocement, shotcrete and grout/epoxy injection are some of the most often used ones.

However, the conventional methods usually have the disadvantages of affecting aesthetics and being considerably time consuming etc. Fibre Reinforced Polymer (FRP) is a more state-of-the-art strengthening/retrofitting technique. The enhancement of masonry walls using FRP material has the common advantage of little added mass. However, the main drawbacks are the high cost, the high technical skill required for their installation, the effect on the architectural aesthetics and the basic lack of experience with these materials particularly relevant to their aging. Furthermore, one other major problem is that typically in developing countries the masonry surface is not smooth and this causes stress points for the FPR wrap and therefore results in premature failure/unpredictable failure, thereby making the application of this technique very unpractical in the developing countries.

This thesis is concerned with the strengthening/retrofitting of masonry structures and a new strengthening/retrofitting approach using a collar joint technique has been proposed. Namely, the approach is implemented by building another masonry wall parallel to the existing single-leaf wall and bonding the two together using a mortar (collar) joint. This method does not require sophisticated workmanship because of its easy implementation, which renders it practical. In addition, the material is easy and cheap to obtain, which helps to prove its cost-effectiveness. Furthermore, double-leaf or collar-jointed masonry wall systems are common in construction as they can improve the sound, water and fire resistance of the structures.

However, this construction system has received little attention in the past. Therefore, the influence of this building system on the whole structure has not been extensively studied. Though the similar approach using cement/epoxy injection has been applied in multi-stone masonry walls, the research work on clay brickwork has not been done according to the author's observation. The actual research of this thesis investigates experimentally the merits of the collar-joint technique that differs from any

previous published work in terms of masonry materials and collar joint type. In conclusion, this thesis aims to investigate the improvement of this approach and the influence of this approach on the mechanical behaviour of masonry structures. Furthermore, this collar jointed technique was extended and applied to infilled RC frame to investigate its influence on the composite structure.

In the past decades, extensive studies have been carried out to investigate the mechanical behaviour of masonry (Hendry 1998, Rots 1997, Van der Pluijm 1993). However, it is prohibitively expensive to conduct experiments, therefore, it is fundamentally important to also develop a numerical approach to predict the in-service behaviour of masonry walls. In the past decades, an enormous growth in the development of numerical methods for structural analysis has been achieved by researchers. Among them, micro- and macro-scale methods are the most often used. In the micro-scale modelling, Finite Element Method (FEM) and Discrete Element Method (DEM) are the two most frequently studied. This research has also used numerical analysis in order to have a better understanding on the improvement and influence of this collar-joint technique, as well as to address the load transfer between the two masonry leaves.

1. 2   Research aims and objectives

As the collar joint construction system is still popular nowadays, the principal aimof this research is to experimentally and numerically quantify the in-plane performance of the unreinforced masonry wall panels reinforced using the collar jointed technique under a combined in-plane lateral quasi-static loading, in order to investigate the effectiveness and practicability of this construction system used as strengthening/retrofitting. As stated earlier, the collar-jointed construction system is common in practice, This could be a very economic and easy method for those residents in the developing

countries or masonry-popular area. The strengthening/retrofitting technique and the computational model can be used by engineers and researchers to compare and evaluate alternative methods of retrofitting or strengthening the masonry structures. Although this research was conducted in the UK, which earthquake is a rarity, and also using local materials, it is expected that these research results can be referred and easily extrapolated to other countries, thus it providing another alternative strengthening/retrofitting method for the engineers and householders

The objectives of this study are summarized as:

1. To review the current literature to obtain an up-to-date understanding on the structural behaviour of the single- and double-leaf masonry wall panels.

2. To review and compare the existing strengthening/retrofitting approaches in order to assess the advantages and disadvantages of the different approaches.

3. To propose a new strengthening/retrofitting approach in order to overcome the shortcomings of the existing approaches.

4. To review and evaluate the computational methods that are currently available to predict the mechanical behaviour of masonry walls under a combined quasi-static in-plane lateral loading.

5. To conduct an experimental study on masonry wall panels in order to investigate their mechanical behaviour, including single- and double-leaf masonry wall panels, as well as to assess the improvement of the proposed approach.

6. To develop a simplified micro-scale model which is capable of predicting quantitatively and qualitatively the serviceability and ultimate limit state behaviour of masonry walls by including tensile, shear and compressive failure.

7. To select an appropriate method to determine and calibrate the material parameters for the constitutive model for the masonry material.

8. To verify and validate the models developed by comparing the predicted behaviour with the behaviour observed in the experiments. The result of the study will provide recommendations for the assessment and strengthening of unreinforced masonry buildings using a collar jointed technique.

9. To extend and apply the collar jointed technique to infill panels found in RC frame structures and investigate the potential benefits to the composite structure.

1. 3 Thesis outline

This thesis is divided into nine chapters. Following this introductory chapter, a review of the literature on masonry is presented in **Chapter 2**. **Chapter 2** serves as an overview of the past research conducted on masonry structures. The aim of this chapter is to establish a base of knowledge and understanding for the author's research. Firstly, this chapter presents a brief description of the material properties and the inherent variations in the properties of masonry. Then, the possible failure patterns of masonry wall panels are discussed, followed by a review of the existing strengthening approaches for the masonry wall panels. After that, a typical review of double-leaf (collar jointed) walls is presented as the double-leaf wall is the

main focus of this research. Finally, the analytical investigations and the different modelling approaches that have been used in the past are discussed. A summary is provided which highlights the extent of current knowledge and the areas where new knowledge is required.

Chapter 3 describes the experimental work. The experimental tests are carried out on both single- and double-leaf masonry wall panels. For the double-leaf ones, pre- and post-damaged collar jointed walls are designed in order to investigate the influence of different types of collar joint on the mechanical behaviour of double-leaf masonry wall panels.

The experimental results of the tests described in **Chapter 3** are presented and discussed in **Chapter 4**. In this chapter, the mechanical behaviour of both single-leaf and double-leaf wall panels are thoroughly analysed and discussed. Furthermore, the experimental results are compared with each other in order to find out the effectiveness of the proposed method in this research.

Chapter 5 has identified a suitable numerical model to simulate masonry walls, both at the serviceability state (pre-cracking) and at the ultimate limit state (post-cracking). A number of existing modelling approaches are assessed and compared before the selection of the most appropriate one. The selected model is then used as the basis of the author's research. For this research, Finite Element Method (FEM) is selected and the commercial finite element software, MIDAS FEA, is utilised.

Chapter 6 investigates the calibration of material parameters in the modelling of masonry structures using MIDAS FEA. The investigation includes a series of sensitivity studies of the parameters influencing the mechanical behaviour of a single-leaf masonry wall. The calibration is carried out based upon the sensitivity of the study results. It can be found in both the experimental and numerical results that the performance of a masonry wall has three stages: the linearly elastic stage (stage one), load

re-distribution stage (stage two), and the failure stage (stage three). The numerical results of each stage will be compared with those obtained from the laboratory testing as described in **Chapter 4.** The material parameters are manually "tuned" step by step to achieve similar responses to those obtained in the laboratory.

In **Chapter 7**, the parameters obtained in **Chapter 6** are assigned to the model in MIDAS FEA. The application of these parameters to the single-leaf wall 3 is performed so as to numerically validate the model by capturing all the failure modes. The characterized parameters are also used in double-leaf walls, including the pre- and post-damaged types, to predict their mechanical behaviour. The predicted numerical results are also compared with the experimental results obtained in **Chapter 4**.

In **Chapter 8**, the proposed strengthening approach using a collar jointed technique will be extended and applied to the masonry wall panels in reinforced concrete (RC) frame structures. In this chapter, a new infilled RC frame is designed by replacing Mehrabi's (1996) infilled RC frame structures with the masonry wall presented and studied in **Chapter 3** and **4**. The infilled masonry walls can be solid or contain openings, and the newly designed structures will be strengthened using the collar jointed technique. This chapter is carried only numerically. Furthermore, the bare masonry infill panel tested in the laboratory is compared with the masonry infill wall restrained by a RC frame.

Finally, the principal and secondary findings from this research are summarized in **Chapter 9**. The limitations of the current research are presented as well as the recommendations for further research.

Chapter 2   Review of previous research on masonry

2. 1 Introduction

Masonry is a brittle, anisotropic, composite material that exhibits distinct directional properties due to the mortar joints which act as planes of weakness. In the past decades, extensive studies have been carried out to investigate the mechanical behaviour of the masonry structures (Van der Pluijm 1993, Rots 1997, Hendry 1998, Abrams et al. 2001, Stavridis and Shing 2010).   The analysis of the mechanical behaviour of masonry structures is difficult due to its heterogeneous and anisotropic behaviour. Furthermore, there is still a lack of good understanding in the complex fracture behaviour of masonry. The behaviour of masonry is complicated further by the inherent variations in the constituent materials, variations in workmanship, and the effects of deterioration caused by weathering processes and the development of other defects during the life of the masonry structure. It is well known that masonry material has relatively high resistance to compressive stress while has poor resistance to tensile stress.. When subjected to very low levels of stress, masonry behaves approximately linearly elastically (Mosalam et al. 2009). However, it becomes nonlinear after the formation of cracks and the subsequent redistribution of stress through the uncracked elements. Nevertheless, Kaushik et al. (2007) concluded that masonry does not behave elastically under lateral loads, even in the range of small deformations.

This chapter provides basic knowledge on masonry materials and structures and helps the author to generate a comprehensive understanding on the performance of masonry materials and structures. Researches on different aspects of masonry walls that have been studied over the past decades will

be reviewed here. The following sections will briefly summarize previous researches relating to the material components, strengthening methods, in-plane performance, and modelling of masonry walls.

2. 2   Material properties

It is well known that the analysis of a masonry structure is very difficult mainly due to its complex components. The most important components identified in a masonry wall panel are: brick characteristics; mortar joint characteristics and brick/mortar bond characteristics. In this section, the previous researches on the material properties of masonry components will be presented and discussed in detail. This helps to understand the mechanical behaviour of masonry wall panels in the following study and provides initial data for the numerical work.

2.2.1 Brick

Bricks are a big part in a masonry structure and make up most percentage of the structure. From a structural viewpoint, bricks used today are generally made from a variety of raw materials such as clay, calcium silicate (sand-lime), stone and concrete by a variety of production methods. This study will be mainly focused on clay bricks as it is the most extensively used type of masonry unit throughout the world. It is estimated that approximately 96% of the bricks used in the United Kingdom are manufactured from clay (MIA, 2013). Clay brick used as a building material is made of clay with or without a mixture of other substances, burned at an adequately high temperature to prevent it from crumbling again when soaked in water. The properties of bricks vary in a wide range of values in every structure. Even though the bricks are made of the same material, the mechanical behaviour of bricks is not homogeneous nor isotropic, especially for hollow or perforated bricks.

Information on the mechanical properties of clay bricks is required when assessing existing URM buildings, which can be used as a guidance in the following research, both experimentally and numerically. The most important characteristics of a brick element are the compressive strength, tensile strength and Young's modulus, which are described in detail in the following section.

Compressive strength

BS-3921 (1985) has presented a standardised procedure to obtain the compressive strength of a masonry unit. Compressive strength has been known to be influenced by several external factors such as loading rate, specimen size and shape, and specimen boundary conditions. Figure 2.1 represents the compressive behaviour of a typical brick unit. In the figure, the compressive behaviour starts with a linear elastic part up until the first micro-cracks appear. The hardening starts at this moment, which means that the stiffness of the material starts to decrease but the load can still increase. Gradually, the micro-cracks propagate and finally result in bigger macro-cracks by connecting several smaller ones. The softening part follows, and the size and number of cracks increase significantly until it is crushed. In the final stage, there is still a small amount of strength remaining regardless of the amount of cracks that have developed (Van Noort 2012). The compressive strength of clay bricks can vary from 20 to 145 MPa depending on various factors such as the constituents of materials, firing conditions, and the size and shape of unit (Charimoon 2007).
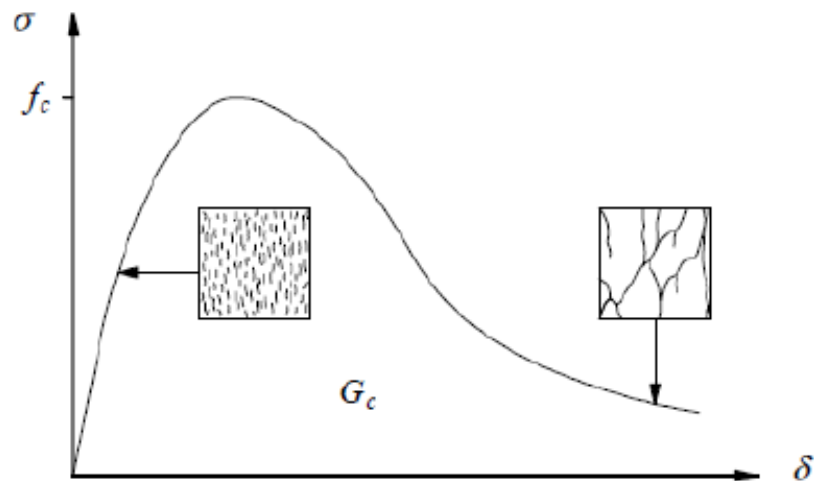
Figure 2.1 Compressive behaviour of brick like materials

Tensile strength

The measurement of the tensile strength of masonry is more difficult. Although it can be determined by a direct tensile test, such testing is difficult to perform. Even if possible, the test produces quite variable results because of the complicated test apparatus and stress concentrations on the specimen. Van der Pluijm (1997) demonstrated that the behaviour of masonry units and mortar joints under tension showed a great similarity to that of concrete. Figure 2.2 illustrates the tensile behaviour of a typical brick unit. In the figure, the tensile behaviour starts with a linear elastic part up until the tensile strength is reached and first cracking occurs. After that point softening takes place, which is indicated by a decrease of the stiffness of the material and also a decrease of the load applied to the material specimen. The material is considered completely failed when the strength and stiffness equal zero.

Generally, experiments have shown that the tensile strength of clay bricks is best measured by indirect methods, which increases with the increase of brick compressive strength (Chaimoon 2007). Based upon the previous researches, a simple relationship between the compressive strength and tensile strength was found. The other one can be approximately obtained if

only one is known already. Schubert (1988) found that the ratio between the tensile and compressive strength ranges from 0.03 to 0.10 for the longitudinal tensile strength of bricks. However, Sahlin (1971) reviewed the test data and found that the ratio of the tensile strength to the compressive strength of brick is around 1:20 for solid bricks and 1:30 for hollow bricks.

There is little investigation about the mode I fracture energy (the amount of energy to create a unitary area of a crack) of a single brick unit reported in the literature. Still, Van der Plujim (1992) had carried out some experiments regarding the tensile behaviour of bricks where the tensile strength ranges from 1.5 to 3.5 N/mm^2 and fracture energy from 0.06 to 0.13N/mm. Similarly, Almeida et al. (2002) found that the average value of the tensile strength was in the order of $3N/mm^2$, while the average fracture energy values ranged between 0.0512 to 0.081N/mm.
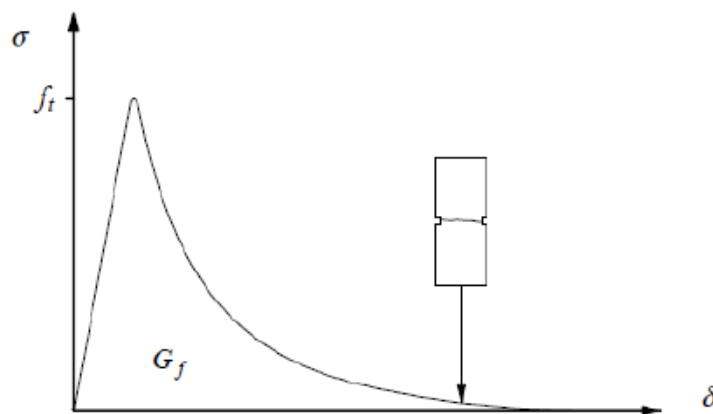
Figure 2.2 Tensile behaviour of brick like materials

Young's modulus

The mechanical behaviour of a brick element is described as elastic-brittle, and the Young's modulus of brick can be directly obtained via tests. The most common approach is to measure the deflection change under compressive load on brick specimens. Besides directly test, some researchers have proposed empirical methods to obtain Young's modulus.

Sahlin (1971) proposed that the ratio of modulus of rupture varies roughly between 10% and 30% of the compressive strength of clay brick. Furthermore, (Kaushik et al. 2007) recommended a range of values depending on the compression strength of the brick to estimate the elasticity modulus of clay bricks, which is shown in Equation 2.1.

$$150. f_b \leq E_b \leq 500. f_b \qquad (2.1)$$

Where f_b represents the compressive strength of brick unit and E_b is the elastic modulus of brick unit.

2.2.2 Mortar

Although mortar forms only a small proportion of brickwork as a whole, its characteristics play a big influence on the mechanical behaviour of the brickwork. Mortar is a mixture of different materials, such as cement, sand, water, lime etc. with different portions. Mortar is used in masonry construction as a binding material to bind individual masonry units into a composite assemblage and take up all irregularities in the bricks. Fundamentally, the cement adds strength, the lime and water contribute to workability and the sand provides inexpensive filler. The moment the fresh mortar contacts the brick, the brick absorbs water from the fresh mortar and the moisture transmission process starts (Pel et al. 1995, Forth et al. 2000). There are various types of mortar which have been used over several centuries such as lime-pozzolanic, cement-lime and cement mortar. Different admixtures and additives (milk, oils, starches, or natural resins, etc.) can be added to mortar to form mortars with particular characteristics, such as adhesion, water repellence, etc. (Harries and Sharma, 2016). Mortars with general purposes are used to build masonry with joints of 10 to 15mm in thickness while thin layer masonry use special thickness mortar with a thickness of 3 to 4mm (Vermeltfoort 2005).

According to BS EN 998-2 (2010), mortar should have good workability, sufficient bond and appropriate strength, and the first two properties are more critical. The bonding is dependent upon a satisfactory value of the brick suction and mortar water retention. The workability is the ability of the mortar to flow easily over the surface of bricks. Though the use of more water can improve the workability, it can also reduce the mortar strength. Therefore, the amount of water needs to be added according to the ball dropping test. Additionally, the standard specimens test results cannot represent the real mortar strength in masonry joint as the standard non-absorbent mould doesn't take the water absorption effect of the masonry unit into consideration. Therefore, mortar properties are mainly used as a measure of quality control rather than representative of the actual properties. Generally, it is the bond strength that matters more in the analysis (Chaimoon 2007).

Mortar compressive strength can be determined using either cube or prism tests (BS EN 1015-11:1999). The compressive strength (f_{mc}) of mortar depends on its inherent material. The lime mortar has a strength of 0.5 to 1MPa, cement-lime mortar varies from 1 to 10MPa and pure cement mortar strength ranges from 10 to 20MPa (Wijanto 2007). Furthermore, the strength of bed and head mortar joints are different. According to Dialer (1990), the strength of the head or perpend joints is usually lower than the strength of the bed joints. This is a result of the greater degree of mortar shrinkage in the perpend joints and also these joints are often not filled fully with mortar. The modulus of elasticity of mortars, E_{mc}, is approximately equal to $10f_{mc}$ (Wijanto 2007) while Kaushik et al. (2007) recommended a range of values shown in Equation 2.2. Poisson's ratio of most hydraulic cement and lime mortars is on the order of 0.2 (Wijanto 2007).

$$100. f_{mc} \leq E_{mc} \leq 400. f_{mc} \qquad (2.2)$$

Where f_{mc} is the compressive strength of mortar while E_{mc} is the elastic modulus of mortar.

2.2.3 Brick-mortar interface

The connection between the bricks and mortar often is the weakest link in a masonry structure, therefore cracks often occur along these interfaces (Lourenco 1996). The property of the brick-mortar interface is very important in the mechanical behaviour of masonry as it has a considerable effect on the load transfer and cracking. Groot (1993) demonstrated that water is an important factor in the strength development of these interfaces. After the mortar has been applied on the bricks, the water in the mortar will be sucked into the pores of the bricks. Cement particles from the mortar move along with the water and will be spread along the surface of the brick, resulting in a bond between the mortar joint and brick. Very high water-cement ratio or very low water-cement ratio can both result in relatively low strength even if the bricks and the mortar both have a very high strength. The reason is that not enough cement particles are sucked into the brick's holes in both cases. Generally, it is better to have a good bond between mortar and brick than a high resistance mortar (Campbell Barraza 2012).

There are two modes of failure occurring in the brick-mortar interface, which are tensile failure (mode I) and shear failure (mode II) as discussed by Lourenco (1996). The mechanical behaviour of brick/mortar has been conducted in the work of van der Pluijm (1992, 1993).

Brick-mortar interface tensile failure (mode I)

The tensile mechanical properties of the contact between brick and mortar can be estimated from laboratory tests. Experiments on the direct tensile strength of brick-mortar were performed by Van der Pluijm (1992). Figure 2.3 (Almeida et al. 2002) is a tensile bond test rig, which shows how to determine the tensile behaviour of the interface between brick and mortar. The tensile results showed that the tension softening response was an exponential curve as shown in Figure 2.4.

16
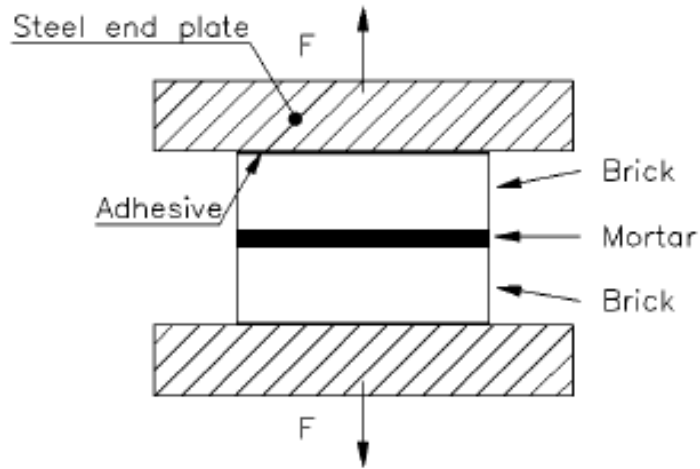
Figure 2.3 Tension test rig for brick-mortar interface (Almeida et al. 2002)
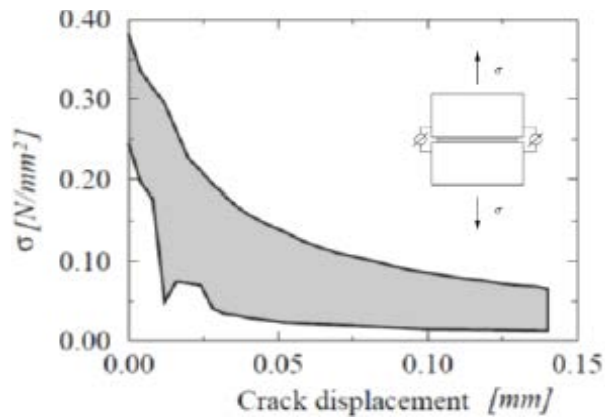
Figure 2.4 Stress-displacement relation for the interface (van der Pluijm 1992)

The brick-mortar interface tensile strength is a key parameter for numerical modelling of masonry structures. It can be seen that the mode I softening curve is exponential, similar with the tensile behaviour of the bricks and mortar. Van der Pluijm (1992) found that the bond strength varies between 0.3 to $0.9 N/mm^2$ and the mode I fracture energy, which is defined as the amount of energy to create a unitary area of a crack along the brick/mortar interface, ranges from 0.005 to $0.03 Nmm/mm^2$. Almeida et al. (2002), quantified the tensile strength and mode I fracture energy for different types of brick-mortar interfaces. The average bond tensile strength was in the

order of $2 N/mm^2$ and the average mode I fracture energy was around $0.008 Nmm/mm^2$. However, the test results were considerably scattered, as well as the shape of the softening branch.

Brick-mortar interface shear failure (mode II)

Beattie et al. (2001) proposed that the failure of masonry joints under shear can be represented by a Mohr-Coulomb failure law which expresses a linear relationship between the shear stress and the normal stress as Equation 2.3:

$$\tau = c + \tan \Phi . \sigma \qquad (2.3)$$

Where   represents the cohesion or the shear strength at zero pre-compression. is the tangent of the friction angle of the interface between unit and mortar joint. The values of cohesion and friction angle that define the brick/mortar interface may vary considerably according to different unit/mortar combinations.

The estimation of the shear behaviour of the interface between brick and mortar can be carried out by shear bond test rig (Van Der Pluijm 1993), which is shown in Figure 2.5. Figure 2.6 (Van Der Pluijm 1992) shows the mechanical shear behaviour (mode II failure).

BS 5628 (2005) gives design values for cohesion ranging from 0.35 to 1.75 N/mm^2 and $\tan \psi$ equals to 0.6 for mortar designation. However, the published values of the cohesion are reported to range between 0.1 and 1.8 N/mm^2 (Lourenco, 1998b; Hendry, 1998, Van der Pluijm 1992). Van der Pluijm (1992) found that the value of mode II fracture energy G_f^{II}, ranges from 0.01 to $0.25 N/mm$. In addition, Van der Pluijm found that the tangent of the initial internal friction angle $tan \Phi_0$ ranges from 0.7 to 1.2 for different

unit/mortar combinations. The tangent of the residual internal friction angle $tan\,\Phi_r$ is approximately constant and equals to 0.75.
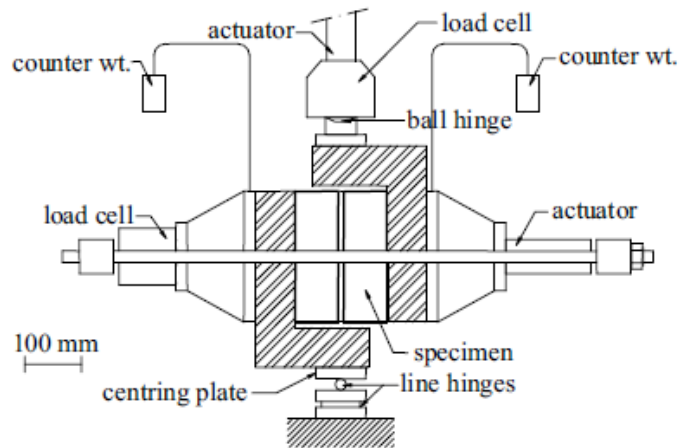
Figure 2.5 Shear test rig for brick-mortar interface (Van Der Pluijm 1993)
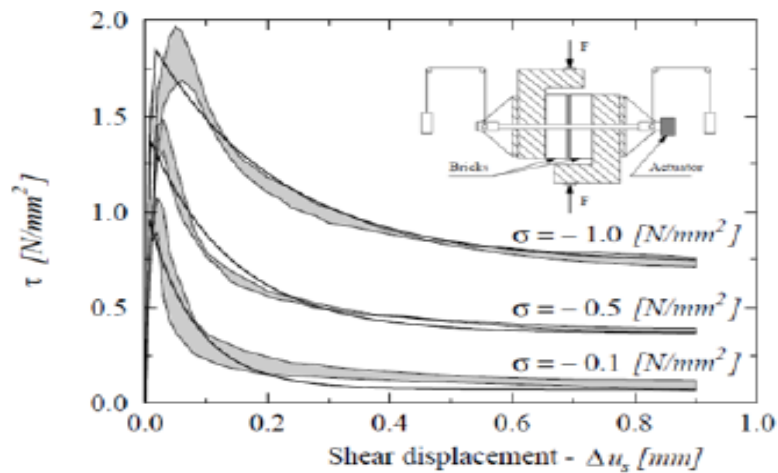
Figure 2.6 Stress-displacement diagram for shear with various confining stresses
(van der Pluijm 1992)

Another relevant feature of masonry joints is the dilatancy angle (Ψ), which measures the uplift of one unit over the other upon shearing, depends on the level of the confining stress. The dilatancy angle is positive but tends to zero upon increasing normal confining stress (Van der Pluijm, 1999). The average value of $tan\,\psi$ ranges from 0.2 to 0.7 depending on the roughness of the brick surface for low confining pressures (Roca et al. 1998).

19

The brick/mortar interface can be influenced by many factors, and the factors have been determined by Lawrence et al. (2008) and Vermeltfoort et al. (2007). These factors are: the surface texture and the suction rate of units; the mortar composition; the grain size distribution of the aggregate in mortar; and the type of binders and the use of admixtures and additions for the preparation of the mortar. Abdou et al. (2006) studied the influence of holes on joint mortar behaviour by testing on half brick couplet specimens made of both solid and hollow bricks. In both cases, the experimental results showed that there was no stiffness degradation even in the softening regime. However, it seems that the presence of holes increases the stiffness due to mortar filling in the holes but does not affect the internal friction angle of the mortar joint. Wang et al. (2013) found that the presence of perforations help to increase shear strength by forcing failure to be both along the brick/mortar interface and through the mortar in the perforation.

2.2.4 Masonry

The tensile strength and compressive strength are two of the most important material parameters for the analysis and design of masonry structures. The uniaxial tensile behaviour of masonry is dependent upon the direction of loading. Lourenco (1996) found out that the failure is generally caused by the failure of the relatively low tensile bond strength of the brick-mortar interface if the tensile loading is perpendicular to the bed joints. There are two different types of failure when tensile loading is parallel to the bed joints, displayed in Figure 2.7, depending on the relative strength of joints and units. The first type is represented by zigzag cracks (Figure 2.7 (a)) through the head and bed joint. In the second type of failure, cracks run almost vertically through the bricks and head joints (Figure 2.7 (b)). In this case, the tensile strength of bricks is approximately the same with the mortar. The compressive strength of brick masonry can be determined either from brick and mortar strength using an approximating approach or from compression

tests on masonry prisms. The real uniaxial compressive strength of masonry is suggested to be obtained from the so-called RILEM test, see Figure 2.8. However, the RILEM (1985) specimen is relatively large and costly to carry out. Therefore, the stacked bond prism (Figure 2.9) is frequently used to obtain the uniaxial compressive strength instead (Dhanasekar, 1985).

There are several factors influencing the compressive behaviour of masonry. Brick and mortar characteristics are the most important ones. Both brick and mortar tend to expand laterally at different rates due to Poisson's effect under compression. The mortar normally has a higher value of Poisson's ratio and will therefore expand laterally more than the bricks. However, this expansion is restrained by the bond and friction at the brick-mortar interface leading to a state of tri-axial compression in the mortar and a state of compression/ tension in the brick. This phenomenon has occurred in both numerical analyses by Rots (1991) and in practice and can cause the masonry to fail earlier than expected when loaded under compression.

(a)   (b)
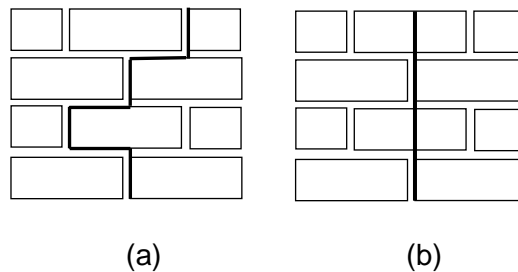
Figure 2.7 Failure patterns of masonry wall subjected to tensile load parallel to bed joint

$$h \geq b$$
$$h \geq 5\,h_b$$
$$h \geq 3\,t_b$$
$$h \leq 5\,t_b$$
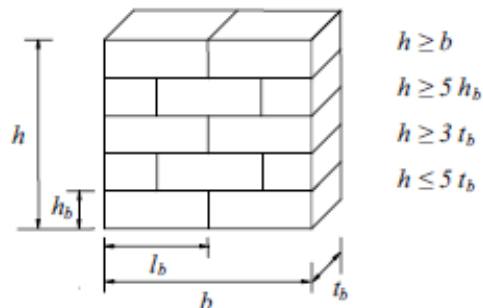
Figure 2.8 Specimen for determination of masonry compressive strength (RILEM, 1985)

21
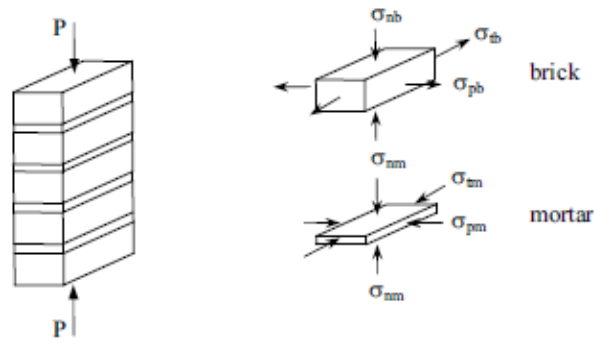
Figure 2.9 Test rig for determination of masonry compressive strength (Dhanasekar, 1985)

The curing of masonry after construction is very important as it affects the global behaviour of masonry structure by helping the hydration of the cement in the mortar. A few researchers (Anderson and Held, 1986, Marquis and Borchelt, 1986) have investigated the effects of curing conditions on the masonry strength in the past, and they have concluded that the masonry cured wrapped under polyethylene sheeting has higher bond strength than when it is cured open to air. Another factor that can influence the masonry strength is the thickness of mortar joint. Thicker masonry joints decrease the compressive strength because the flexible mortar tends to spread more and causes tensile splitting of brick units at lower loads (Chaimoon 2007).

2. 3   Masonry failure pattern

Movements in masonry may arise from the application of external load, foundation settlement, temperature changes, moisture content changes, creep, and chemical reactions in the materials such as chemical attack or corrosion of any carbon steel components embedded in the mortar such as ties or reinforcement (Hendry 1998, Forth 2009). If the movement of the masonry wall is restrained, the applied load may exceed the masonry wall's

bearing capacity, thus making the masonry wall start to crack. Small and invisible cracks can be gradually formed into big and visible cracks under external loading. If cracks keep forming and finally propagate through the structure, they may reduce the masonry's load carrying capacity and could lead, eventually, to collapse. One or combined cracking patterns can be found in the failed masonry wall panels.

The cracking patterns are totally different with those found in other structures made of different materials (concrete, steel, etc.). These special crack patterns are attributed to the composite nature of masonry and the characteristics of brick and mortar. Lourenco and Rots (1997) pointed out that the basic failure mechanisms of masonry have five basic types: (1) tensile cracking of the joints, (2) sliding along a bed/head joint at low values of normal stress, (3) cracking of the masonry units in direct tension, (4) diagonal tension cracking of masonry units at value of normal stress sufficient to develop friction in joints and (5) compressive failure, characterised by splitting of units in tension as a result of mortar dilatancy at high compression values. Type (a) and (b) are joint mechanisms, (c, e) are combined mechanisms involving bricks and joints and (d) is a brick mechanism. The detailed cracking patterns are showing in Figure 2.10.

However, in terms of global failure patterns of masonry wall panels, Campbell Barrza (2012) divided the failure modes into three main types: i) sliding shear failure; ii) shear failure and iii) bending failure depending on failure characteristics (Figure 2.11). Sliding shear failure is formed when the predominantly horizontal force exceeds the shear strength. Shear failure is exhibited when a wall is loaded with significant vertical as well as horizontal forces and this is the most common mode of failure. Bending failure can occur where walls have high shear resistance. This failure is characterized by a toe crushing on the lower side of the wall and/or an opening on the other side.

a) Joint tensile cracking   b) Joint slip   c) Cracking of unit in direct tension

e) Unit diagonal tension crack   d) Masonry crushing
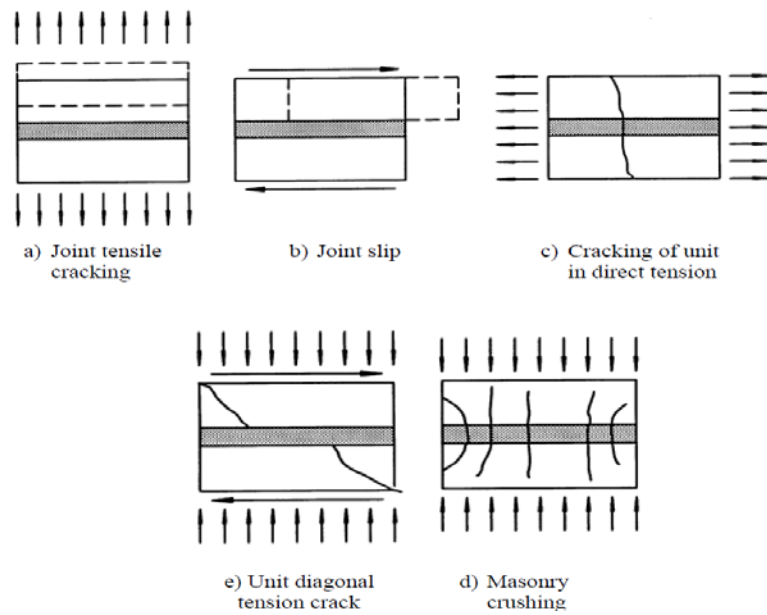
Figure 2.10 Cracking patterns of masonry walls (Lourenco and Rot 1997)

(a) Sliding shear failure   (b) Shear failure   (c) Bending failure
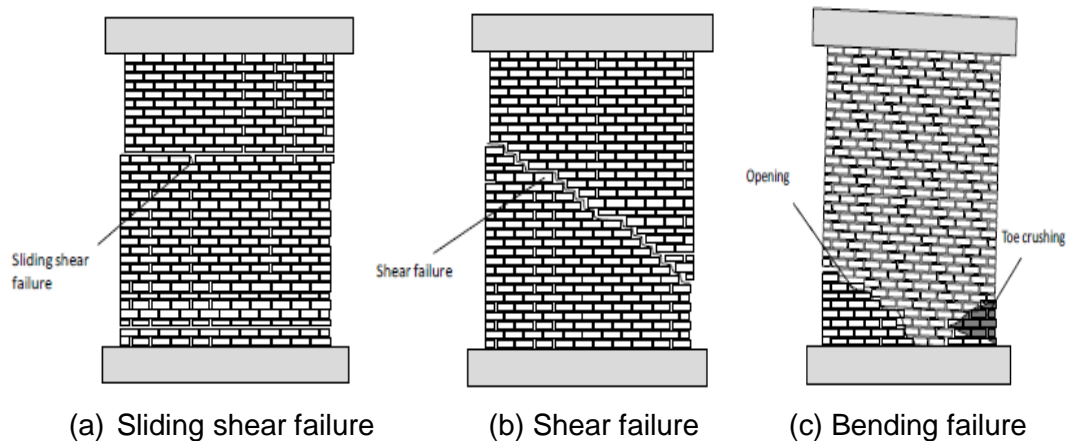
Figure 2.11 Failure pattern of masonry walls (Campbell Barrza 2012)

Generally in the experimental tests, one mode or combined failure modes can be found in the failed masonry walls. A combined failure mode happened in the structure can lead to a more complicated failure mechanism in analysing masonry (Melbourne and Tomor, 2005). The formation and occurrence of failure patterns of masonry walls vary depending on a lot of factors. The aspect ratio (height to length) and the loading patterns are some of the significant factors that may influence the failure pattern. The

other factors includes the strength ratio between masonry unit and mortar, boundary conditions and building skills etc. Abrams and Shah (1992) have investigated the influence of these factors by reporting on a series of unreinforced masonry wall tests with different length-to-height aspect ratios under different combinations of loadings. The first wall had an aspect ratio of 2.0 and was subjected to a vertical stress of 0.52MPa. This wall failed in shear (diagonal tension) with no flexural cracking. The second wall had an aspect ratio of 1.5 and was subjected to a stress of 0.34MPa. This wall, which was subjected to a smaller vertical compressive stress, had a flexure-shear failure as it was a toe compression failure. The third wall was a slender wall with aspect ratio of 1.0 and subjected to a stress of 0.34MPa. A flexure failure happened as the horizontal crack initiated along the bed joint immediately above the bottom course.

Furthermore, the failure pattern is also influenced by the loading patterns, and the biaxial behaviour is more complex than uniaxial one. The overall biaxial behaviour is a result of the combination of stress redistribution, local cracking and progressive failure in the localised regions (Chaimoon 2007). A testing programme on masonry subjected to proportional biaxial loading was performed by Dhanasekar (1985) to illustrate the influence of stress ratio and stress orientation. Under uniaxial tension, cracking and sliding of the head and bed joints governed failure while under tension-compression, failure occurred either by cracking and sliding of the joints alone or in a combined mechanism involving both units and joints.

In this chapter, only the performance of masonry wall without surrounding constraints is presented. Regarding the failure patterns and mechanical behaviour of masonry infill within infilled RC frame structures, the detail will be presented in Chapter 8.

2. 4   Strengthening approaches for masonry walls

Unreinforced masonry buildings constitute a significant portion of existing buildings around the world, and some of them are historically and culturally important. Matthys and Noland (1989) estimated that more than 70% of the buildings throughout the world are masonry buildings. Besides masonry buildings, reinforced concrete frame structures infilled with masonry walls are another popular construction system in the modern world. However, the masonry infill can be a contributing factor to the catastrophic structural failure if the structures are not properly designed. Moderate to strong earthquakes can devastate buildings, resulting in massive death toll and extensive economic losses. Especially for the developing countries, the vicious cycle whereby they do not possess the wealth to develop their infrastructure sufficiently to withstand the damages caused by earthquake and conversely, earthquake destroys their economy development (Bhattachary et al. 2014). As it is not feasible to demolish and replace these masonry buildings due to some factors, this raises the problem of finding methods to strengthen and retrofit the masonry buildings to ensure that they can perform their highly sought energy absorption role.

In the past decades, researchers have proposed a variety of technical methods to enhance the seismic behaviour of unreinforced masonry structures. These methods have been investigated both experimentally and numerically. However, as many repair and retrofit techniques have been developed by practicing engineers on an individual basis, therefore there is still little technical guidelines with which an engineer or researcher can determine the relative merits of these methods (ElGawady et al. 2004).

The basic concept of retrofitting is to upgrade the structural strength and improve the inelastic deformation capacity or ductility of the structure. This section reviewed the previous studies on strengthening and retrofitting of masonry structures in order to assess the advantages and disadvantages of

different approaches. Thus to develop a new method that differs with the existing ones as well as to overcome the shortcomings.

2.4.1 Existing URM retrofitting techniques

In the past decades, a large amount of research have been carried out investigating the retrofitting or enhancing of existing URM buildings. So far, the methods which have been implemented include conventional techniques (ElGawady et al. 2004a) and modern retrofitting techniques (ElGawady et al. 2004b).

2.4.1.1 Conventional techniques

Shotcrete

Figure 2.12 Application of shotcrete to URM wall (ElGawady et al. 2006)

Shotcrete overlays are sprayed onto the surface of a masonry wall over a mesh of reinforcing bars (Figure 2.12). ElGawady et al. (2006) carried out tests on retrofitted masonry walls by applying shotcrete technique, and the

ultimate lateral load resistance of the walls was increased by a factor of approximately 3.6. Shotcrete is advantageous in situations when formwork is cost prohibitive or impractical and where forms can be reduced or eliminated, or normal casting techniques cannot be employed. However, the disadvantages are much time consumed in the implementation, available spaces reduced and the affecting on the aesthetics.

Grout/epoxy injection

This method does not alter the aesthetic and architectural features of the existing buildings and it is considered to be one of the most efficient methods for repairing or strengthening structures of historical importance. The main purpose of injections is to restore the original integrity of the retrofitted wall and to fill the voids and cracks, which are presented in the masonry due to physical and chemical deterioration and/or mechanical actions (Bhattacharya et al. 2014). This method became popular and practical because of its minimal cost and ease of implementation. An ideal area of application is multi-leaf masonry walls where it is necessary to connect the different layers of the wall and which also appear high amount of voids in the dry rubble stones' inner core. The most important aspect of its vast use lies with the fact that it is sustainable. However, this approach will be successful only if the mechanical property of the mix and its physical chemical compatibility with the masonry to be retrofitted is achieved (Alcaino and Santa-Maria, 2008).

Ferrocement

Ferrocement is relatively cheap, strong and durable, and the basic technique is easily acquired. It consists of a thin cement mortar laid over wire mesh, which acts as a reinforcement. The mechanical properties of ferrocement depend on mesh properties as the mesh helps to confine the masonry units

after cracking and thus improving in-plane inelastic deformation capacity. Ferrocement is ideal for low cost housing since it is cheap and can be done with unskilled workers. This retrofitting technique increases the in-plane lateral resistance and improves wall out-of-plane stability and arching action since it increases the wall height-to-thickness ratio (Garofano, 2011). However, this method is much more time consumed in the implementation and it affects the aesthetics.

Re-pointing

Sometimes, the bricks in the masonry buildings are still of good quality but the mortar is poor. In this case, the mortar can be replaced to some extent with a higher strength bonding material. However, this method is not sustainable and the effectiveness is not remarkable as Tetley and Madabhushi (2007) found that the addition of 2% Ordinary Portland Cement to the mortar made little or no difference to the ultimate acceleration resistance.

External reinforcement

Figure 2.13 External reinforcement using vertical and diagonal bracing (Rai and Goel 1996)

It has been found that the lateral load resistance and ductility of URM walls have been improved greatly by mechanically attaching the exterior of existing masonry walls with a structural system (Hamid et al. 1994). Rai and Goel (1996) carried out a study by attaching a steel system directly to the existing diaphragm and wall (Figure 2.13). In an earthquake, cracking in the original masonry structure is expected and after sufficient cracking has occurred, the new steel system will have comparable stiffness and be effective (Hamid et al. 1994, Rai and Goel 1996). The steel strip system, proposed to retrofit low-rise masonry and concrete walls, is effective in increasing their in-plane strength, ductility, and energy dissipation capacity (Rai and Goel 1996, Taghdi 2000).

Confinement of URM with RC tie columns
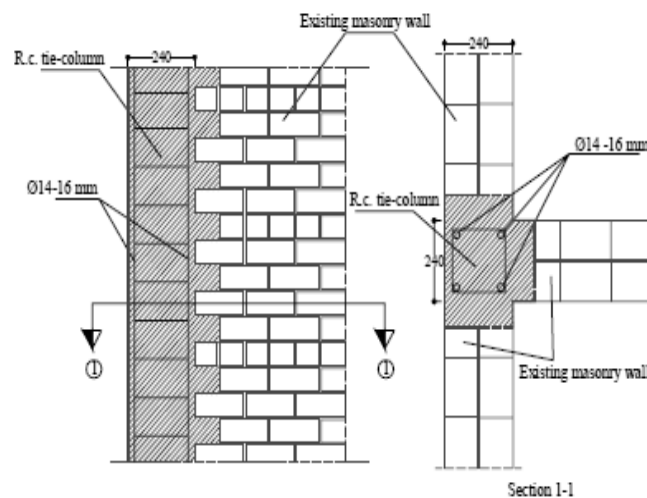
Figure 2.14 Reinforced tie columns confining masonry wall panels (ElGawady et al. 2004a)

This method (Figure 2.14) involves reinforced masonry tie columns confining the walls at all corners and wall intersections as well as the vertical borders of door and windows openings (ElGawady et al. 2004a). In order to be effective, tie columns should connect with a tie beam along the walls at floors levels. Eurocode 8 (1996) recommends the usage of such confined

30

system for masonry constructions. The confinement prevents disintegration and improves ductility and energy dissipation of URM buildings, but has limited effect on the ultimate load resistance (Chuxian et al. 1997). Tomaževič and Klemenc (1997) found out that this strengthening method can increase the lateral resistance by a factor of 1.5 as well as improve the lateral deformations and energy dissipation by more than 50%.

Centre core technique

This method involves placing a grouted and reinforced core in the centre of the building's wall. In detail, a continuous vertical hole is drilled from the top of the wall into its basement wall. After placing reinforcement in the centre of the hole, a filler material is pumped from the top of the wall to the bottom such that the core is filled from the bottom under pressure controlled by the height of the grout. This strengthening method can improve the capability of a wall to resist both in-plane and out-of-plane loading. This technique is successfully used to double the resistance of URM wall in a static cyclic test (Abrams and Lynch 2001).

Bamboo reinforcement

This method was proposed by Dowling et al. (2005) to use bamboo as part of a system involving buttresses, a ring beam, internal vertical reinforcement and horizontal internal reinforcement, which is shown in Figure 2.15. The experimental tests showed that all reinforced structures survived up to a 100% increase in displacement intensity. However, this remarkable improvement is found on adobe walls, which is a very weak masonry material. With higher strength material, the increase might not be so remarkable.

Figure 2.15 Bamboo reinforced wall with ring beam (Dowling et al. 2005)

Polypropylene (PP) band technique
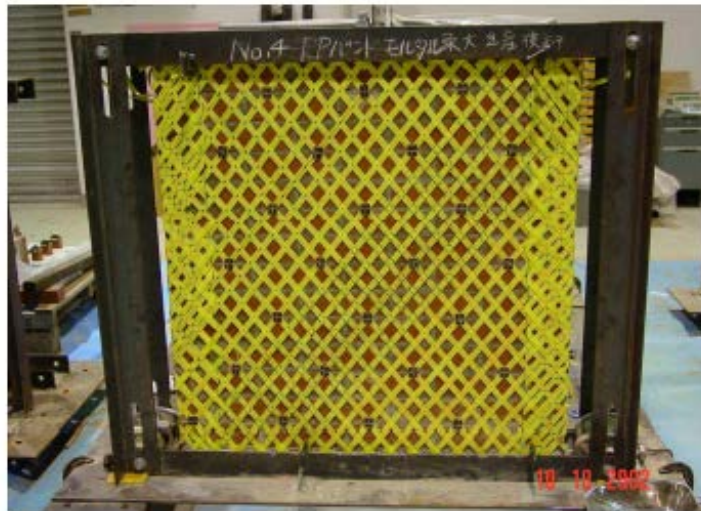
Figure 2.16 Retrofitted wall with PP-band

Polypropylene (PP) bands have been applied as an inexpensive retrofitting material in Japan. Sathiparan et al. (2005) tested both reinforced and unreinforced wallets, and found out that the diagonal compression tests showed that strengthened wall with PP mesh provide higher residual strength after formation of the first diagonal shear cracks. Furthermore, Mayorca and Meguro (2004) experimentally verified this method on strengthening URM (Figure 2.16). The experiments showed that although

the reinforcement did not increase the structure peak strength, it contributed to improve its performance after the crack occurrence. Though this approach has the advantages of low-cost and simplicity of installation with available resources and skills, the improvement of a structure's mechanical behaviour is not significant and the aesthetic of the original structure is affected significantly.

2.4.1.2 Modern retrofitting methods

The drawbacks of the conventional methods can be overcome by using Fibre Reinforced Polymer (FRP) reinforcement. FRP probably is the most widely used state-of-the-art approach to enhance masonry walls. Since the early 1990s, FRP composites used as retrofitting or strengthening method on existing concrete and other (masonry, timber) structures have been extensively studied (Teng et al. 2003). The most widely used FRP composites are Carbon FRP (CFRP), Glass FRP (GFRP) and Aramid FRP (AFRP). Figure 2.17 illustrates a typical application of FRP on masonry wall panels. In general, retrofitting of unreinforced masonry walls using FRP can increase the lateral resistance by a factor ranges from 1.1 to 3 (ElGawady et al. 2004b). Alcaino and Santa-Maria (2008) presented an analysis of the experimental results of clay brick masonry walls retrofitted with carbon FRP, and the results showed that the strength of the walls could be increased by 13-84%. In addition, Mohmood and Ingham (2011) conducted a research programme in order to investigate the effectiveness of FRP additions as seismic retrofit interventions for in-plane loaded unreinforced masonry walls. The experimental results showed that the shear strength increased by up to a factor of 3.25. Valluzzi et al (2002) performed a study in order to investigate the efficiency of the strengthening of FRP with different configurations. One was strips with grid arrangement and other was diagonal strips. The panels were strengthened on both sides and only at one side as well. It was noted that, the asymmetrical application of the reinforcement is associate to a limited effectiveness in the improvement of

the shear resistance of masonry panels. Moreover, it is shown that the diagonal configuration can be more efficient concerning the enhancement of the shear capacity, while the configuration of strips as a grid allows a better stress redistribution producing a less brittle failure due to crack.
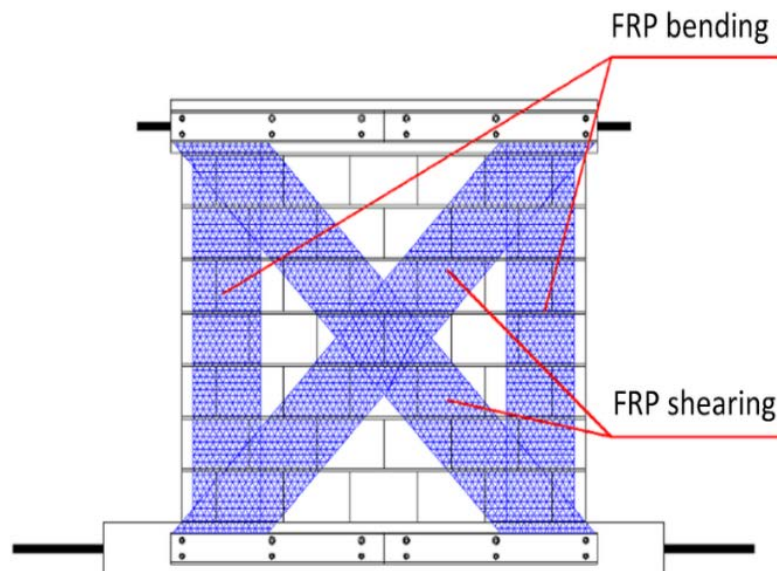
Figure 2.17 Application of a typical FRP strengthening approach

The retrofitting of masonry wall using FRP has become popular recently. The reasons are that it has the advantages of little added mass, low disturbance and relatively high improvement in strength. However, the drawbacks of this method are its high cost, high technical skill and affecting on architectural aesthetics. The initial cost of FRP material is about 5 to 10 times more than steel (Burgoyne 2004), which is a huge burden for the house owners in the developing countries. Moreover, many engineers have not obtained enough knowledge of FRP materials; especially as their long-term behaviour needs to be understood. In addition, one other major problem is that typically in developing countries the masonry surface is not smooth and this causes stress points for the FPR wrap and therefore results in premature failure/unpredictable failure. Moreover, the FRP is usually made by continuous strips or sheets externally and applied on the surface of masonry wall. This may create a water-proof barrier and natural transpiration of stone or ceramic material. Furthermore, the problem of fire resistance of

this strengthening approach may arise as well. Finally, this reinforced buildings can be particularly vulnerable when FRP is used in combination with epoxy-based bonding material, which made this technique detrimental (Garofano 2011).

2.4.2 Discussion of the existing methods

The strengthening methods have been presented in the above section, and the results illustrate that the improvement of different methods varies. Each approach has its own advantages and disadvantages. The significance of the improvement of each strengthening method depends on the structure material and strengthening material. Therefore, the application of the strengthening methods should be selected carefully. Table 2.1 summarizes the characteristics of all the above methods. Table 2.2 assesses the suitability of the methods based on the scores. The score ranges from 1 to 10 with 1 representing poor approach and 10 an excellent approach. The rating system on Table 2.2 is based on the strengthening approach's characteristics. For example, in terms of economic feature, FRP is about 10 times more expensive than steel, while mortar is much cheaper than steel. Therefore, the economic score is assessed based on its cost, and they are taken as FRP 1, steel 3 and mortar 9, respectively. In terms of strengthen improvement, the FRP is more efficient as it can improve the strength about 1.1 to 3 times. However, for the grout injection, it can only restore the initial strength. Therefore, the assessment score of the improvement for FRP is 10, steel 7, and mortar4. It should be noted that this numbering is not taken as accurate but as approximate assessment. As the exact value is not easy to obtain. However, the value given in Table 2.2 is assessed carefully based on the characteristics listed in Table 2.1 as well as the literature review, and it is very close to the accurate value. Moreover, it should be noted that the assessment and judgement was carried out on individual case, which means the features of each retrofitting approach might be different when used in other cases.

Figure 2.18 Summary of the characteristics of the methods

Strengthening method	Characteristics
Shotcrete	The improvement of this method is significant. However it is too expensive for application in poor communities as it requires the use of concrete and steel reinforcement, as well as great effect on the aesthetics.
Grout/epoxy injection	It requires minimal cost and it is easily applied. However it works only when the mechanical property of the mix and its physical chemical compatibility with the masonry is achieved.
Ferrocement	The improvement is remarkable. However, it is expensive due to the use of steel reinforcement and it also affects the aesthetics.
Re-pointing	It needs minimal cost as it only requires the manufacture of a stronger mortar as well as little technique knowledge required. However, it only restores the initial strength of masonry.
External reinforcement	It has relatively remarkable improvement. However it is expensive to apply. It also affects the aesthetic.
Confinement	It is cost-effective for application in new building. However, it is uneconomical as a retrofit for existing buildings, as it requires demolition and reconstruction of wall sections
Centre core	It could improve the performance remarkably. However, it is expensive and complicated to implement.
Bamboo	It requires very little cost and it is easily buildable. The improvement is significant on the adobe structure. However, it might not be effective with brickwork masonry structure.
Polypropylene (PP) band	It requires very little cost, about 5% total cost of house. It is simple enough for application by local craftsmen without specific knowledge. However, it has huge effect on the aesthetic and relatively small improvement.
FRP	It is expensive compared with other strengthening materials. It requires sophisticated skills and it has an effect on the aesthetic of the buildings. However, it has the advantages of remarkable improvement and little added mass.

Figure 2.19 Assessment of the existing methods

Strengthening method	Economic	Improvement	Sustainability	Buildability	Total score
Shotcrete	2	8	5	5	20
Grout/epoxy injection	9	4	8	8	29
Ferrocement	1	8	5	6	20
Re-pointing	10	1	8	8	27
External reinforcement	3	7	5	6	21
Confinement	5	8	3	4	20
Centre core	2	9	6	3	20
Bamboo	7	5	7	6	25
Polypropylene (PP) band	9	1	8	8	26
FRP	1	10	5	5	21

Based on Tables 2.1 and 2.2, it can be known that each approach has its own characteristics and there is no best strengthening approach. Each retrofitting technique has its own advantages and disadvantages. When a technique is appropriate for one building, it may not necessarily be appropriate for another. The strengthening/retrofitting approach must be consistent with aesthetics, function, strength, ductility and stiffness and the cost requirements. The selection should be decided by the owner depends on which characteristic is more concerned. For example, if the improvement is the only concern, FRP is the best choice. If the finance issue is more concerned, grout injection or re-pointing should be preferred.

Chuang and Zhuge (2005) proposed a general procedure for retrofitting masonry structures, and it is: (1) understanding the performance of the building; (2) determination of required seismic capacity; (3) development and

selection of strengthening schemes; (4) design of connection details; and (5) re-evaluating the retrofitted building. This chapter briefly followed this procedure in order to find a retrofitting approach. In this chapter, section 2.2 and 2.3 have presented a basic understanding on the performance of masonry building. After knowing the performance, the determination of required seismic capacity should be made. Before the selection of strengthening scheme, the retrofitting criteria are selected in conjunction with the importance of the structure and seismic activities/intensities expected at the site. Section 2.4 compared and assessed the existing approaches, which provide a guidance on the selection of retrofitting approaches. The engineer needs to identify the building's structural deficiencies and understand the local and global mechanical characteristics of the building. A good retrofitting solution requires consideration of technical, economic and social aspects. After the selection of retrofitting method, the craftsmen should implement the retrofitting strictly following the suggested procedure.

In this research, the author has proposed and tested a new approach too, which can been seen as a conventional, though practical retrofitting approach. Namely, the traditional method of building a wall parallel to an existing single-leaf wall and bonding the two leaves together using a mortar (collar) joint is being considered as a possible strengthening and retrofitting technique. The method does not require sophisticated workmanship because of its easy implementation, which further renders it cost-effective. Moreover, the material is easy and cheap to obtain in most countries. Therefore, according to the literature review and compared with the mentioned characteristics in Table 2.2, the score of this proposed method in terms of economy, sustainability and buildability is 8, 8, and 9, respectively. However, the improvement and influence of this technique is not known yet. Therefore, it is necessary to conduct this research to investigate the improvement.

Furthermore, the double-leaf wall system is also a popular construction system as it can improve the soundproofing, waterproofing and fireproofing. The actual research investigates experimentally the merits of the technique that does differ from any previous published work. Based on the author's knowledge and observation, it has not been extensively studied. Therefore, the author intends to implement this construction system as a strengthening/retrofitting approach and investigate its improvement. The further intention of the study is to apply the suggested measure's influence on the holistic behaviour of infilled RC frames; this can actually be both beneficial, e.g. due to adding strength, or detrimental, e.g. due to impact damage on relatively weak columns and the influence on the structure period because of added stiffness.

A preliminary parametric study has been conducted to evaluate the performance of the enhancement method using a monotonically increasing quasi-static loading scheme both experimentally and analytically. Notably, the whole study is not only relevant to earthquake engineering, which is a rarity in the UK; double-leaf (collar jointed) walls can also be used to improve a structure's lateral stability (e.g. against wind or blast loading) through adding stiffness. Thus, this research broadly aims to generate knowledge and understanding which can be directly applied in a number of structural applications. The details of this approach will be presented in Chapter 3 and 4.

2. 5   Double- and multi-leaf wall

As the proposed strengthening approach involves the double-leaf wall, therefore, it is necessary to know the mechanical behaviour of this type of wall. As far as the author knows, most of the researches on masonry retrofitting or masonry mechanics were mainly on single-leaf walls, only few researchers have conducted such studies on double- or multi-leaf masonry walls. Still, double-leaf walls can be found in many historic structures and

they have regularly been exposed to considerable earthquakes, which obviously affects the holistic structural dynamic performance. Furthermore, double-leaf masonry walls are common in modern construction as they can enhance soundproofing, fireproofing, and waterproofing characteristics. As the proposed method to strengthen/retrofit masonry walls in this research involves the double-leaf masonry walls too, therefore, the author feels necessary to conduct research on such a construction system shedding light to previous gaps in knowledge.

According to BS 5628-1: (2005), a double-leaf (collar jointed) wall is defined as *"two parallel single-leaf walls, with a space between not exceeding 25 mm, filled solidly with mortar and so tied together as to result in common action under load".* Similarly definition can be found in Eurocode 6 (2005), that *"a wall consisting of two parallel leaves with the longitudinal joint between filled solidly with mortar and securely tied together with wall ties so as to result in common action under load." A typical double-leaf (collar jointed) masonry wall is illustrated in Figure 2.18.*
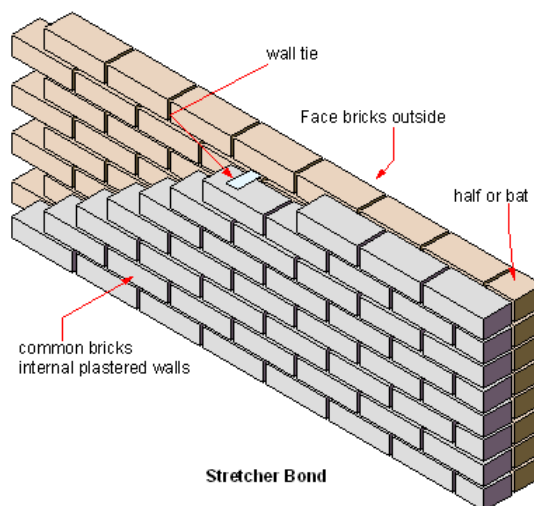
Figure 2.20 Geometrical arrangement of a typical double-leaf masonry wall

Over the last few decades, few researchers have conducted studies on double- or multi-leaf masonry structures. Among those researchers, Anand

and Yalamanchili (1996) analysed a composite masonry wall made of a hollow block leaf and a brick leaf connected by two types of collar joint (9.55mm and 51mm). The composite masonry walls were subjected to both vertical and horizontal loads in a 3D arrangement to find out that collar joint failed in brittle in nature and it kept propagating at a constant load once initiated. However, as the double-leaf wall in this research is made up of two leaves both with same material while the composite masonry leaves were made of different materials (block and brick), therefore, it is still unknown whether the same result can be acquired if the two leaves are made of same materials. Moreover, Peraza (2009) found out that if the two masonry leaves were made with different materials (clay brick and concrete block), the collar joint may be harmful to the whole structure over the life time. As the clay brick tends to expand over time while concrete block tends to shrink, and the collar joint will constrain this change, thus causing the composite wall to bow slightly. In this research, both the leaves are made of brick units, therefore, this issue is not concerned herein.

Ferguson (2002) investigated the performance of collar joint masonry wall, and found out that the collar joint fully infilled wall failed at a higher peak load than those walls with empty collar joints. The same results were confirmed in the work of Mirza et al. (2002) as well. In addition, the collar joint was not fully infilled sometimes and improperly constructed collar joint can reduce the structural integrity. This deficiency can be repaired by grout injection (Krauth et al. 2001). Similarly, Vintzileou and Tassios (1995) and Vintzileou and Miltiadou-Fezans (2008) used the grout injection to repair the masonry which was made up of two exterior leaves. The grout injection contributed to the increase of tensile and compressive strength of masonry. However, this increase was not followed by substantial increase in the stiffness of masonry. Moreover, the grout injection is different with the proposed approach in this research in terms of building process. The grout injection is normally done after the building of masonry walls while this approach can be carried out during the constructions of the collar jointed masonry walls.

Pina-Henriques et al. (2004) and Ramalho et al. (2005) conducted a few series tests on three-leaf masonry walls under shear and compression to predict the mechanical behaviour. The specimens consisted of two external leaves made of stone bricks and mortar joints, and an internal leaf made of mortar and stone aggregate. The leaves were connected with two different types of collar joints (Figure 2.19): a) straight collar joint; and b) keyed collar joint. They found that the structures made with different types of collar joints behave differently under the application of external load. For the wall panels constructed with a straight collar joint, vertical shear failure occurred. However, for the wall panels constructed with keyed collar joints, failure was mainly due to diagonal cracks in the inner leaf. Ramalho et al. (2008) undertook numerical investigations with the aim to simulate the aforementioned experimental tests (Pina-heriques et al. 2004, Ramalho et al. 2005) by applying a unique damage model which was developed to interpret the time evolution of mechanical damage in brittle materials. The model was implemented in two finite element codes (ABAQUS and FEAP) to make a comparison. The proposed numerical model captures different features of nonlinear response of multi-leaf walls. Nevertheless, as perfect bonding was assumed between the adjacent layers during the modelling, some of the numerical results were overestimated. Similarly, Binda et al. (2006) conducted research on multi-leaf stone masonry walls bonded by two different types of collar joint (straight joint and keyed joint, see Figure 2.19) in order to understand the load-transfer mechanisms between the individual walls. However, the collar joint in any case was much thicker than what is suggested in British Standard 5628-1 (2005) that the space between two parallel single-leaf walls does not exceeding 25mm.

The failure patterns of double- or multi-leaf masonry structures have some difference with single-leaf wall. Pappas (2012) concluded that the failure modes in multi-leaf masonry walls can be mainly categorised into detachment of the leaves, the global or local overturning and the local expulsions of the material. In the case of the three-leaf masonry wall, the applied load is resisted mainly by the external leaves (Vintzileou 2007)

(Figure 2.20). In general, the compressive strength as well as the Young's modulus of the internal leave is smaller than that of the external leaves. As the inner core is confined by the external leaves, the inner leave will fail in higher compressive strength while external leaves fail in lower values. When the internal core yields, three failure patterns may occur: (a) the detachment of the external and internal leaves; (b) global or local crushing of external and internal leaves; (c) the external leaves fail out-of-plane due to the larger lateral dilatancy of the internal leaf. However, as the proposed method is carried on double-leaf wall, the failure pattern will be different.
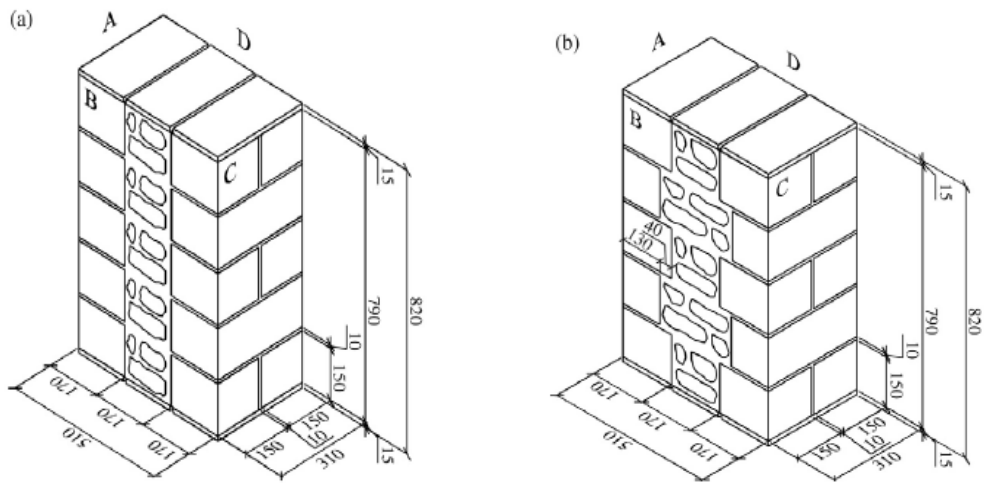
Figure 2.21 Wallets dimensions in mm: (a) straight collar joint and (b) keyed collar joint (Pina-Heriques et al. 2004)
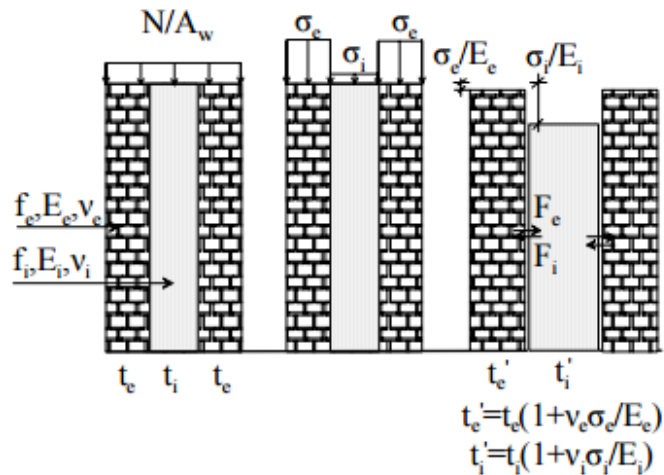
Figure 2.22 Stresses and deformations of a three-leaf masonry subjected to compression (Vintzileou 2007)

2. 6 Modelling of masonry walls

The development of a computational model is for the sake of avoiding the need for costly, repetitive laboratory testing of large-scale wall panels. One of the objectives of this research is to develop a numerical model to simulate double-leaf (collar jointed) masonry walls. However, the modelling of load bearing masonry wall panels or masonry infill under in-plane combined loading is difficult and still has not been completely resolved. The great number of influencing factors, such as dimension and anisotropy of the bricks, joint width and arrangement of bed and head joints, material properties of both brick and mortar, and quality of workmanship, make the simulation of brick masonry extremely difficult (Tzamtzis and Asteris 2003).

The need to predict the in-service behaviour and load carrying capacity of masonry structures has led researchers to develop numerical methods which are capable of solving those problems. The ability of a method to reproduce the structure's behaviour in a realistic way and the computational demands can be important criteria for the selection of the method (Pappas 2012). Up until now, researchers have proposed different approaches to simulate the masonry walls under static or dynamic loading, both for in-plane or out-of-plane behaviour. In order to model and represent the real behaviour of masonry structures, both the constitutive model and the input material properties must be selected carefully. Lourenco (2002) suggested a few factors in selecting the most appropriate method to use, and they are: the structure itself under analysis, the level of simplicity desired, the knowledge of the experimental data available; the amount of financial resources; time requirements and the experience of the modeller. It should be noted that results of different approaches might result in different outcomes. Among those popular non-linear simulation methods, there are three main types of simulation methods, and they are: (i) detailed micro-scale modelling, (ii) simplified micro-scale modelling and (iii) macro-scale modelling. Depending on the level of accuracy and simplicity required,

different model strategy will be applied (Lourenco 1996). The methods are summarized in Figure 2.21:
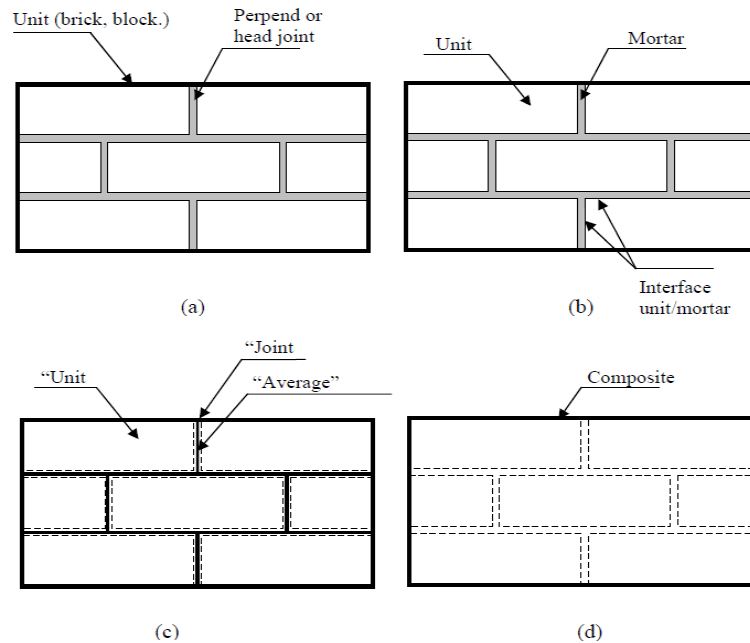
Figure 2.23 Modelling strategies for masonry: (a) typical masonry specimen; (b) detailed micro-modelling; (c) simplified micro-modelling; and (d) macro-modelling (Lourenco, 1996)

Detailed micro-scale modelling: Figure 2.21(b) is a detailed micro-modelling method. In this method, both the masonry units and the mortar are discretised and modelled with continuum elements while the unit/mortar interface is represented by discontinuous elements. Detailed micro-modelling is probably the most accurate method to simulate the real behaviour of masonry as it can take the elastic and inelastic properties of both the unit and the mortar into account. However, it requires large computational effort to analyse by applying this method. Therefore, this method is used mainly to simulate tests on small specimens in order to determine accurately the stress distribution in the masonry materials (Lourenco and Pina-Henriques, 2006; Zucchini and Lourenco, 2006).

Simplified micro-scale modelling: Figure 2.21(c) is simplified micro-scale modelling method. This method is refined based on the detailed micro-scale modelling. In this method, the mortar joints are smeared into zero-thickness interface while the masonry units are expanded by taking into the dimensions of mortar joints in order to keep the whole geometry unchanged. The expanded units are modelled as continuous elements while the behaviour of the zero-thickness unit-mortar interface as dis-continuous elements. Cracking in the masonry units can also be simulated by assigning potential vertical zero thickness interfaces at the unit's centre lines (Lourenco 1996). The drawback of the large computational effort required by detailed micro-modelling is partially overcome by the simplified micro-scale modelling method as it can capture quite accurate results but take less computational time. However, Lofti and Shing (1994), Lourenco and Rots (1997) pointed out that the accuracy is lost since Poisson's effect on the mortar cannot be included and, as a result, the brick-mortar interaction can only be partially described.

Macro-scale modelling: Figure 2.21(d) is macro-scale modelling. In this method, the units, mortar joints and unit-mortar interfaces are smeared out into a homogeneous anisotropic continuum. There is no distinction between individual masonry units and the mortar joints within this method and masonry is considered as a homogeneous anisotropic material. The behaviour of masonry is described in terms of average stress and strains. This approach is very attractive for large-scale masonry structures as it can reduce much computational time as well as mesh generation flexibly. In spite of this, it is not adequate for detailed studies and for capturing failure mechanisms (Lourenco, 1996).

2.6.1 Simplified micro-scale modelling

Though the simplified micro-scale models are relatively costly to use due to requiring a lot of input data and their failure criterion has a complicated form due to the brick-mortar interaction. However, it can capture all possible failure modes, thus giving a better understanding of the failure behaviour of the masonry walls. The main methods available for modelling masonry structures using the simplified micro-modelling approach include: (a) Finite Element Method (FEM); (b) Discrete Element Method (DEM). These two types of modelling will be described in detail in the following section.

2.6.1.1 Finite Element Method (FEM)

The finite element method (FEM) is the dominant and powerful approach for the analysis of structures, which is able to simulate complex structures with linear or non-linear material properties either at a micro or macro scale. When modelling masonry using the FEM, discontinuities are generally introduced using interface elements, for which the constitutive model is in direct relation with the stress vector and the relative displacement vector along the interface (Oliveira 2003). Therefore, for an accurate simulation of masonry behaviour, it is essential to obtain a constitutive model for the interface elements which is able to capture realistically the behaviour of masonry and be able to simulate all the failure mechanisms.

Simplified micro-scale FEM describes masonry as a two phase material where its constituents are considered separately. The bricks are represented with plane stress quadrilateral finite elements. The mortar joints are represented by non-linear interface elements, which can only deform in normal and shear directions. This model was first proposed and applied to solid masonry by Page (1978). Ali et al. (1987) used this method to study the non-linear behaviour of masonry subjected to concentrated loads. Lourenco

(1996) introduced a compressive cap to the failure surface in Page's model. By this, the crushing of the masonry bricks is also enabled beyond the interfaces, allowing for all possible failure modes to be taken into account.

In Lourenco's (1996) work, this model is applied where bricks are subdivided into a number of rigid elements and mortar joints are smeared into zero-thickness interfaces. Al-Chaar and Mehrabi (2008) modelled RC frames infilled with masonry walls using this method in DIANA. In addition, a lot of other researchers have applied this method to model masonry structures and good agreement was found (Van Zijl 2004, Dolatshahi and Aref 2011).

2.6.1.2 Discrete Element Method (DEM)

Discrete Element Method (DEM) is characterized by modelling the materials as an assemblage of distinct blocks or particles interacting along their boundaries and the mortar joints as zero thickness interfaces between the distinct blocks. It was first introduced by Cundall (1971), which was applied in the study of jointed rock engineering. Later this approach was extended to other fields of engineering requiring a detailed study of the contact between blocks or particles such as soil and other granular materials (Ghaboussi and Barbosa 1990).

The discrete element method is based on discontinuous mechanics and treats the model as discontinuous materials with the ability to have progressive failure, crack propagation and large displacements and rotations between the block. By the automatic rounding of the corners of the blocks, it is possible to avoid the problem of the interlocking blocks which makes the DEM a very convenient tool for analysis of masonry structures (Azevedo and Sincraian 2001).

In the last two decades, the approach was applied successfully to model masonry structures by Lemos (2007) and Zhuge (2008) in which the collapse modes were typically governed by the mechanisms in which the deformability of the blocks plays little or no role. Also, the possibility of frequent changes in the connectivity and the type of contact as well as marked non-linearity induced by the inability of the masonry joints to withstand tension makes DE a suitable method for solving problems involving discontinuities in the case with low bond strength masonry (Sarhosis and Sheng 2014, Sarhosis et al. 2015).

2.6.2 Macro-scale modelling

There is no distinction between individual masonry units and the mortar joints in macro-modelling approach. Masonry is simplified as a homogeneous anisotropic composite by smearing units and mortar joints into an average continuum.

Saw (1974) assumed masonry as an isotropic elastic behaviour by ignoring the influence of mortar joints acting as planes of weakness. Dhanasekar et al. (1985) proposed a non-linear finite element model for solid masonry based on average properties. This assumption can work in predicting deformations at low stress level, but not at higher stress levels where extensive stress redistribution caused by non-linear material behaviour and local failure would occur (Tzamtzis and Asteris 2003).

Macro-scale modelling neglects the influence of mortar joints, which makes this modelling approach suitable for the study of the global behaviour of masonry. Therefore, this model is applicable when the dimensions of a structure are large enough so that the relationship between average stresses and strains is acceptable (Lourenco 1996). This method is relatively simple to use and requires less input data and a more simple failure criterion.

Thus remarkable simulation time can be saved by applying this method. However, unconditionally accurate results and fine-detail of the behaviour cannot be captured by the nature of this approach.

2. 7　Summary

This chapter reviewed the previous researches based on the aims and the objectives of this research, which provides a general overview and basic understanding on masonry. The literature is summarized briefly as following.

Masonry is a brittle, anisotropic, composite material, which has a better performance in resisting compression rather than tension. It has been experimentally and numerically studied in the past decades on the mechanical behaviour of masonry. However, the mechanical behaviour is still not thoroughly understood yet due to its inherent complexity. There is still a lack of good understanding in the complex fracture behaviour of masonry, especially on the double-leaf masonry wall.

As a building material, masonry can be often found in the residential buildings as well as the historical heritages. Most of these buildings and heritages are located in the seismic prone and populated areas, which are vulnerable to damage if moderate to strong earthquake happens. Even if without earthquake, these structures are facing different potential damages, such as, wind, weather corrosion, and foundation settlement etc. The damage of masonry structures might cause massive economic loss and death toll. Therefore, it is necessary to strengthen the structure before earthquake happens or retrofit after the damage occurs.

In order to have an effective strengthening/retrofitting, Chuang and Zhuge (2005) proposed a general procedure, and it is: (1) understanding the performance of the building; (2) determination of required seismic capacity;

(3) development and selection of strengthening schemes; (4) design of connection details; and (5) re-evaluation of the retrofitted building. This research was carried out followed this procedure. Sections 2.2 and 2.3 in this research provide a basic knowledge on the performance of masonry building. In section 2.4, different approaches on strengthening/retrofitting the masonry structures have been proposed, and a comparison has been assessed in Tables 2.1 and 2.2. According to the tables, each type of strengthening approach has its own advantages and disadvantages, there is no best strengthening/retrofitting approach. The application of the strengthening approach needs to be assessed and selected based upon a few factors: masonry material of the structure, finance problem, aesthetics etc. Therefore, this research introduces a new strengthening/retrofitting approach using collar jointed technique. This approach differs with the existing strengthening approaches. Besides, collar jointed masonry wall is quite a common and popular construction system in masonry structures as it can improve the water, sound, and fire proofness. However, this topic has not been extensively studied, let alone used as a strengthening method. Therefore, in this research, the author proposed this construction system as a new strengthening approach, namely, building a wall parallel to a single-leaf wall and bounding the two leaves together using 10mm thick collar joint.

Though the basic concept of this approach has some similarities with the grout/epoxy injection, it is totally different in terms of building process and construction materials. The grout/epoxy injection is carried out after the building of masonry structures in order to infill the cavity of the structure. Furthermore, the grout/epoxy injection is most often carried out on stone masonry structures as this type of structures is more easily to have cavity between each leaves. The proposed strengthening approach using collar jointed technique has its own characteristics. The collar jointed technique is easy to be carried out in different types of masonry structures, including adobe, brick and stone. Also, the material is cheap and easy to obtain in most countries, which is a cost-effective choice for the householders in the developing countries. Furthermore, this approach does not need

sophisticated skill, which is buildable for the local craftsmen. In addition, the aesthetics of the structure can be affected least if the strengthening material was chosen similarly with the original one. In conclusion, this method has its advantages in economy, sustainability and buildability. However, the improvement of this method is not known yet, which will be conducted in the following chapters. In order to have a more comprehensive understanding on the mechanical behaviour of masonry wall panels reinforced/unreinforced using collar jointed techniques, experimental tests should be carried out in the laboratory. More details of this approach will be presented in Chapter 3 and the test results will be demonstrated in Chapter 4.

Chapter 3   Experimental work on masonry walls

3. 1   Introduction

This chapter describes the materials and experimental details that have been used and conducted throughout the research. Seven tests investigating two different types of masonry walls, i.e. the benchmark single-leaf and the innovative double-leaf, have been carried out in George Earle Laboratory in the University of Leeds. The tests breaking down includes four tests on single-leaf and three on double-leaf masonry wall panels, wherein critical variables were modified. The experimental observations were primarily focused on static displacement and load capacities clearly supports a quasi-static rationale for performing any earthquake load related assessments. In addition to the large scale tests on masonry walls, some experimental tests on small specimens, including mortar cubes and brick units, were conducted respectively as well, to obtain the mechanical properties of the materials used in the experimental work.

3. 2   Specimen materials

The materials used in this research have been tested and assessed by carrying out a series of preliminary small scale tests to obtain all the relevant material properties. The types of materials are discussed in detail and presented according to the requirements needed.

3.2.1 Brick

Bricks make up most percentage of the masonry wall, and play an important role in the whole mechanical behaviour of a masonry element. In general,

bricks used today are usually made from clay, calcium silicate and concrete. It is estimated that approximately 96% of bricks used in the United Kingdom are manufactured from clay (MIS 2013). In this study, all the bricks used in this research are red Engineering Class B perforated bricks and they are made from loam with brick-earth or shale and subsequently fired at high temperature. The standard dimension of each brick is 215mm$\times$102.5mm$\times$ 65mm. The geometry and detailed dimensions of the brick is shown in Figure 3.1. It should be noted that the clay brick used in this research has a relatively higher strength than most masonry unit, so that the failure cracks will be more unlikely occurred among bricks. Furthermore, the brick has some small slots on the back as well as the holes in the unit, which helps to improve the connection among the two leaves. Therefore, the integrity of the collar joint will be better than using the smooth type of brick.

a)   Geometry of brick   b) Dimensions of brick
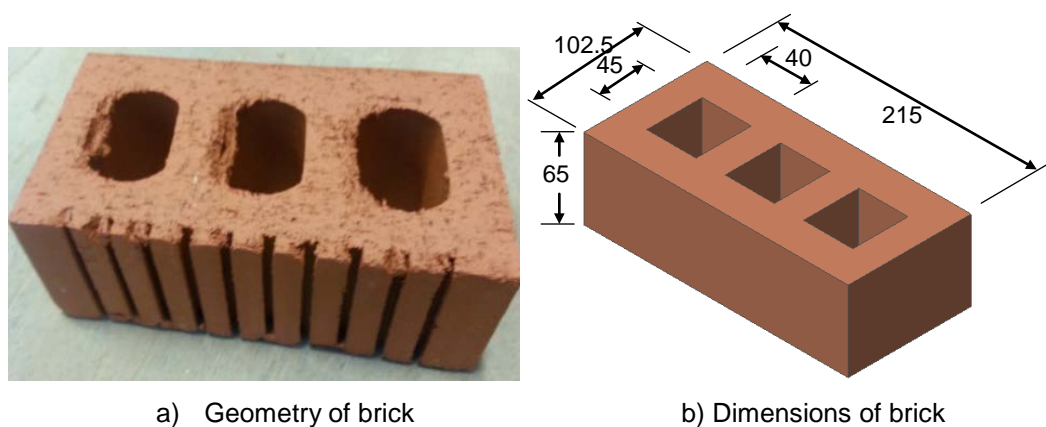
Figure 3.1 The detail of brick used in this research

Some important specifications of the clay brick are given as follows:

Compressive strength: Greater than 70 MPa

Water absorption: Less than7%

Durability: F2

Perforation: 24%

The bricks have been tested under the guidance of British Standard BS 3921 (BSI 2005) and BS EN 772-1 (BSI 2011). The bricks were compressed under the equipment TONI PACT 3000, which is shown in Figure 3.2, to obtain brick's compressive strength. Prior to the test, the bricks were immersed in water for 24 hours before loading on bed face via 10mm plywood plates as required by the standard. The results showed that the bricks have a mean compressive strength of 74MPa.

Furthermore, the water absorption tests were carried out as well based on British Standard BS 3921 (2005). Water absorption of brick affects the performance of mortar and the deformation of masonry. The water absorption of 10 bricks immersed in water for 24 hours was 5.6% (±0.6%).

However, there is no standard method available to date for measuring the elasticity modulus of masonry units. Therefore, the elastic modulus test were carried out in the traditional method, which is calculated by dividing the tensile stress (stress is a force that tends to deform the body on which it acts per unit area) by the extensional strain (strain is the measure of the extent to which a body deforms under stress, which has no unit) in the elastic portion of the stress-strain curve. The equation to obtain the modulus is shown as following.

$$E = \frac{\sigma}{\varepsilon} = \frac{FL_0}{A_0 \Delta L} \qquad (3.1)$$

In this research, the elastic modulus of brick has been tested by using strain gauges to measure the strain change under compression. Though as mentioned in the literature review section that brick is anisotropic, the elastic modulus perpendicular to bed face is taken as $\mathbf{19.9 kN/mm^2}$ from the test results. However, as the brick was extruded perpendicular to its bed face during the manufacturing process, the strength and stiffness of a brick parallel with bed face will be different due to the presence of perforations, method of manufacture, and type of clay. In the majority of cases, bed-face

modulus are equal to or greater than header-face modulus, but for pressed clay bricks, the bed-face modulus is only about 50% of the header face modulus (Brooks 2014). Based on the literature review that the masonry behaves in a linear stress-strain manner when loaded below their strength limit. Similar experimental result is also found in Chapter 4. Therefore, in this study, the property of a single brick unit is taken as isotropic.

Figure 3.2 TONI PACK for compression test

3.2.2 Sand

Sand is mainly used as an inert material to give volume which results in reduction of cost. Type S sand was provided in this research in order to achieve the required strength and durability. The results of a sieve analysis are shown in Figure 3.3, which complied with BS 1199 and 1200 (1976) and BS 410-2 (2000).
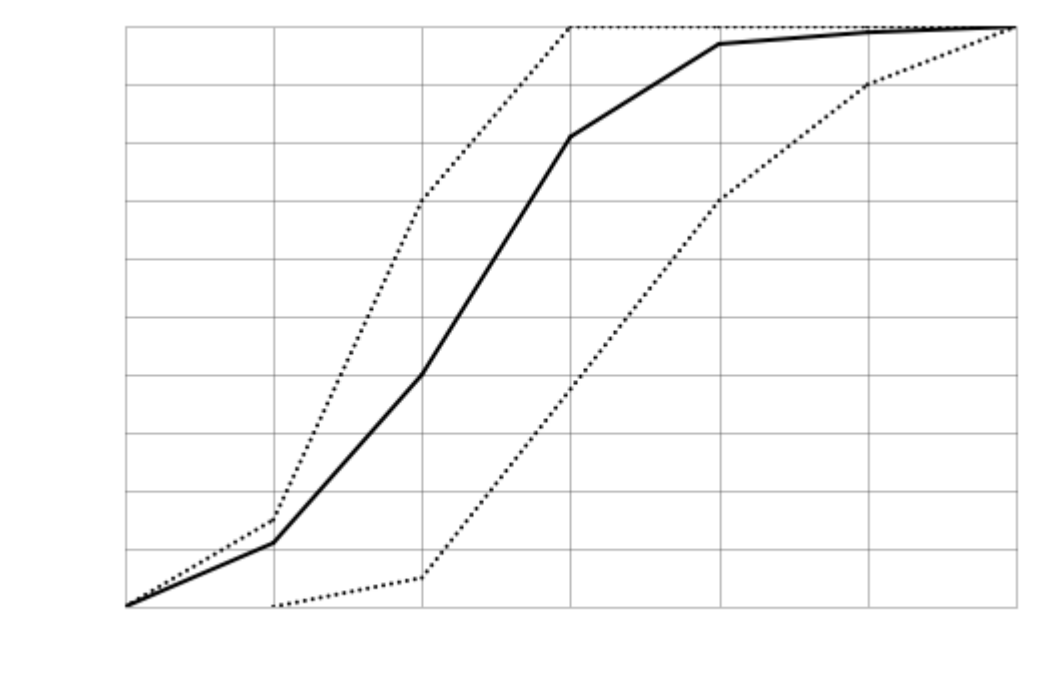
Figure 3.3 Sieve analysis of sand

3.2.3 Cement

High strength Portland cement is used to construct all masonry wall panels. The cement is based on BS EN 197-1 (2011). It is supplied by Hanson Heidelberg Cement Group, packed in bags of 25Kg.

3.2.4 Lime

Lime is used in this research because it improves the plasticity and workability of mortar, while providing a high degree of cohesiveness. Furthermore, lime mortars have high water retention, creating an improved bond as there is more contact between the unit and the mortar. In this research, the white hydrated building lime was used in the construction of masonry walls, which is based on BS EN 459-1 (2015).

3.2.5 Water

Clean tap water is used throughout the research work.

3.2.6 Mortar

Mortar is used as a means of sticking or bonding bricks together and to take up all irregularities in the bricks. Although mortars form only a small proportion of a masonry wall as a whole, its characteristics have a large influence on the quality of the brickwork and mechanical behaviour of masonry walls. To do this the mortar must be workable so that all joints are filled completely. The stiffness and plasticity are two things of importance for the workability (Wijanto 2007). The mortar stiffness depends on the quantity of water added to the mortar mix. The ratio of water to be added to the mortar depends on the application of the mortar, and does not indicate anything about its quality but it is a characteristic of the condition. Therefore, the workability of the mortar should be assessed before it being used in the construction.

The tests on masonry mortar in this research were based on BS EN 1015-11 (1999). There were two different types of mortar used in the experiments, Type S and Type N. Type S has mix proportions of Portland cement: lime: sand by volume equal to 1:1/2:4½. The mix proportions of mortar by mass can be estimated from the bulk density of each constituent. The mix proportions by mass is 6.8:1.3:35.5 for cement, lime, and sand respectively. For Type N mix proportions are changed to 1:1:6 by volume, and 6.3:2.5:42.6 by mass.

The mortar is mixed by machine to ensure a thorough mixing mortar. The cement, lime and sand are mixed dry first to ensure a uniform mix. Then the water will be added to the mixture and mixed thoroughly by machine until the mortar is easily workable. Before the mortar is used in construction, the

consistency required should be determined in advance. The consistency of the mortar is determined by the dropping ball test and the water/cement ratio would be adjusted according to the penetration result. The dropping ball test is based on BS 4551-1 (1998). The test involves dropping a plastic ball of 10mm diameter from a distance of 300mm onto the surface of the mortar and measuring its penetration. The consistency shall be adjusted to a penetration of (10±0.5mm). The ball dropping apparatus together with a device for measuring the penetration are shown in Figure 3.4.

Figure 3.4 Dropping ball apparatus

For Type S mortar, the compressive strength, for cubes of 100mm dimension cured in a fog room with 99% RH and 21 C^o was 12.7MPa (±1.2MPa) under the curing age of 14 days. The same cube compressive strength, for similar curing conditions to Type S, is found to be 6.7MPa (±0.4MPa) under the curing age of 14 days. However, there is an exception that the mortar cubes have been cured for 42 days for one certain test, which have an average compressive strength of 8.2MPa (±0.3MPa). In terms of elastic modulus, the approach to obtain is the same with the one applied on bricks, by using strain gauges to measure the strain difference under compression. The modulus of mortar is from the test results.

3. 3 Tests description

In this research, two different types of specimens have been tested: single-leaf and double-leaf (collar-jointed) masonry walls. Collar jointed masonry walls include the pre-damaged and post-damaged type. Based on the British Standard BS 5628-1 (2005), the collar jointed wall is defined as two parallel single-leaf walls, with a space between not exceeding 25mm, filled solidly with mortar and so tied together as to result in common action under external load.

3.3.1 Single-leaf wall panels

First of all, tests on single-leaf walls have been carried out. The test rig of the single-leaf wall is demonstrated in Figure 3.5. The in-plane dimensions of each built panel were 975mm×900mm×102.5mm (thirteen courses high and four bricks wide). All the bricks were constructed in stretcher bond type and tied together with 10mm thick mortar joint. Furthermore, the holes in the brick were filled with mortar during the construction process of the wall. The holes were filled straight away after each layer being completed so that the holes can be taken as nearly fully filled. All construction work was completed by an experienced mason in order to obtain uniformity.

Panels rested on a steel base-plate, which was constrained by the steel portal. The wall was also restricted on the top-left corner by external –in-plane quasi static loading. To avoid localised crushing of the masonry at the point of application of the loads, a steel plate was placed on the top-left corner of the wall to distribute and reduce stresses. The steel plates were spanned in a vertical direction over the top three courses and one brick length horizontally. There was a wide gap (10mm for the first two walls and then 20mm for the rest) between the unloaded side of the panel and the portal frame column in order to provide clearance for displacements. For the

first three courses, starting from the base, this gap was filled with mortar to restrict any horizontal movement of the wall. The mortar filled in the gap was the same with the mortar used as bed and head joints. Sixteen demountable mechanical strain gauges (DEMEC) points were mounted on the wall to measure strains during testing. This instrument consists of a digital indicator attached to an invar bar with hardened steel cones attached to one fixed and one movable end. Stainless steel measurement discs with a blind drilled circular hole were attached to the specimen surface with a suitable adhesive. The distance between every adjacent two DEMEC gauge points was 200mm. The DEMEC gauge measurement tools are shown in Figure 3.6. Each increment on the digital indicator represents 3.9 micro-strains. Furthermore, a LVDT was set to measure the wall top horizontal deflection. Figures 3.7 and 3.8 represent the real test rig of the single-leaf wall panel carried out in the laboratory.
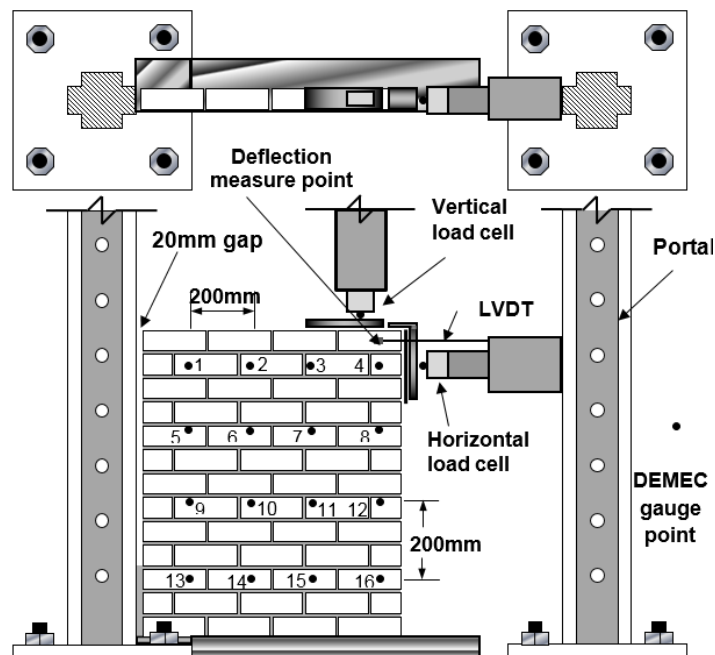
Figure 3.5 Testing rig of single-leaf panel

Figure 3.6 DEMEC gauge measurement

Figure 3.7 Test rig of single-leaf wall on the front side
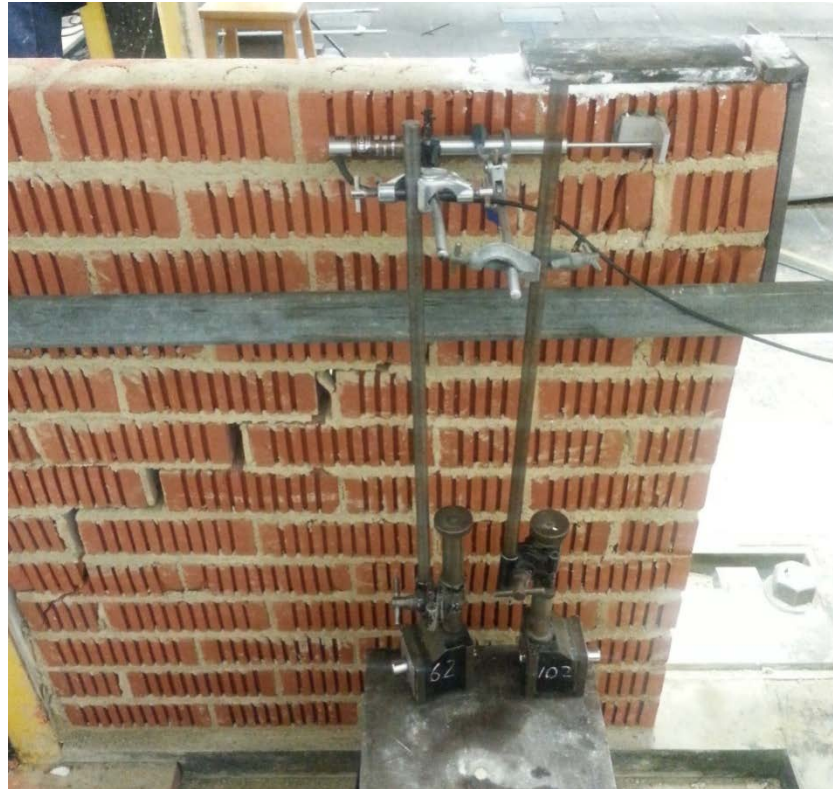
Figure 3.8 Test rig of single-leaf wall on the back side

3.3.2 Double-leaf wall panels

After the tests on single-leaf walls, a second series of tests were subsequently carried out for all double-leaf walls on an updated apparatus based on the single-leaf wall panel, which are shown in Figure 3.9. The second leaf was built parallel to the existing one and got 'tied' to it using a 10mm thick collar joint. The mortar used in the collar joint was exactly the same as the mortar used in the other tests. Mortar was successively filled up to the bricks' top and the collar joint after constructing each new layer of bricks. Therefore, it could be simply assumed that the holes in the bricks and collar joint between the two walls were filled with mortar fully. As the brick has many slots on the back side (shown in Figure 3.8) and the surface is relatively rough, therefore, the mortar was filled directly into the vertical collar joint without doing any surface treatment in advance. The new panel (second leaf) was not restricted in any way by the portal frame, which meant that it could move freely throughout its length along its in-plane axis. The

63

load was only applied to the initial panel which was restrained by the portal frame, and the loading setup was exactly the same with the single-leaf wall. Thus, there was no direct loading applied to the second wall; the only load sustained was transferred by shear from the initial panel via collar joint between the two walls.

In this research, steel ties have not been used. The main purpose of the steel tie is to link the different leaves and to promote a more monolithic structural element, therefore, to prevent the out-of-plane instability of the leaves. The main purpose of this research is to investigate the shear performance of the collar joint wall under lateral load, thus only the collar joint is considered in the experiments. The steel tie may have some influence on the mechanical performance of collar jointed masonry wall, for instance, preventing the two leaves from separating from each other. Therefore,. in order to exclude the influence of the steel tie, the collar joint without steel ties is conducted in this research. After knowing the behaviour of the collar joint, then the steels could be included in the further research in order to obtain the combined behaviour of the collar joint and steel tie.
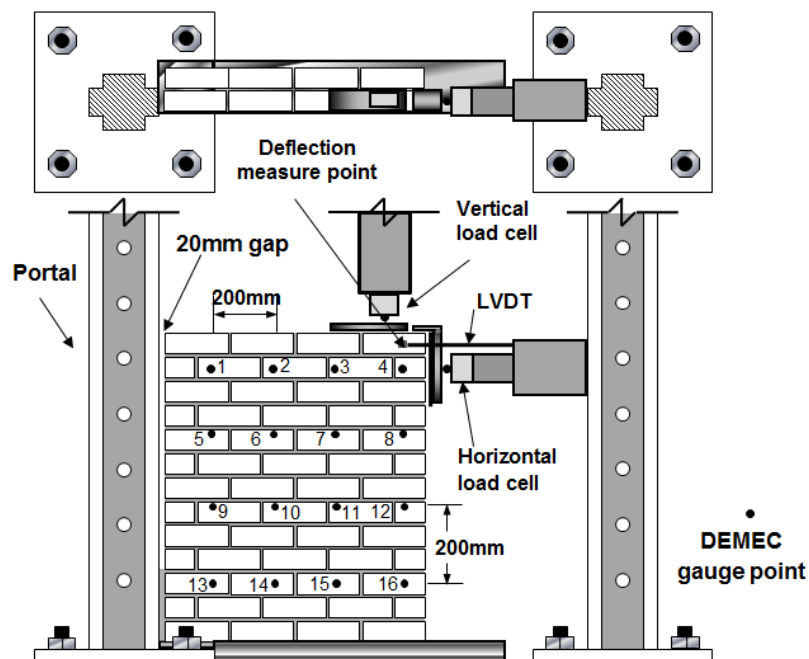
Figure 3.9 Testing rig of double-leaf panel

For the double-leaf walls, there was a further division into two categories relevant to their damage stage. These will be quoted as pre-damaged and post-damaged type.

For the pre-damaged case, the second-leaf was attached to the first leaf before the first leaf was tested. In detail, the two leaves were built at the same time with the same material and connected by a 10mm thick collar joint. After that, the newly formed wall (double-leaf) could be assumed to work as a whole panel as the mortar joint can provide a good bond connection between the two leaves. The collar-jointed wall panel was tested under the apparatus after curing for 14 days under polythene. For the post-damaged type, the second leaf was attached to the first leaf only after the latter had nominally failed making it essentially a means of retrofitting. In detail, the first leaf was built by the mason first and then tested after it had cured for certain number of days. However, the test was interrupted when initial fine cracks (no big cracks) appeared along the mortar joints. This case represents the small crack occurred on masonry walls because of unexpected external loadings, foundation settlement, temperature changes and moisture content changes etc happened. Therefore, in this case, it is unlikely or unnecessary to replace the cracked masonry wall as the cracks are too small. However, it is practicable to apply the post-damaged retrofitting method proposed in this research. By using this method, the wall could restore its initial strength without destructing the structure. Based on the single-leaf wall panels' tests that have been done previously, it could be observed that the wall had nearly failed in this circumstance. Subsequently it did not get any crack repair as the cracks were too small to fix, but got retrofitted by "attaching" a second wall to it using the previously discussed collar joint technique, thus becoming a post-damaged double-leaf wall. The test rig of the double-leaf wall carried out in the laboratory is shown in Figures 3.10 and 3.11.

Figure 3.10 Test rig of double-leaf wall on the front side

Figure 3.11 Test rig of double-leaf wall on the back side

3. 4   Curing

In all cases, masonry wall panels were cured for 14 days under polythene before being loaded with one exception. Wall 6 (a single-leaf wall) was cured

for an extended period of 42 days before being tested in order to have some indication of the curing impact. Eight mortar cubes had been cast every time during the construction in order to control the mortar strength. All the cubes were cured in the steaming room for the same period with the masonry wall. A summary of the test configurations indicating the adopted tests' naming conventions for any later reference is provided in Table 3.1.

Figure 3.12 Summary of tests specimens

Wall name	Wall type	Mortar type	Cured days	Pre/Post-damaged
W1	Single-leaf	S	14	
W2	Single-leaf	S	14	
W3	Single-leaf	N	14	
W4	Double-leaf	N	14	Pre-damaged
W5	Double-leaf	N	14	Pre-damaged
W6	Single-leaf	N	42	
W7	Double-leaf	N	14	Post-damaged

3. 5   Load design and history

The horizontal/lateral force was applied to the restricted panel by a horizontal actuator. The lateral load was applied on the free side of the masonry wall (the other side was restricted by steel portal frame), as it is displayed in Figures 3.5 and 3.9. Among others, the scope of the test rig was to potentially simulate the RC frame restraint as experienced by a real infill wall. Therefore, a vertical load cell was also used to suppress the vertical uplift of the restrained leaf, mimicking the interaction with an RC frame, which is shown in Figure 3.12. Here in this research, the quasi-static in-plane load is applied, which means the loading was added laterally to the masonry wall with a slow rate and the deflection was recorded at the same time. The nonlinear static (pushover) analysis is the often used procedure

for evaluation of the seismic response of the buildings, and it could approximately model its mechanical behaviour.
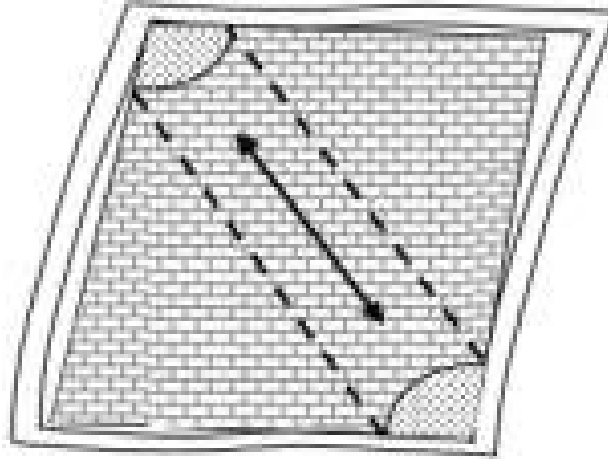
Figure 3.13 Typical deformed shape of RC frame infilled with masonry wall

To avoid localised crushing of the masonry at the point of application of the loads, steel plates were used to distribute and reduce stresses, which was shown in Figure 3.5 and 3.9. The vertical load was set up to 20kN from the start to represent the vertical load coming from the above beam, and then increased slowly with the increase of horizontal/lateral load.

What happened unexpectedly to Wall 1 and Wall 2 is that the test stopped before failure. As described that the gap between Wall 1 and the frame is not big enough for the total deflection. Therefore, Wall 1 failed during the test but it did not totally collapse. Wall 2, has been tested twice. In the first test, the vertical load was kept constant at 20kN. However, the wall was lifted up during the test. Therefore, for the second test, the vertical direction was restrained so that the vertical load increased gradually. The horizontal load was increased at a rate of 2kN/min. However, the test was paused at every 5kN increment. In order to minimize the time relaxation effects, the measure of the DEMEC gauge points was carried out as soon as possible. In the future research, automatic data recording method should be applied..

Once the walls failed, the lateral force-deflection and the relevant failure patterns were recorded.

3. 6 Summary

Masonry is a composite material and masonry structure is difficult to analyse due to its complexity, especially for the collar jointed (double-leaf) masonry wall panels. In this research, unreinforced masonry wall panel is strengthened/retrofitted using collar jointed technique to form a collar jointed masonry wall. In order to obtain a general overview and basic understanding on the mechanical performance on both strengthened and unstrengthened masonry wall panels, a detailed description of the experimental test rigs on masonry wall panels, including four specimens on single-leaf and three specimens on double-leaf, has been presented in this chapter. The experimental results will be analysed and demonstrated in detail in Chapter 4.

Chapter 4   Experimental results

The masonry wall specimens have been tested in Chapter 3 and the results will be discussed and presented here in this chapter.

4. 1   Failure patterns; an initial qualitative assessment

This section describes the failure patterns of the single- and double-leaf (collar jointed) masonry wall panels.

4.1.1   Single-leaf wall panels

The failure patterns of single-leaf Wall 1, 2, 3, and 6 are shown in Figures 4.1, 4.2, 4.3 and 4.4, respectively, which will be explained in detail as following.

Figure 4.1 Failure pattern of single-leaf Wall 1

According to the failure patterns illustrated in Figures 4.1 and 4.3, the failure mode of a single-leaf masonry wall panel is described by a major diagonal crack (except Wall 2, which will be discussed in the next paragraph). Based on the experimental results observed on Wall 1, before this diagonal crack was being developed, some small, hairline (shear) cracks appeared along the bed joint length when the lateral load reached around 30kN. Further, with the increase of the horizontal load, the top-corner of the wall (indicated as area 1 in Figure 4.1 and Figure 4.3) began to rotate. However, the rotation was restrained by the vertical actuator placed on the left-top corner of the wall. Therefore the stress around the corner kept accumulating, until it surpassed the strength of the masonry wall. When the lateral in-plane resistance reached approximately 50kN, the corner was crushed around area 1 and cracks started propagating from that region down through the wall body. Stresses kept increasing with the applied load as long as the rotation is restrained until it reached the wall's failure load, 58kN.

The failure process of Wall 3 is very similar with Wall 1. The small cracks showed up around 35kN. The cracks kept expanding until the load reached 62kN, then the big diagonal crack formed. However, the wall still kept carrying more load until the lateral load reached about 70kN. Once the external load exceeded the strength of the masonry, the failure occurred in the form of the earlier quoted diagonal crack spanning widely from area 1 to area 3, following a staircase path along the mortar interface.

In conclusion, these failure patterns demonstrated in Figures 4.1 and 4.3 have also been found and described in the work of Lourenco and Rots (1997) in terms of local failures and in the work of Campbell Barrza (2012) in terms of global failures which were demonstrated in Chapter 2. In Lourenco and Rots' work, the cracking of unit in direct tension and masonry crushing can be found in area 1 in both Figures 4.1 and 4.3. The joint tensile cracking and unit diagonal tension crack can be found in area 2 in Figure 4.3. In terms of global failures, the shear failure and bending failure described in Campbell Barrza's work can be found in area 2 and 3 in both figures, respectively. This

71

typical mechanical behaviour of a masonry wall under lateral load can also be seen in the work of Vermeltfoort and Raijmakers (1993). This is because the mortar is usually weaker compared with the brick in masonry walls and it is the place where the cracks most likely occurred.

However, at some point, the cracks may pass through bricks as well as shown in area 3 in Figure 4.3. This is because that the mortar was in a state of approximate tri-axial compression, while the brick is subjected to compression combined with bi-axial tension. The expansion of mortar under compression was confined by bricks and therefore induced an approximate state of tri-axial stress in mortar. The mortar could carry much higher compression due to internal confining stresses. However, the expansion of mortar could cause tension among bricks in reverse. If this tension exceeded the tensile strength of the brick, cracks occurred. The point at the top of the edge gap-filling mortar in area 3 is clearly a point of rotation and as expected no local crushing of the masonry was observed below this region. After the big diagonal crack appeared, the wall could carry no more lateral load and failed soon after.

For Wall 2, which is shown in Figure 4.2, there are no obvious cracks occurring in the whole panel. The reason is that Wall 2 had been tested twice. For the first test, the vertical load was kept constant at 20kN. However, as the rotation was not restrained (the vertical actuator was adjusted to free the extra vertical load resulted from rotation), the wall was lifted up from the base in the middle of the test. In this case, the wall failed by detaching from the steel base while the whole masonry wall body was nearly intact during the test. Then the wall was tested again with rotation restrained like Wall 1. However, during this time the wall touched the frame before any obvious cracks appeared. In this case, this experiment acted like a control test to prove that the failure of a masonry panel are relevant with the boundary conditions.
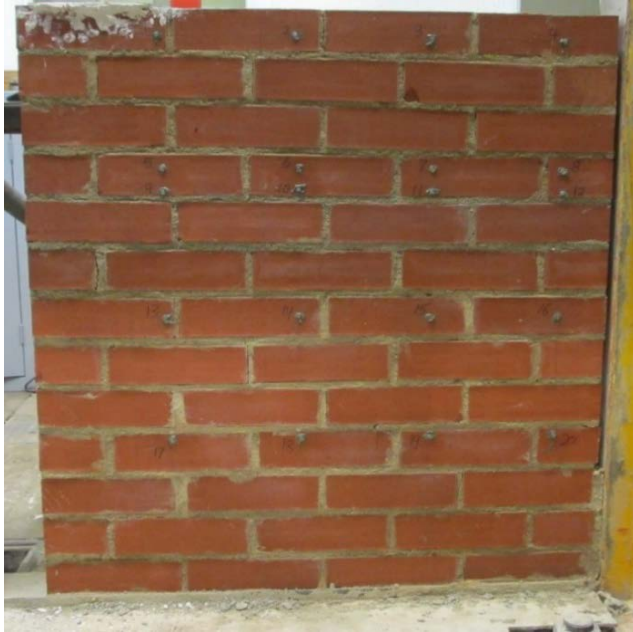
Figure 4.2 Failure pattern of single-leaf Wall 2
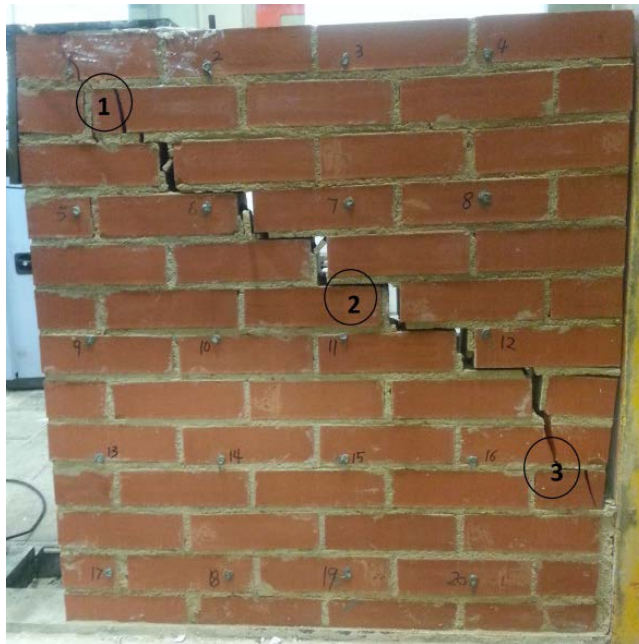
Figure 4.3 Failure pattern of single-leaf Wall 3

For Wall 6, which is still a single-leaf wall. However, as it was explained in the experiments section in Chapter 3, this wall was not totally failed and there were no apparent cracks occurring in the wall, only some small and hair-line cracks appeared along the mortar joints when the lateral load

reached around 45kN. The number of cracks kept increasing unit the test was stopped on purpose. This is because at this stage, the lateral load reached about 70kN and the cracks were visible and the crack sound could be heard clearly. Based on the findings from previous experiments the wall was very close to failure. These cracks are highlighted with black line for clarity, which is shown in Figure 4.4. However, compared with previous researches and the totally failed experimental walls, the crack patterns were very alike. It could be assumed that Wall 6 is nearly at the failure point and the failure pattern would be represented by diagonal crack if it failed totally. This wall will be strengthened and tested as a post-damaged approach. The result of it is shown in section 4.1.2 in this chapter.

Figure 4.4 Failure pattern of single-leaf Wall 6

4.1.2 Double-leaf walls

The double-leaf walls consists of two types of masonry walls (as previously defined) pre-damaged and post-damaged walls. As these two types were built in different approaches, they will be presented separately as following.

4.1.2.1 Pre-damaged test

Figures 4.5 and 4.6 represent the failure patterns of Wall 4, while Figures 4.7 and 4.8 represent Wall 5. As displayed in Figures 4.5 and 4.7, it is clear that the failure pattern is represented by diagonal cracking in pre-damaged walls, similar to the single-leaf wall cases.

However, at this instance, masonry walls had more cracks than their single-leaf counterparts prior to the formation of the decisive diagonal crack that signified the ultimate failure, this is a sign that for the double-leaf walls, ductility (i.e. extent of plastic deformation) had improved through the presence of a second leaf. In terms of the failure process, there were three notable features of behaviour of this type of masonry wall, namely: i) initial flexural cracking in the bed joints of the wall; followed by, ii) propagation of stepped shear cracks, with increasing load leading to, iii) complete collapse.

In detail, some hairline cracks appeared along the bed joints on both leaves, first when the lateral load reached around 42kN, similar with single-leaf wall. With the increase of lateral load, the wall started to rotate. However, this rotation was restrained by the vertical actuator. The stress among mortars started to accumulate. The cracks kept increasing and propagating during this stage. When the lateral load reached about 75kN, the cracks became very obvious and crack sound could be heard. After that, the lateral load kept increasing until it reached approximately 92kN, a big and remarkable diagonal crack was formed and failure happened. From the test failure process, it was clearly seen that the two leaves worked and failed as a whole panel.

Note the cracks in the second leaf appeared later than the ones on the first leaf, which is because the load from the first leaf was spread evenly by the collar joint before it passed to the second leaf. Also, in all cases the cracks on the second leaf were less compared to these of the first one and mainly occurred along mortar joints, which are shown in Figures 4.6 and 4.8.

Therefore, it became apparent that the stress transfer between the two leaves was effective throughout the different loading stages as initially envisaged. Namely, the load was applied directly to the first wall and distributed to the second wall consistently via the collar-joint and there was less stress concentration on the second leaf.

Although the two leaves are joined and the width of the loaded area effectively equals to the double of the initial thickness, the real stress is not distributed evenly, being concentrated at the top corner of the first wall and "flowing" inhomogeneously through into the second wall. The uneven distribution of the stress between the two walls is also influenced by the boundary conditions imposed. The second leaf was not restrained by the gap-filling mortar and is therefore being less stiff, it attracted less of the load. From Figures 4.11 and 4.12, it can be seen that the two leaves are still bound together, which means the composite masonry wall works as a whole panel in general.

Figure 4.5 Failure pattern of double leaf wall W4 on the loaded leaf

Figure 4.6 Failure pattern of double-leaf wall W4 on the unloaded leaf

Figure 4.7 Failure pattern of double leaf wall W5 on the loaded leaf

Figure 4.8 Failure pattern of double-leaf wall W5 on the unloaded leaf

4.1.2.2 Post-damaged test

For the post-damaged double-leaf masonry wall panel, the failure process and failure patterns were different with the pre-damaged masonry wall. In terms of failure process, there were four notable features of behaviour namely: i) initial flexural crack; followed by ii) formation of diagonal stepped cracks from the top right hand side of the panel to the bottom left hand side with increasing load leading to iii) detachment of the collar joint from the wall; and finally iv) collapse as a result of shear failure.

In detail, the first leaf of the pre-damaged wall behaved in a similar manner to the single-leaf walls tested previously (failure was governed by a wide diagonal crack), as Figure 4.9 illustrates. This was obviously affected strongly by the preloading and incipient damage induced to the wall.

However, the second wall behaved quite differently to that seen on the first leaf as well as the previous tests. The actual failure for the second leaf was established by a horizontal shear crack, initiated by the failure of the collar joint. The collar joint actually detached itself from the first leaf wall whilst remained connected to the second wall – see Figure 4.13. Based on the deformation figures, it can be seen that the collar joint was totally connected to the second leaf. However, the collar joint was connected to the first leaf only among the bottom three-layer bricks (about 20-30% of the first leaf). This finding shows that the collar joint won't provide a perfect connection between the two leaves under exceeding load. Unfortunately, the result shows that the collar joint in post-damaged wall does not improve the whole integrity of the composite masonry wall in this case as it detaches when external load is large enough. The composite masonry wall works individually after they were separated. However, detachment of the masonry leaves is a common failure pattern of double- and multi-leaf masonry walls (Pappas 2002).

On the front side it can be seen that the diagonal cracks passed through the mortar joints and crossed some bricks. In terms of detailed failure process, the first leaf already has small cracks along the joints. These cracks didn't expand remarkably until the lateral load reached around 30kN. When the load reach about 53kN, the big diagonal crack formed and some other small cracks appeared above the main diagonal crack. The cracks kept increasing and expanding until the wall reached its failure load, 74kN.

However, in the back side, only a small sliding and stepped crack appeared at the bottom of the wall, which is shown in Figure 4.10. This crack occurred around 40kN. However, after the first leaf detached from collar joint, the crack stopped growing until the wall totally failed. The localization of this sliding and stepped crack must intuitively follow a weakest link path through the mortar joints.

Figure 4.9 Failure pattern of double-leaf wall W7 on the front side

Figure 4.10 Failure pattern of double-leaf wall W7 on the back side

4.1.3 The failure pattern of collar joint

The failure patterns of the collar joints on the pre-damaged and post-damaged masonry wall panels are presented in Figures 4.11, 4.12 and 4.13.

4.1.3.1 Pre-damaged test

It can be seen in both Figures 4.11 and 4.12 that, the collar joint between two leaves hardly separated, only a small part cracked in the loaded corner in Figure 4.12. This is because the two leaves were constructed in the same time, and the two leaves were cured in the same condition and within the same curing age. This could help to improve the bond between the two leaves as the cement particles in the mortar joints could penetrate into each other during the curing process.

In the pre-damaged test, the panels failed with a diagonal crack on both leaves. The same failure pattern on both leaves means that the collar joint helped the two leaves work together as a whole panel.

Figure 4.11 Failure pattern of the collar joint on top side of W4

Figure 4.12 Failure pattern of the collar joint on top side of W5

4.1.3.2 Post-damaged test

Based on Figure 4.13, it can be seen that the collar joint actually detached itself from the first leaf wall (loaded one) whilst remained connected to the second leaf wall. This failure pattern is totally different with the one in the pre-damaged test. This is because the two leaves were built in different times and cured with a different curing age.

The mortar in the first leaf had been cured for 6 weeks and the mortar had almost reached its ultimate strength. Though the cement particles could get into the bricks in both leaves, it is very hard for the cement particles in the collar joint to penetrate into the already cured mortar joints in the first leaf. However, for the second leaf, the cement particles can easily penetrate into the mortar joints during the curing process, thereby resulting a stronger bond between the collar joint and second leaf compared with the bond between the collar joint and first leaf. Therefore, as it can be seen in the figure, the collar joint separated from the first leaf while remained connected with the second leaf.

Figure 4.13 Failure pattern of the collar joint on top side of W7

4.1.4 Discussion

In the single leaf wall tests, the failure patterns found are in an agreement with the findings in the literature review. For the current test series, the occurrence of the diagonal crack signified the end of each test. However, in practice it is common that a masonry panel loaded in-plane within a frame will become locked in and continue performing a structural role, even after the diagonal crack is formed. The most notable aspect of such a role is the potential for additional energy dissipation (Mehrabi et al. 1996) allowed within the restrained sliding of the damaged interfaces. These tests do not consider any load cycling or dynamic effect that is critical for assessing holistically the masonry performance. However they still constitute an insightful first attempt to explain and comprehend the up to failure performance of the masonry wall.

The failure patterns of the collar jointed masonry walls studied in this research differs with the literature review. The reason is due to the loading

patterns and boundary conditions as they can lead to totally different failure patterns. In the work of Vintzileou (2007), the multi-leaf masonry wall was loaded vertically, which leaded to the detachment of the internal and external leaves, global or local crushing of external and internal leaves and the external leaves out-of-plane failure. In this research, the experimental tests on collar jointed walls were carried out under combined in-plane loading. The failure pattern in the pre-damaged masonry wall is represented by diagonal shear crack while for the post-damaged masonry wall, the failure pattern is represented by diagonal crack as well as separation in the collar joint. The failure patterns of the two types of masonry walls (pre-damaged and post-damaged) were different even under the same loading, which indicated that collar joint is an important influence factor in the failure pattern of collar jointed masonry wall. Therefore, the collar joint type should be considered in investigating the performance of collar jointed masonry wall.

It should also be noted that the type of brick used in this research is a special brick (ribbed), which has some influence on the connection between collar joint and brick leaf. As the ribs can prevent the collar joint from moving along its in-plane direction, thus improving the bond of the collar joint to some degree. However, for other types of brick (for instance, smooth texture brick), the connection between the collar joint and the brick leave will not be as strong as the ribbed brick has. The interaction between the ribbed brick and mortar joint as well as the smooth brick and mortar joint is demonstrated in detail in Figure 4.14. From the figure, it can be known that only friction and shear force existed between the smooth brick and mortar joint. However, there is compressive force existed between ribbed bricks and mortar joint besides the friction and shear force. It is widely known that the compressive strength of mortar joint is much stronger than its shear and tensile strength. Thus the collar joint between the ribbed bricks is able to provide a better connection. Therefore, the failure patterns of both brick leaf and collar joint will be different if different types of masonry unit and collar joint are used. Furthermore, by combining the experimental results and the literature review (mainly from the work of Binda et al. 2006, see Figure 2.19), the failure

pattern of double-leaf (collar jointed) masonry wall can be summarized in Table 4.1.

(a) Smooth brick   (b) Ribbed brick
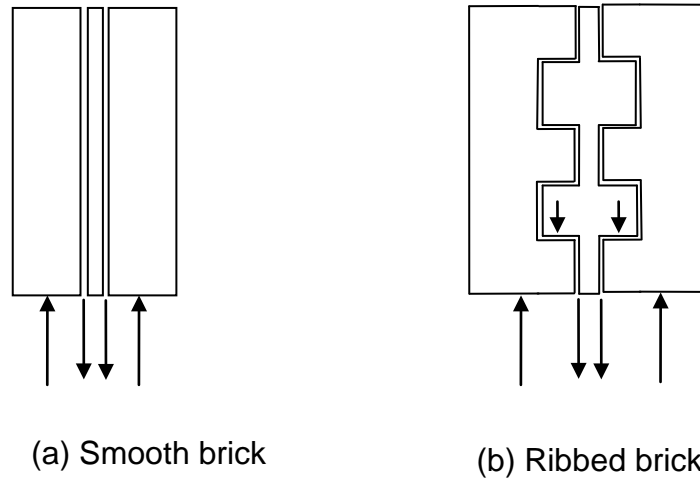
Figure 4.14 Interaction between bricks and mortar joint: (a) Smooth brick; (b) Ribbed brick

Figure 4.15 Failure pattern of collar jointed (double-leaf) masonry wall

	This research		Previous research	
	Pre-damaged	Post-damaged	Straight collar joint	Keyed collar joint
Failure pattern	Mainly diagonal cracks and some shear cracks on both leaves	Mainly diagonal cracks and shear cracks on first leaf, only shear cracks and sliding on second leaf, separation of the collar joint	Spalling of the outer leaves and separation of collar joint (nearly undamaged)	Spalling of the outer leaves as well as the keyed collar joint
Loading pattern				

4. 2 Failure load and deflection

All the tests results have been recorded during the tests and analysed at a later stage. In this section, the lateral load and displacement of both single-leaf and double-leaf wall panels will be discussed and compared. The ultimate failure loads along with critical deflection parameters for all tests are summarised in Table 4.1:

Figure 4.16 Failure load and deflection of all tests

Wall No.	Wall type	Lateral load (kN)	Displacement at yield point (mm)	Maximum displacement (mm)	Mortar compressive strength (MPa)
W1	Single-leaf	58	9.7	13.1	12.7
W2	Single-leaf	64	10.1	11.2	15.3
W3	Single-leaf	70	8.2	20.0	6.7
W4	Double-leaf	91	10.1	11.4	6.3
W5	Double-leaf	93	10.3	12.6	6.6
W6	Single-leaf	75	9.03	9.03	8.1
W7	Double-leaf	77	8.8	17.6	7.1

4.2.1 Comparison of single-leaf walls

The horizontal load-deflection relationship for the ensemble of the single-leaf walls is shown in Figure 4.15. It can be clearly seen that the curves are almost linear before the maximum load. This agrees with the works of Kanyeto (2006) and Campbell Barraza (2012) that masonry structures under small load behave linearly. The stiffness of Wall 1 is very similar to, although slightly below that of Wall 2. More importantly some extensive capability for plastic deformation is observed in Wall 1, while this was not the case for Wall 2. As a matter of fact Wall 1 could deform even more as its full plastic range was not pursued as the limitation of the apparatus clearance was

reached (this was increased thereafter). Such experimental deviations are expected in similar masonry constructions, as the results may vary a lot even exactly the same materials are used, though the deviation is always attributed to a substantial material difference. When referring to the different mortar type of Wall 3 all the strength and deformation variables were increased consistently and significantly. The post-peak stage of Wall 3 implies that the masonry wall is plastic and not as brittle as concluded in the literature review. However, this remained in doubt as the tests were not sufficient to rule out all contingencies. One of the reasons which might cause this is the sudden failure of masonry wall. This sudden failure might cause the wall to deflect remarkably.
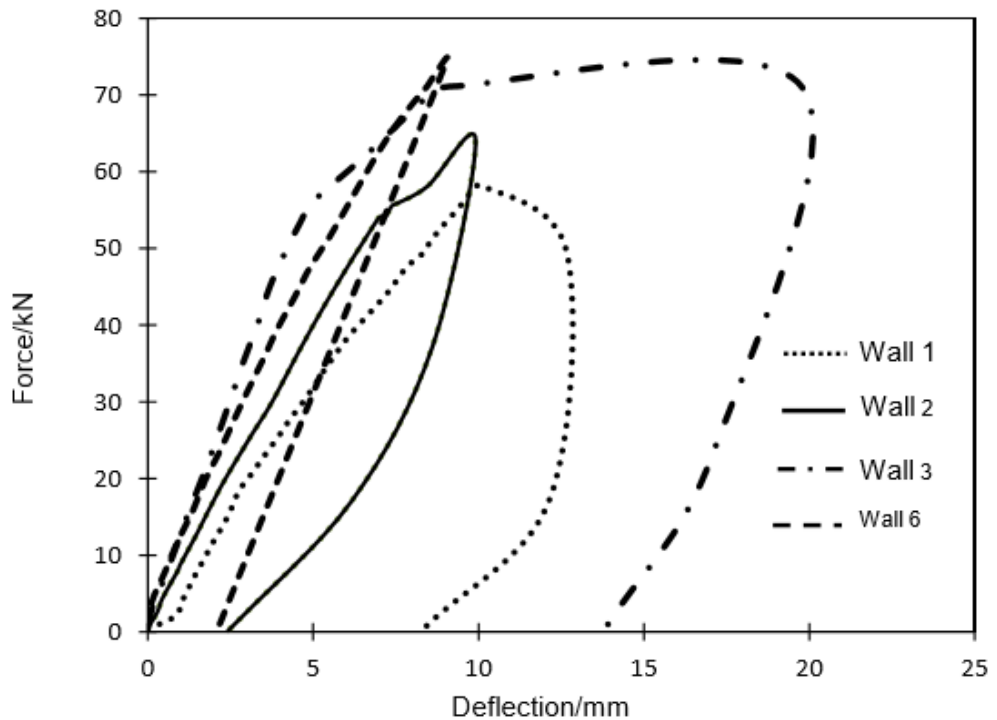
Figure 4.17 Load-Deflection relationship of single-leaf walls

The testing of Wall 6 was stopped when it had nominally been assumed to have yielded. This state was taken at the point when initial 'fine' cracking appeared and the horizontal load-deflection relation started deviating increasingly from the elastic region. At that point Wall 6 was unloaded and its damaged stage was considered the benchmark for the later post-damage retrofitting study.

It can be seen in the above figure that there was no post-peak behaviour captured for Wall 6.The stiffness of Wall 6 was evidently greater than that of Wall 1 and 2. Although this can be attributed to the increased curing time when compared to Wall 1 and 2, Wall 6 was cured for 42 days instead of 14 days. This increased stiffness which was also apparent in the case of Wall 3 seems mainly a product of the different mortar type. Interestingly, the Wall 6 stiffness is lower than that of Wall 3 and further imposing the small effect of additional curing time beyond a certain limit. For the combined influence of mortar type and curing age, it requires further experimental investigation.

4.2.2 Comparison of double-leaf walls

Figure 4.16 illustrates the horizontal load-deflection behaviour for all the collar-jointed masonry walls. As probably expected for these walls, Wall 4 and 5 (pre-damaged method) exhibited a much higher failure load (91 and 93kN, respectively) than any of the single leaf walls, which failed at loads ranging between 58kN to 70kN.

In this figure, Wall 4 and 5 have similar failure loads yet their ultimate deflection capability looks different at first look. This is an artificial output with the measurement of Wall 5 encompassing a slip without which the displacement behaviour becomes quite alike with any difference falling within the acceptable experimental deviation bands. Interestingly, Wall 7 (the post-damaged wall), although only achieving a failure load more in-line with the single-leaf walls (around 75kN) going approximately halfway through the capability of pre-damaged method, exhibits sustained ductility with much more gradual strain-softening. The improved stiffness of Wall 7 in comparison to Wall 4 and 5 is probably an unexpected surprise. It has been cured for longer and the reduced damage seems to not have compromised the stiffness but noting the small effect of the curing time previously evidenced this output looks slightly strange. Compared with Wall 4 and 5,

Wall 7 have a bigger ductility as the lateral load dropped gradually for quite a long time after the peak stage.
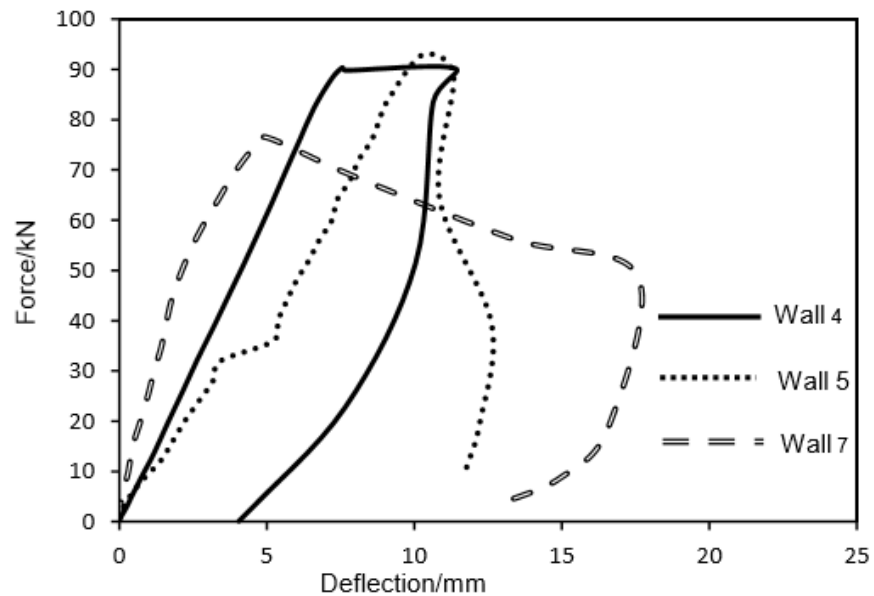
Figure 4.18 Load-Deflection relationship the of double-leaf walls

4.2.3 Comparison of pre-damaged approach

Figure 4.17 illustrates the improvement of pre-damaged earthquake strengthening in terms of the load-deflection relationship. The construction process has been described in Chapter 3 (experimental work). As it was explained in the above paragraph there was a slip on the displacement measurement of Wall 5, therefore, only the lateral force and deformation of Wall 4 is considered here. Compared with Wall 1 and 2, Wall 4 (double-leaf wall) increased the failure load approximately about 60% and stiffness around 50%, which is a remarkable result in terms of brittle material.

However, when it is compared with Wall 3, Wall 4 can only increase the failure load about 40%. Furthermore, it didn't increase the stiffness as it can be seen that Wall 4 and Wall 3 had almost the same stiffness. This might be related to the LVDT deflection measurement of Wall 3, as the stiffness of Wall 3 is unexpectedly high. Therefore, further research should be carried

out on the stiffness of single-leaf wall panel. Overall, it still can be concluded that the pre-damaged approach helps to improve the mechanical behaviour of single-leaf masonry walls.
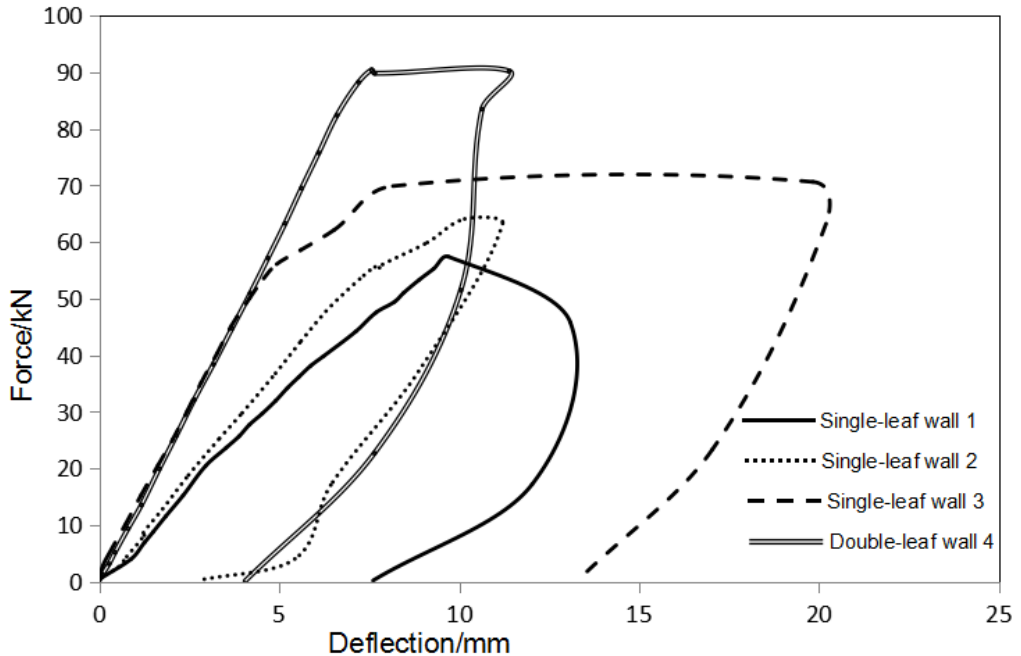
Figure 4.19 Load-Deflection relationship of pre-damage strengthening

4.2.4 Comparison of post-damaged approach

Figure 4.18 presents the load-deflection curves of Wall 6, a single-leaf masonry wall and Wall 7, a double-leaf wall repaired using the collar joint technique. The construction and test process had been described in detail in Chapter 3 (experimental work). It obviously shows that though the failure load of the repaired and strengthened double-leaf wall was not increased, the initial stiffness had been improved significantly to almost twice as the single-leaf one. As the test of Wall 6 was stopped when some initial small cracks appeared on the wall. There was no chance to know the ductility of Wall 6. However, for Wall 7, the repaired double-leaf wall, obviously had a relatively high ductility in terms of a brittle material.
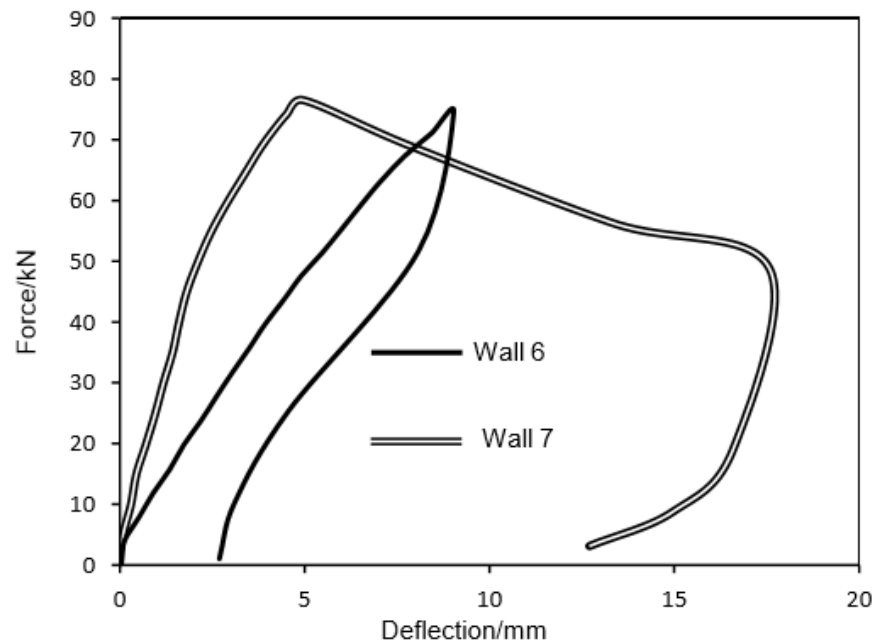
Figure 4.20 Load-Deflection relationship of post-damage strengthening

4. 3   Analysis of DEMEC gauge readings

As it had been described in the experiment's section in Chapter 3 that there are 16 DEMEC gauge points mounted on the wall and the DEMEC strain gauge is ideal for strain measurement and crack monitoring. The masonry element will shorten under compression load or elongate subjected to tension. Therefore, this change can be recorded by DEMEC gauge points. After knowing the strain change of the masonry wall, the stress distribution of the masonry wall is known as the masonry is simplified to an isotropic material in this research. Therefore, the DEMEC gauge readings could provide a helpful overview and understanding on the load transfer among single- and double-leaf masonry walls.

During the test, it was paused to measure DEMEC gauge readings at every 5kN increment. The DEMEC gauge points can only measure the strain change vertically or horizontally. In order to have a clear visual impression

about the analysed results, only some representative points are selected to be presented here, including horizontal points and vertical points. The locations of the DEMEC gauge points are illustrated again in Figure 4.19.
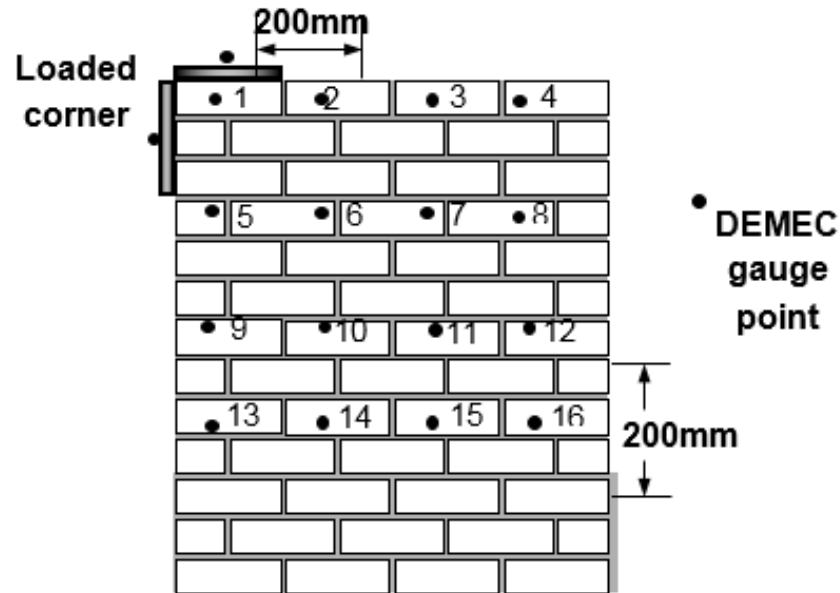
Figure 4.21 The location of DEMEC gauge points on masonry wall

4.3.1 Single-leaf masonry walls

In this section, only the DEMEC gauge reading results on Wall 3 and 6 have been analysed. The reason that Wall 1 and 2 were not analysed here is because the DEMEC gauge points were not mounted at the same locations with the rest specimens (Figures 4.1, 4.2, 4.3 and 4.4). Furthermore for Wall 2, it had been tested twice. The first loading might have already produced some cracks. Therefore, Wall 3 and Wall 6 would give a better overview on the strain change on masonry walls during the test.

4.3.1.1 Wall 3
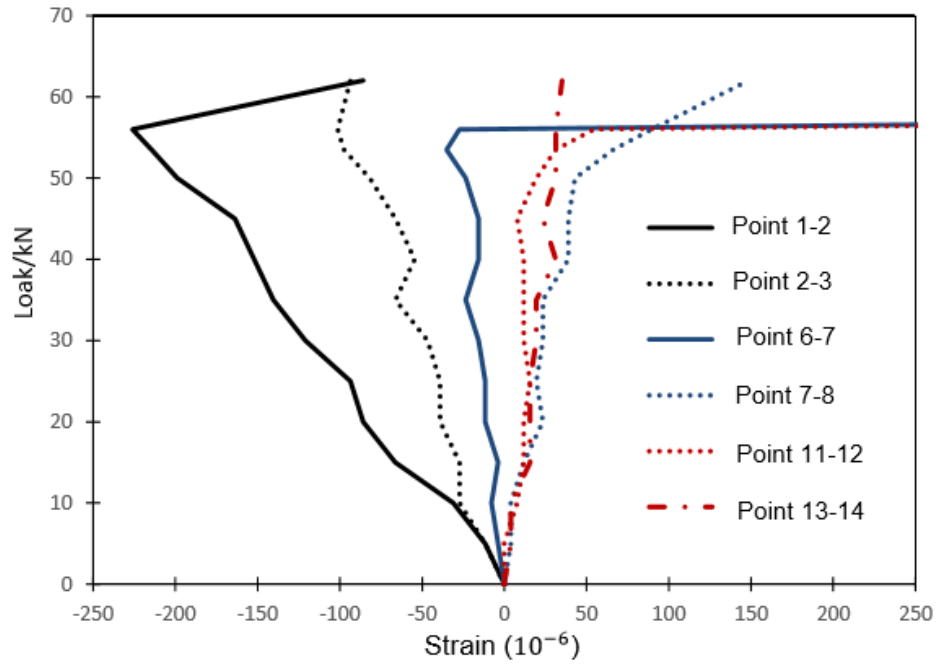
Figure 4.20Load-strain curve of horizontal DEMEC gauge points of Wall 3
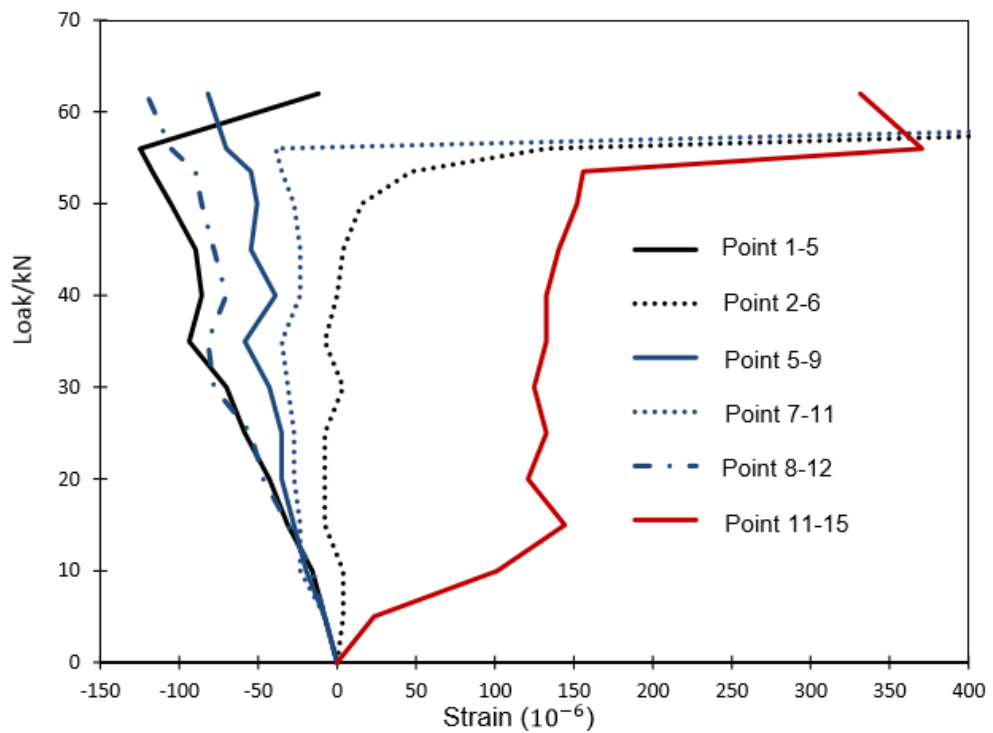
Figure 4.22Load-strain curve of vertical DEMEC gauge points of Wall 3

The load-strain relationship curves of horizontal DEMEC gauge points of Wall 3 are demonstrated in Figure 4.20. The strain value in negative represents compression while positive means tension. Point 1-2 represented the strain around the loaded corner, which was in compression until it reached around 55kN. Before this stage, the strain increased almost linearly until the final failure happened. This finding agreed with Mosalam et al. (2009) that masonry behaves in an approximately linearly elastically under low levels of stress. It could be calculated that the failure stress of point 1-2 was around 4MPa. There was a sudden strain jump at this stage, which meant a big crack occurred suddenly around the loaded corner. It was proved in Figure 4.3 that the brick was crushed near point 1.

Point 2-3 was at the same height with Point 1-2 but a little further from the loading point. It was shown that Point 2-3 was in compression but smaller compared with Point 1-2, which means the lateral in-plane load reduced gradually along the horizontal direction. For point 6-7 and10-11, they were all in compression before the big diagonal crack occurred. The compression strain was not large compared with point 1-2 due to the lateral load spreading to the whole panel. However, point 7-8, 11-12 and 13-14 were in minor tension before the failure occurred. It could be clearly seen that when the lateral load reached about 55kN, the big diagonal crack, as described in section 4.1.1, occurred. This big diagonal crack caused the strain of most points increased abruptly. It reveals that the failure of masonry element is brittle.

For the vertical points on Wall 3, as illustrated in Figure 4.21, most of the points were in compression during the test, except for point 11-15, which was in tension from the beginning. Similar with the horizontal points, when the lateral load reached about 55kN, there was a small jump of the strain because of the occurrence of diagonal crack. Point 5-9 and 8-12 did not have any crack as they were always in small compression, and Figure 4.3 did not show any obvious crack among them.

4.3.1.2 Wall 6

Figure 4.22 illustrates the load-strain curves of the horizontal DEMEC gauge points of Wall 6. For Wall 6, the strain results behaved very similar with Wall 3. It could be seen that the strains of some points were changed when the load reached around 40 to 45kN, as explained in section 4.1.1, some small cracks occurred along the mortar joints in the centre area of Wall 4. Compared with Wall 3, this increase was not abrupt. Instead it increased gradually (determined by the acceleration). Therefore, this meant the small cracks occurred, and the cracks kept expanding slowly under lateral loading. Some of these cracks were too small to be observed as the wall was failed. Furthermore, it could be seen that point 1-2 was not crushed even when the strain reached -400 micro strain (nearly 6.5MPa in stress). As it was explained that Wall 3 was crushed at a stress of 4MPa, while Wall 6 was still working without any cracking. Besides the variation of masonry wall test, the other reason was that Wall 6 was cured much longer than Wall 3, therefore having a higher failure strength.

While for the vertical points, as demonstrated in Figure 4.23, point 1-5 was still in compression as there was no failure happening around that area. Point 11-15 behaved exactly the same compared with Wall 3, that in tension first and then strain increased because of crack occurred when the lateral load reached around 45kN. As for the other points, most of them were in minor compression or minor tension, until the small cracks occurred along the joints. Still, the increase of strain at the stage when the small cracks occurred was mild and gradual.

The DEMEC gauge readings briefly revealed the failure process of single-leaf masonry wall under combined loading. Fine cracks first occurred along the mortar joints. With the accumulation of the stress in the loaded corner, brick and mortar crushing cracks may appear suddenly, which caused the fine cracks expanding abruptly, thereby causing the masonry wall fail in a brittle manner.
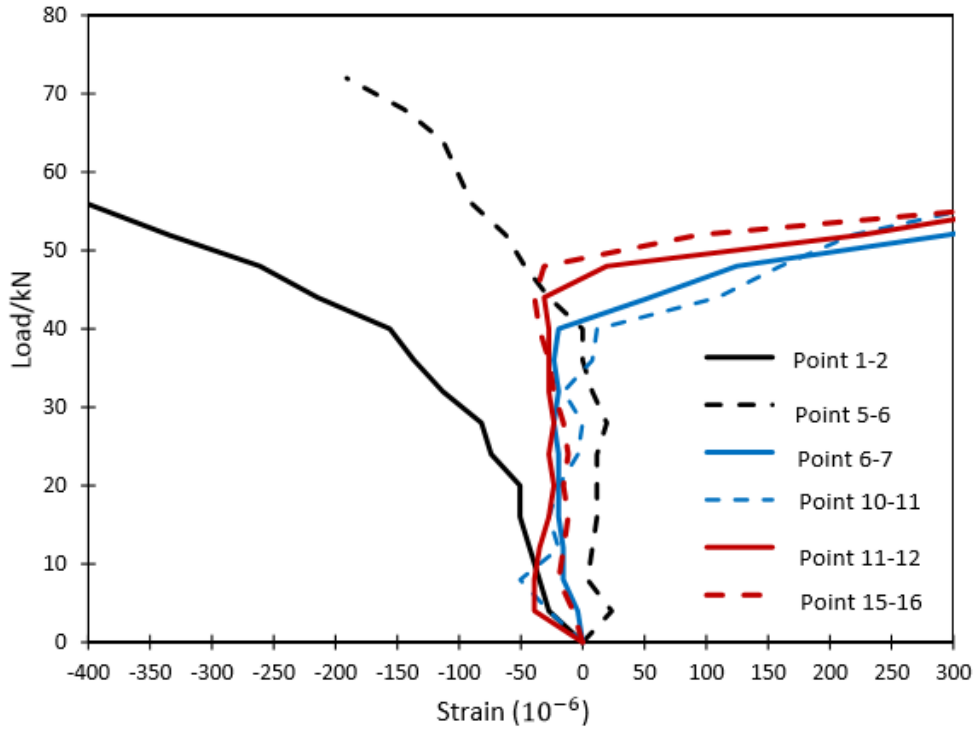
Figure 4.23 Load-strain curve of horizontal DEMEC gauge points of Wall 6
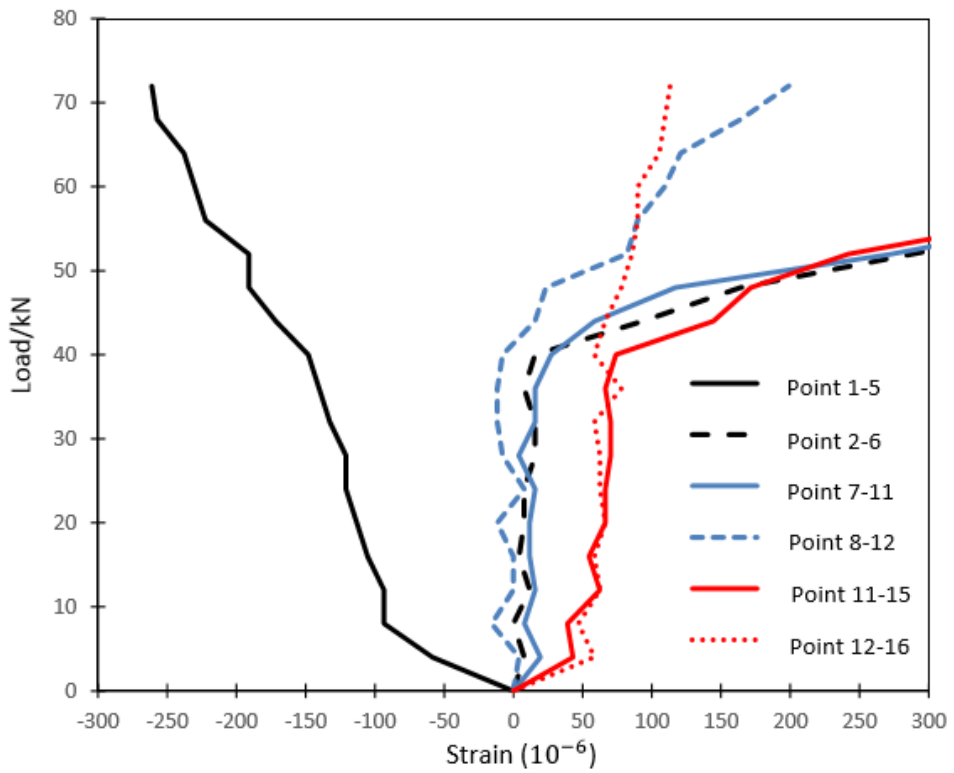
Figure 4.24 Load-strain curve of vertical DEMEC gauge points of Wall 6

4.3.2 Double-leaf walls

Similar with single-leaf walls, the strains of all points behaved very much alike in the double-leaf masonry walls. For the pre-damaged wall, Wall 5 was selected and Wall 7 for post-damaged wall. Only the first leaf in the double-leaf walls has DEMEC points. The DEMEC gauge readings were recorded during the test and analysed after the test. The following sections present a detailed description and discussion on the results.

4.3.2.1 Wall 5 (Pre-damaged)
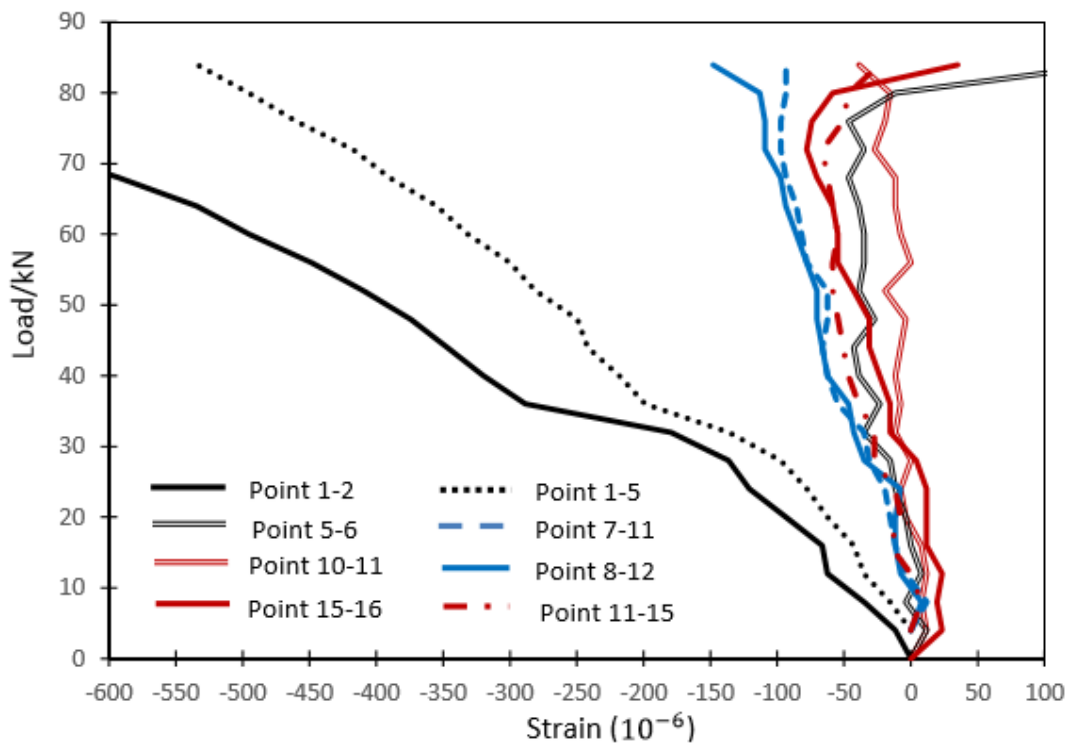
Figure 4.25 Horizontal and vertical load-strain curve of DEMEC gauge points of Double-leaf Wall 5

Figure 4.24 shows the load-strain relationships of some representative points on Wall 5. Point 1-2 and point 1-5 were always under compression with the increase of lateral load, as was the same with the single-leaf walls.

However it can be calculated that when the strain of point 1-2 was -600 micro strains, the stress was nearly 9.6MPa, much higher than both single-leaf Wall 3 and 6. As shown in Figure 4.7 there is no crack between points 1-2, which means that double-leaf wall does increase the failure strength of masonry wall, at least around the loaded corner.

However, for point 1-5, there was a crack which passed through the brick, but the load-strain curve indicated no cracks occurred. This was because the measurement stopped around 80kN for safety reasons, and the crushing of bricks happened around failure load (90kN). Therefore no cracks were recorded by the DEMEC gauge at this stage. Most importantly, it can be seen that most of the points were under minor compression during the test. This is a good sign for the masonry wall as it could resist much higher compressive load than tensile load. Therefore, the collar joint could help to postpone the occurrence of cracks. However, there was still a small jump on the strain when the lateral load reached about 75kN. This meant a few big cracks occurred. The masonry wall tended to fail quickly after big diagonal crack appeared. For the sake of safety, no more DEMEC gauge readings were recorded after the occurrence of the big cracks.

4.3.2.2 Wall 7 (Post-damaged)

Figure 4.25 represents the load-strain relationship of DEMEC gauge points on masonry Wall 7, which is a post-damaged retrofitted wall. The first leaf had been tested and some minor cracks had already occurred along some mortar joints, highlighted in Figure 4.4. The strain of point 1-2 increased gradually under lateral load, which was still under compression. While for point 1-5, the strain increased remarkably in the first 5kN and then increased slowly after that. This was because there were some minor cracks happened already. The second loading, which can be taken as a cyclic loading, compressed the cracks at the very beginning of the test. The strain

increased significantly after the occurrence of big crack when the lateral load reached around 35kN. This is because the crack that appeared between Point 11-15 was compressed under small lateral load. However, the crack will expand after the re-distribution of external load. For point 2-6, 7-11, and 10-11, they were in tension from the beginning and the tension strain increased slowly, which was because some minor cracks already occurred between these points. Then the second load caused these cracks expand again. However, bigger cracks occurred only when the lateral load reached around 40 to 50kN. However, the strain increase of Wall 7 was not as remarkable as Wall 5. This proves that post-damaged approach can improve masonry wall's ductility as it didn't fail abruptly like brittle material, thereby causing the post-damaged masonry wall to fail in a less brittle manner.
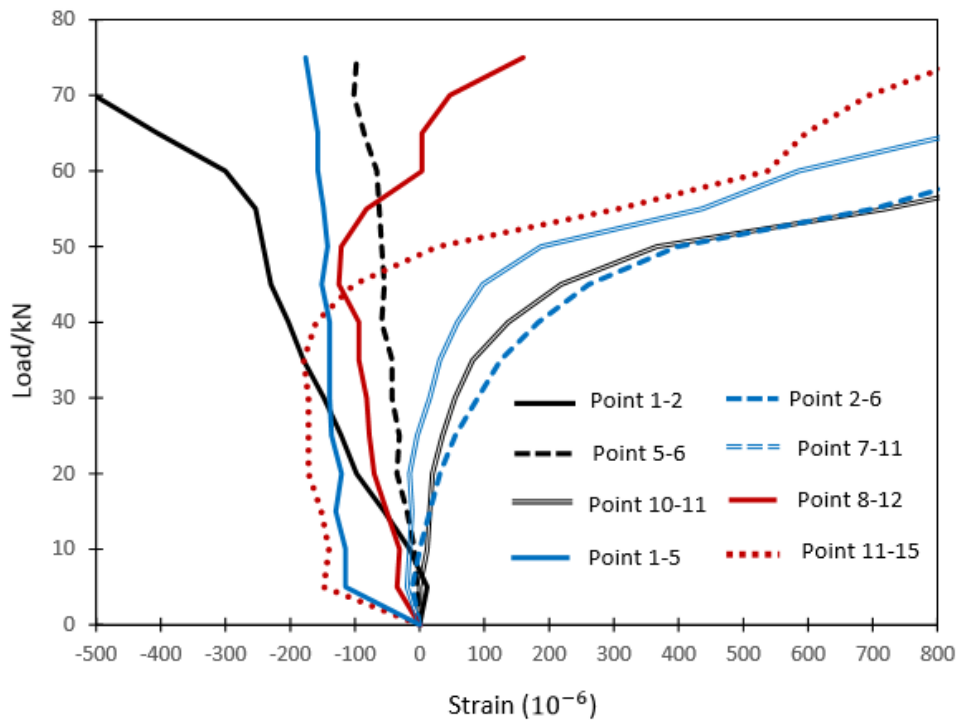
Figure 4.26 Horizontal and vertical load-strain curve of DEMEC gauge points of Double leaf Wall 7

4.3.3 Strain (stress) distribution of masonry wall

The strain change can be obtained via the DEMCE gauge readings. Though the property of masonry wall is anisotropic, it is taken approximately isotropic. Therefore, as long as the strain was known, the stress can be found. In this section, the DEMEC gauge readings were recorded when the lateral load reached about 40kN. In this case, the walls were failed and are still in their elastic stage according to the results displayed in Figure 4.15 and 4.16. Furthermore, the stress is in this stage was large enough to be recorded and analysed. In this section, only single-leaf wall 3 and double-leaf wall 5 have been selected to be researched.

4.3.3.1 Single-leaf wall 3
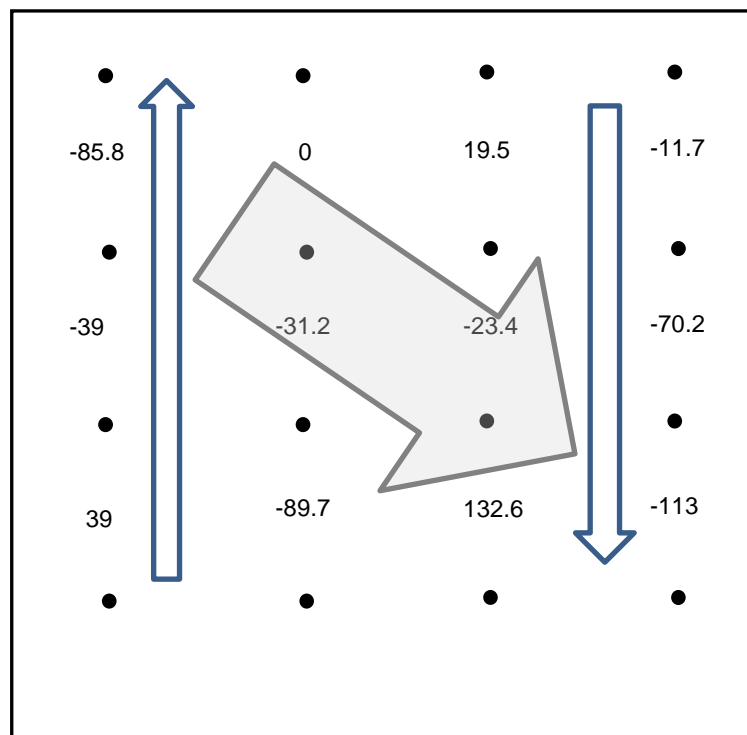
Figure 4.27 Strain (Stress) distribution of wall 3 in the vertical direction
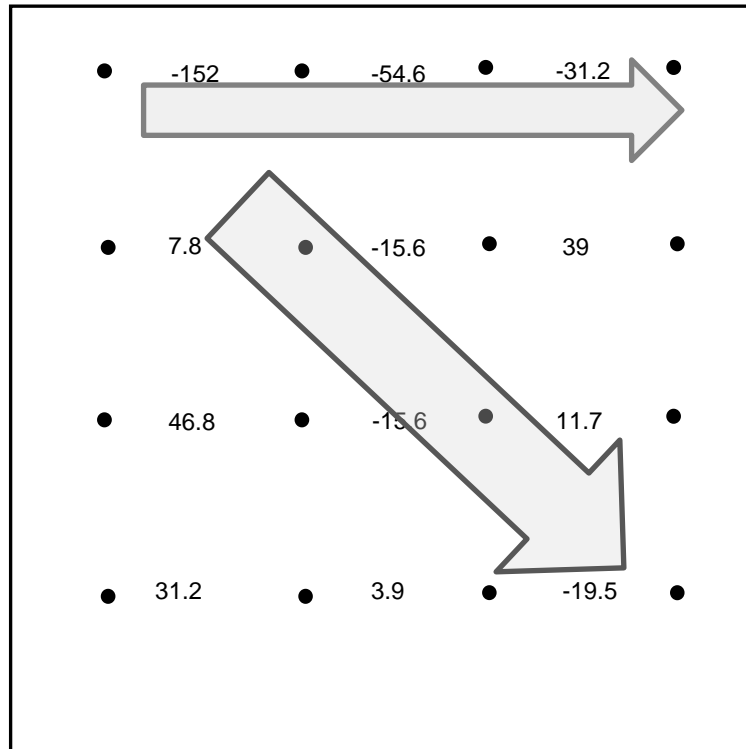
Figure 4.28 Strain (Stress) distribution of wall 3 in the horizontal direction

Figure 4.26 and 4.27 demonstrates the stress distribution of the single-leaf wall 3 in the vertical and horizontal directions, respectively. The value between every two dots represents the strain change between these two dots. Therefore, the stress value between these two dots can be obtained if the Young's modulus of masonry wall is known.

In Figure 4.26, it is seen on the left side that the stress was changed from compression to tension from top to bottom. This was because the left side was compressed by the vertical load but it was still subjected to lateral loading. The lateral loading caused the wall rotate and lift up the wall from the left-bottom side, which is the reason for the stress change. Similarly, this change can be found on the right side as well.

The wall was in compression on the right side. However, in the middle part of the wall, it is more complex to determine the compression area or tension area as it is related to both vertical and lateral loading. The vertical and

horizontal load may both cause tension and compression in the diagonal area. Nevertheless, it is still can be assured that the lateral and vertical loading were passed via the diagonal area to the left bottom side (displayed as the grey angle in Figure 4.26). Figure 4.27 illustrates that the top side of the wall was in compression because of the lateral load. However, the stress decreased in the area further from the loaded corner as the load was partially passed to base via diagonal strut (Shown in grey angle in Figure 4.27). Furthermore, in this stage, it shows that the left side and right side both are in tension because of the combined loading. Both Figure 4.26 and 4.27 demonstrated that the combined loading was mainly passed via the diagonal strut to base.

4.3.3.2 Double-leaf wall 5

Figure 4.28 and 4.29 represent the stress distribution of the double-leaf wall 5 in the horizontal and vertical directions, respectively. The stress distribution on the left side, right side and top side are quite similar with the single-leaf wall. The load corner always has the largest stress, this is because the external was concentrated in this area and will always cause crushing cracks. Figure 4.28 and 4.29 reveal that the combined loading is passed diagonally from the top-left corner to the bottom-right corner to the base. However, there is a big difference between the double-leaf and single-leaf masonry walls. The diagonal area (strut) is much bigger than the single leaf wall, which was caused by the collar joint.

 The combined loading was passed to the second leaf of the double-leaf wall via the collar joint. However, the stress distributed on the second leaf wall "flowed" back again to the first leaf. By this process, the combined loading was spread to the further area from the loading point, thus making the diagonal strut much bigger.

Based upon the DEMEC gauge strain readings on single- and double-leaf walls, the stress distribution can be obtained. Mainly, the external loading is passed to the base via the diagonal strut, also, the collar joint of the double-leaf wall has a big influence on the stress distribution. The collar joint greatly increases the diagonal strut area, which helps the tension stress change to compression.
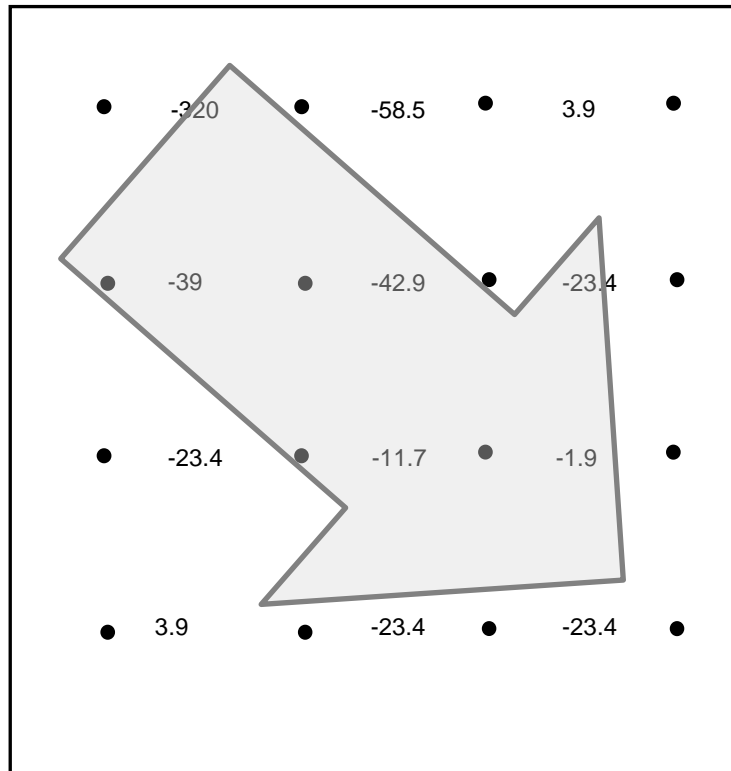
Figure 4.29 Strain (Stress) distribution of wall 5 in the horizontal direction on the loaded leaf
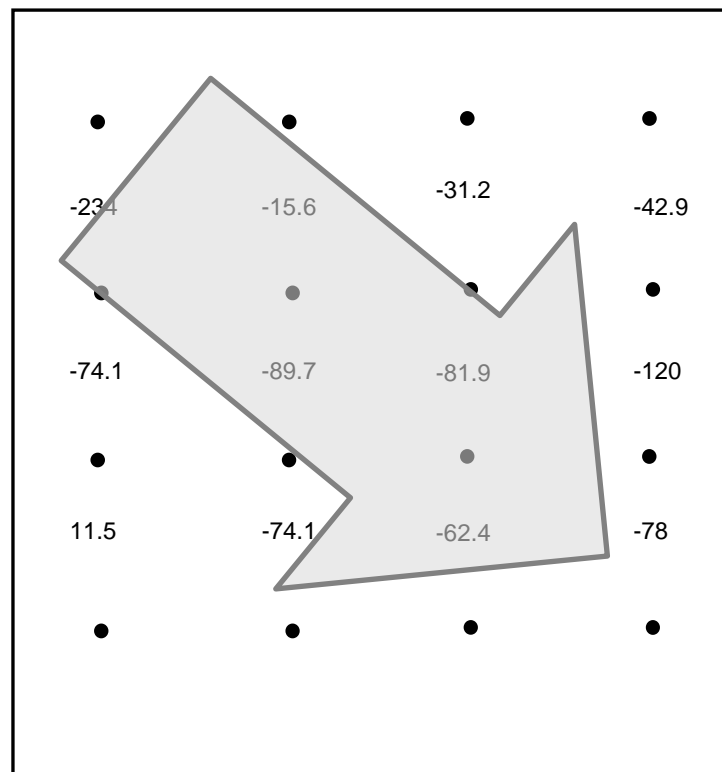
Figure 4.30 Strain (Stress) distribution of wall 5 in the vertical direction on the loaded leaf

4. 4   Discussion of the strengthening/retrofitting approaches

The results suggest that the post-damaged retrofitting method works less effectively in terms of strength improvement than the pre-damaged method. This is possibly an unfair comparison and this outcome is not really that surprising owing to the different methods of construction adopted for the two types of double-leaf walls. For example, the two walls in the pre-damaged enhancement configuration were constructed at the same time, therefore, the interlocking of the collar-joint within the two leaves is maximised.

However, for the post-damaged retrofitting, the second wall was bonded to the first one after it had been tested and without any pre-treatment, i.e. the mortar joints of the existing (first leaf) wall were not shaped to help the collar joint to key into the walls. This meant that the bond between the two walls was much weaker; there was effectively an interface weak region between

the collar-joint and the first wall. Future work should investigate certain realistically and acceptably practical methods of 'pre-treating' the first wall to ensure a stronger bond and a more efficient collar-joint along with indicators of the sustained damage, yet this was not at all considered here. For example, steel ties could be used to improve the bond between the two leaves in post-damaged walls (shown in Figure 4.30). As illustrated in Figure 4.13 the two leaves were separated and the collar joint stopped working as a binding material. The application of steel ties could prevent the separation or at least postpone the separation and the improvement of post-damaged method could be larger.
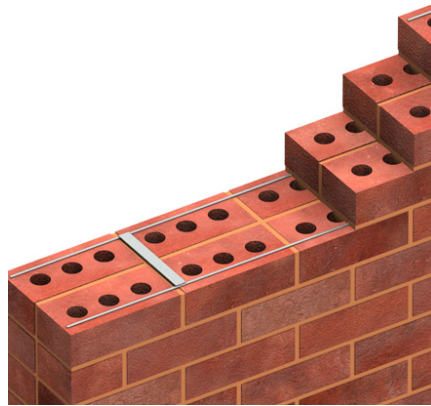
Figure 4.31 Collar jointed wall with steel ties

In addition, the collar joint in this research is assumed to be fully infilled between the two leaves. This is the reason that the construction work was carried out layer by layer and collar joint was also filled layer by layer. With this process, the collar between the two leaves can be fully infilled with mortar joint. However, in some cases the filling of the collar joint is carried out after the two leaves have already been constructed. When this occurs, the collar joint is hard to be fully infilled. Therefore, the possibility of partially infilled collar joints should also be taken into consideration.

Moreover, as it is mentioned in Section 4.1.4, the brick in this research has some slots on the back side. When the mortar is filled into the slots, the formed collar jointed between the masonry leaves can be taken as keyed joint, this is similar with the collar jointed conducted in the work of Pian-

Heriques et al. (2004) (4.31(b)). In the work of Pina-Heriques et al., two cases were considered, straight collar joint (4.31(a)) and keyed collar joint. It was found that shear failure occurred in the panels constructed with a straight collar joint. However, for the wall panels constructed with keyed collar joints, failure was mainly due to diagonal cracks in the inner leaf. Furthermore, the shear strength value for straight collar joints are between 0.09 and 0.17, whereas for the keyed joints, the values are in the 0.58-0.81 range, which means, the strength for keyed joints is 3.5 to 9 times stronger than straight collar joints. In this research, only one case, i.e., keyed collar joint is considered and the results showed that the bond of collar joint was quite strong as well. However, not all the bricks are ribbed like the bricks used in this research. If the back side of the brick unit is relatively smooth and solid, then the type of straight collar joint should be taken into account. The bond of the straight collar joint may have a totally different influence on the failure pattern as well as the failure load. The results found in this research are based on the ribbed bricks, which is not applicable in other types of bricks. Therefore, in the future work, a straight collar joint should be included in the research, which means different types of bricks (especially smooth one) should be used.

In addition, the DEMCE gauges mounted on the first leave help to understand the load transfer among the masonry wall. There are no DEMEC gauges mounted on the second leaf, which means the load transfer among the second leaf is not clearly known, although it can be known from the numerical results. Therefore, in the future work, the DEMEC gauges should also be mounted on the second leaf in order to have a sound understanding on the load transfer.

Figure 4.32 Masonry prisms' dimensions in mm: (a) straight collar joint and (b) keyed collar joint (Pina-Heriques et al. 2004)

4. 5 Summary

In this Chapter, the results of a preliminary analysis of the experimental tests that have been carried out in Chapter 3, have been presented and discussed in detail. The tests were carried out both on single- and double-leaf masonry wall panels. Double-leaf masonry walls consist two types: pre-damaged and post-damaged masonry walls. The results are analysed in terms of failure patterns, load-deflection relationship (failure load and maximum deflection), and strain/stress distribution by using DEMEC gauge points.

The results showed that pre-damaged approach works better than post-damaged approach in terms of increasing failure load. The pre-damaged double-leaf wall can improve the failure load of single-leaf wall up to 40% to 60%, while the post-damaged double-leaf wall can only restore the initial failure load. However, in terms of stiffness improvement, post-damaged type works better compared with the pre-damaged one. The stiffness of the post-damaged wall was increased remarkably, almost twice that of single-leaf wall. While for the pre-damaged type, the stiffness can be increased but not

as significantly as post-damaged wall. Also, the improvement of the ductility of the post-damaged wall was greater. Therefore, the pre-damaged strengthening approach should be carried out in building the masonry structures in order to improve the load resistance capability. For the existed masonry structure with collar jointed masonry walls, this result assures the safety of the building. However, for the masonry structuresthat have been constructed, the post-damaged retrofitting approach can be applied. Surface treatment prior to the retrofitting process may be needed in order to improve the final effectiveness.

According to the failure patterns, the failure of single-leaf wall was represented by a big and remarkable diagonal crack. The cracks occurred mainly along mortar joint with only few passing through the bricks, which agrees with the literature review. For the collar jointed walls, the failure was represented by a big diagonal crack as well as some other small cracks. Moreover, it can be seen that the cracks on the collar jointed walls were much more than the single-leaf wall, which means the collar joint has spread the stress more evenly through the whole panel. The results showed that the collar joint could help to improve the integrity of the masonry wall panels.

In addition, two types of mortar, type S and Type N, had been used in the single-leaf wall tests. The results of the single-leaf wall showed that the mortar type doesn't affect the failure load or failure pattern. However, this conclusion needs more research. Besides, the longer the curing age is, the stronger strength and stiffness the masonry wall can acquire. However, by using the high strength cement, masonry wall and mortar can reach most of its designed strength after cured for 14 days.

Furthermore, the failure process of the masonry wall can be easily explained by using DEMEC gauge points. Strain in negative represents compression while positive means tension. The readings represent the strain change during the test and the stress can be obtained if the modulus of elasticity of masonry wall is known. The DEMEC gauge results in section 4.3 shows that

it can explain the failure process of masonry wall and stress distribution among masonry wall panels very well. Therefore, more DEMEC gauge can be used on both of the walls in order to get a more detailed understanding on the performance. However, the analysis of DEMEC gauge is time consuming and only the stress/strain on the brick leave's surface can be known. The mechanical behaviour of the collar joint is not able to know. Therefore, in order to provide a detailed understanding on the stress/strain distribution through the collar joint, a numerical analysis is necessary. Furthermore, the simulation result is able to rule out the contingency occurred in the experiments. The numerical work is carried out in Chapters 5 to 7.

Chapter 5   Micro-scale simulation model

5. 1   Introduction

In the past decades, relevant research on numerical methods to predict the in-service behaviour and load carrying capacity of masonry walls has been advanced considerably. However the modelling of a load bearing masonry wall or masonry infill under in-plane combined loading remains difficult primarily due to the complex mechanics developed within the different materials of the wall. So far, a number of different approaches have been implemented to simulate the mechanical behaviour of masonry walls subjected to static or dynamic loading that can act in-plane, out-of-plane or even simultaneously in both planes. Different approaches are available, with linear elastic or non-linear inelastic material behaviour, at a micro or macro level, with different ways of damage representation and with damage models obeying different constitutive laws (Papps 2007). A review of the current strategies for modelling masonry has been presented in Chapter 2 (literature review). This chapter aims to develop a numerical model for masonry walls that is able to validate the current experimental outcomes presented in Chapter 4.

5. 2   Selection of numerical models

There is a broad range of numerical models to choose from the literature review. It is necessary to select the most appropriate one in order to predict the most accurate results. Lourenco (2002) proposed a few factors that need to be taken into account in choosing the most appropriate methods, which

are: the structure itself; the simplicity desired; the experimental data available; the amount of financial resources; time requirements and the experience of the modeller.

In order to choose the best appropriate numerical model to simulate the masonry wall panels tested in the laboratory, a comparison of the numerical models that have been presented in Chapter 2 will be carried out as following.

5.2.1 Comparison of macro-scale and micro-scale models

In macro-scale modelling, the masonry units and mortar joints are smeared into an averaged continuum. There are no distinctions between the units, the mortar and their interfaces. This model can be applicable when the dimensions of a structure are large enough so that a description involving average stresses and strains becomes acceptable. Considerable computational time can be saved by applying this method. However, unconditionally accurate results and fine-detail of the behaviour cannot be captured by the nature of this approach.

On the other hand, the micro-scale modelling has two approaches: (a) detailed micro-scale modelling; (b) simplified micro-scale modelling. In the detailed micro-scale modelling approach, both the masonry units and the mortar are discretised and modelled with continuum elements while the unit/mortar interface is represented by discontinuous elements accounting for potential crack of slip planes. While in the simplified micro-scale modelling approach expanded units are modelled as continuous elements while the behaviour of the mortar joints and unit-mortar interface is lumped into discontinuous elements. Detailed micro-scale modelling is probably the most accurate approach available today to simulate the real behaviour of masonry as the elastic and inelastic properties of both the units and the

mortar can be realistically taken into account. With this method, a suitable constitutive law is introduced in order to reproduce not only the behaviour of the masonry units and mortar, but also their interaction. However, any analysis with this level of refinement requires large computational effort. Thus this method is used mainly to simulate tests on small specimens in order to determine accurately the stress distribution in the masonry materials. The drawback of the large computational effort required by detailed micro-scale modelling is partially overcome by the simplified micro-scale modelling strategy.

The dimensions of the experimental masonry wall carried out in the laboratory are $900{\times}975{\times}102.5\text{mm}^3$. The dimensions are not large enough to apply macro-scale modelling nor small enough to use detailed micro-scale modelling. Furthermore, simplified micro-scale model can give a good understanding of the local behaviour of masonry structures, meanwhile, it also reduces computational time and computer memory requirements. Therefore, simplified micro-scale modelling will be applied in this research.

5.2.2 Comparison of Finite Element Method (FEM) and Discrete Element Method (DEM)

Both FEM and DEM have been presented in detail in Chapter 2. Here in this section, a comparison is carried out in order to select the more appropriate one.

Finite element method is the most often used and well developed method in calculation of masonry structures due to its long tradition. However, DEM has only been used to model masonry in the last two decades (Zhuge et al. 2004). Stavridis and Shing (2008) concluded that nonlinear finite element modelling is the most powerful analysis tool, which is able to simulate complex structures with linear or non-linear material properties either at a

micro or macro scale. Researchers have carried out studies to compare the effectiveness of FEM and DEM. Giordana et al. (2002) investigated the applicability of both types of modelling. The comparison of numerical and experimental results are shown in Figure 5.1. It can be seen that the load-displacement curve obtained from the analysis by using FEM is in better agreement with the experimental envelope, although a slightly stiffer compared with the experimental one. In additional, there is a main drawback for DEM, which is the poor constitutive law for the internal elements when deformable blocks are taken into account. In the past, most numerical models that are based on the discrete element method treated blocks as rigid. This makes this method inappropriate for the analysis of the type of the structures in which the state of strain and deformations inside a discrete element cannot be ignored. However, this drawback can be overcome by FEM modelling.
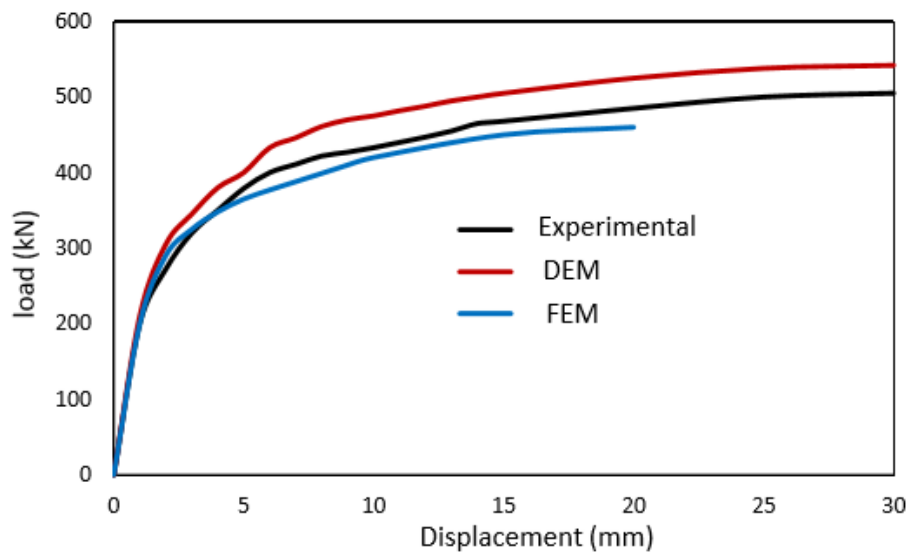
Figure 5.1 Comparison of experimental against numerical results (Giordano et al. 2002)

5. 3   Model in MIDAS FEA

The commercial finite element software MIDAS FEA was selected for the modelling in this research. The reason to choose MIDAS FEA is because it is a state-of-the-art software, which defines a new paradigm for advanced nonlinear and detail analysis for civil and structural engineering applications. In addition, MIDAS FEA combines a powerful pre/post processor and solver that stands for reliability and accurate solutions. Furthermore, MIDAS FEA possess the following characteristics:

- It provides an inherent material called "Combined tension-shearing-cracking" for the brick-mortar interface, which combines all the failure modes mentioned above;

- It allows users to assign different parameters that are obtained via experimental tests or numerical calibration to different materials;

- It allows the user to assign different material properties at different locations of the structure. This is important, especially when bed mortar joint, head mortar joint or collar joint are totally different;

- It provides both 2D and 3D models;

- It is able to capture all the failure modes, including tensile failure, de-bonding and shear slip at the brick-mortar interfaces;

- It is able to capture the onset and propagation of cracking on the masonry wall, and also the measurement of crack width;

- It is able to simulate the post-cracking behaviour of masonry wall;

- It is able to provide a load-displacement relationship for analysis;

- And it is able to provide results with a satisfactory degree of accuracy.

5. 4　Micro-scale modelling

As the compared results showed in Section 5.2 in this chapter, simplified micro-scale finite element modelling will be adopted，more details can be found in the work of Lourenco (1996). Here in this section, the simplified micro-scale finite element modelling will be described and presented in detail.

As previously noted, the joints (including the collar joint in this research) in masonry are typically the weakest parts. Therefore, it can be naturally assumed that any cracks would develop along the joints. Such a simplified micro-modelling approach whereby predefined cracks are included at the joints is herein practiced. The mortar joints and the brick-mortar interfaces are lumped into a zero-thickness interface while the dimensions of the brick units are slightly expanded to keep the whole geometry of the given masonry structure unchanged. Furthermore, a potential vertical crack is placed in the middle part of every brick. This is due to the fact that in masonry structures, as also evidenced in the current experimental failure patterns, most of the propagating cracks beyond being located in the mortar they can also develop in the middle of bricks (Dolatshahi and Aref 2011) making these regions similarly quite prone to forming separations (Lourenco and Rots 1997). Indicatively, this is shown in Figure 5.2.
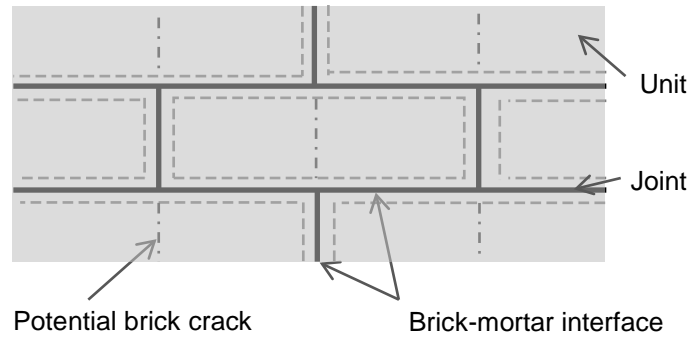
Figure 5.2 Simplified micro-modelling strategy for masonry panel (Lourenco 1996)

5.4.1 Brick representation

As the mortar joints are represented by a zero thickness interface, the dimensions of the bricks have to be expanded slightly to maintain the geometry of the brickwork. Each individual brick can be taken as rigid or deformable element. The rigid block does not change its geometry as a result of any applied loading. Rigid elements can be applied when the behaviour of the system is dominated by the mortar joints or alternatively high strength and low deformability brick has been used. In the case of brick modelled as deformable element, bricks can be assumed to be linear elastic or non-linear according to the Mohr-Coulomb criterion. The bricks in this research were assumed to be deformable behaving in a linear elastic manner. For the 2D models, practiced in the case of single leaf walls, the brick units were represented by eight-node plane stress continuum elements while for the 3D models which are practiced in the case of double leaf walls, the brick units were represented by eight-node hexahedron solid elements (shown in Figure 5.3). The material parameters for the linear elastic model are the unit weight of the brick, the Young's modulus and the Poisson's ratio. The value of these parameters can be obtained via experimental tests on small specimens.

5.4.2 Mortar joint representation

As explained previously, the mortar joints are smeared into zero thickness interfaces between adjacent bricks. This approach by making a significant simplification and representing an entire mortar joint with a zero-thickness cohesive interface model has been proved by Lotfi and Shing (1994). At the interfaces, the bricks are connected to each other by sets of interface elements. These interfaces are located at the outside perimeter of the bricks, see Figure 5.3. It needs to be noted that the nodes on each element mesh should match so that they can be connected together in the model. In the 2D model, the brick-mortar joint interfaces were represented by six-node line interface elements while for the 3D models relevant to collar jointed walls, the surface interface elements were used to analyse the interface behaviour. The interface behaviour was simulated using a Mohr-Coulomb failure surface combined with a tension cut-off and a compression cap.
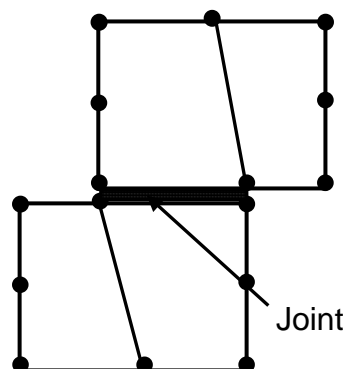
Figure 5.3 Deformable bricks with interface element

5.4.3 Constitutive law for the interface element

The zero thickness interface is based on multi-surface plasticity, comprising a Coulomb friction model (mode II) for shear failure, a tension cut-off (mode I) for tensile failure, and a cap mode for compressive failure, which is shown in Figure 5.4. This model was described in detail by Lourenco (1996).
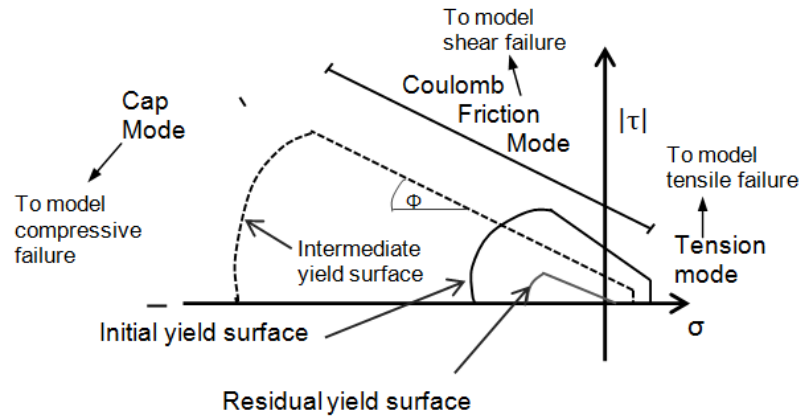
Figure 5.4 Interface model proposed by Lourenco (1996)

As it is known that there is an interface material model called "Combined Cracking-Shearing-Crushing" in MIDAS FEA, which is capable of capturing all the possible failure mechanisms of the masonry joints, such as sliding, tensile cracking and crushing. The parameters needed to define the interface model in MIDAS FEA are listed in Table 5.1. The model works by combining different yield surfaces, including tension, shear, and compression with softening in all three modes (Lourenco, 1996). Each of these three yield surfaces is described in more detail as following.

Figure 5.5 Modelling parameters for the interface model and their definition

Parameter	Symbol
Normal stiffness	k_n (N/mm^3)
Shear Stiffness	k_s (N/mm^3)
Tensile strength	f_t (N/mm^2)
Mode I fracture energy	$G_f^I (N/mm)$
Cohesion	C (N/mm^2)
Friction coefficient	ϕ
Dilatancy coefficient	Ψ
Mode II fracture energy	$G_f^{II} (N/mm)$
Compressive strength	f_c (N/mm^2)
Compressive fracture energy	$G_f^c (N/mm)$

Tensile behaviour

The tensile cracking of the interface model is represented with a tension cut-off with exponential softening. The tension cut-off is illustrated as a vertical line in the positive region of normal stress in Figure 5.4, which can simulate the brittle failure of mortar joint under tensile force. The exponential softening behaviour in tension is consistent with experimental results from Pluijm (1992) (Lourenco, 1996), which is shown in Figure 2.4 in Chapter 2. The yield function for tension mode reads

$$f_1(\sigma, \kappa_1) = \sigma - \overline{\sigma_1}(\kappa_1) \tag{5.1}$$

where the yield value $\overline{\sigma_1}$ reads

$$\overline{\sigma_1} = f_t \exp\left(-\frac{f_t}{G_f^I}\kappa_1\right) \tag{5.2}$$

where f_t is the tensile strength of the unit-mortar interface, G_f^I is the mode I fracture energy, and κ_1 is introduced as a measure for the amount of hardening or softening of tension mode.

Shear behaviour

As it is described in Chapter 2 that the shear behaviour of the interface element can be modelled with the Mohr-Coulomb failure law, which is defined in Equation 5.3:

$$f_2(\sigma, \kappa_2) = |\tau| + \sigma \tan \Phi(\kappa_2) - \overline{\sigma_2}(\kappa_2) \tag{5.3}$$

where the yield value $\overline{\sigma_2}$ reads

$$\overline{\sigma_2} = c \exp\left(-\frac{c}{G_f^{II}}\kappa_2\right) \tag{5.4}$$

and the friction angle Φ is coupled with cohesion softening via the following equation:

$$\tan\varPhi = \tan\varPhi_0 + (\tan\varPhi_r - \tan\varPhi_0)\frac{c-\overline{\sigma_2}}{c} \tag{5.5}$$

The interface material model considers exponential softening for both the cohesion and friction angle, which are demonstrated in Equations. The softening of the friction angle is assumed to be proportional to the softening of the cohesion (Lourenco, 1996). The dilatancy effect and strain softening behaviour are also incorporated in this model.

In the above, C is the cohesion of the unit-mortar interface, $\varPhi_0$ is the initial friction angle, $\varPhi_r$ is the residual friction angle, G_f^{II} is the mode II fracture energy and κ_2 is the amount of hardening or softening of mode II.

Compressive behaviour

For the cap mode, an ellipsoid interface model is used. The compressive model is representative of the maximum compression strength of the interface element. For the hardening/softening behaviour, the law shown in Figure 5.5 was considered, where represents the amount of softening (Lourenco and Rots 1997). The energy under the curve can be related to a "compressive fracture energy". For the yield function for a 2D model, it is shown in Equation 5.6:

$$f_3(\sigma,\kappa_3) = C_{nn}\sigma^2 + C_{ss}\tau^2 + C_n\boxed{?} - (\overline{\sigma_3}(\kappa_3))^2 \tag{5.6}$$

with C_{nn}, C_{ss} and C_n a set of material parameters and $\overline{\sigma_3}$ the yield value. The parameters C_{nn} and C_n control the centre of the cap whereas the parameter C_{ss} controls the contribution of the shear stress to failure. In this study a centred cap with $C_{nn} = 1$ and $C_n = 0$ is adopted because a tension cut-off will be included in the composite yield surface. Furthermore, C_{ss} is taken as 9 as this value provides the best result (Lourenco 1996).
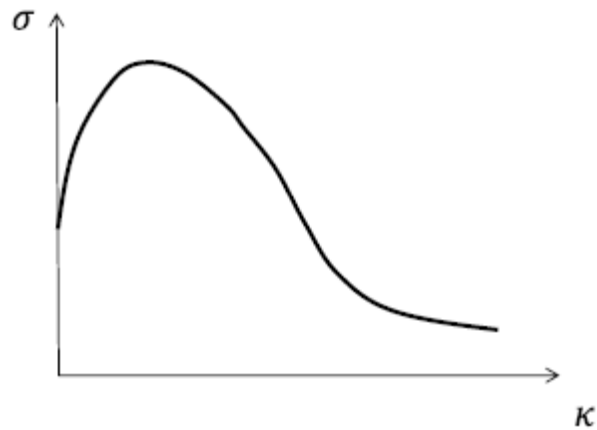
Figure 5.6 Nonlinear compressive behaviour of the cap model (Lourenco and Rots 1997)

5. 5 Review on the application of this method

Lourenco (1996) applied this model to simulate the experimental test of (Raijmakers and Vermeltfoort 1992). The experimental tests were two shear walls, a solid clay brickwork and a clay brickwork with opening, which are shown in Figures 5.6 (a) and (b). The numerical model was checked both qualitatively and quantitatively against experimental data and a high degree of correlation was found, which are shown in Figures 5.7 (a) and (b). Tarque (2011) applied the finite element method MIDAS FEA to model the adobe masonry wall, and good agreement with the experimental result was found. The load-displacement diagrams are shown in Figure 5.8. Similarly, Lofti (1992) and Attard et al. (2007) applied this method by modelling masonry walls with a combination of continuum elements and interface elements.
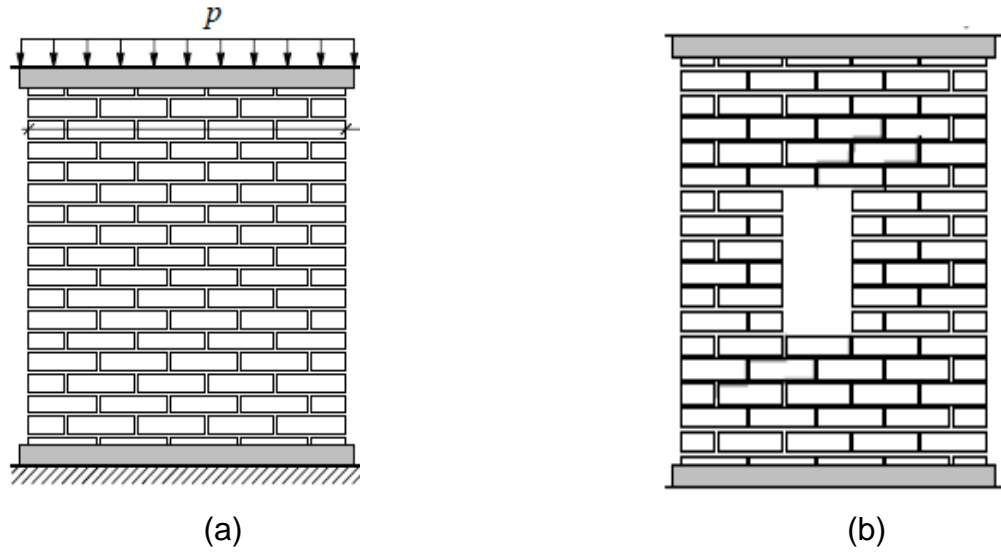
Figure 5.7 Test setup for shear masonry wall: (a) solid wall; (b) wall with opening (Raijmakers and Vermeltfoort 1992)
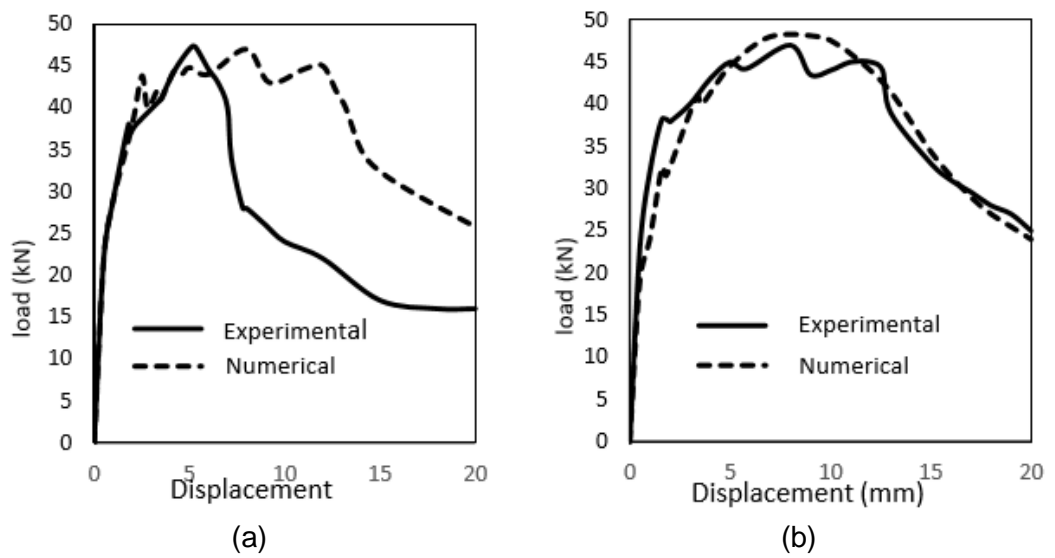
Figure 5.8 Load-displacement diagram of shear wall: (a) solid wall; (b) wall with opening (Lourenco 1996).
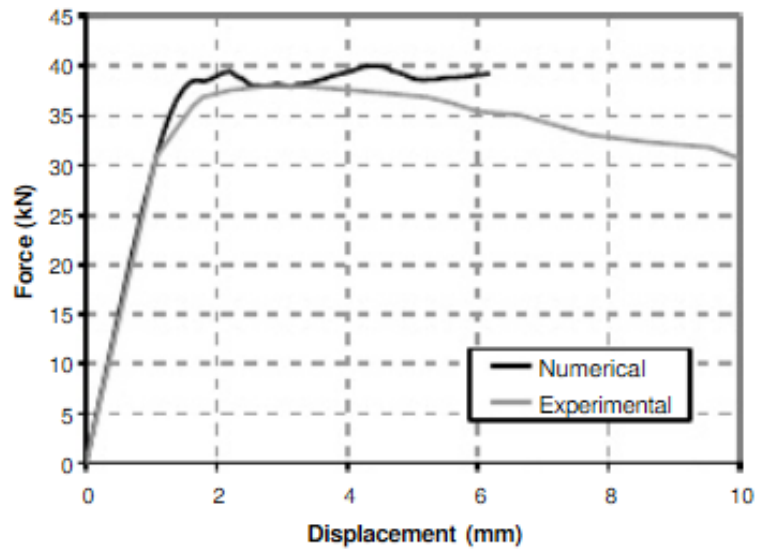
Figure 5.9 Load-displacement diagrams of the adobe masonry wall (Tarque 2011)

Also, Al-Chaar and Mehrabi (2008) used this method to model the masonry infill of an infilled RC frame, which was tested by (Mehrabi et al. 1996). By applying this method, a good agreement with experimental results was found. The load-displacement curves for infilled RC frame is shown in Figure 5.9.
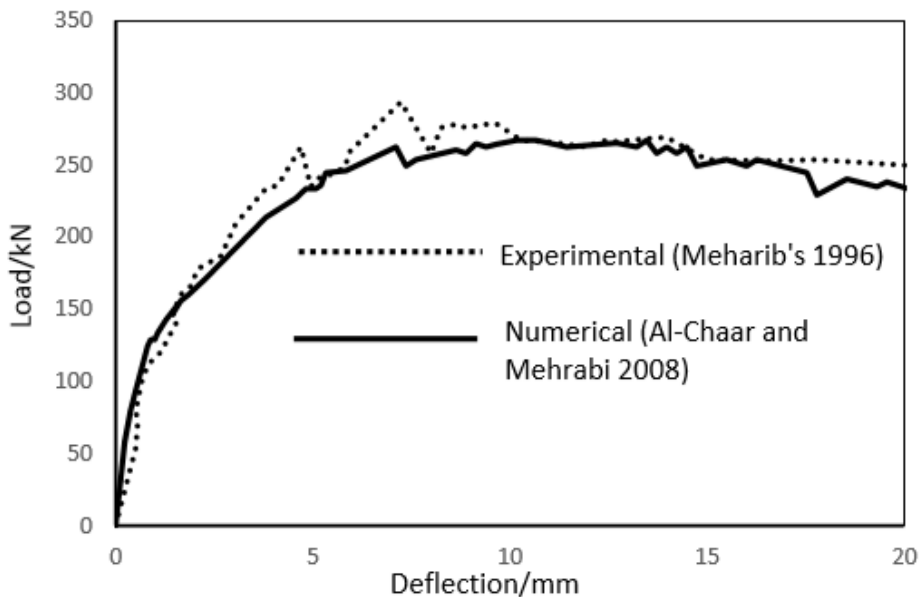
Figure 5.10 Load-displacement curves for infilled RC frame

123

5. 6 **Summary**

In this chapter, a simplified micro-scale finite element model was developed. Within this model, the mortar joints were smeared out into zero-thickness interface, while the bricks were expanded in order to keep the whole geometry unchanged. Furthermore, a potential vertical crack was pre-defined in the middle of every brick as this is where the brick crack mostly likely occur. This model was proposed and presented in the work of Lourenco (1996), and it has been proved to be workable and effective by many researchers (Al-Chaar and Mehrabi 2008, Lofti 1992, Attard et al. 2007). In this research, the commercial software MIDAS FEA was used due to its powerful advantages in analysing masonry wall panels. Furthermore, the inherent material model "combined cracking-shearing-crushing" is able to capture all the failure modes occurred in masonry structure. However, as the masonry material is composite and a lot of parameters are involved, therefore, these parameters should be known before the numerical analysis work. Some of the parameters are able to be obtained via tests on small scale samples (Chapter 3) while the others can only be estimated or calibrated numerically. The detail of the calibration work on those parameters are carried out in Chapter 6.

Chapter 6   Calibration of material parameters of masonry wall

6. 1   Introduction

The material properties of the masonry wall are difficult to obtain via small scale specimen tests and the results could be variable. Therefore, the parameters that cannot be obtained via tests need to be characterized by the calibration method before the simulation work. In this chapter, the calibration work is carried out based on the experimental results of a single-leaf masonry wall. Firstly, a sensitivity study was carried out on the single leaf masonry wall in order to identify the most influential parameters. Then, the parameter calibration was conducted based on these sensitivity study results. After the calibration work, the parameters will be assigned to the masonry model in the simulation work in Chapter 7 to simulate the single-leaf wall panel and to predicate the double-leaf wall panels. For a more detailed calibration process, the flowchart is demonstrated in Figure 6.1
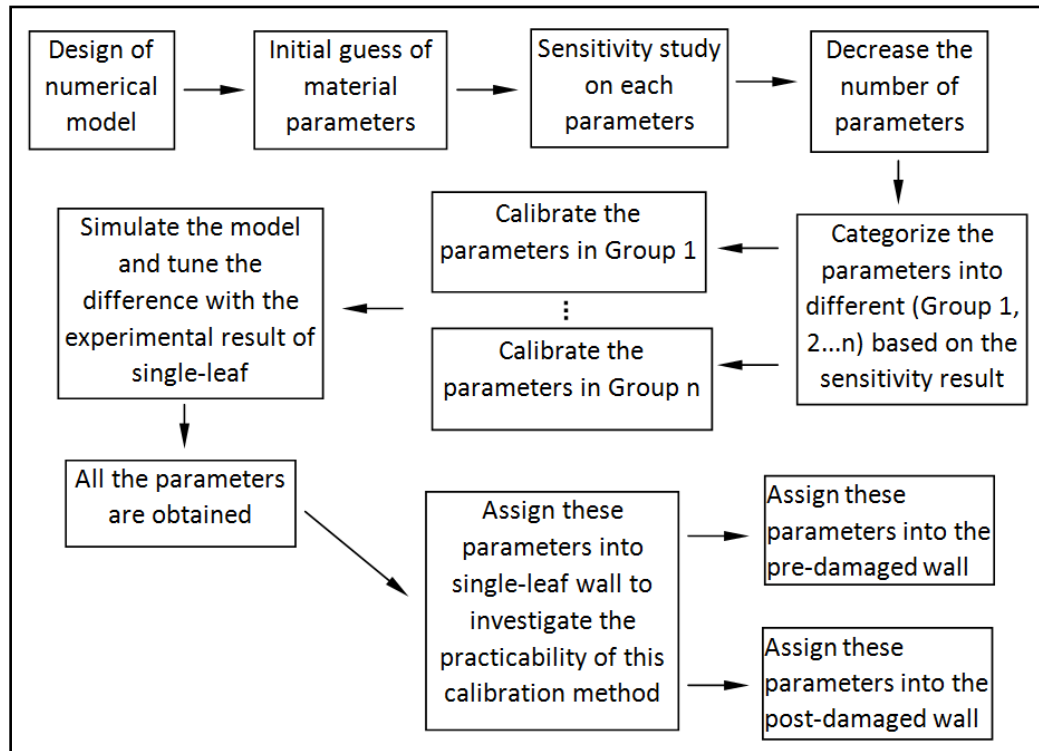
Figure 6.1 Detailed process of calibration process

6. 2   Generation of initial model in MIDAS FEA

6.2.1 Geometry

The geometrical model representing the brickwork wall panels described in Chapter 5 was created in MIDAS FEA. The brick was represented by an elastic deformable element, while the mortar joints are represented by zero thickness interfaces. As the mortar joints have been smeared out in the modelling, this change needs to be taken into account. To allow for the 10mm thick mortar joints, each brick element was increased by 5mm in each face direction to give it a size of 225 X 102.5 X 75mm^3. This is illustrated in Figure 6.2. In a more elaborate approach vertical-potential cracks are placed through the bricks as well. This is due to the fact that in masonry structures, as also evidenced in the current experimental failure patterns, most of the propagating cracks beyond being located in the mortar also develop in the

middle of bricks (Dolatshahi and Aref 2011) making these regions similarly prone to forming separations (Lourenco and Rots 1997).
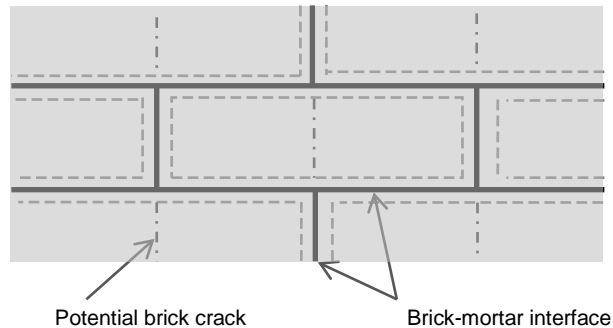
Figure 6.2 Micro-modelling strategy for masonry (Lourenco 1996)

6.2.2 Materials details

In MIDAS FEA, each brick was assumed to behave as a homogeneous, isotropic continuum which exhibits linear stress-strain behaviour. The brick element remained intact at all stages of applied loading while the predominant failure mode would be sliding along the brick/mortar interface and brick element slip along the pre-defined brick crack in the middle part of the brick. Such failure modes have also been observed in the experiments described in Chapter 4.

For the mortar joints and pre-defined brick cracks, these were represented by a zero thickness interface. These interfaces were modelled using "combined cracking-shearing-crushing" material in MIDAS FEA. As explained in Chapter 5, this material captures all the failure modes. The material is based on the elastic normal and shear stiffness, tensile and cohesive strength, compressive strength, Mode I fracture energy, Mode II fracture energy, compressive fracture energy, friction angle as well as the dilation characteristics of the mortar joints. All these parameters need to be calibrated in order to validate the experimental masonry walls.

In this chapter, as all the parameters are not known yet, therefore, the material property is assumed and selected for the initial simulation. This assumption and selection were based on the previous researches. The method can also be found in the work of Tarque (2011).

The selection of the initial value of the material parameters was mainly based on the work of Van der Pluijm (1992) and Lourenco (1996). Obviously, these material parameters do not accurately represent those for the wall panels tested in the laboratory because it is impossible to obtain the accurate value of each parameter as the curing condition, boundary condition as well as other factors are different . The obtained parameters via numerical work are perfect and they don't consider the deviation existed in masonry material. Therefore, these material parameters can provide an initial qualitative evaluation to represent the formation and propagation of cracks and the global structural behaviour of the masonry walls with sufficient reliability. For the pilot study, the initial value of the parameters are taken the same with the literature review, thus only reasonable values are considered. According to the literature review, the strength and stiffness of head joint is about 75%-100% percent of its bed joint (Lourenco 1996, Al-Chaar and Mehrabi 2008, Sarhosis 2012, Sattar 2013). In this research, the material properties for bed mortar joints and head mortar joints are treated as the same for simplicity. Although they may differ in real masonry walls, it was considered to be acceptable as any significant differences that may occur in practice would influence the behaviour of the panels in the laboratory tests. Also, by taking the bed and head joints as the same, a large amount of the numerical work and time in the calibration part can be saved.

6.2.3 Boundary conditions

As shown in Figure 3.1 in Chapter 3, the base of the masonry wall and the right-bottom corner were restrained by a steel base and frame. Therefore, they were modelled as rigid supports. The left-top part of the wall was restrained as a roller after the vertical load being applied as the vertical displacement is restrained while the wall still can move along the horizontal direction.

6.2.4 Loading

A 20kN vertical load was applied to the left-top steel plate before the test. The vertical load would increase gradually during the test as the vertical deflection was restrained by the vertical load actuator. The horizontal load was applied to the vertical steel plate on the left side of panel and it was displacement controlled. The self-weight of the masonry wall was not considered in this model.

6. 3 Parameters sensitivity study

6.3.1 Methodology

The sensitivity analysis took place in order to evaluate the influence of different parameters on the calibrated numerical behaviour curves. As mentioned above, there are quite a few parameters that need to be calibrated and some of them can significantly affect the modelling results. Some of the material parameters can be measured via small scale tests. However, some others are very difficult to obtain via experimental tests, such as the mode I fracture energy, mode II fracture energy etc. As the material parameters define the characteristics of the zero thickness interfaces between the mortar joints and the blocks, they can be difficult to

measure directly from physical tests. Even if it is able to carry out the experimental tests, the results always vary and are not trustworthy. For instance, the tensile strength and the compressive strength etc. of the mortar joint obtained from experimental tests on small samples is stronger than its counterparts in masonry wall panels because of the effect of scale factor and boundary conditions etc. Therefore, another method is needed to obtain these parameters. In theory, every parameter needs to be calibrated by taking other parameters into consideration. It would be very unlikely that parametric studies are carried out by taking every parameter into account, as it would be extremely time consuming. There are more than 16 parameters needed to be characterized in this research. Even if each parameter has 5 different variables, it would take 16^5=1,048,576 simulations. Therefore, it is impossible to conduct a parametric study by taking every parameter into consideration.

In order to save computational time in the simulation work, some parameters were calibrated together. The initial range of every parameter is selected according to the literature review. As the previous researches have done similar simulations on masonry structures. The parameters used in those researches have been considered here as well. Therefore, only reasonable values are considered here, which can save a lot of consuming time by excluding the unnecessary ranges.

6.3.2 The influence of brick-mortar interface' parameters

The shear/normal stiffness (K_n/K_s)

Firstly, the stiffness of brick-mortar interface was conducted. The mortar joints have been smeared out as a zero-thickness interface in the modelling. Therefore, the properties of both brick and mortar should be taken into consideration in the elastic interface stiffness (K_n andK_s).

Lourenco (1996) used detailed dis-continuum finite element analysis to demonstrate that the interface stiffness can be directly related to the brick and mortar properties as follows:

$$K_n = \frac{E_b E_m}{h_m (E_b - E_m)} \tag{6.1}$$

$$K_s = \frac{G_b G_m}{h_m (G_b - G_m)} \tag{6.2}$$

If the Poisson's ratio (v) is taken into account, the relation between Young's modulus and shear modulus will be known. K_s can be rewritten as following:

$$K_s = \frac{E_b E_m}{2 h_m [E_b (1 + v_m) - E_m (1 + v_b)]} \tag{6.3}$$

By dividing equations (6.1) and (6.3), the relation between and is obtained, this is shown in the Equation (6.4) to (6.7):

$$\frac{K_n}{K_s} = \frac{\frac{E_b E_m}{h_m (E_b - E_m)}}{\frac{E_b E_m}{2 h_m [E_b (1 + v_m) - E_m (1 + v_b)]}} \tag{6.4}$$

$$\frac{K_n}{K_s} = \frac{2 (E_b + E_b v_m - E_m - E_m v_b)}{E_b - E_m} \tag{6.5}$$

$$\frac{K_n}{K_s} = 2 \left[1 + \frac{E_b v_m - E_m v_b}{E_b - E_m} \right] \tag{6.6}$$

$$K_n = 2 \left[1 + \frac{E_b v_m - E_m v_b}{E_b - E_m} \right] K_s \tag{6.7}$$

Where E_b and E_m are the Young's module for the brick and mortar; G_b and G_m are the shear module for the brick and mortar; v_b and v_m are the Poisson's ratio for brick and mortar and h_m is the actual thickness of mortar joint.

According to Equation (6.7), the relation between K_n and K_s can be obtained if the value of each parameter is given. The range of each parameter is adopted from micro-scale experiments reported by Hendry (1998), Van der pluijm (1992) and Sarangapani et al. (2005), which is shown in Table 6.1.

Table 6.1 Range of brick and mortar properties identified from the literature

Interface parameter	Young's modulus of brick (N/mm^2)	Young's modulus of mortar (N/mm^2)	Poisson's ration of brick	Poisson's ration of mortar
Symbol	E_b	E_m	v_b	v_m
Range	$(4\sim100)\times10^3$	$(1\sim11)\times10^3$	$0.1\sim0.2$	$0.1\sim0.2$

After combining of the material parameters, the ratio of the normal to shear stiffness ranges from 2.0852.514. Therefore, the value of the ratio can be taken as the average of 2.085 and 2.514, namely 2.3.

As ratio between normal stiffness to shear stiffness is 2.3, therefore, only the normal stiffness needs to be calibrated in the following study. As long as normal stiffness is known, the shear stiffness will be known straightforward. The initial parameters ranges are selected from the work of Van der Pluijm (1992) and Lourenco (1996), which are listed in Table 6.2.

Table 6.2 Initial brick and interface material parameters (Lourenco, 1996)

	Properties	Symbol	Value
Brick properties	Elastic Modulus	$E (MPa)$	16700
	Poisson's ration	v	0.15
	Normal stiffness	k_{bn} (N/mm^3)	82
	Shear stiffness	k_{bs} (N/mm^3)	36
	Tensile strength	$f_{bt} (N/mm^2)$	2
	Tensile fracture energy	G_f^{bt} (N/mm)	0.08
Brick-mortar properties	Normal stiffness	k_n (N/mm^3)	82
	Shear stiffness	k_s (N/mm^3)	36
	Tensile strength	$f_t (N/mm^2)$	0.25
	cohesion	C (N/mm^2)	0.35
	Mode I fracture energy	G_f^I (N/mm)	0.018
	Mode II fracture energy	G_f^{II} (N/mm)	0.125
	Friction angle	Φ	40
	Dilatancy angle	Ψ	0
	Compressive strength	f_C (N/mm^2)	8.5
	Compressive fracture energy	G_f^C (N/mm)	5

A range value of K_n has been selected, which is between 8.2 (1/10 of initial value) to 820 N/mm^3 (10 times of initial value). Figure 6.3 demonstrates the load-deflection curves of normal stiffness with different values. From the figure, it can be seen that the normal stiffness has an extremely significant influence on the mechanical behaviour of the masonry wall. Larger normal stiffness tends to result in stiffer masonry wall. Also, the normal stiffness plays a remarkable role on the failure load and deflection. Masonry walls with smaller normal stiffnesses tend to fail at lower loads.

It can also be seen that the experimental result falls between the normal stiffness of 8.2 and 17.2 N/mm^3 and when normal stiffness is $17.2N/mm^3$, the modelling result is close to the experimental one. Obviously, it cannot be claimed that the assumed normal stiffness (k_n=17.2N/mm^3) is exactly the same normal stiffness of the interface. Presumably, this normal stiffness value is close to the real value, and it can be applied in the initial sensitivity study.
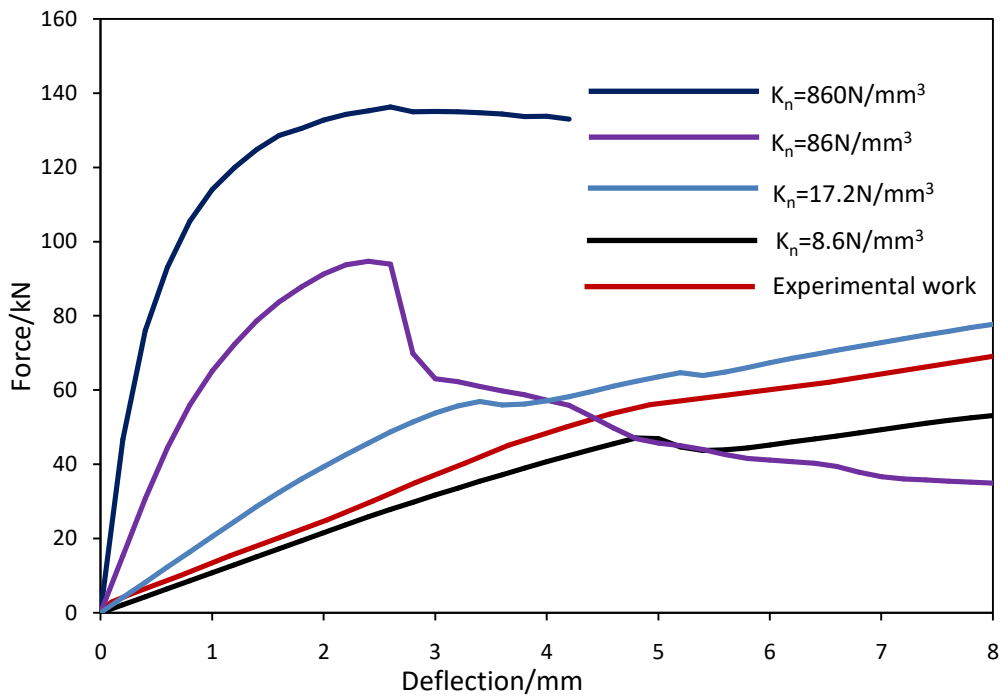
Figure 6.3 Influence of normal stiffness

Tensile strength (f_t) or cohesion (C)

Pluijm (1993) reported that the ratio of shear bond strength to direct tensile bond strength varied between 1.3 and 6.5 and the ratio was largest for low values of tensile bond strength. In addition Pluijm et al. (2000) take the ratio as 1.5 when and this ratio is often found in masonry specimens (Binda et al. 2006). In the work of Lourenco (1996), the ratio of clay brickwork's cohesion

to tensile strength was taken as 1.4. In this research, value 1.4 will also be used. Therefore, if the ratio of cohesion to tensile strength is known, then only one parameter needs to be calibrated.

The selected range of tensile strength is between 0.1 to $1 N/mm^2$. Figure 6.4 presents the influence of the tensile strength of the interface on the mechanical behaviour of the masonry wall. It can be seen that the tensile strength has quite a big influence on the stiffness of the wall. Furthermore, a larger tensile strength can increase the failure load, thus postponing the occurrence of the crack.
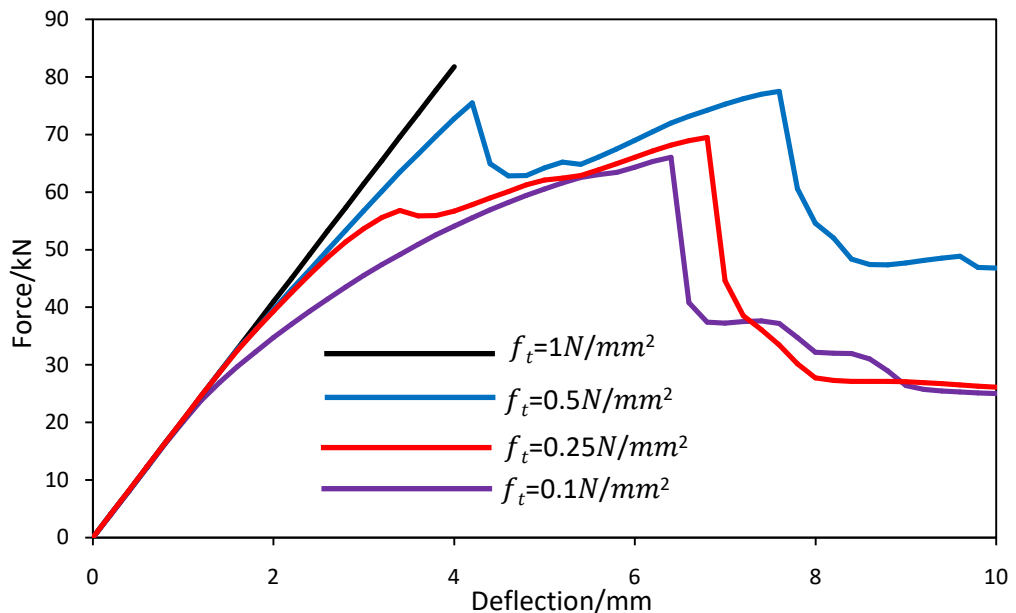
Figure 6.4 Influence of tensile strength

Mode I fracture energy (G_f^I)

The range of mode I fracture energy is between 0.009 to 0.07 N/mm according to Van der Pluijm (1992). Figure 6.5 illustrates the influence of mode I fracture energy on the load-deflection relationship of the masonry wall. It can be seen that the mode I fracture energy does not have a remarkable influence on the overall result, especially with the stiffness of the

whole wall. However, bigger mode I fracture energy can slightly increase the maximum load thus postponing the occurrence of failure.
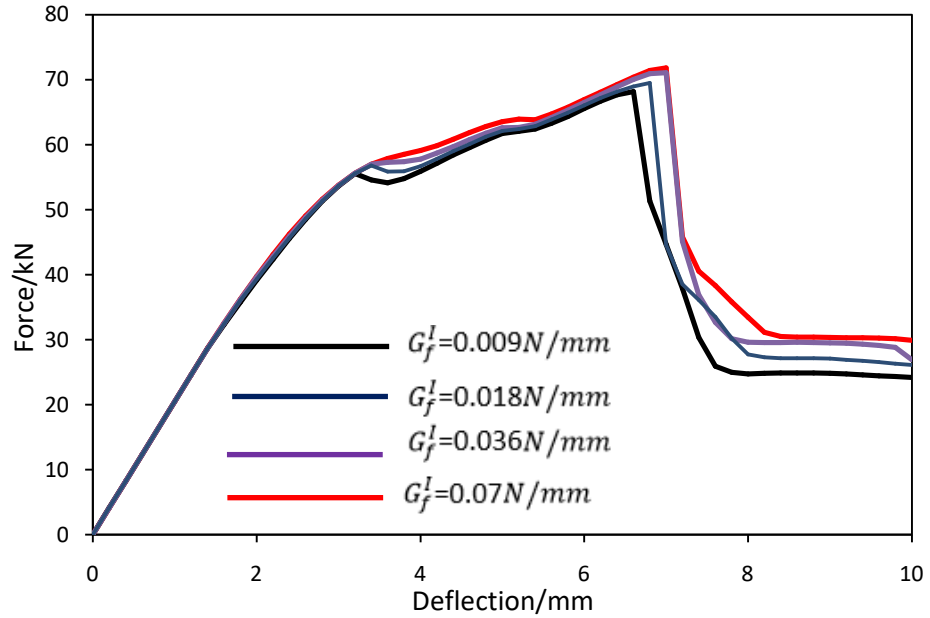
Figure 6.5 Influence of mode I fracture energy

*Coefficient of friction angle (**tan Φ**))*
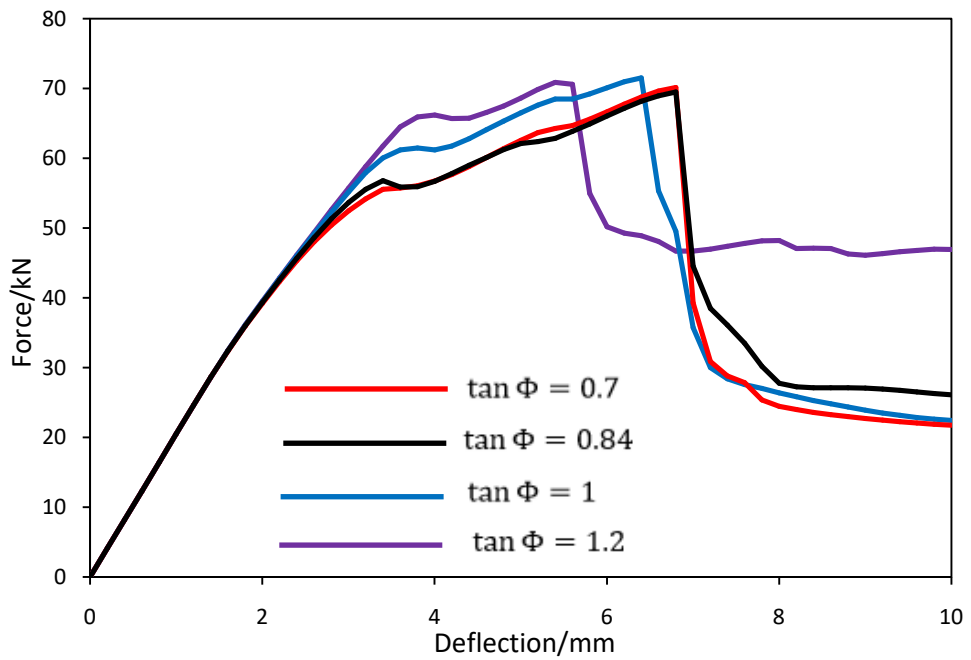
Figure 6.6 Influence of coefficient of friction angle

136

The friction coefficient of the interface ranges between 0.7 to 1.2 (Van der Pluijm 1992). Figure 6.6 illustrates the load-deflection relationship under different friction angles. In Figure 6.6, it can be seen that the friction angle does not affect the stiffness of the whole wall. However, the friction angle can affect the failure load and occurrence of cracks to some degree.

Coefficient of dilatancy angle ($\tan\Psi$*)*

According to Van der Pluijm (1992), the coefficient of dilatancy angle ranges from 0.2 to 0.7. The influence of dilatancy angle on the mechanical behaviour of the whole wall is displayed in Figure 6.7. It reveals that before the big crack occurred, the dilatancy angle does not affect the stiffness of the masonry wall at all. However, after the big crack occurred and the re-distribution happened, the dilatancy angle starts to have a significant influence on the masonry wall. Bigger dilatancy angle can postpone the occurrence of big cracks and also improve the failure load of the wall.
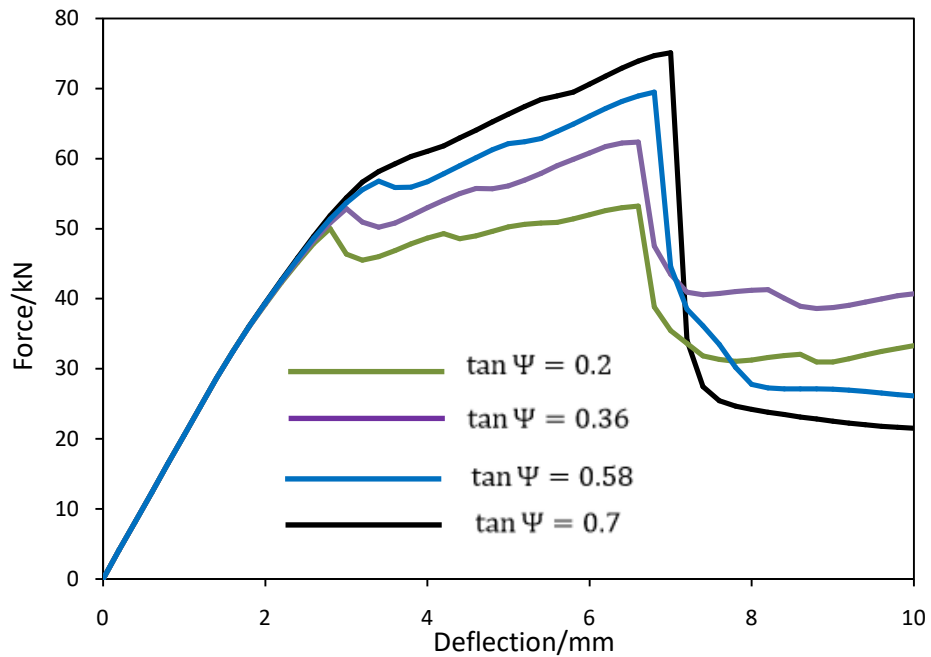
Figure 6.7 Influence of coefficient of dilatancy angle

Mode II fracture energy (G_f^{II})

The selected range of mode II fracture energy is between 0.065 to $0.3\ N/mm$. Figure 6.8 displays the influence of Mode II fracture energy on the behaviour of the masonry wall. Though it can be concluded that the mode II fracture energy does not affect the stiffness of the wall, it does have a relatively remarkable influence on the failure load and crack occurrence. Larger value of mode II fracture energy can increase the failure load and postpone the occurrence of big crack.
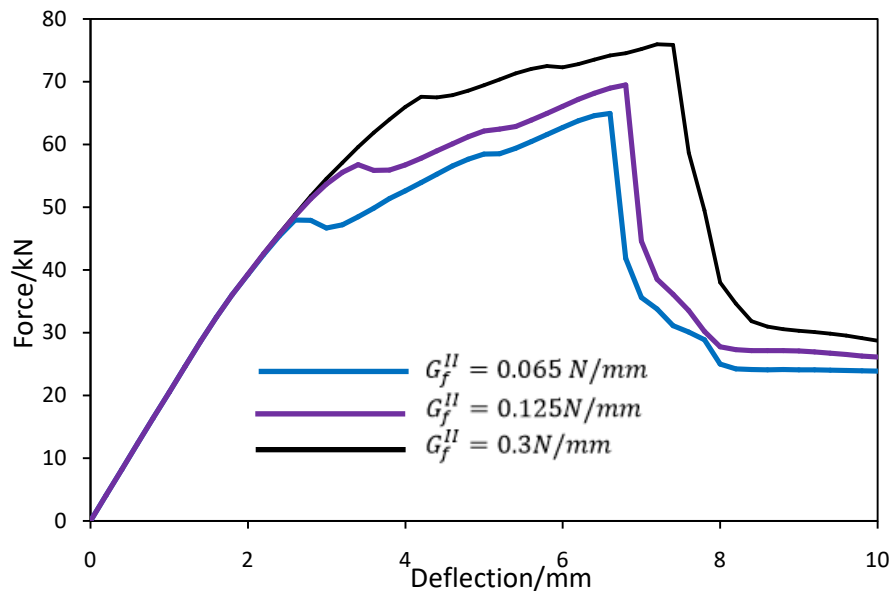
Figure 6.8 Influence of Mode II fracture energy

Compressive strength (f_m)

Figure 6.9 presents the influence of the compressive strength on the load-deflection relationship. It can be clearly observed that the compressive strength does not affect the initial stiffness. However, it does have a great influence on the failure load and post-peak behaviour.
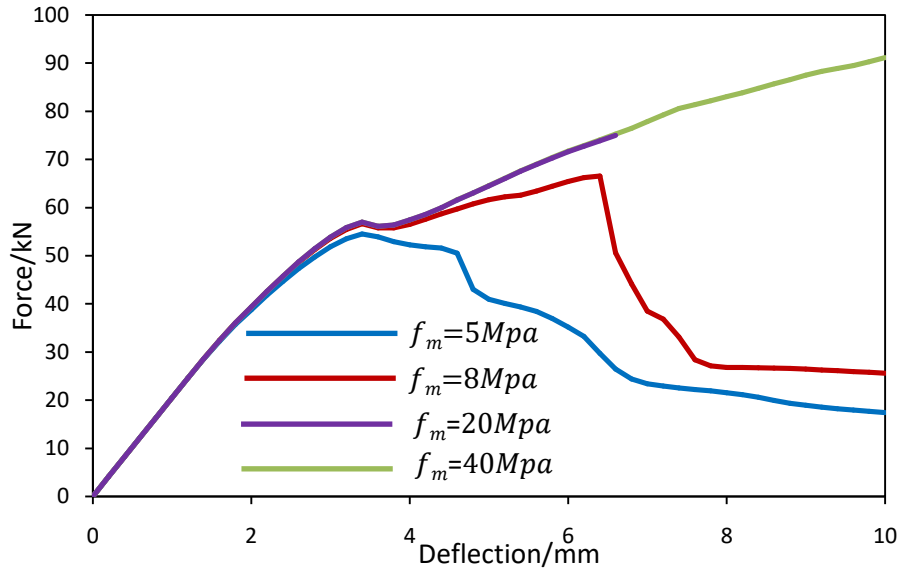
Figure 6.9 Influence of compressive strength

Compressive fracture energy (G_c^f)
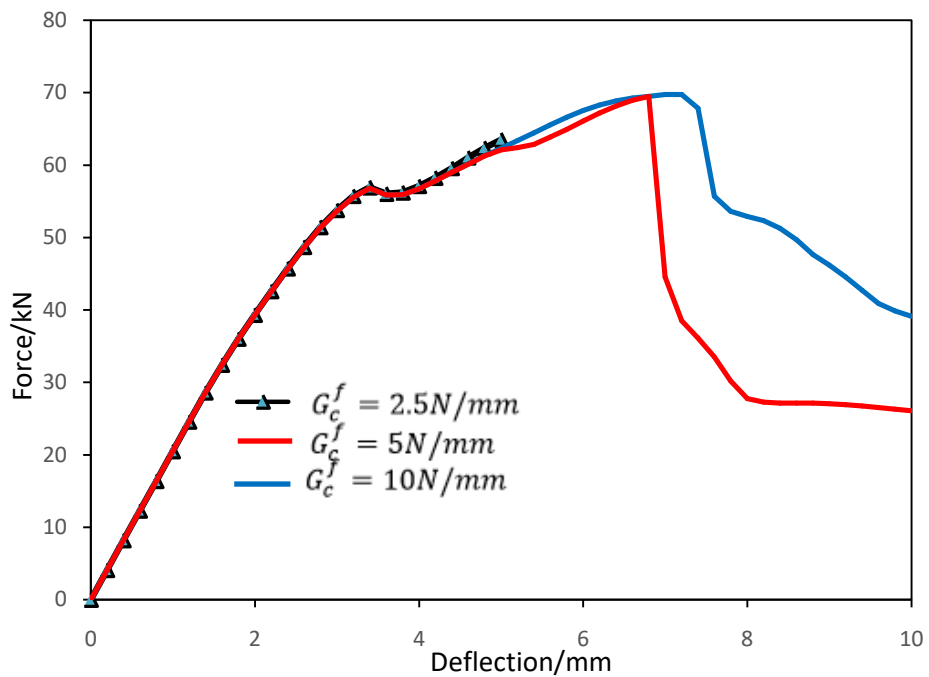
Figure 6.10 Influence of compressive fracture energy

Figure 6.10 illustrates the influence of compressive fracture energy on the behaviour of the masonry wall. It reveals that the parameter compressive

fracture energy does not influence the whole behaviour. However, it does slightly affect the failure point.

6.3.3 The influence of brick's parameters

As described in section two in chapter 5, there is a potential vertical crack placed through the middle part of every brick. This crack is modelled by using the same method with the brick-mortar interface. However, for simplicity, this interface is modelled with a discreet cracking element. In this case, only the normal/shear stiffness of the crack (K_{bn} and K_{bs}), tensile strength (f_{bt}) and fracture energy (G_f^{bt}) should be obtained in advance. The following section is the sensitivity parametric study carried out on these parameters.

Normal/shear stiffness (K_{bn}/K_{bs})

Similarly, the ratio of K_{bn} to K_{bs} is 2.3. The selected value of the normal stiffness ranges from 100 to $1E6 N/mm^3$. Figure 6.11 illustrates the influence of the normal/shear stiffness of the crack interface on the behaviour of the whole masonry wall panel. It clearly shows that the normal/shear stiffness does affect the stiffness and the failure load of the whole wall, however, this effect is minor. Therefore, for simplicity, this minor effect can be ignored in the parametric study. According to Lourenco (1996), the normal stiffness of brick crack can be taken as $1000 N/mm^3$.
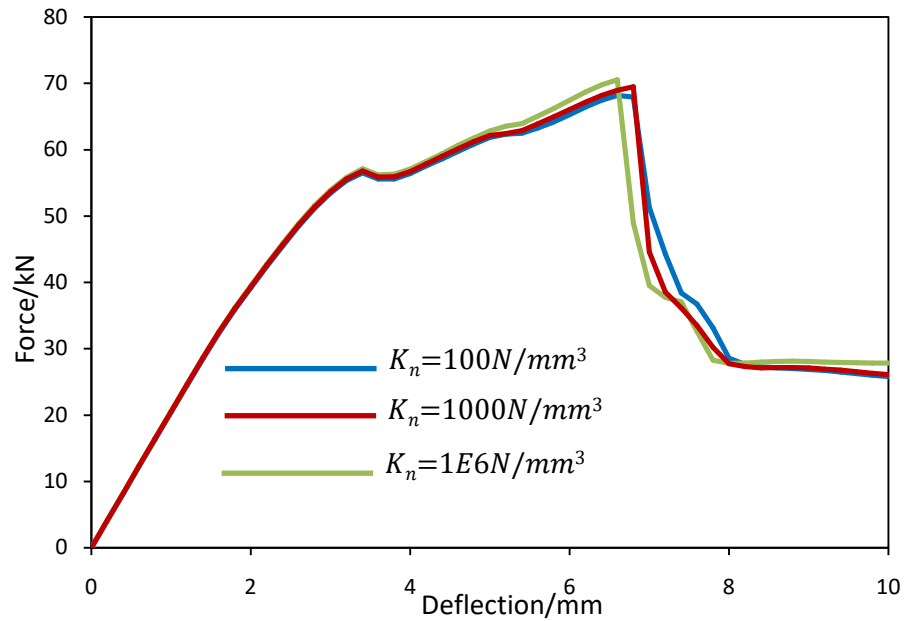
Figure 6.11 Influence of normal stiffness of brick crack

Brick element type

When we model the brick as deformable element, linear elastic and non-linear behaviour can be applied. Here in this section, both cases will be conducted to find out the variation between them.

Figure 6.12 demonstrates the influence of the brick element type on the global behaviour of the whole masonry wall panel. It reveals that no matter which type of element is used, the modelling produced similar results. This is because based on the literature review, the failures most likely occur along the interfaces (brick-mortar interfaces and brick crack interfaces). Therefore, the modelling element type of brick does not influence the final results by much. For simplicity, linear elastic element type will be used in the modelling.
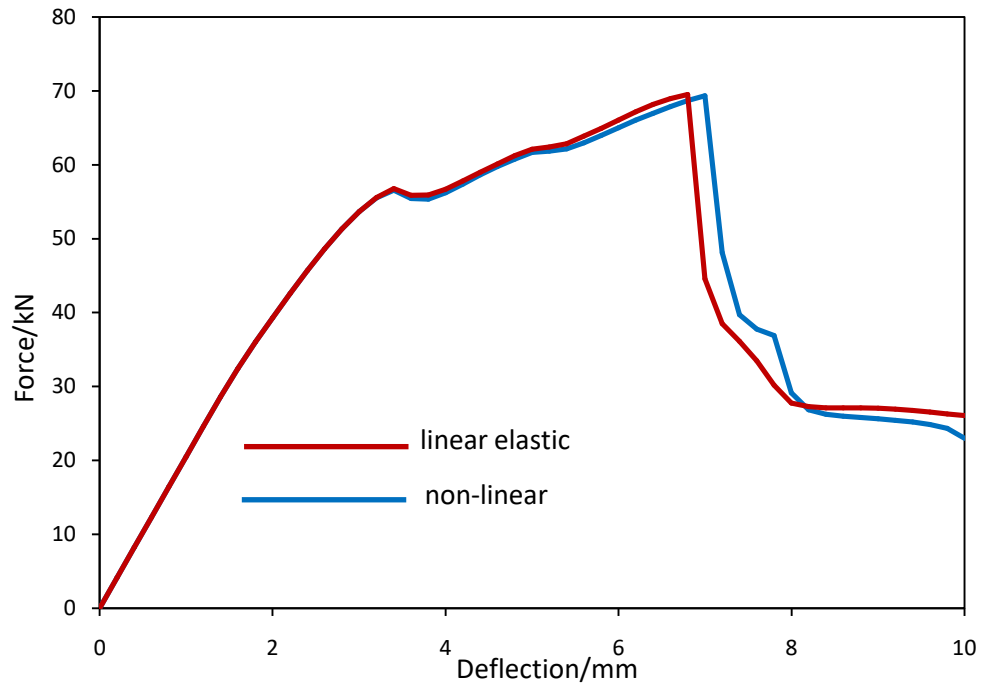
Figure 6.12 Influence of brick type

Tensile strength of brick crack (f_{bt})

Figure 6.13 illustrates the influence of the brick crack tensile strength on the behaviour of the masonry wall panel. The figure clearly reveals that the brick crack tensile strength only presents a minor influence on the behaviour of the final modelling results. This minor influence can be ignored in the simulation. According to the Lourenco (1996), the brick crack tensile strength for clay brick can be taken as $2N/mm^2$.
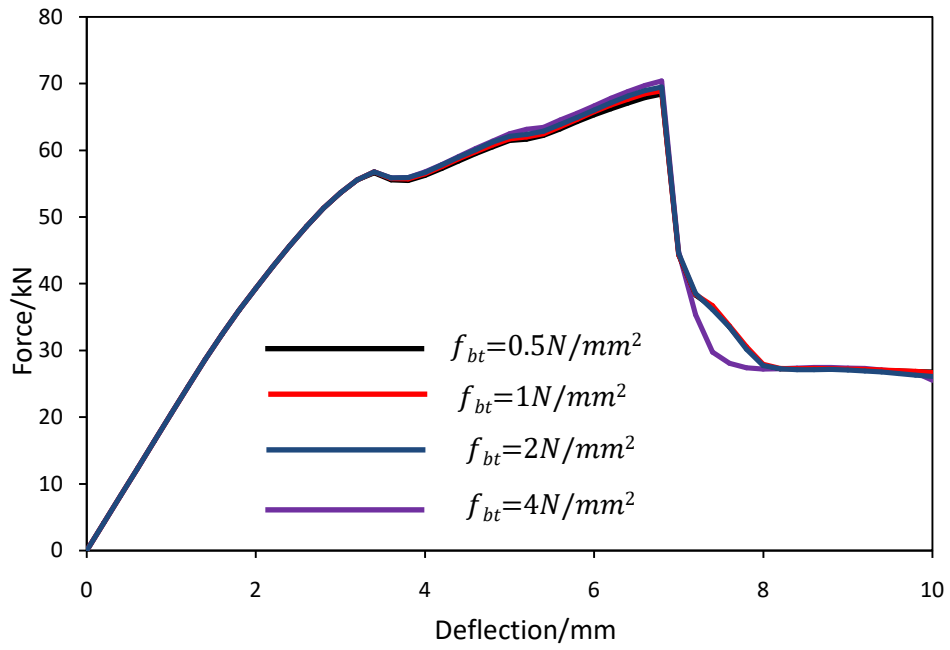
Figure 6.13 Influence of tensile strength of brick crack

Fracture energy of brick crack interface (G_f^{bt})
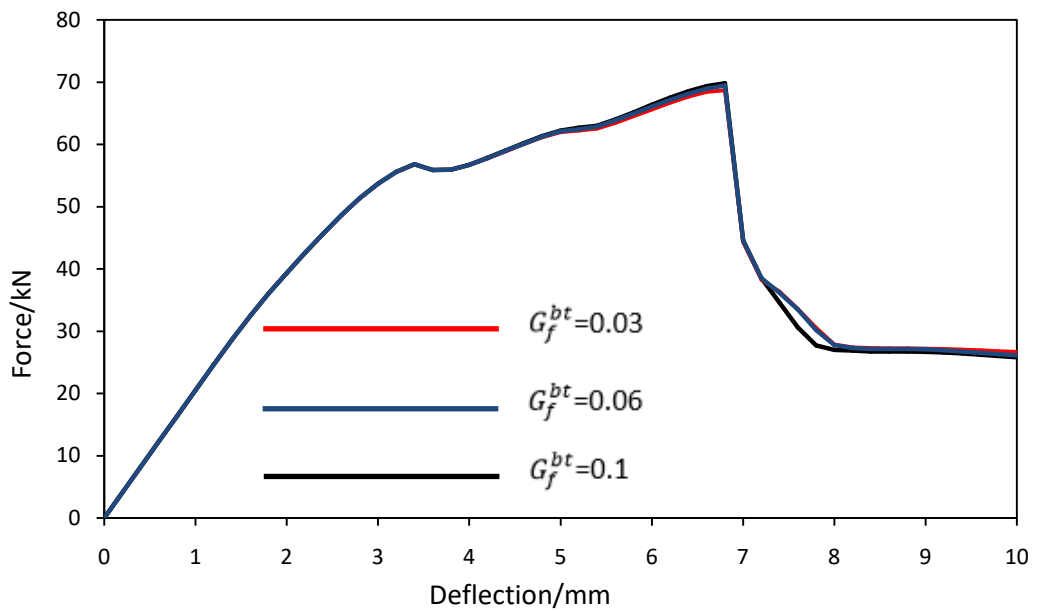
Figure 6.14 Influence of fracture energy of brick crack interface

Figure 6.14 presents the fracture energy of the brick crack on the mechanical behaviour of the masonry wall. It shows that the fracture energy nearly has no influence on the final results. According to the literature review presented in Chapter 2, the fracture energy will be taken as G_f^{bt}=0.08N/mm. This value will be used all through the following research.

6. 4   Results of analysis

Based on the above sensitivity parametric study, a summary on the influence of each parameter on the masonry wall can be concluded. The parameters will be categorized based on the significance of the influence.

6.4.1 Brick crack interface

Firstly, from Figure 6.11 to 6.14, after changing the brick type, normal stiffness, tensile strength, or tensile fracture energy, the final result is almost unchanged. It can be concluded that the influence of these parameters on the final results is very slight. This little influence can be ignored in the simulation work. The value of these parameters will be selected according to the literature review. The properties of a potential crack in a clay brick as shown in Table 6.3. These parameters will be used all through the research.

Table 6.3 Property of clay brick crack interface

Parameter	Normal stiffness	Shear stiffness	Tensile strength	Tensile fracture energy
Symbol	K_{bn} (N/mm^3)	K_{bs} (N/mm^3)	f_{bt} (N/mm^2)	G_f^{bt} (N/mm)
Value	1000	435	2	0.08

6.4.2 Brick-mortar interface

Based on the above sensitivity parametric studies, the property of the brick-mortar interface has had a significant influence on the mechanical behaviour of the masonry wall panel. However, the significance of different parameters varies on different stages. The influence can be categorized into three stages based on their significance. The load-displacement of single-leaf wall 3 is shown in Figure 6.15.
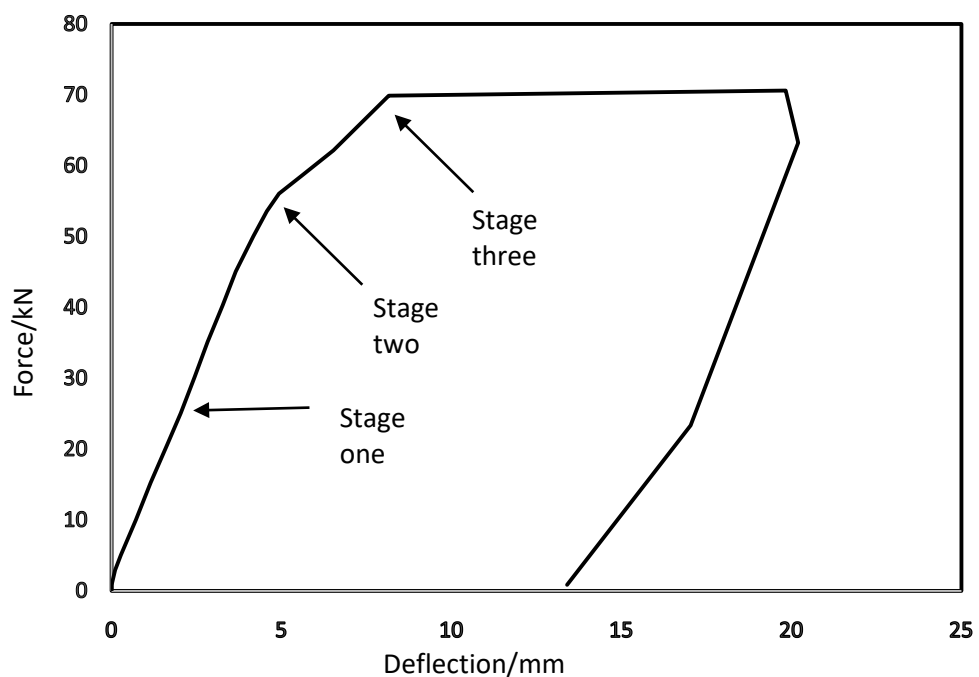
Figure 6.15 Experimental Load-deflection of a single-leaf wall

First stage (elastic stage)

This stage is the linear elastic stage. Here, the masonry wall behaves almost linearly under the combined external load. Based on the results from Figure 6.3 to 6.10, it can be concluded that only K_n/K_s and f_t of the interface have a significant influence on this stage. The influence of other parameters is very slight, which can be ignored in the simulation of this stage.

To prove that the other parameters do not affect stage one, the normal/shear stiffness and tensile strength of the interface will remain constant, while the rest of the parameters will be variable. Figures 6.16 and 6.17 demonstrate the influence of the two combinations of the rest of the parameters if they are taken into account at the same time. From both figures, it is proven that the rest of the parameters do not have a big influence on stage one.
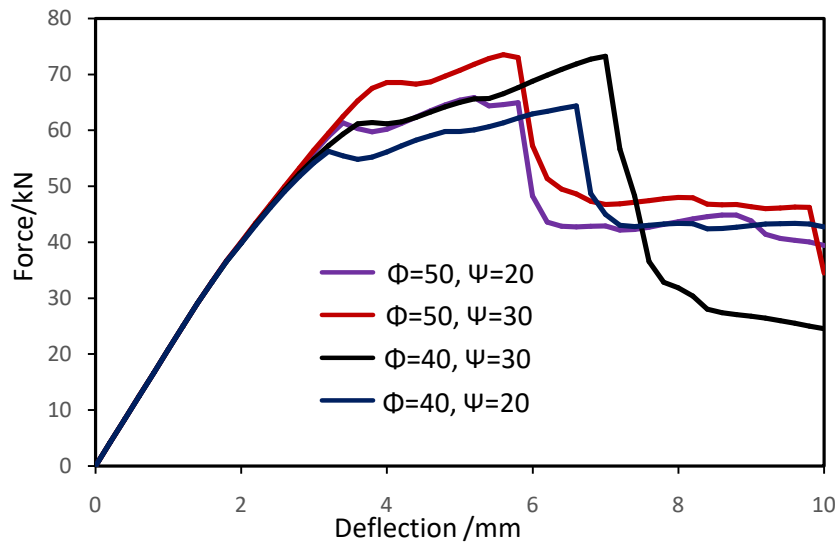
Figure 6.16 Influence of other parameters on stage one
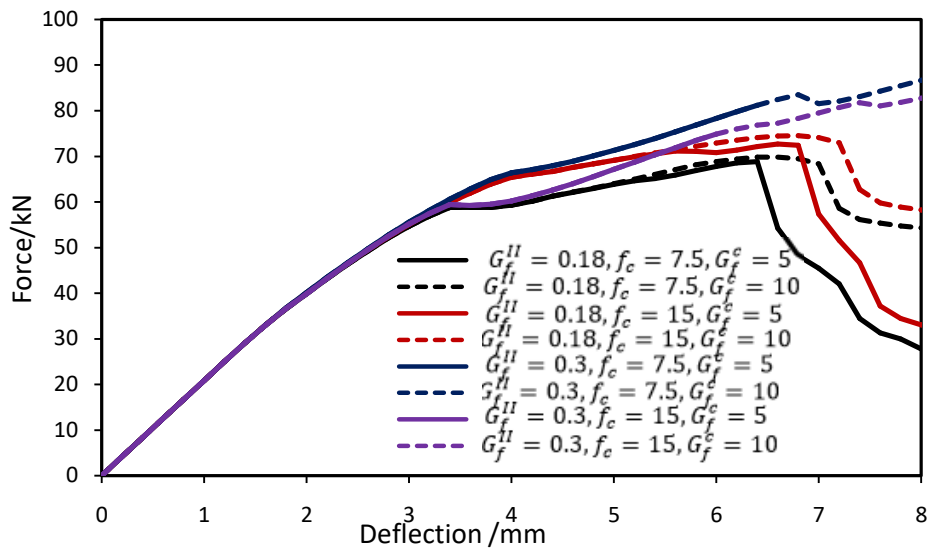
Figure 6.17 Influence of other parameters on stage one

Second stage (re-distribution stage)

This stage is the load re-distribution stage. At this stage, small cracks were connected together and formed big cracks. However, the wall did not fail. The load was re-distributed among the wall. After the re-distribution, the wall continued to carry more load. According to the figures from Figures 6.3 to 6.10, parameters like K_n/K_s, f_t, $\tan \Phi$, $\tan \Psi$, G_f^{II}, G_f^{II} and play an important role in this stage. The other parameters do not have any remarkable influence on the results. As K_n/K_s and f_t have already been calibrated in the first stage, therefore, only $\tan \Phi$, $\tan \Psi$, G_f^{I} and G_f^{II} need to be calibrated via parametric study for in this stage.

To prove that the other parameters do not affect stage two, the aforementioned parameters will remain constant while only f_c and G_c^{f} are variable. Figure 6.18 shows the influence of these two parameters on stage two. From the figure, it can be clearly seen that these two parameters do not influence stage two at all.
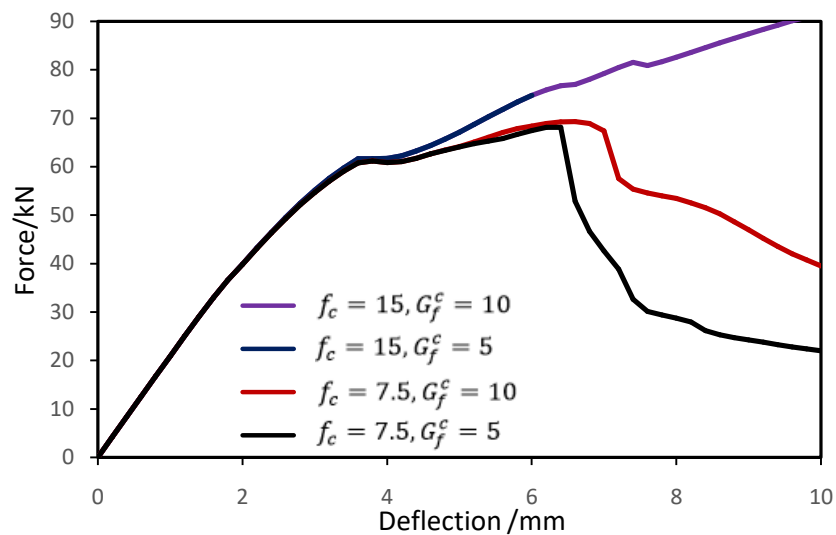
Figure 6.18 Influence of other parameters on stage two

Third stage (Failure point)

The third stage is the failure stage. At this stage, the masonry wall reached its maximum load capacity. After this stage, the wall could not carry any more load, and it started to fail. As demonstrated in Figures 6.3 to 6.10 that parameters like K_n/K_s, f_t, $\tan \Phi$, $\tan \Psi$, G_f^I, G_f^{II}, f_c and G_f^c remarkably influence the mechanical behaviour of masonry wall. However, K_n/K_s, f, $\tan \Phi$, $\tan \Psi$, G_f^{II}, G_f^I have already been obtained in the first two stages. Therefore, only f_c and G_c^f are needed in this stage.

6. 5 Calibration work

6.5.1 Methodology

As the influence of parameters on each stage is known in Section 6.4, the material calibration work can be carried out stage by stage. The aim of the calibration work is to "tune" the difference between the numerical and experimental results.

After the calibration of parameters in stage one, stage two and three can be carried out using the same process and method. The methodology of material parameter calibration for stage one is illustrated in Figure 6.19.

In detail, this calibration approach can be expressed as following steps: (1) Select the initial value of the parameters based on the literature and assign them in the FE model. In this step, the initial value of the parameters that affect stage one will be selected and kept variable while the other parameters will be kept constant based on the literature.(2) Compare the numerical result with the experimental result. Only the results obtained from stage one will be compared and analysed. (3) Shrink the range of the initial parameters based on the comparison and assign them back to the model. By this process, the initial range will be shrunk and more accurate value will

be obtained. (4)Repeat step (2) and (3) until a satisfied result is obtained. (5) Apply the same process to calibrate the parameters in stage two and three until all the parameters needed have been calibrated.

By applying this calibration methodology, the results obtained will not be exactly the same as the experimental results. However, as the properties of masonry materials always vary even if in the same conditions, it is impossible to obtain completely accurate material property. The aim of the calibration work is to obtain the optimum estimation of the unknown model parameters as it is very unlikely to take all the influence factors into account. The estimation of the material parameters obtained from this approach can be referred to as the maximum likely estimates.
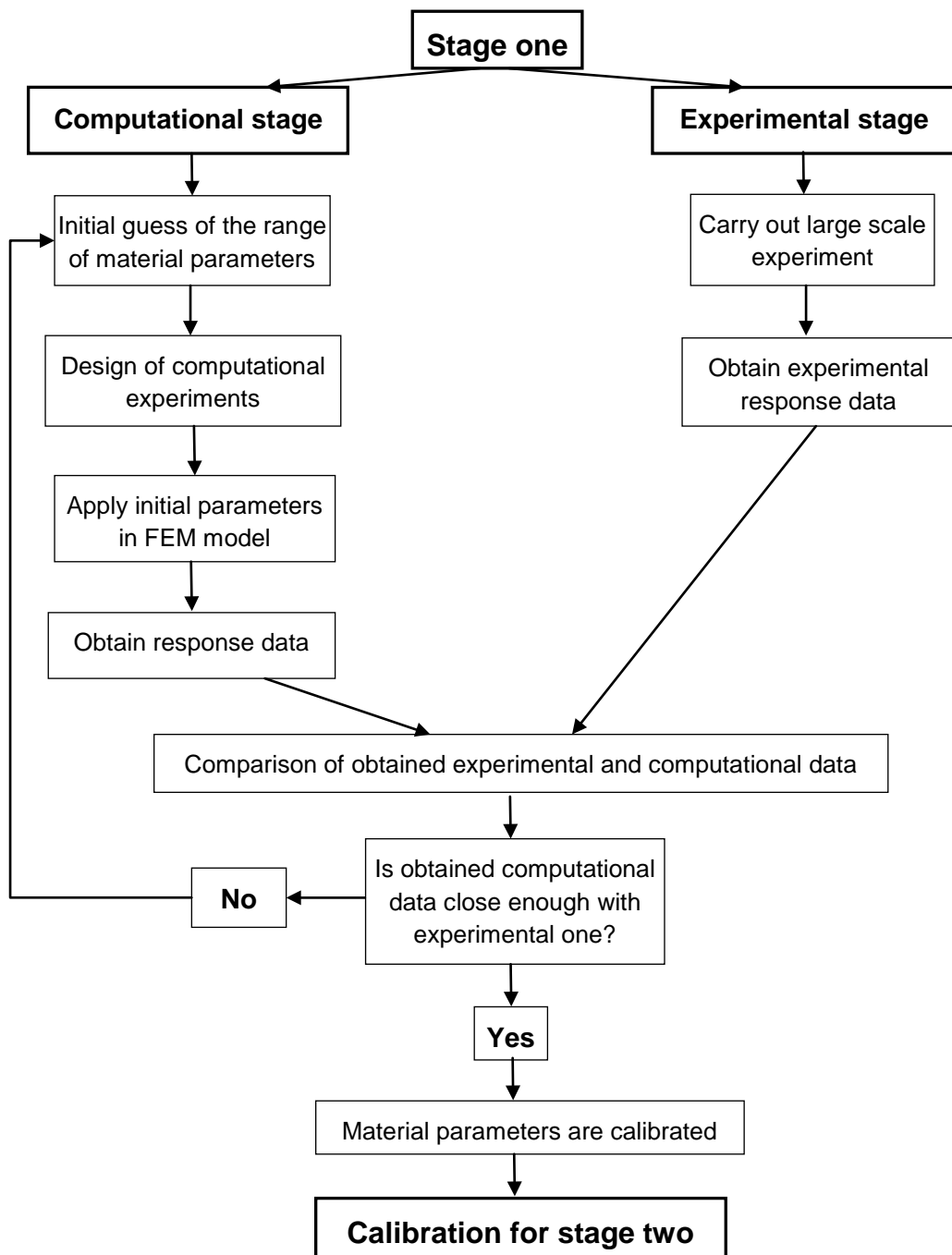
Figure 6.19Methodology for the calibration of material parameters

6.5.2 First stage (Linear stage)

Figure 6.14 shows that the behaviour of masonry wall in first stage is almost linear, therefore, the initial stiffness of the wall can be obtained by dividing the load by displacement, which is shown in the Equation 6.8:

$$K = \frac{F_i}{D_i} \tag{6.8}$$

where K is the initial stiffness of the masonry wall, is the lateral load at point , and is the displacement at point . Point is where the point still lays in the linear stage. It is known from the experimental result (the stiffness of Wall 3 in linear stage) that the stiffness of the masonry wall $K = 12.6 kN/mm$.

Based on Figure 6.3, the normal stiffness (K_n) of the brick-mortar interface is between 8.2 to $17.4 N/mm^3$. The parametric study was carried out with normal stiffness increase of $1.64 N/mm^3$, and the increase of tensile strength is $0.1 N/mm^2$ from 0.1 to $0.5 N/mm^2$. The value range of the parameters are presented in Table 6.4. Only the normal stiffness and tensile strength are variables, the rest are taken from Lourenco's (1996) work and remained constant.

Table 6.4 Ranges of brick-mortar interface used in MIDAS

Parameter		Value
Variables	Normal stiffness(N/mm^3)	**8.2, 9.84,11.48, 13.12,14.76, 16.4**
	Shear Stiffness (N/mm^3)	**/2.3**
	Tensile strength (N/mm^2)	**0.1, 0.2, 0.3, 0.4, 0.5**
Constants	Mode I fracture energy $G_f^I (N/mm)$	0.018
	Cohesion (N/mm^2)	0.35
	Friction coefficient	0.75
	Dilatancy coefficient	0.6
	Mode II fracture energy (N/mm)	0.125
	Compressive strength (N/mm^2)	8.5
	Compressive fracture energy $G_f^c (N/mm)$	5

$\frac{F_i}{D_i}$

By selecting the initial value for each parameter, the results of different combinations are produced. Here the stiffness result of every combination will be compared with the experimental results. After the comparison, the initial range was shrunk and then the further finer calibration was carried out. By repeating the above process, a final value range will be acquired. After applying these parameters in MIDAS FEA, the final results are illustrated in Figures 6.20 and 6.21.
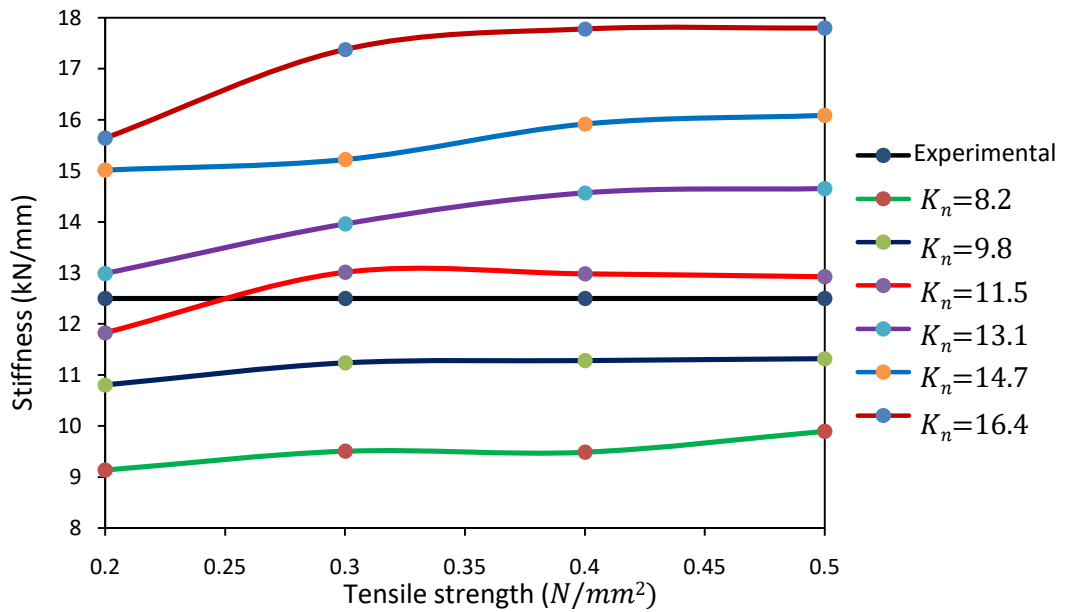
Figure 6.20 Influence of tensile strength and normal stiffness of brick-mortar interface on the first stage
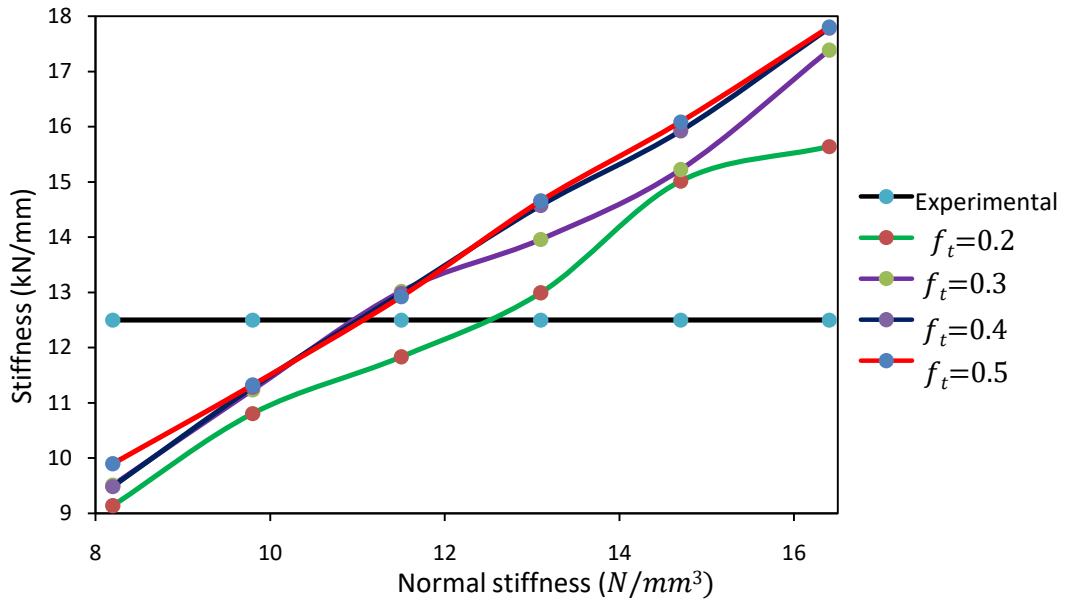
Figure 6.21 Influence of normal stiffness and tensile strength of brick-mortar interface on the first stage of masonry wall

According to Figure 6.20, it can be seen that the tensile strength of the experimental result lies between 0.2 to $0.4 N/mm^2$. Therefore, it can be concluded that the value of the tensile strength of the interface is between 0.2 to $0.4 N/mm^2$. Similarly, the normal stiffness of the interface is between 11 to $13 N/mm^3$. However, both the stiffness and tensile strength vary within a big range. Therefore, a second calibration is needed in order to get a finer value. In the second calibration, the initial range has been shrunk. For the second parametric study, the range of tensile strength is from 0.2 to $0.4 N/mm^2$ with every increment of   while the range of normal stiffness is from 11 to $13 N/mm^3$ with every increment of $0.5 N/mm^3$. The numerical results are demonstrated in Figure 6.22 and 6.23.
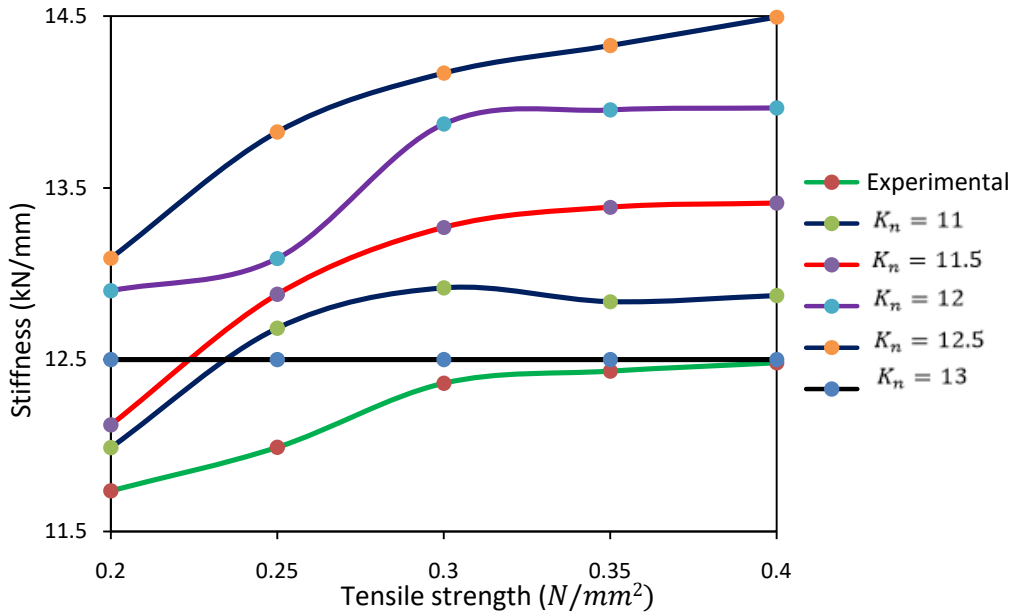
Figure 6.22 Influence of tensile strength and normal stiffness of brick-mortar interface on the first stage of masonry wall
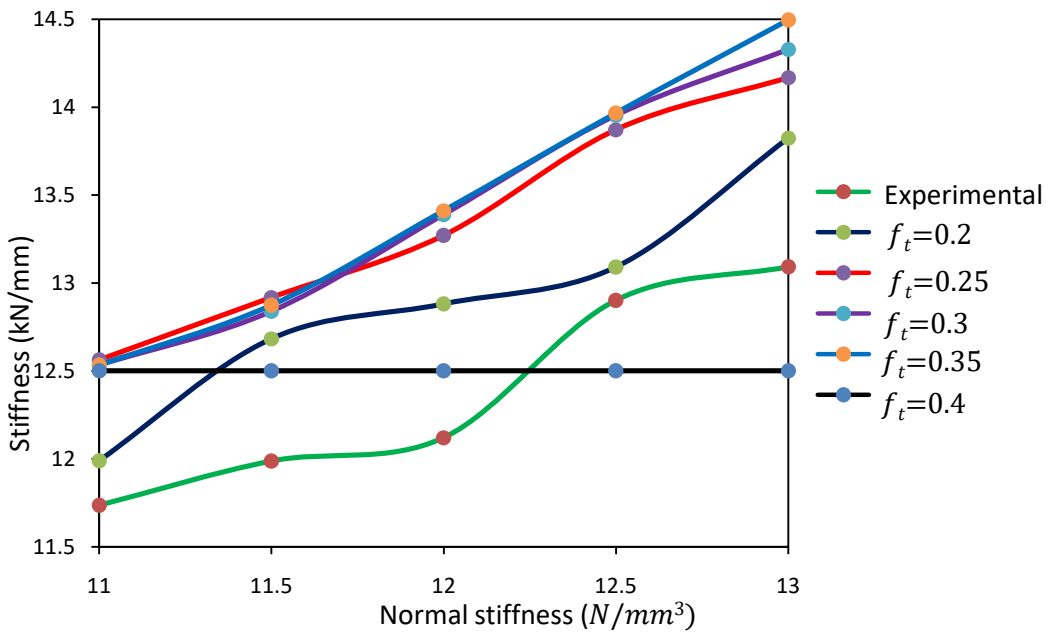
Figure 6.23 Influence of normal stiffness and tensile strength of brick-mortar interface on the first stage of masonry wall

According to Figures 6.22 and 6.23, it can be concluded that the value of the tensile strength of the interface is between 0.22 to $0.25 N/mm^2$, and the

normal stiffness of the interface is between 11.4 to $12.2 N/mm^3$. This range is still a little wide for value selection. Therefore, a third calibration is needed. In the third parametric study, the range of tensile strength is from 0.22 to 0.25 N/mm^2 with every increment of while the range of normal stiffness is from 11.4 to $12.2 N/mm^3$ with every increment of $0.2 N/mm^3$. The numerical results are shown in Figures 6.24 and 6.25
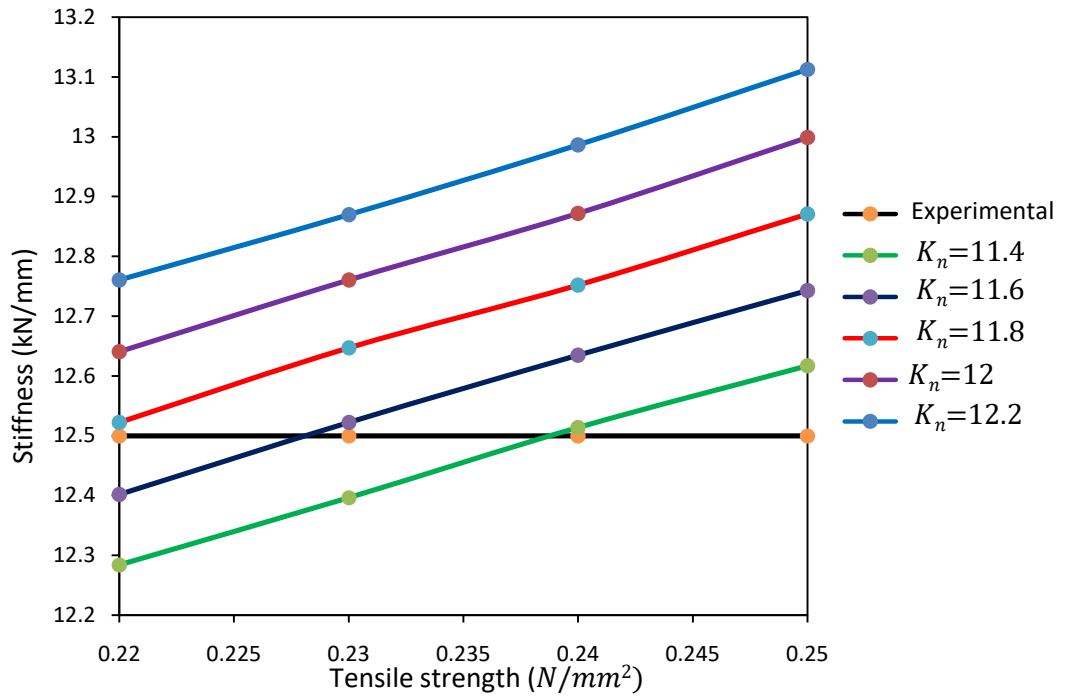
Figure 6.24 Influence of tensile strength and normal stiffness of brick-mortar interface on the first stage of masonry wall
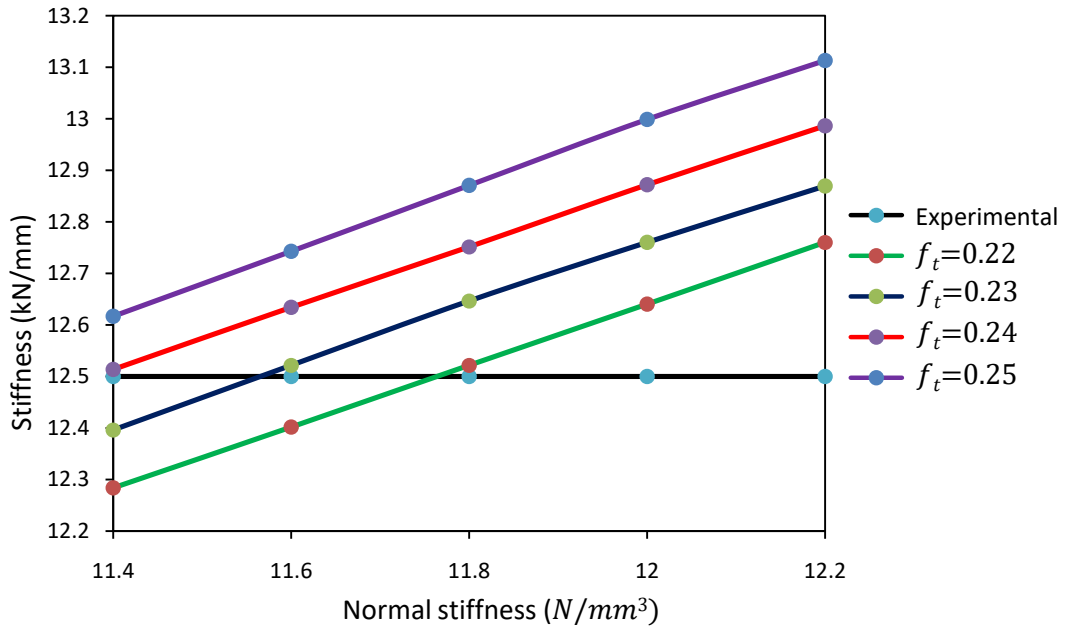
Figure 6.25 Influence of normal stiffness and tensile strength of brick-mortar interface on the first stage of masonry wall

Figures 6.24 and 6.25 reveal that the value of the tensile strength of the masonry wall is between 0.228 to $0.24 N/mm^2$, and the normal stiffness is between 11.55 to $11.8 N/mm^3$. Taken as an average of them, the tensile strength is $0.235 N/mm^2$ and the normal stiffness is $11.7 N/mm^3$. The obtained parameters are shown in Table 6.5:

Table 6.5 Calibrated parameters of interface

Parameter	Symbol	Value
Normal stiffness(N/mm^3)	K_n	11.7
Shear Stiffness (N/mm^3)	K_s	5.1
Tensile strength (N/mm^2)	f_t	0.235

6.5.3 Stage two (Load re-distribution stage)

After the tensile strength and normal stiffness having been obtained, stage two can be carried out. In this stage, four parameter, $\tan\Phi$, $\tan\Psi$, G_f^I and G_f^{II} need to be characterized. It is assumed that G_f^{II} equals to $10G_f^I$ (Stavridis and Shing 2008), therefore, only three parameters should be calibrated in the simulation. Furthermore, the value of $\tan\Phi$ is between 0.7 to 1.2 or the friction angle ranges from 30^0 to 50^0, $\tan\Psi$ is between 0.2 to 0.7 or dilatancy angle ranges from 10^0 to 30^0, and G_f^{II} is between 0.01 o $0.25 N/mm^2$. Therefore, the selection of initial range has already been minimized.

The parametric study will be carried out with the friction angle increase of 5^0, the increase of dilatancy angle is 12.5^0, and the increment of G_f^{II} is $0.1N/mm^2$ from 0.01 to $0.31N/mm^2$. The parameters are shown in Table 6.6, the rest are taken from Lourenco's (1996) work and remained constant.

Table 6.6 Ranges of brick-mortar interface used in MIDAS

Parameter		Symbol	Value
Constants	Normal stiffness(N/mm^3)	K_n	11.7
	Shear Stiffness (N/mm^3)	K_s	5.1
	Tensile strength (N/mm^2)	f_t	0.235
	Cohesion (N/mm^2)	C	0.329
	Compressive strength (N/mm^2)	f_m	8.5
	Compressive fracture energy (N/mm)	G_f^c	5
Variables	Mode I fracture energy (N/mm)	G_f^I	G_f^{II}/10
	Friction coefficient	φ	30,35,40,45,50
	Dilatancy coefficient	Ψ	10,22.5,35
	Mode II fracture energy (N/mm)	G_f^{II}	0.01,0.11,0.21,0.31

In stage two, the load and displacement at the re-distribution point is 57kN and 4.85mm, respectively (Figure 4.14). After assigning the above parameters in the model, the computational results are obtained and they will be compared with the experimental results. For the first calibration, the results are presented in Figures 6.26, 6.27 and 6.28.
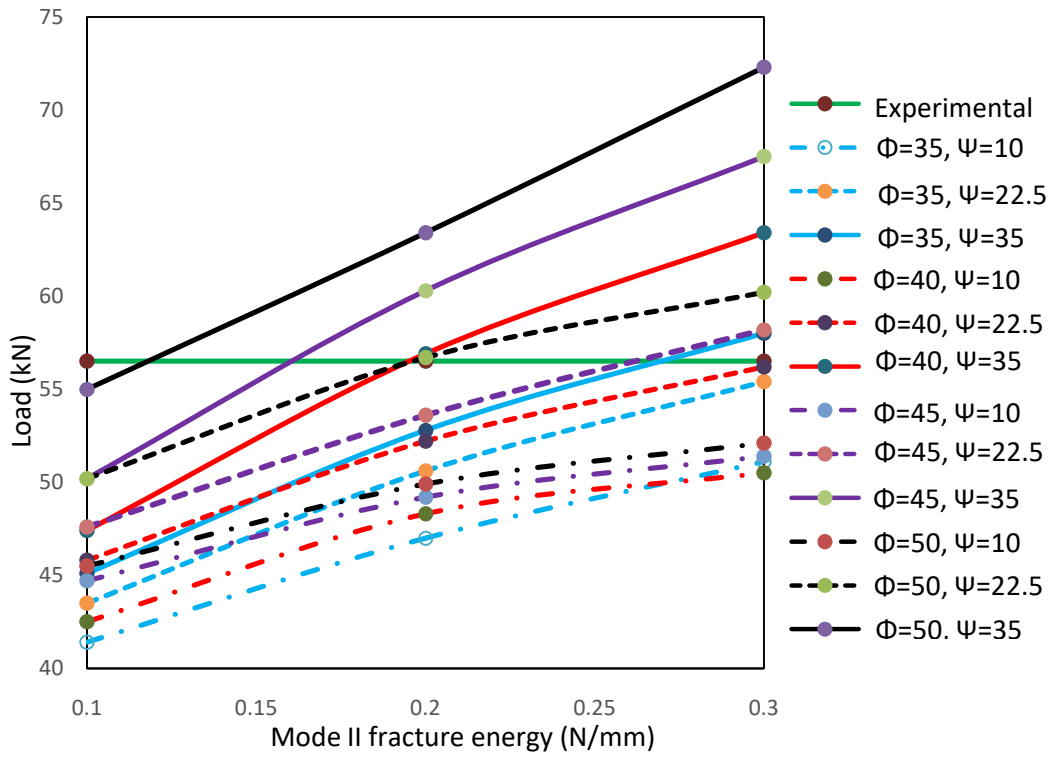
(a). Influence on the load
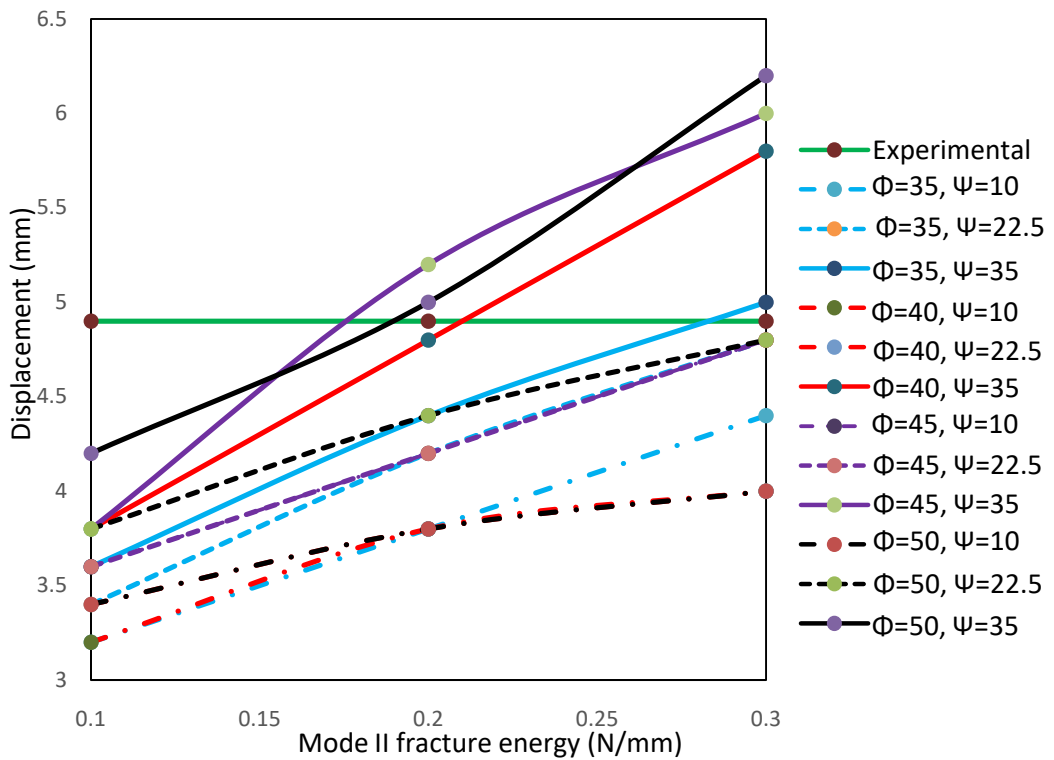
(b). Influence of on the displacement

Figure 6.26 Influence of Mode II fracture energy on stage two
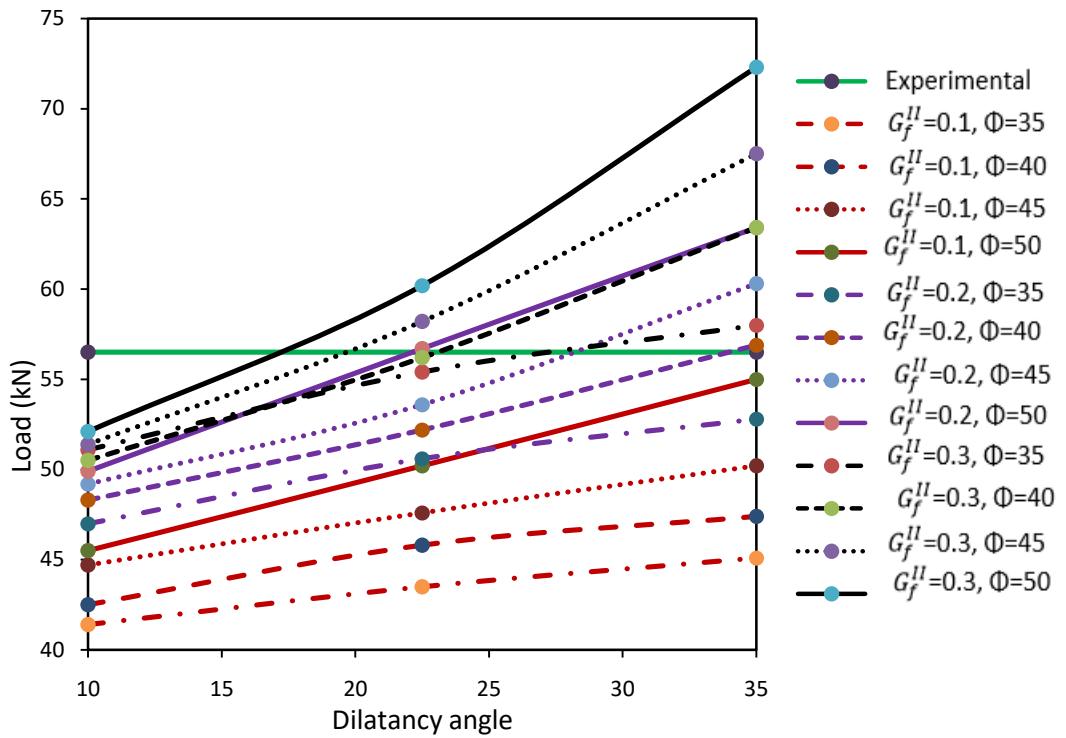
(a). Influence on the load
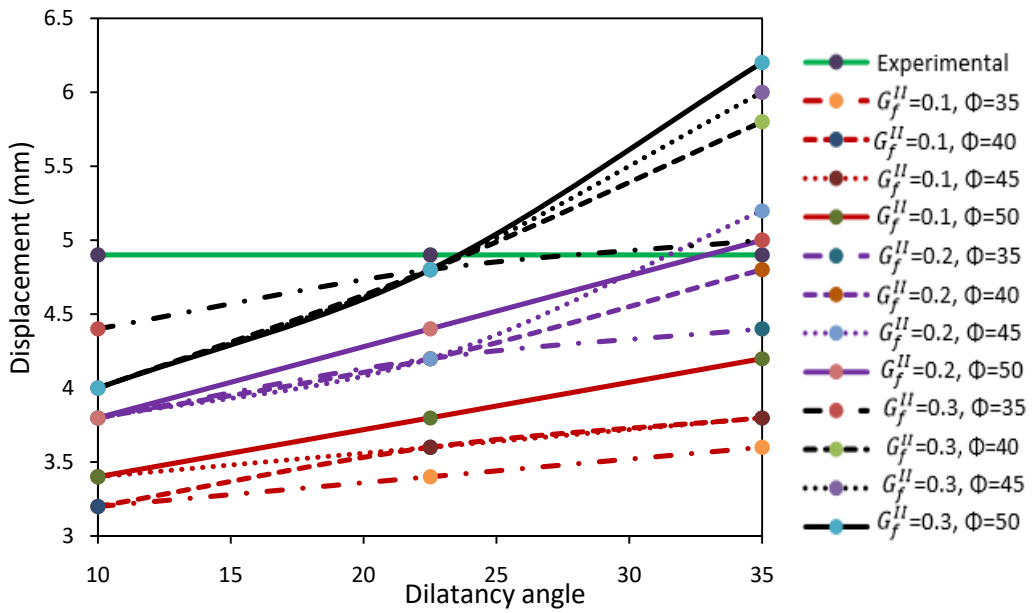
(b). Influence on the displacement

Figure 6.27 Influence of dilatancy angle on stage two
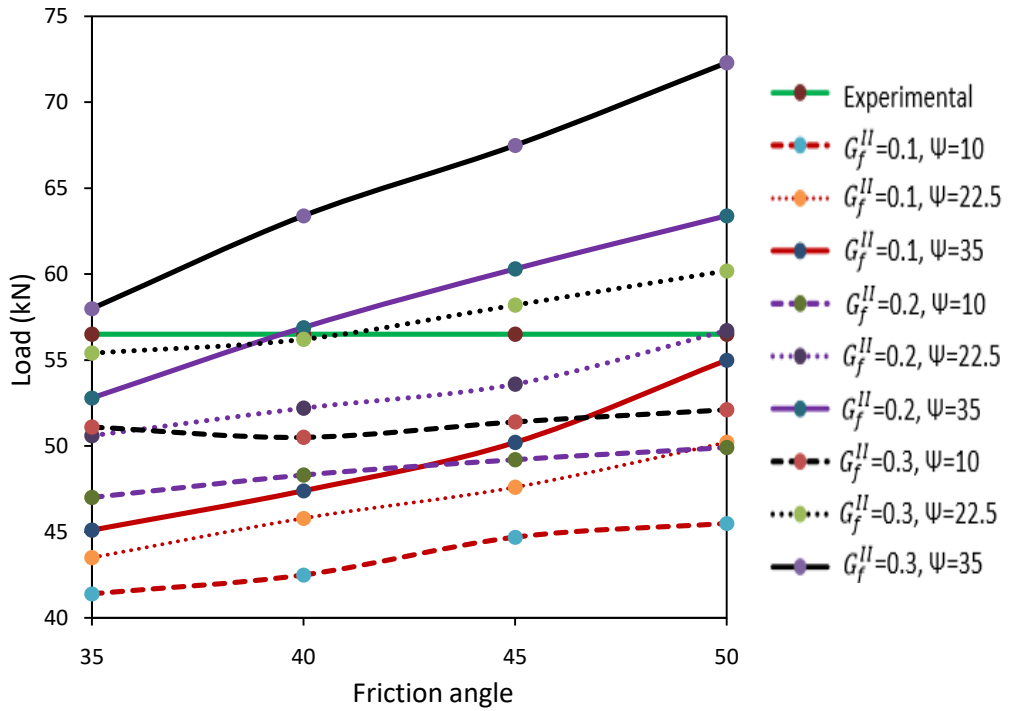
(a). Influence on the load
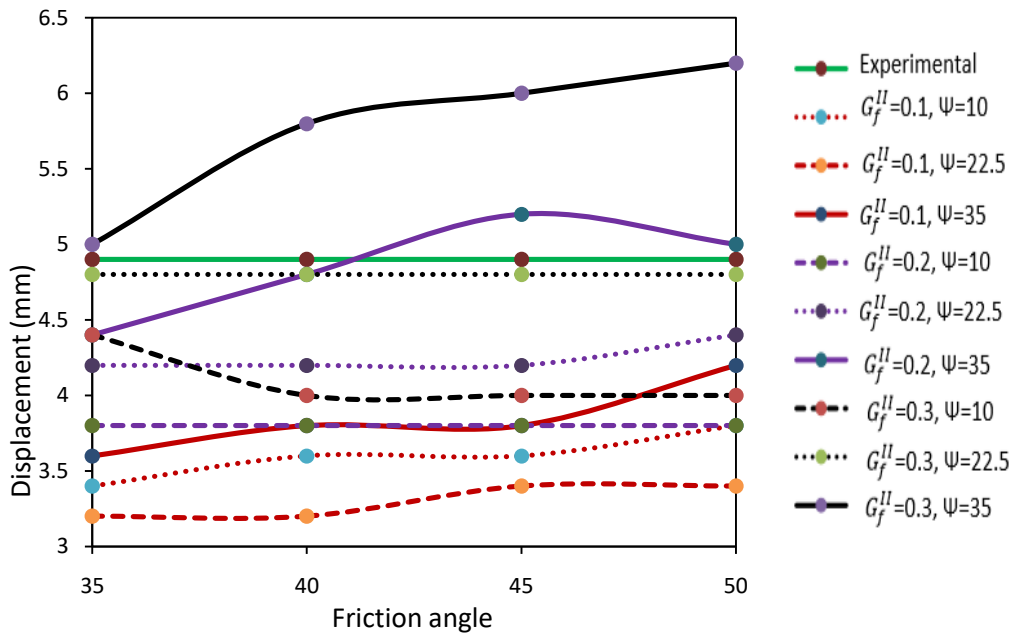
(b). Influence on the displacement

Figure 6.28 Influence of friction angle on stage two

Based on Figure 6.26 (a) and (b), it can be concluded that the value of Mode II fracture energy ranges from 0.15 to 0.25. Similarly, it can be obtained from

Figure 6.27 (a) and (b) that the value of dilatancy angle ranges from 22 to 28. Figure 6.28 (a) and (b) reveal that the value of friction angle ranges from 40^0 to 45^0.

As the value still lies between wide ranges for each parameter, a second calibration is needed. The same procedure needs to be repeated and the results are displayed in Figures 6.29, 6.30 and 6.31.
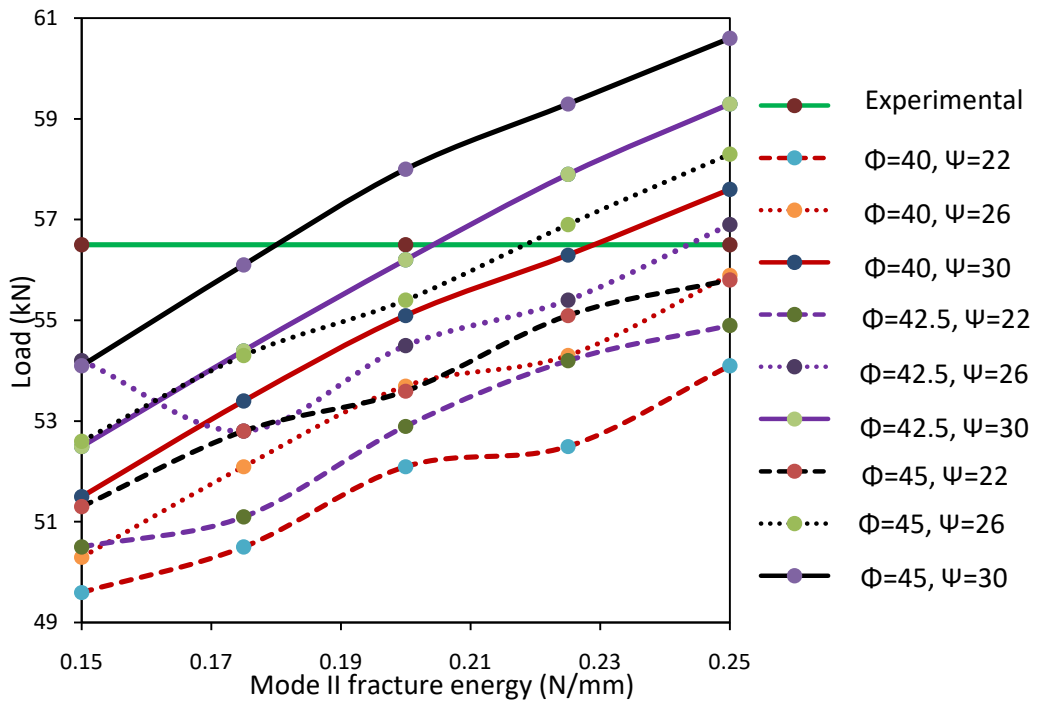
(a). Influence on the load
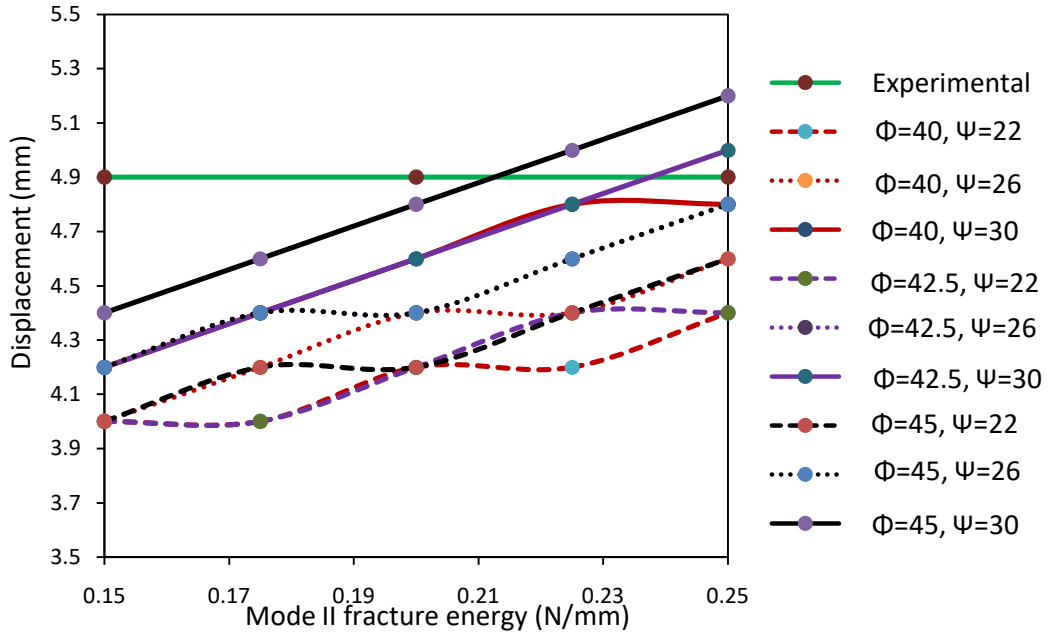
(b). Influence on the displacement

Figure 6.29 Influence of Mode II fracture energy on stage two
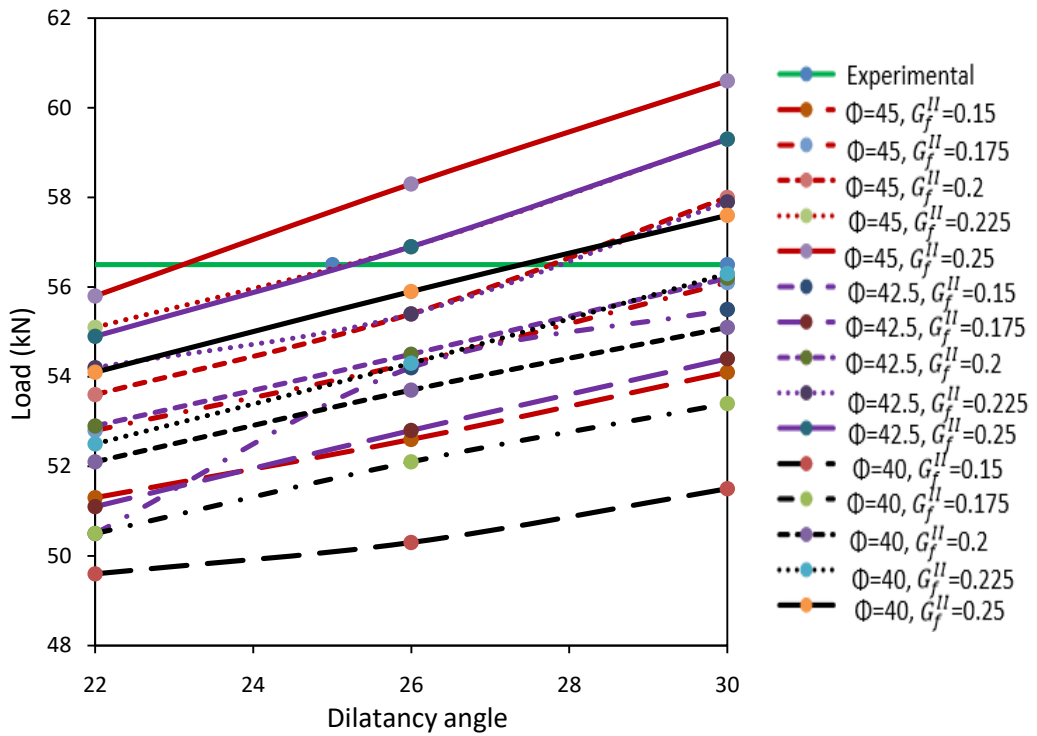
(a). Influence on the load
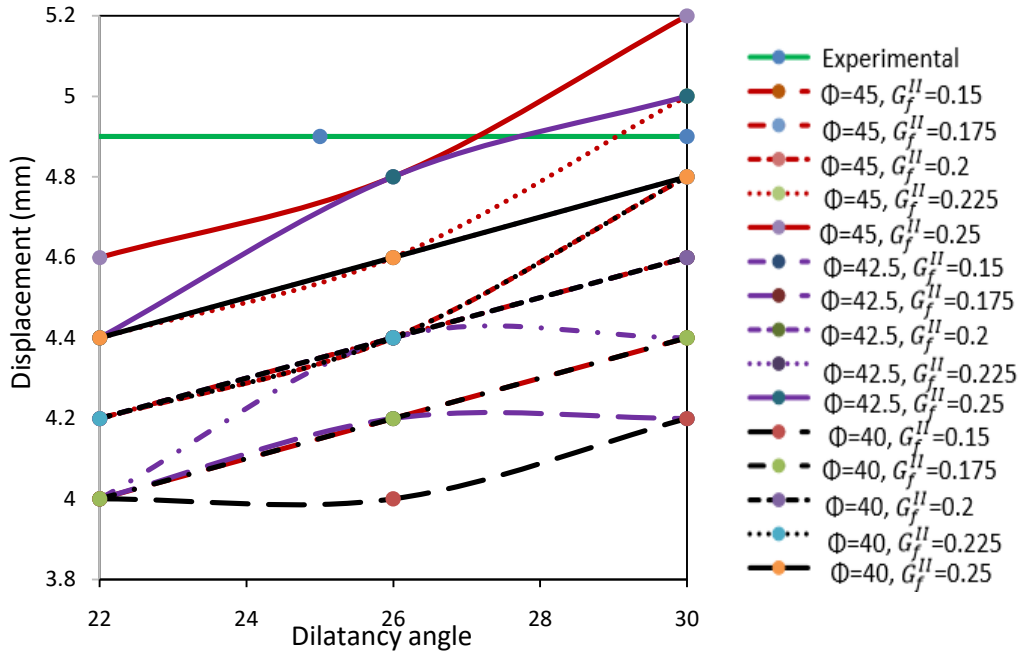
(b). Influence on the displacement

Figure 6.30 Influence of dilatancy angle on stage two
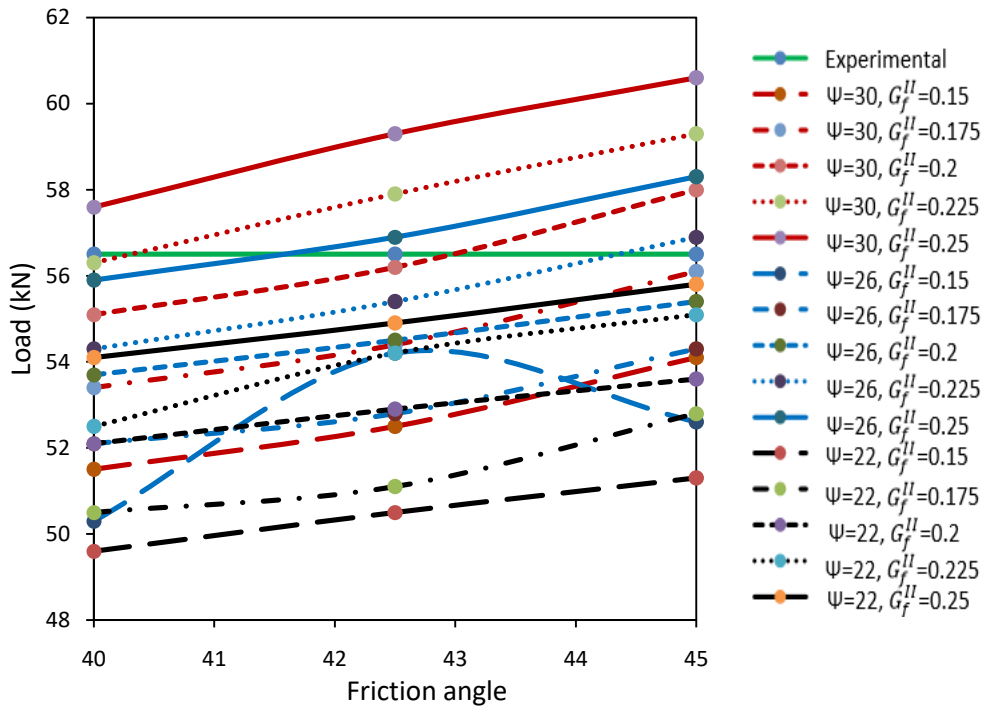
(a). Influence on the load
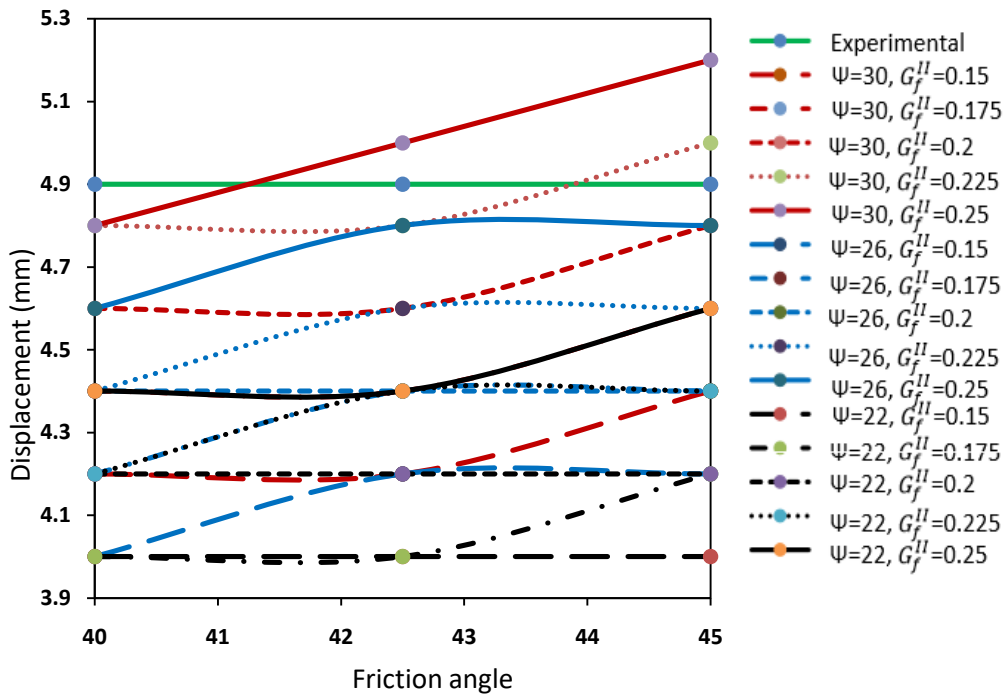
(b). Influence on the displacement

Figure 6.31 Influence of dilatancy angle on stage two

According to Figure 6.29 (a) and (b), it can be concluded that the value of Mode II fracture energy is between 0.21 to 0.24 with an average value of 0.225. From Figure 6.30 (a) and (b), it can be observed that the value of dilatancy angle is between 27^0 and 28^0 with its average value as 27.5^0. Similarly, it can be obtained from Figure 6.31 (a) and (b) that the value of friction angle is between 41.5^0 and 43.5^0 with the average value of 42.5^0. So far, the obtained parameters are shown in Table 6.7.

Table 6.7 Calibrated parameters of the interface

Parameter	Symbol	Value
Normal stiffness(N/mm^3)	K_n	11.7
Shear Stiffness (N/mm^3)	K_s	5.1
Tensile strength (N/mm^2)	f_t	0.235
Mode I fracture energy (N/mm)	G_f^I	0.0225
Cohesion (N/mm^2)	C	0.329
Friction coefficient	ϕ	42.5
Dilatancy coefficient	Ψ	27.5
Mode II fracture energy (N/mm)	G_f^{II}	0.225

6.5.4 Stage three (Failure stage)

After the tensile strength and normal stiffness were obtained in stage one, and friction angle, dilatancy angle, Mode I fracture and Mode II fracture energy were obtained in stage two, the calibration work on stage three can be carried out. In this stage, only two parameters, compressive strength and compressive fracture energy need to be characterized. The parametric study will be carried out with the variables shown in Table 6.8.

In this stage, the maximum load and displacement of masonry wall at failure point is 69kN and 8.2mm, respectively. The numerical results of calibration work will be compared with the experimental results, which are displayed in Figures 6.32 and 6.33.

Table 6.8 Ranges of brick-mortar interface used in MIDAS

|	Parameter	Symbol	Value
Constants	Normal stiffness(N/mm^3)	K_n	11.7
	Shear Stiffness (N/mm^3)	K_s	5.1
	Tensile strength (N/mm^2)	f_t	0.235
	Mode I fracture energy (N/mm)	G_f^I	0.0225
	Cohesion (N/mm^2)	C	0.329
	Friction coefficient	ϕ	42.5
	Dilatancy coefficient	Ψ	27.5
	Mode II fracture energy (N/mm)	G_f^{II}	0.225
Variables	Compressive strength (N/mm^2)	f_c	**1, 5,10, 20, 40**
	Compressive fracture energy (N/mm)	G_f^c	**1, 2.5, 5, 10, 20**
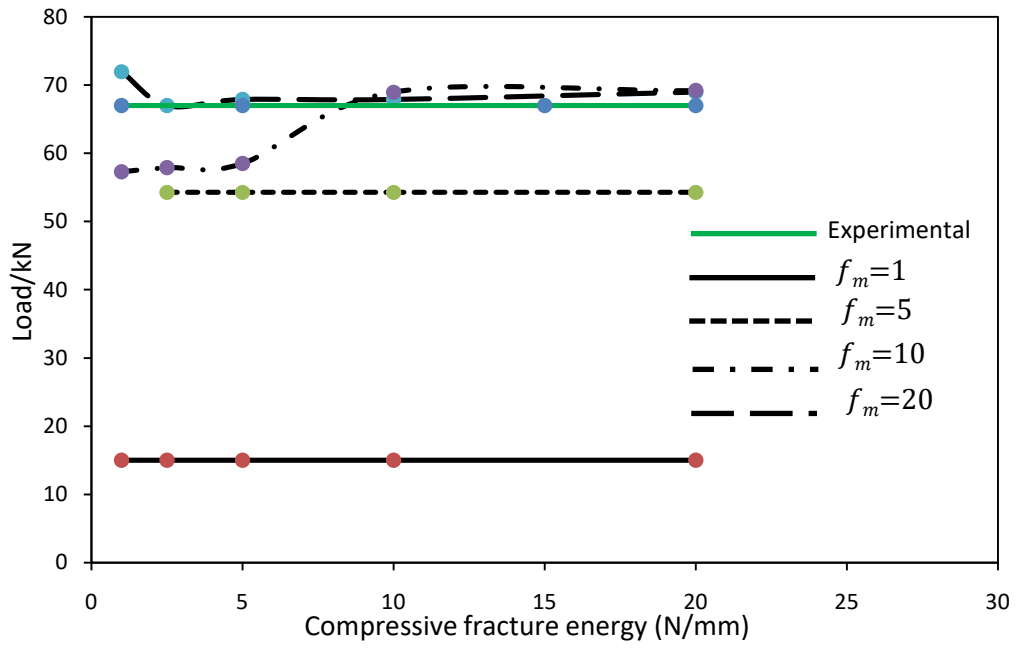
(a) Influence on the load
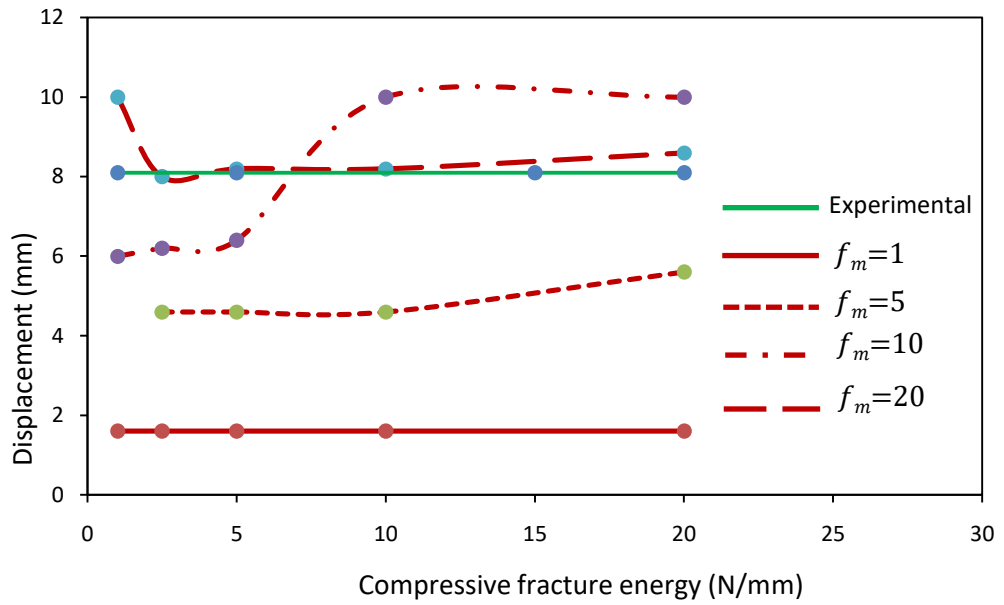
(b) Influence on the displacement

Figure 6.32 Influence of compressive fracture energy on the masonry wall
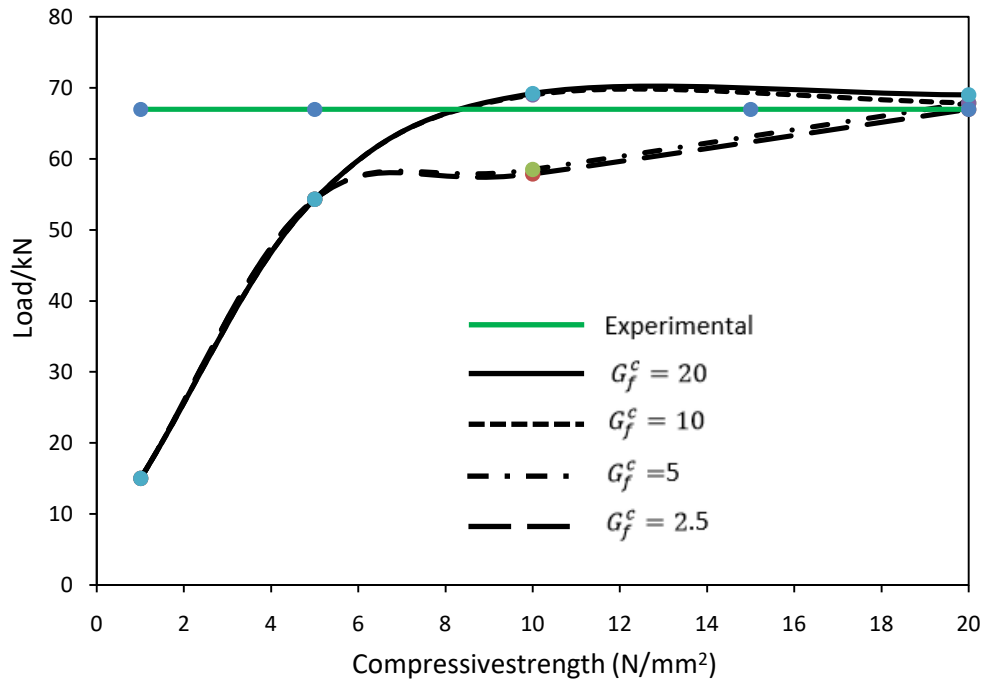
(a). Influence on the load
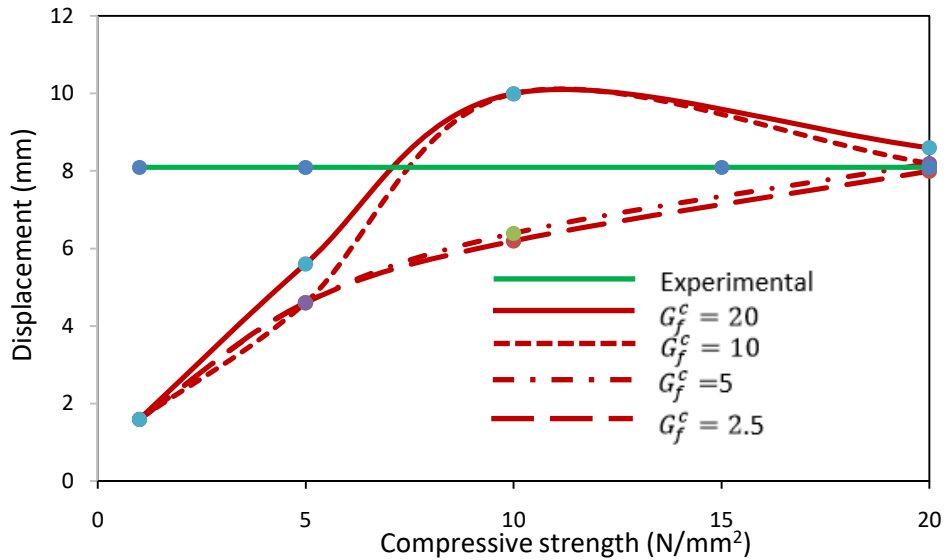
(b). Influence on the displacement

Figure 6.33 Influence of the compressive strength on the masonry wall

Based on Figure 6.32 (a) and (b), the value of the compressive fracture energy ranges from 5 to 10. Similarly for Figure 6.33 (a) and (b), it can be concluded that the value of the compressive strength ranges from 5 to 10. A

finer calibration is needed. The results of the finer calibration are shown in Figures 6.34 and 6.35.
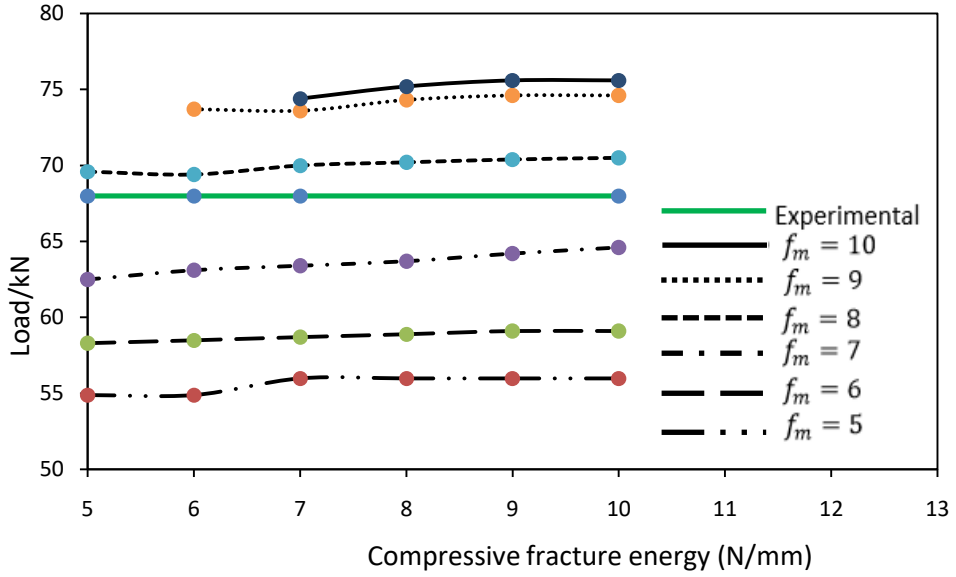
(a) Influence on the load
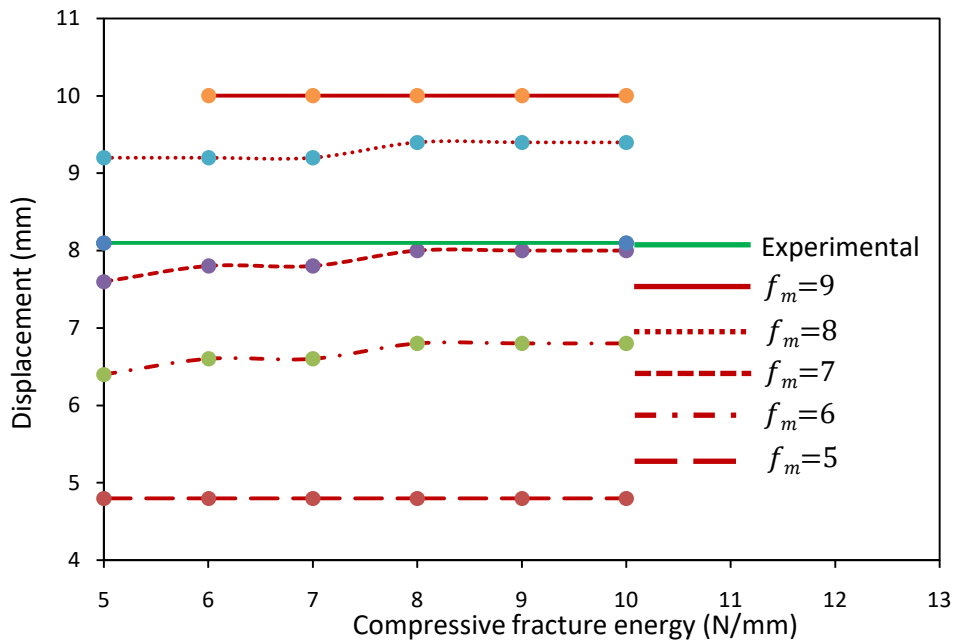
(b) Influence on the displacement

Figure 6.34 Influence of compressive fracture energy on the masonry wall
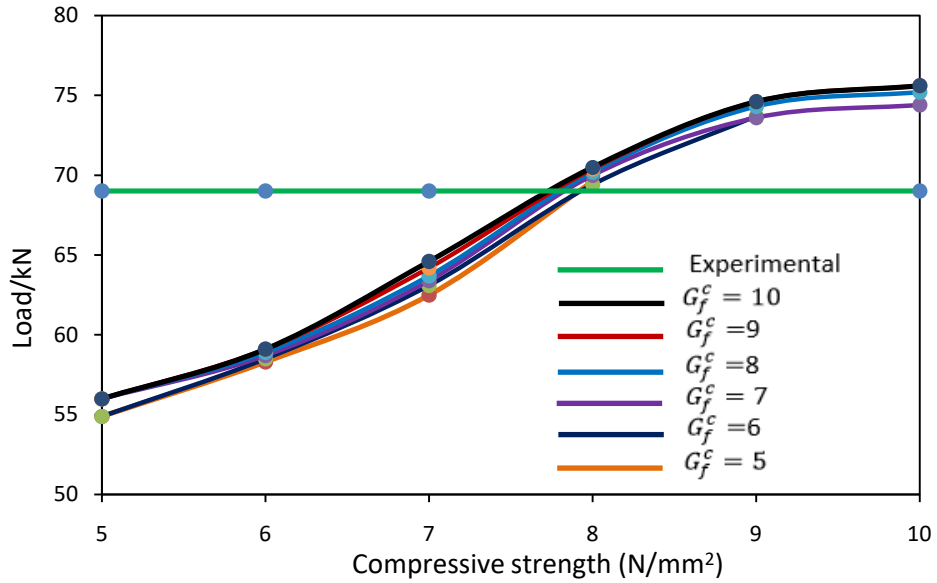
(a). Influence on the load
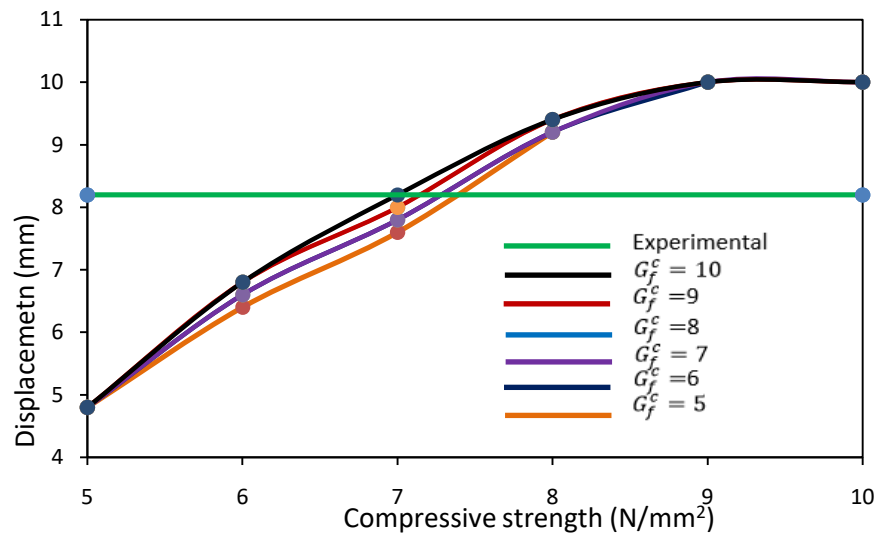
(b). Influence on the displacement

Figure 6.35 Influence of compressive strength on the masonry wall

Based on Figures 6.34 (a) and (b), it can be concluded that the value of the compressive fracture energy can be any number between 5 and $10 N/mm$, as any number among this range does not have a remarkable influence on the failure load or displacement. According to the literature review, was selected. In Figures 6.35 (a) and (b), it can be obtained that the value of the compressive strength lies between 7 to 8, and the average value can be taken as $7.5 \, N/mm^2$.

6. 6   Discussion of the calibration

In this chapter, the calibration of the material parameters has been carried out, and the detailed process of the calibration work is displayed in Figure 6.1. In the modelling work, some parameters, like elastic modulus and Poisson's ratio, have be acquired from tests on small specimens. However, for the parameters that are not able to or difficult to obtain via experimental tests on small samples, such as normal/shear stiffness and mode I/II fracture energy, are calibrated by using the above method.

The calibration method used in this research has its own characteristics. First of all, the calibration work was carried out based on the experimental result, which means that the calibration result agrees with the experimental one. Thus the reliability of the result is improved. The practicability will be proved in Chapter 6. Secondly, the sensitivity study of each parameter has been conducted and all the parameters have been categorized according to the sensitivity result. The aim of this process was trying to find out the most significantly influential parameter on each stage. In this research, all the parameters are divided into three groups, which is shown in Section 6.4.2. The influence of each group is demonstrated in Figures 6.17, 6.18 and 6.19. The figures clearly shows that the parameters in Group one only have remarkable influence on stage one, and they don't have much influence on other stages. Same findings are found in the parameters in Groups two and three. Therefore, this calibration work has decreased and minimized the interaction effect of parameters in different groups. For example, it is unnecessary to consider the interaction between the parameters in Group one and Group two as the numerical result doesn't change much. Thirdly, the calibration work was carried out manually, which is simple and easy to carry out. From the literature review, it is known that the failure process of masonry wall follows the failure process showed in this research. It always starts from small cracks appeared on masonry wall, to big cracks occurred and then to fail finally. Similarly experimental result was found as well in the

work of Sarhosis (2012). Therefore, this same process can be extended and applied to other research conducted on masonry panels.

However, this method has its own shortcomings, which need to be overcome and improved in further research. First of all, the calibration work is cumbersome and time consuming because of its manual operation. Other method, for example, optimization using software Altair Hyperstudy, could be applied. Secondly, the interaction of each parameter in each group has not been carried out. Though the parameters in one group do not have significant influence on the parameters in different groups, the interaction effect between each parameter within the same group is not known yet. Therefore, further work on the interaction between each parameter within the same group should be carried out in order to obtain more a accurate calibration result.

In order to apply this method used in this research, the researchers should follow the recommended process: (1) To obtain the parameters which can be obtained via experimental tests on small specimens. The experimental calibration could save much calibration work and time. (2). Divide the parameters into different categories, which is based on the sensitivity study. The sensitivity study investigates the influence of each parameter on the whole masonry wall. Thus the parameters that have the same influence can be categorized into the same group. (3)Then the calibration work can be carried out as demonstrated in Section 6.5. (4) Assign the calibrated parameters back to the finite element model to determine the accuracy of the calibration results.

6. 7 Summary

The model proposed in Chapter 5 has been implemented in this chapter in order to calibrate the unknown parameters. First of all, the sensitivity study of each parameter has been carried out first in order to know influence of

the parameters on the whole wall. The sensitivity study shows that different parameters influence the masonry wall in different stage and therefore they can be divided into three stages. In the first stage, which is elastic stage, only normal/shear stiffness and tensile strength have a big influence on the whole behaviour and only these two parameters need to be calibrated. For the second stage, which is the stress-redistribution stage, parameters friction angle, dilatancy angle, cohesion, mode I fracture energy and mode II fracture energy need to be calibrated. While for the final stage, i.e. failure stage, only compressive strength and compressive fracture energy need to be calibrated. After that, the calibration work on each parameter can be carried out and the detailed process has been described in Section 6.5. After the calibration study had been carried out in the above sections, all the parameters were obtained and listed in Table 6.9. These parameters will be assigned to single-leaf wall 3 in Chapter 7 to reproduce the experimental results, as well as the collar jointed wall to validate its applicability.

Table 6.9 Calibrated parameters of interface

Parameter		Symbol	Value
	Normal stiffness	K_n (N/mm^3)	11.7
	Shear Stiffness	K_s (N/mm^3)	5.1
	Tensile strength (	$f_t N/mm^2)$	0.235
	Mode I fracture energy	G_f^I (N/mm)	0.0225
	Cohesion	C (N/mm^2)	0.329
	Friction coefficient	ф	42.5
	Dilatancy coefficient	Ψ	27.5
	Mode II fracture energy	G_f^{II} (N/mm)	0.225
	Compressive strength	f_c (N/mm^2)	7.5
	Compressive fracture energy	G_f^c (N/mm)	5
Brick crack	Normal stiffness	k_{bn} (N/mm^3)	1000
	Shear stiffness	k_{bs} (N/mm^3)	435
	Tensile strength	$f_{bt}(N/mm^2)$	2
	Tensile fracture energy	G_f^{bt} (N/mm)	0.08

Chapter 7 Computational work of masonry walls

7. 1 Introduction

In this chapter, the validity of the material parameters obtained in Chapter 6 will be checked against the experimental tests presented in Chapter 3 and 4. These masonry walls are: (a) single-leaf masonry wall panel; (b) pre-damaged masonry wall panel; and (c) post-damaged masonry wall panel.

The masonry wall is created in MIDAS FEA using linear elastic solid elements to represent bricks and zero thickness non-linear interface elements to represent brick-mortar interface. In Midas FEA, there is an inherent material called 'combined-cracking-shearing-crushing', which is used to represent the non-linear behaviour of the brick-mortar interfaces. This material model has been explained in Chapter 5. All the solid elements are considered elastic and isotropic. As the parameters of a single-leaf wall were characterized in Chapter 6, the assigned parameters here are selected straightforward and the numerical result will be compared with the experimental result in order to demonstrate the ability of the model to capture the behaviour observed in the experiments. Furthermore, these parameters will be extended and applied to the double-leaf (collar jointed) wall panels to predict their behaviour.

7. 2 Single-leaf wall panel

7.2.1 Generation of model in MIDAS FEA

For the single-leaf wall, a 2D micro model was developed. As the single-leaf wall is taken as isotropic in the out-of-plane direction, 2D modelling can still

173

obtain a good numerical result. For the numerical analysis, units are represented by plane stress continuum elements. While line interface elements are adopted for the brick-mortar interfaces as well as the potential vertical cracks in the middle part of the unit. The base was simulated as fixed to replicate the restraint by the frame. The left-top corner of the specimen was allowed to move only along the horizontal axis and a perfect vertical constraint by the relevant actuator was assumed. The idealised numerical model is presented in Figure 7.1, which clearly demonstrates the matching of the geometries with the physical model. Figure 7.2 represents the single-leaf model implemented in MIDAS FEA.
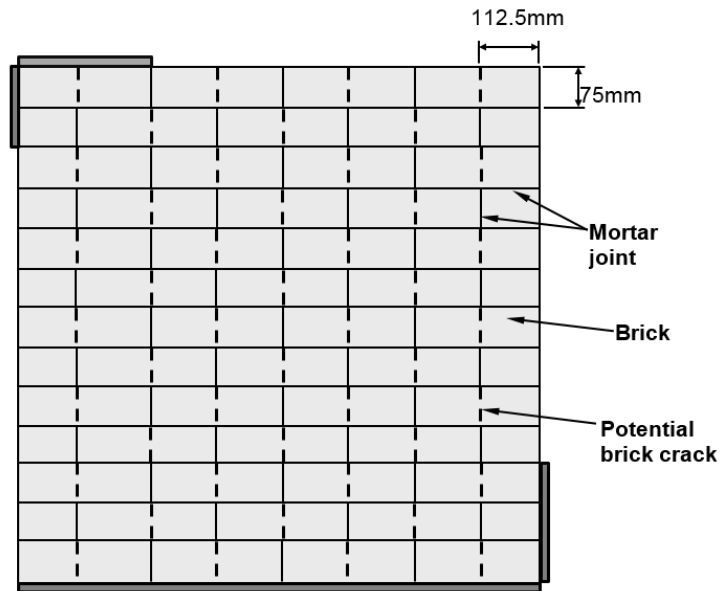
Figure 7.1 The validation 2D model in MIDAS FEA

174
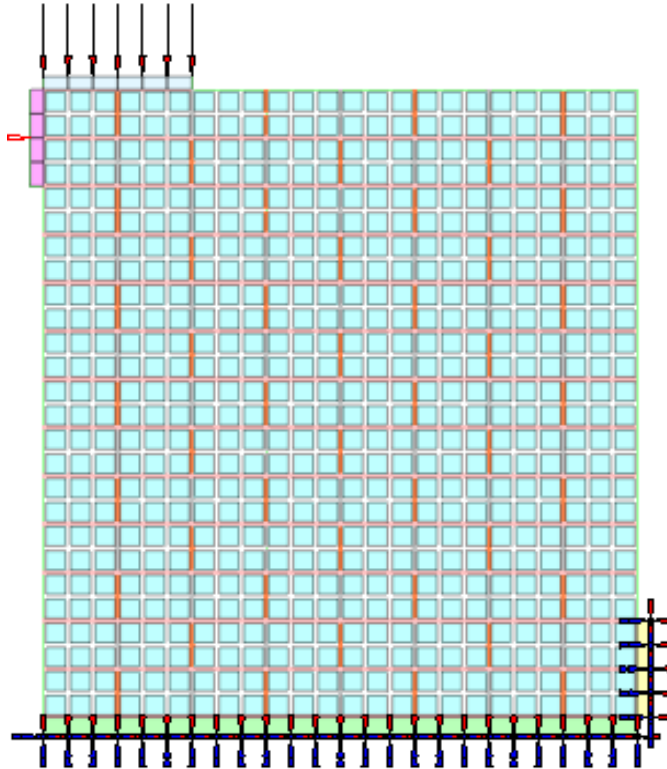
Figure 7.2 Numerical model of single-leaf wall implemented in MIDAS FEA

7.2.2 Model material parameters

In Chapter 6, each parameter has been characterized, and the values have been obtained, and are shown in the Table 6.9 in Chapter 6. The parameters will be applied in this model to simulate the single-leaf wall panel. Also please note that the self-weight of the wall was not considered in this research.

7.2.3 Numerical results

After assigning the parameters, the numerical results are obtained. The comparison of numerical and experimental results are presented in Figure 7.3, 7.4 and 7.5.

Figure 7.3 illustrates the comparison of the load-deflection relationship of the experimental and numerical results. Figures 7.4 and 7.5 display the experimental and numerical failure patterns of single-leaf wall panel. From Figure 7.3, both the experimental and numerical results display that there are three notable stages for the mechanical behaviour of the single-leaf masonry wall:

(1) A linearly elastic stage before it reached its load-redistribution point; followed by (2) load-redistribution stage where big cracks were formed by connecting small cracks together; and (3) failure stage where the masonry wall reached its maximum load capacity. However, there is a big difference after the peak stage. The reason for the difference can be explained. For the experimental result, the loading and deflection was recorded by a hydraulic actuator and a LVDT.

The failure of the masonry wall is brittle and sudden, therefore, the deflection change can be very remarkable in a very short time. Only the behaviour before the peak stage should be compared. Both the experimental and numerical results clearly indicate that the simplified micro-scale modelling could simulate the masonry wall very well. The crack pattern follows the experimental result, which starts from the top-left corner leading to the bottom-right corner. For the loaded corners, it can be seen that there are some brick units penetrate into each other. This is due to the reasons: (1) The explanation provided by the MIDAS Group that the penetration represents the brick crushing, which can also be seen in Figure 7.5. The crush of the brick unit in the masonry wall panel is now being simulated as well. (2) In order to have a more clearly read on the deformed shape, the deformation of the masonry wall pane has been magnified, therefore, the penetration effect looks much more significant. The comparison of Figures 7.4 and 7.5 reveal that the crack patterns and the development of crack at different stages of the masonry wall can be obtained via numerical model. By applying this interface element in the simplified micro-scale FE model,

the mechanical behaviour of masonry wall panel has been simulated very well.
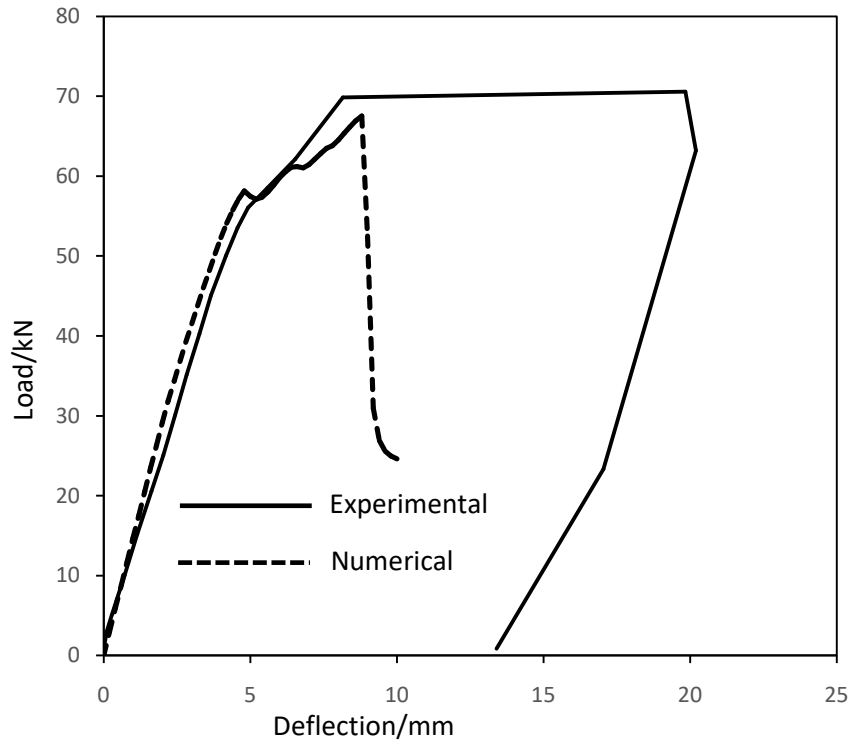
Figure 7.3 Load-deflection relationship of single-leaf masonry wall W3
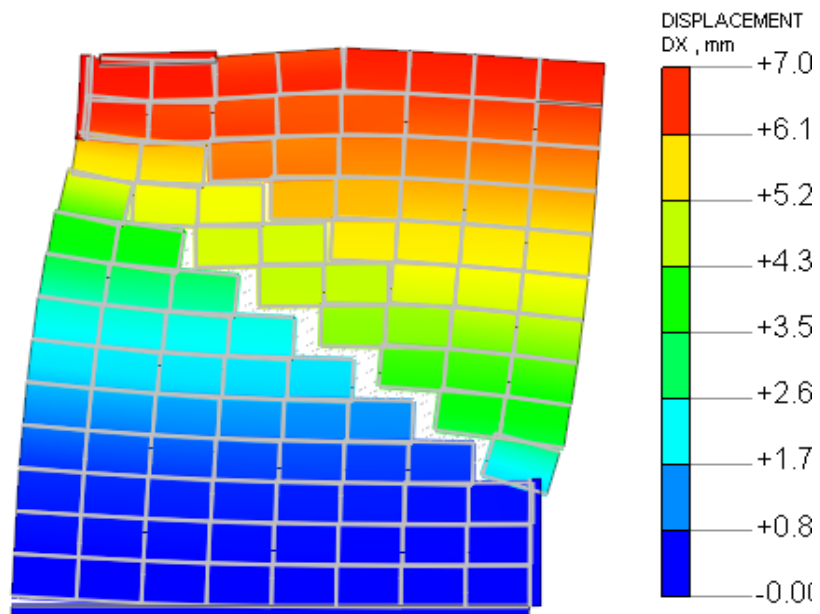
Figure 7.4 Numerical deformation of single-leaf wall W3 at deflection of 7mm
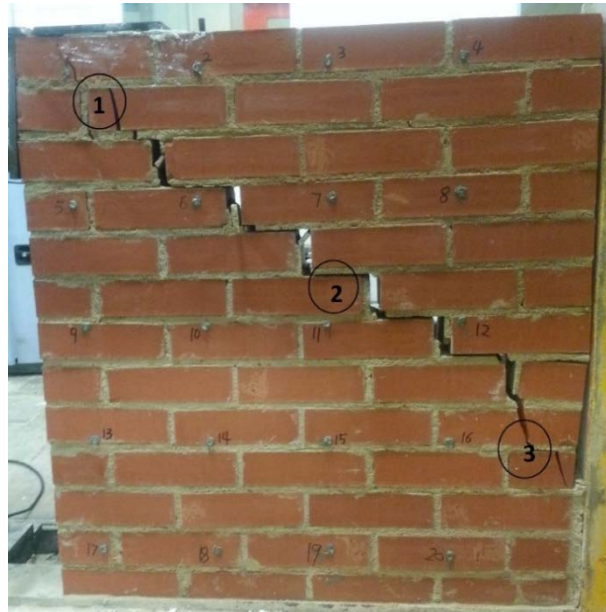
Figure 7.5 Experimental deformation of single-leaf wall W3

7. 3   Double-leaf wall panel (pre-damaged type)

7.3.1 Generation of model in MIDAS

The numerical validation of the double-leaf wall scenario has been implemented through a simplified micro-scale 3D model; this is a prerequisite for accurately considering the mechanical behaviour of the collar-joint, which naturally introduces the depth dimension. The behaviour of this joint is decisive to the overall behaviour of the panel. It should be noted that the cape mode is not included in 3D modelling in MIDAS FEA. Similarly to the brick mortar joints, the collar joint was smeared into an interfacial element for the purposes of this study. This is because the two leaves connected by the collar joint have the same geometry and property, just like two bricks connected by a mortar joint. All the other elements,

including the brick units, mortar joints and potential brick cracks are exactly the same with the single-leaf wall. The boundary conditions for the first leaf remained identical to the single-leaf wall case while for the second leaf wall, no other restriction apart from the base being fixed was prescribed. The illustration of the numerical model is given in Figure 7.6, which can be compared to the previous single-leaf wall for identifying all changes. Figure 7.7 represents the double-leaf model implemented in MIDAS FEA.
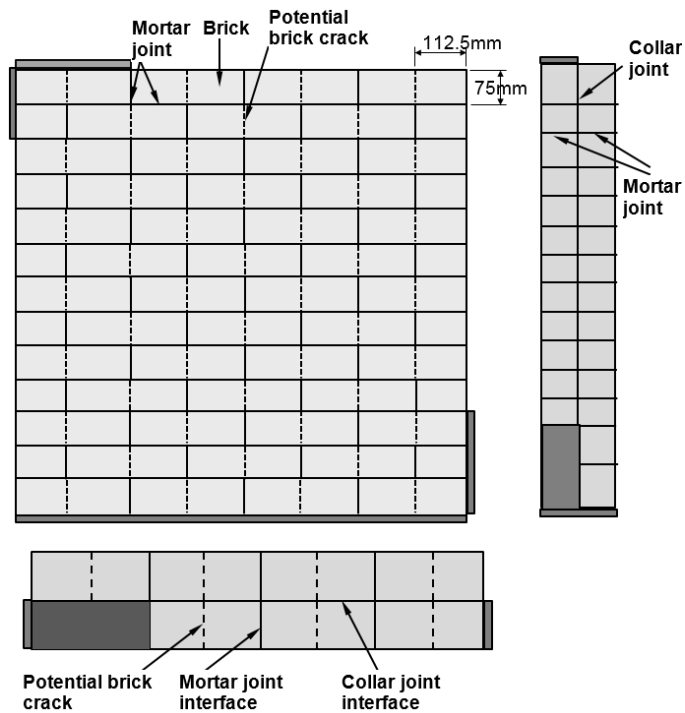

Figure 7.6 The validation 3D model in MIDAS FEA
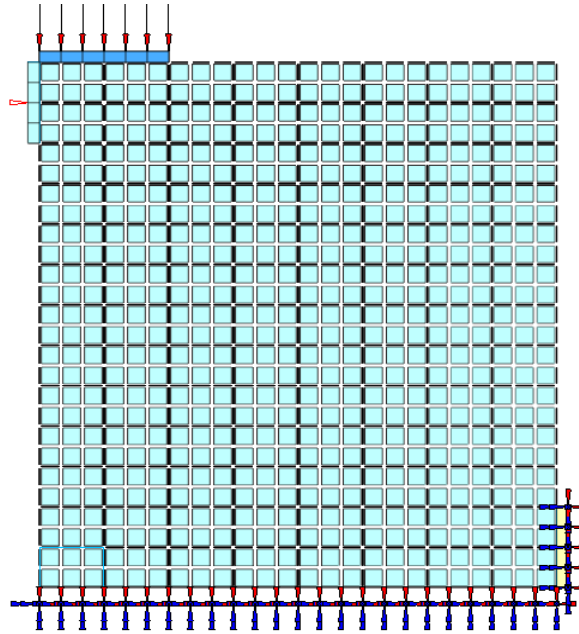
Figure 7.7 Numerical model of double-leaf wall implemented in MIDAS FEA

7.3.2 Model material

The construction material and curing age for the first and second leaf are the same. Though the properties of the two leaves may vary because of their inherent variation in materials and workmanship, it is still assumed that they are the same. Therefore, the material parameters applied to single-leaf wall can be directly assigned to the pre-damaged masonry wall, as the construction of the collar jointed masonry wall used the same materials as the single-leaf masonry wall and the curing age was also the same. Therefore, the parameters obtained from Chapter 6 can also be used in the simulation of the collar jointed masonry wall, shown as Collar Joint 1 in Table 7.1. However, the geometry and boundary conditions of the collar joint are different to the mortar joints. Therefore, the properties of collar joint may be different. In order to determine the influence of the collar joint on the mechanical behaviour of whole wall, another two types of collar joints are assumed, their properties being taken as 0.8 and 1.2 time here of the initial

Collar Joint. They are denoted as Collar Joint 2 and Collar Joint 3, and shown in Table 7.1.

Figure 7.8 Parameters for interface element of pre-damaged wall

Parameter	Symbol	Mortar Joint	Collar Joint 1	Collar Joint 2	Collar Joint 3
Normal stiffness	$K_n(N/mm^3)$	11.7	11.7	9.4	14.1
Shear Stiffness	$K_s(N/mm^3)$	5.1	5.1	4.1	6.1
Tensile strength	$f_t(N/mm^2)$	0.235	0.235	0.19	0.282
Mode I fracture energy	$G_f^I(N/mm)$	0.0225	0.0225	0.018	0.027
Cohesion	$C(N/mm^2)$	0.329	0.329	0.263	0.395
Friction coefficient	ϕ	42.5	42.5	42.5	42.5
Dilatancy coefficient	Ψ	27.5	27.5	27.5	27.5
Mode II fracture energy	$G_f^{II}(N/mm)$	0.225	0.225	0.18	0.27

7.3.3 Numerical results

The numerical results are obtained after assigning the parameters in the model. The comparisons of the numerical and experimental results are displayed in the following figures.

Firstly, Figure 7.8 reveals that the property of the collar joint does not have a remarkable influence on the mechanical behaviour of the double-leaf masonry wall as the numerical results are nearly the same with different types of collar joint. Though the numerical results do not exactly agree with the experimental results, the numerical model still can capture the trend, the maximum load and deflection of the collar jointed wall. Figures 7.9 and 7.10 compare the numerical and experimental failure patterns of the collar jointed masonry wall on the front side, while Figures 7.11 and 7.12 compare the results on the back side. It is found that by applying the parameters obtained in Chapter 6, the numerical model can predict the onset and propagation of

cracks in collar jointed masonry walls. Figure 7.13 demonstrates the failure pattern of collar joint. It reveals that the collar joint of the pre-damaged double leaf masonry wall fails slightly near the loaded corner. This agrees with the experimental results displayed in Figure 4.12 in Chapter 4. Figures 7.14 and 7.15 illustrate the stress distribution of the double-leaf wall at the deflection of 5mm. Figure 7.14 reveals that the combined quasi-static load was passed to the base via the diagonal strut, which agrees with the experimental findings presented in Section 4.3 in Chapter 4. Figure 7.15 shows that the stress on the second leaf is more evenly spread than the first leaf, which means that the load was spread evenly to the second leaf from the first leaf via collar joint. This helps the double-leaf wall carry more load by reducing the stress concentration.
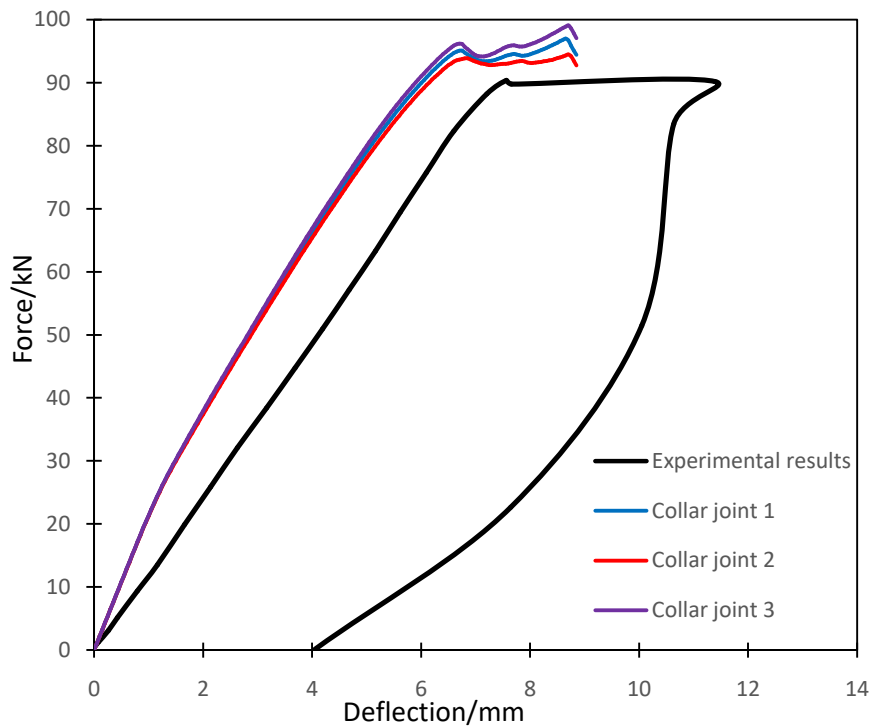
Figure 7.9 Load-deflection relationship of collar jointed masonry wall W4
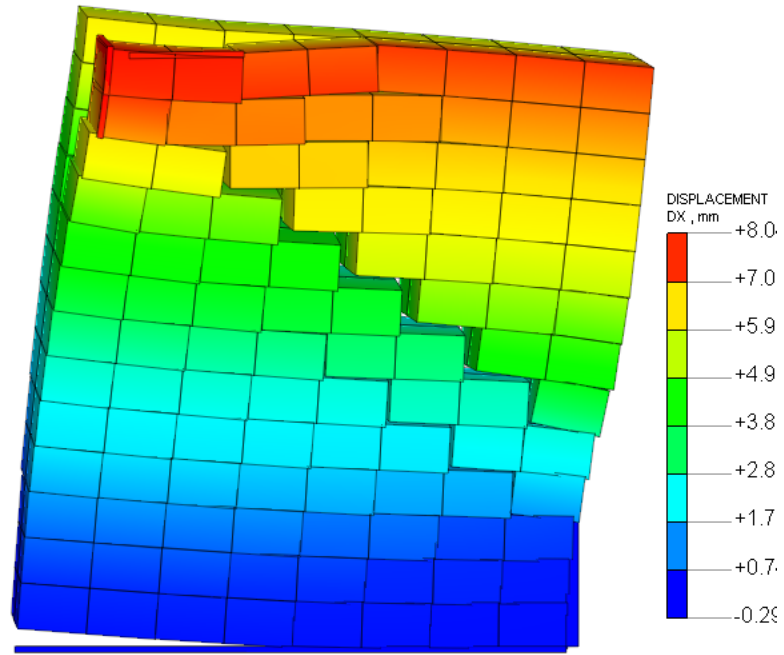
Figure 7.10 Numerical deformation of collar jointed wall W4 on the front side at deflection of 8mm

Figure 7.11 Experimental deformation of collar jointed wall W4 on the front side
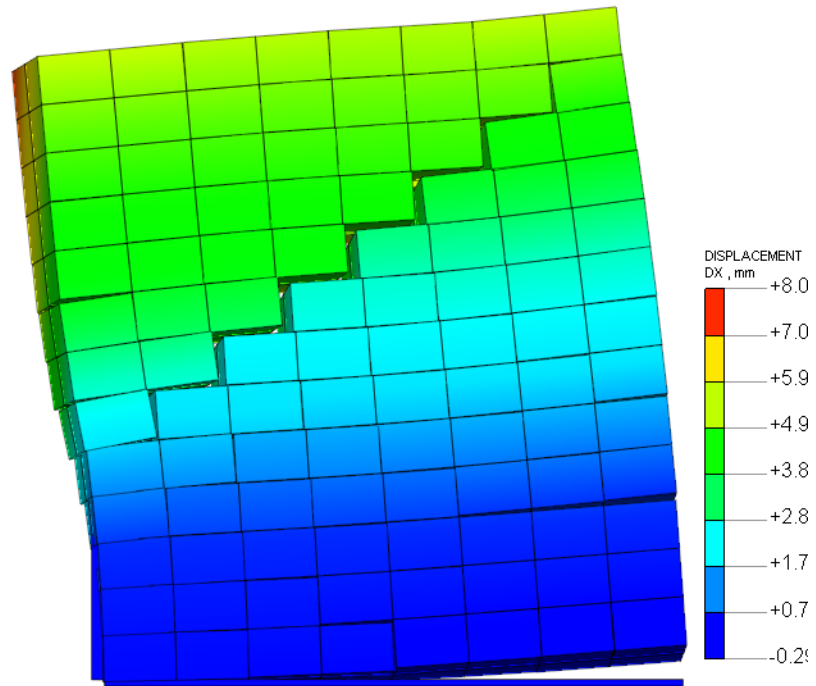
Figure 7.12 Numerical deformation of collar jointed wall W4 on the back side at deflection of 8mm

Figure 7.13 Experimental deformation of collar jointed wall W4 on the back side
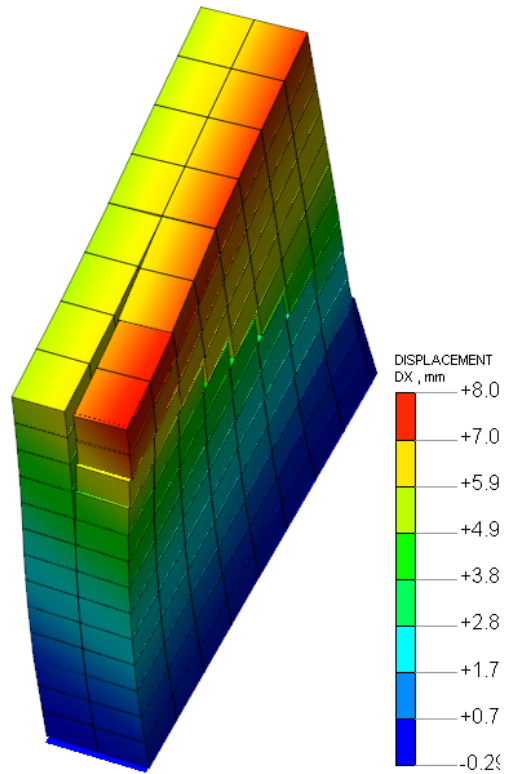
Figure 7.14 Failure patter of collar joint of numerical result
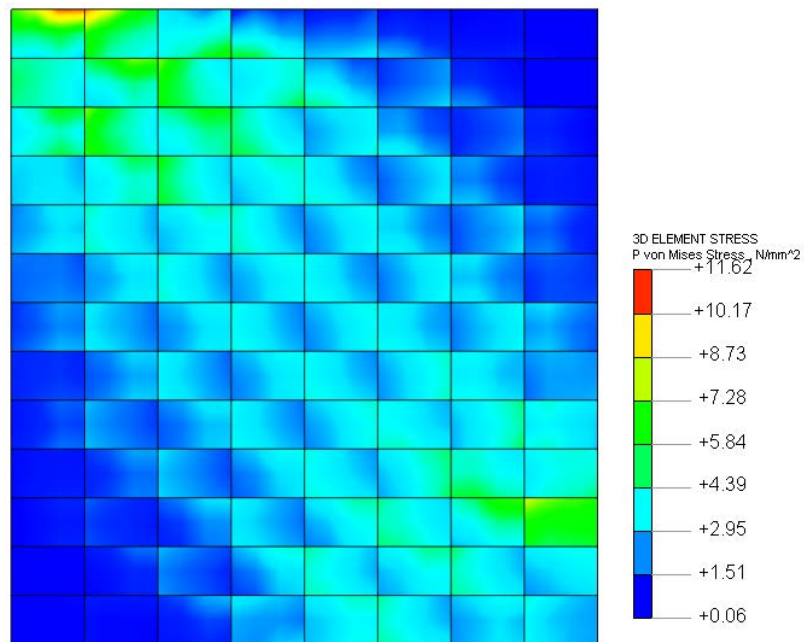
Figure 7.15 Stress distribution on the first leaf at deflection of 6mm

3D ELEMENT STRESS
P von Mises Stress, N/mm^2
+11.62
+10.17
+8.73
+7.28
+5.84
+4.39
+2.95
+1.51
+0.06
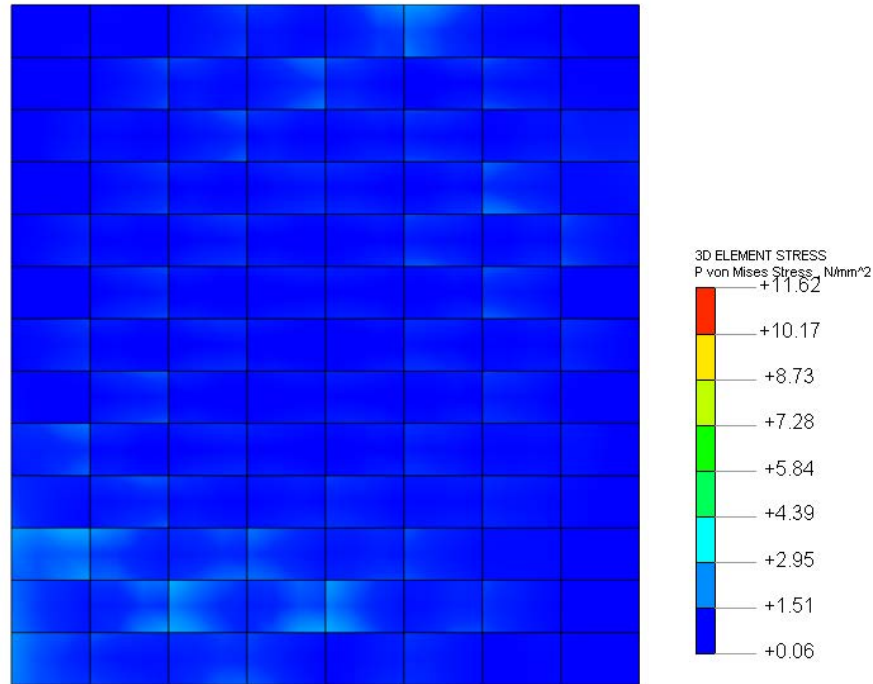
Figure 7.16 Stress distribution on the second leaf at deflection of 6mm

7. 4   Double-leaf wall (post-damaged type)

7.4.1 Generation of model in MIDAS

For the post-damaged masonry wall (previously named Wall 7) the damage results introduced some interesting modelling idiosyncrasies. The existence of some initial minute cracks in the first wall need also to be estimated correctly if accurate behaviour is to surface from the modelling attempt. The first leaf had already been tested and some initial cracks had occurred in the wall. Based on the experimental observations (shown in Figure 7.16), a grid of existing cracks was pre-defined. This is represented by red dashed lines in Figure 7.17, showing the numerical implementation of the wall. By this method, the cracks were assumed not to have any interaction. Although there might be some residual friction among the bricks along the crack

trajectory, it is very difficult to determine the residual behaviour of the interfaces as it is unable to see the cracks inside of the masonry wall. Furthermore, the worst case, which means there is no residual friction existed, should be considered in order to confirm the safety of post-damaged retrofitting method. Therefore, for simplicity, it was assumed not to have any friction or binding effect. However, for a more accurate modelling, the assumption of different percentages of residual friction should be carried out in further research or experimental inspection should be carried out on ti. The rest unit-mortar interfaces are still modelled as discontinuous elements. The boundary conditions and loading scheme were envisaged to be identical to the previous double-leaf wall setup (i.e. pre-damaged wall).

Figure 7.17Cracks on first leaf in experimental results
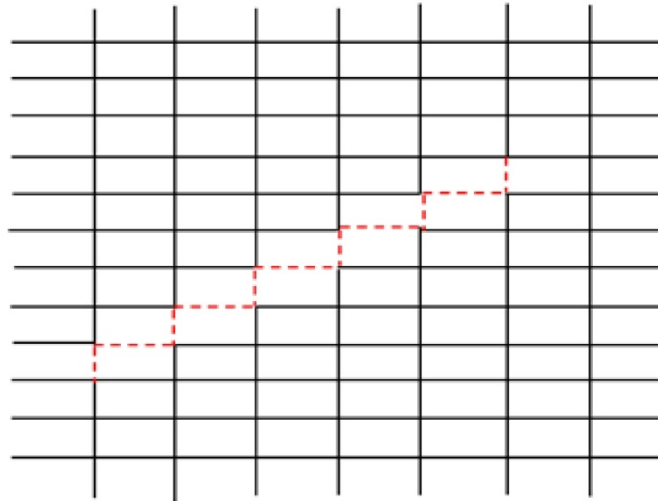
Figure 7.18 Pre-defined cracks on first leaf in finite element modelling

7.4.2 Material model

For the post-damaged collar jointed masonry wall, the second leaf masonry wall used the same material and cured at the same time as the single-leaf and pre-damaged masonry wall. Therefore the property is taken as the same with the single-leaf masonry wall. The "preliminary" leaf was constructed first and cured for over 6 weeks, while the "secondary" leaf was constructed later and cured only for 2 weeks. Therefore, the brick-mortar interfaces in two leaves are totally different. As the "preliminary" wall has been cured for a longer time than the "secondary" one, the strength properties of the "preliminary" wall are expected to be naturally higher than the properties of the "secondary" one. In this research, the property of the interface element in the first leaf was taken as 1.2 times of the single-leaf wall. The number was selected based on the characteristics of masonry material as well as the literature review. The first leaf has been cured for 6 weeks, where the mortar joint has nearly reached its designed strength. However, for the second leaf masonry wall panel was cured for only 14 days, which has reached 70%-80% of its designed strength (based on the tests of mortar cubes on small samples). However, for a more precise assumption, experimental tests should be carried out in order to know the strength of

both first and second leaf masonry wall panel. The collar joint in the post-damaged wall is modelled differently to the one in the pre-damaged walls. In this model, the collar joint hasn't been smeared out. This is because the interface 1(interface between first leaf and collar joint) is different with the interface 2 (interface between the second leaf and collar joint). The bond strength of interface 2 is stronger because of the collar joint and the second leaf were cured together, which can provide a better bond effect. This was confirmed from the experimental results (Figure 4.13 in Chapter 4) where the collar joint was still connected with the "secondary" wall. According to the numerical results of the pre-damaged wall, the interface 2 can be taken as the same with the second leaf. For the interface 1, the property can be taken as much smaller than interface 2. Based on the above findings from experiments as well as the literature review, the extended table of material parameters are given in Table 7.2.

Figure 7.19 Parameters for interface element of post-damaged wall

Parameter	1st leaf mortar	2nd leaf mortar	Collar joint interface 1	Collar joint interface 2
Normal stiffness(N/mm^3)	14.5	11.7	8.5	11.7
Shear Stiffness (N/mm^3)	6	5.1	3.6	5.1
Tensile strength (N/mm^2)	0.28	0.235	0.16	0.235
Mode I fracture energy(N/mm)	0.027	0.0225	0.015	0.0225
Cohesion (N/mm^2)	0.4	0.329	0.23	0.329
Friction coefficient	0.75	0.75	0.75	0.75
Dilatancy coefficient	0.56	0.56	0.56	0.56
Mode II fracture energy(N/mm)	0.27	0.225	0.15	0.225

7.4.3 Numerical results

After assigning the parameters in the model, the numerical results are produced and the comparisons of the numerical and experimental results are displayed in the following figures.

In Figure 7.18, it reveals that the numerical model can capture the trend, the maximum load and deflection of the post-damaged collar jointed masonry Wall 7. Figures 7.19 and 7.20 compare the numerical and experimental failure patterns of collar jointed wall on the front side, while Figures 7.21 and 7.22 compare the results on the rear. Figure 7.23 demonstrates the failure patterns of the collar joint in the post-damaged masonry wall. It can be seen that with the parameters obtained in Chapter 6 along with the estimated parameters, the numerical model can predict the onset and propagation of cracks in collar jointed masonry wall very well.
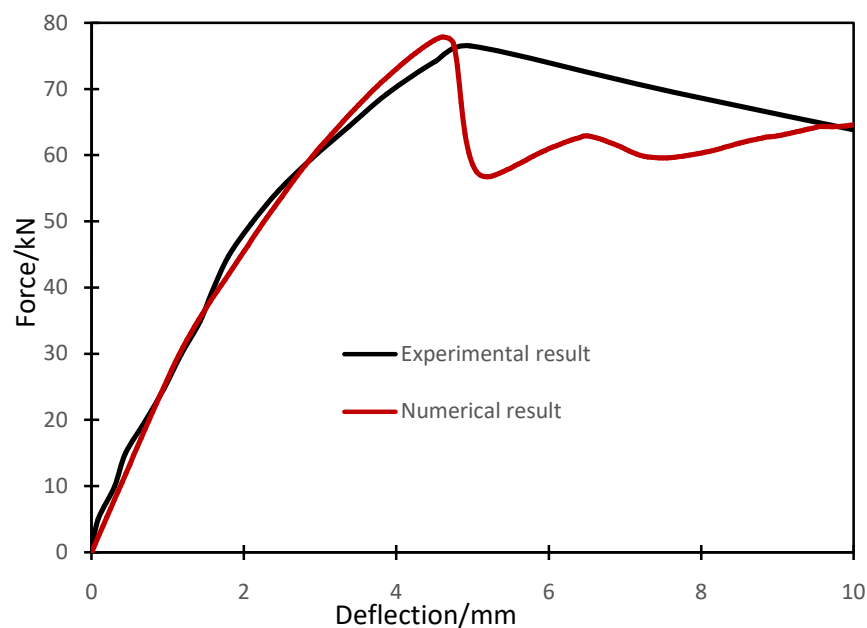
Figure 7.20 Load-deflection relationship of collar jointed masonry wall W7
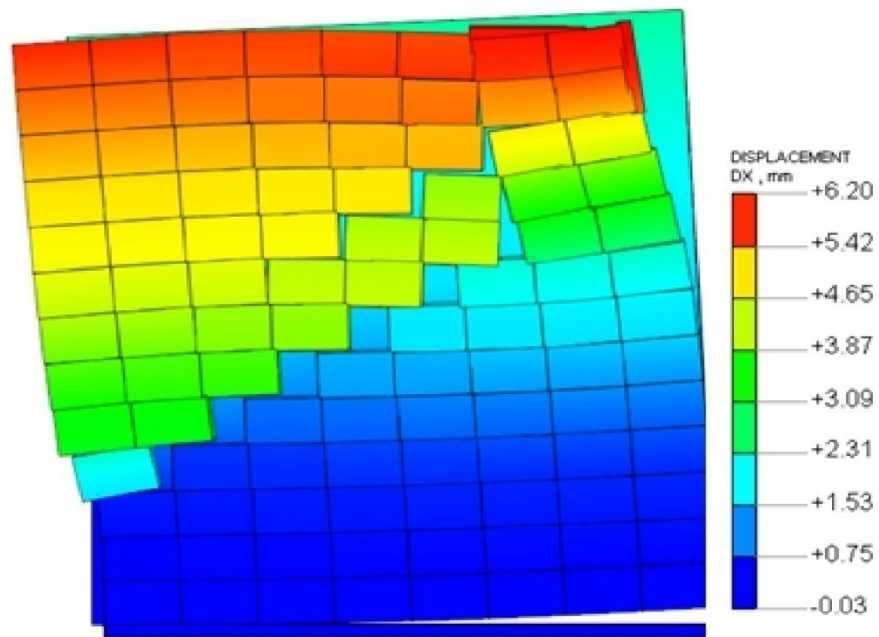
Figure 7.21 Numerical deformation of collar jointed wall W7 on the front side at deflection of 6mm

Figure 7.22 Experimental deformation of collar jointed wall W7 on the front side
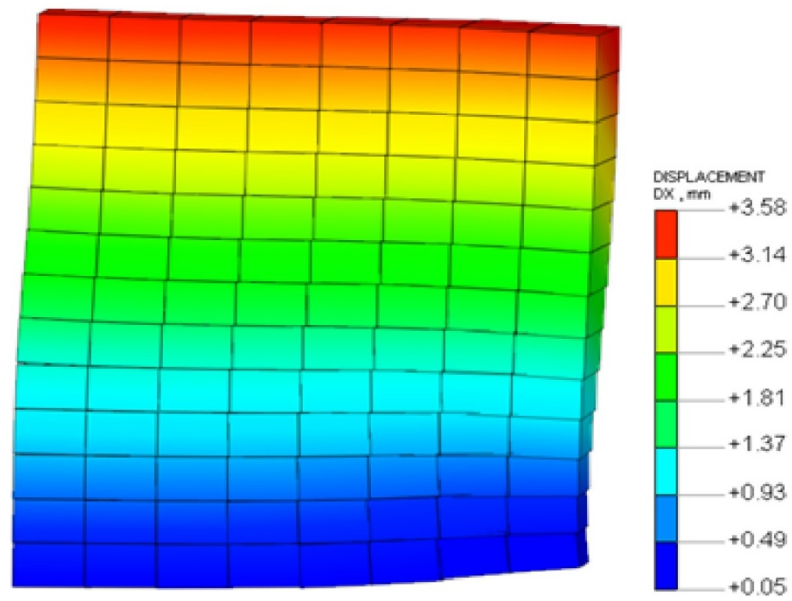
Figure 7.23 Numerical deformation of collar jointed wall W7 on the back side at deflection of 9mm

Figure 7.24 Experimental deformation of collar jointed wall W7 on the back side
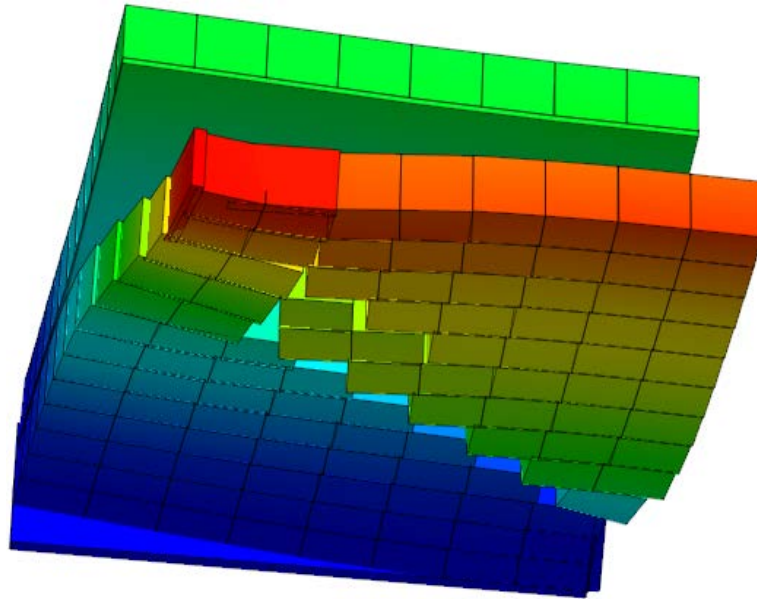
Figure 7.25 The failure pattern of collar joint

7. 5   Strain distribution (Comparison with DEMEC gauge readings)

The strain distribution of the single leaf Wall 3 is displayed in Figure 7.25, and the double-leaf masonry Wall 4 in Figure 7.26. Compared with Figure 4.25 and 4.26 in Chapter 4, the strain distribution of numerical work agrees with the experimental results. The strain distribution shows that the load passed to the base via the diagonal strut.

Specifically, for the single-leaf wall, the strain of Point 1-2 is between 103 to 204 micro strains, while 70 to 128 micro strains for Point 1-5, which is in agreement with the experimental results. For the double-leaf wall, the strain of Point 6-7 and 6-10, are both between 36 to 105 micro strains, which falls in line with the experimental results.

As the masonry is an anisotropic material, the numerical results won't exactly agree with the experimental results. However, the numerical work still can prove that the DEMEC gauge points could experimentally represent the stress and strain distribution of masonry wall in a quantitatively manner.
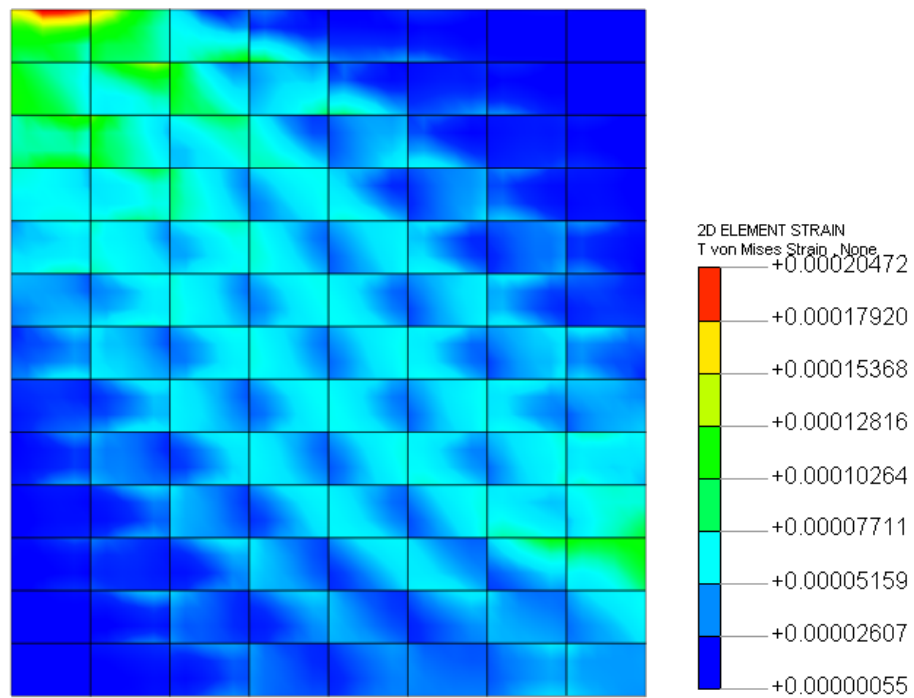
Figure 7.26Total von Mises strain distribution of single-leaf Wall 3 at the load of 40kN
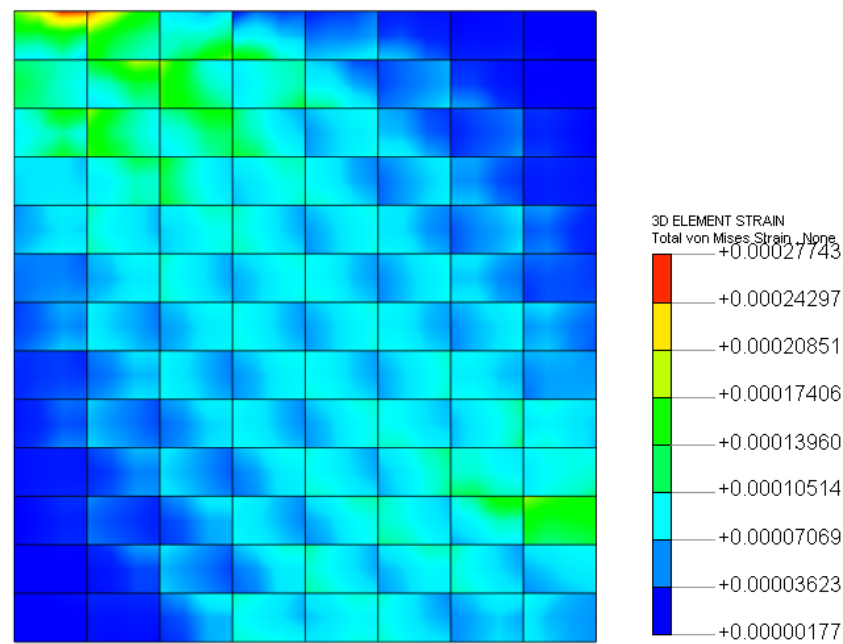
Figure 7.27 Total von Mises strain distribution of double-leaf Wall 4 at the load of 40kN

7. 6   Summary

The simplified micro-scale finite element model proposed in Chapter 5 and the parameters calibrated in Chapter 6 have been implemented to simulate the masonry wall panels, including single-leaf and double-leaf, and good agreement with the experimental result has been found. For different types of masonry wall panels, different idiosyncrasies has been implemented. For the single-leaf wall, a 2D modelling is applied while for the double-leaf wall, 3D modelling is needed. In terms of the double-leaf wall modelling, collar joint could be smeared out in the pre-damaged wall as the interfaces between collarjoint and the brick leave are the same. While for the post-damaged wall, not only the collar joint should be taken into account, but also the cracks occurred through the walls should also be considered. The results proved that this numerical model is capable of simulating the complex masonry material. Further masonry numerical work, including the reinforced concrete frame infilled with masonry walls, could also be

conducted by this approach. In the following chapter, RC frame infilled with masonry is conducted and the analysis of masonry infill has applied this simplified micro-scale finite element model.

Chapter 8   Mechanical behaviour of masonry infilled RC frame

8. 1   Introduction

The masonry wall has been studied experimentally and numerically in the previous chapters. In this chapter the author intends to extend the research to masonry infill panels within RC frame structures as the masonry is also often used as infill in the infilled RC frame to provide partitions. As the collar jointed technique has been investigated and proved to be beneficial in bare masonry wall panels, the author intends to extend the proposed method to the infilled RC frame. The aim of this chapter is to investigate its influence on the composite structure.

An infilled frame is a composite structure formed by the combination of a moment resisting frame and infill walls (Pradhan et al. 2012). This building system has been constructed all around the world, especially in the seismic prone areas. In most infilled frames, the infills are made of masonry. Infill walls are usually provided for functional and architectural reasons, such as durable and economical partitions, and they are normally considered as non-structural elements. On one hand, infilled frame structures have been recognized to exhibit poor seismic performance as numerous buildings have failed during earthquakes. On the other hand, it has been indicated from experimental observations and analytical studies that masonry infills may produce some beneficial effects on the response of the building. Therefore, these contradictory conclusions indicate that masonry infilled frames exhibit a poor or good performance depending on how the masonry is used in the infilled RC structures.

8. 2   Brief literature review on infilled RC frame

This sections describes current knowledge about the behaviour and failure mechanisms of masonry-infilled RC frames in order to give a basic understanding on this type of structure.

The performance of masonry infilled RC frames has intrigued the interest of many researchers worldwide in the past decades (Mehrabi et al. 1994, Fardis et al. 1999). These studies indicated that the in-plane lateral resistance of an infilled RC frame is usually greater than the sum of the resistance of the masonry wall and the bare frame separately (Mainstone 1971). Similar results can be found in the work of Anil and Altin (2007). The ductility of the infilled frame is larger than that of the unreinforced masonry wall structures due to the composite action developed between panel and frame (Zarnic and Tomazevic, 1988). In addition, the stiffness will be increased because of the in-plane bracing action of the masonry panel, thus reducing the lateral deformation when compared with that of the bare frame (Crisafulli, 1997). Mehrabi et al (1996) confirmed that the stiffness and strength of an infilled frame can be much greater compared to the bare frame. However, the greatness depends both on the masonry panel and surrounding frame. For the weak frame-weak panel structure, the stiffness is about 15 times greater, while 50 times greater for the weak frame-strong panel structure. For the resistance, it is 1.5 times and 2.3 times, greater respectively. Nevertheless, the maximum resistance of strong frames were increased by the weak and strong infills by factors of 1.4 and 3.2, respectively.

The failure mechanisms of the masonry infilled frames are complex due to the involvement of the high number of parameters in the mechanical behaviour of the structure, such as the material property, configuration, and relative stiffness of the frame to the infill, etc. (Sattar 2013). Stavridis (2009) and Mehrabi (1994) have summarized the failure patterns as three main mechanisms, and they are:

(i)   Diagonal cracking in the infill with column shear failure or, more rarely, plastic hinges in columns. This failure typically occurs in weak/non-ductile frames with strong infill;

(ii)   Horizontal sliding of the masonry with flexural or shear failure of the columns. Infill crushing is sometimes observed in these tests. This failure mechanism was observed in the weak frames with panels and also in the strong and ductile frames with weak infill panels;

(iii)   Infill corner crushing with flexural failure in the columns. This mechanism is most likely to be found in strong and ductile frames with strong infill.

Similarly, El-Dakhakhni et al. (2003) categorized the failure mechanisms of masonry infilled RC frames into five distinct modes, i.e. (a) corner crushing failure, which is associated with a strong frame with weak infill, (b) sliding shear failure, associated with a weak mortar joint infill bounded with strong frame, (c) diagonal compression failure, associated with slender flexible infill walls, (d) diagonal cracking failure which is associated with a weak frame with relatively strong infill and (e) a frame bending failure mode which is associated with a weak frame with weak infill. The failure modes are displayed in Figure 8.1.

Based on Figure 8.1, it should be noted that the failure modes of the masonry infill restrained by a surrounding RC frame have some similarities but also some differences compared with those found in the bare masonry wall panels. Corner crushing, sliding shear and diagonal cracking are the three most observed failure patterns in the bare masonry wall panels. However, the diagonal compression failure is very rarely found in the bare masonry wall panel.
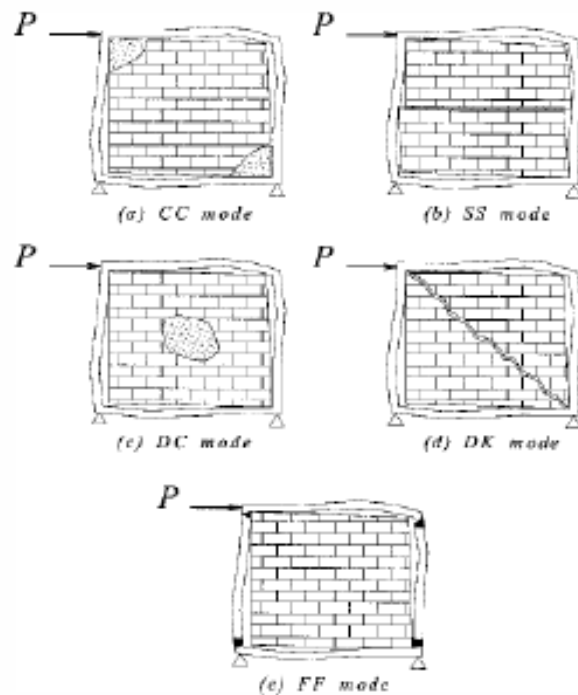
Figure 8.1Different failure modes of the infilled frames: (a) corner curshing; (b) sliding shear; (c) diagonal compression; (d) diagonal cracking; and (e) frame bending failure (El-Dakhakhni et al. 2003)

In an infilled frame structure, infills can be provided fully or with openings depending on the needs for provisions of partitions or for doors and windows. Generally, there are four different types of frames: bare frame, fully infilled frame, infilled with opening and partially infilled frame. Bare frames are rare to see, as they are always to be filled with masonry or other partition materials in order to prevent fire, provide soundproofing and other functions. Some walls will be provided with openings (windows, doors) in terms of different size, location and shape etc. to meet some certain requirements. The partially infilled frames are the least frequently seen type. In some buildings, like hospitals and academic institutions, partial infills are provided in order to get more light in from outside. It was observed that such walls on one hand contribute to enhancing the lateral stiffness of the structure while on the other hand they play a role with an adverse effect called ''short column effect''. The term ''short column effect'' is defined as the effect caused to the full storey slender column whose clear height is reduced by its

part height contact with a relatively stiff non-structural elements such as a masonry infill, which constrains its lateral deformation over the height of contact (Pradhan et al. 2012). The short column effect can cause more severe damage to the structure, which is because there is a big stiffness jump from the lower columns to the upper columns, and this stiffness difference can cause a weak point on the columns, thus making the columns more easily to fall down.

In this Chapter, a study of the mechanical behaviour of the strengthened infilled RC frame structures by applying the collar jointed technique proposed and presented in Chapter 3 has been carried out. The collar joint strengthening technique on the plain masonry wall panels has been investigated in Chapters 3 and 4. Here in this Chapter, the application of the collar joint technique was extended to the infilled RC frame to determine the effectiveness of this technique as well as the influence on the mechanical behaviour of the composite structure. In addition, the masonry wall panel which has been described in Chapter 3 will be used as masonry infill here to fill RC frame.

8. 3   Parametric study

In order to investigate the influence of the masonry wall panel and the collar jointed masonry wall panel on the composite structure, a parametric study will be carried out. This parametric study is conducted based on the work of Mehrabi et al. (1996) and Mehrabi and Shing (1997). Mehrabi et al. had done a series of experimental tests on infilled RC frames under different circumstances. The reasons why Mehrabi's work is selected in this research are due to the comprehensive data available from the tests, as well as the experimental explanation of failure mechanisms. However the most important reason is that the experimental design is highly relevant to this research as it was carried out on the infilled RC frame structures and it is

able to replace the masonry infill easily with the masonry wall presented in Chapter 3. The author combined Mehrabi's surrounding RC frame with the author's masonry wall to form a new structure. The collar jointed technique will be applied to this structure too. Then this newly formed structure will be investigated numerically.

In this study, one specimen from Mehrabi's experimental work is selected, known as Specimen 9, The RC frame is a weak frame, which was designed for a lateral wind load. In this research, Specimen 9 is selected because the lateral wind load can be simplified as equivalent static wind load. The frame was filled with a solid concrete brick panel. The geometry and detail of Mehrabi's experimental test set-up is displayed in Figure 8.2, as well as the member sizes and reinforcement detailing of the surrounding frame.
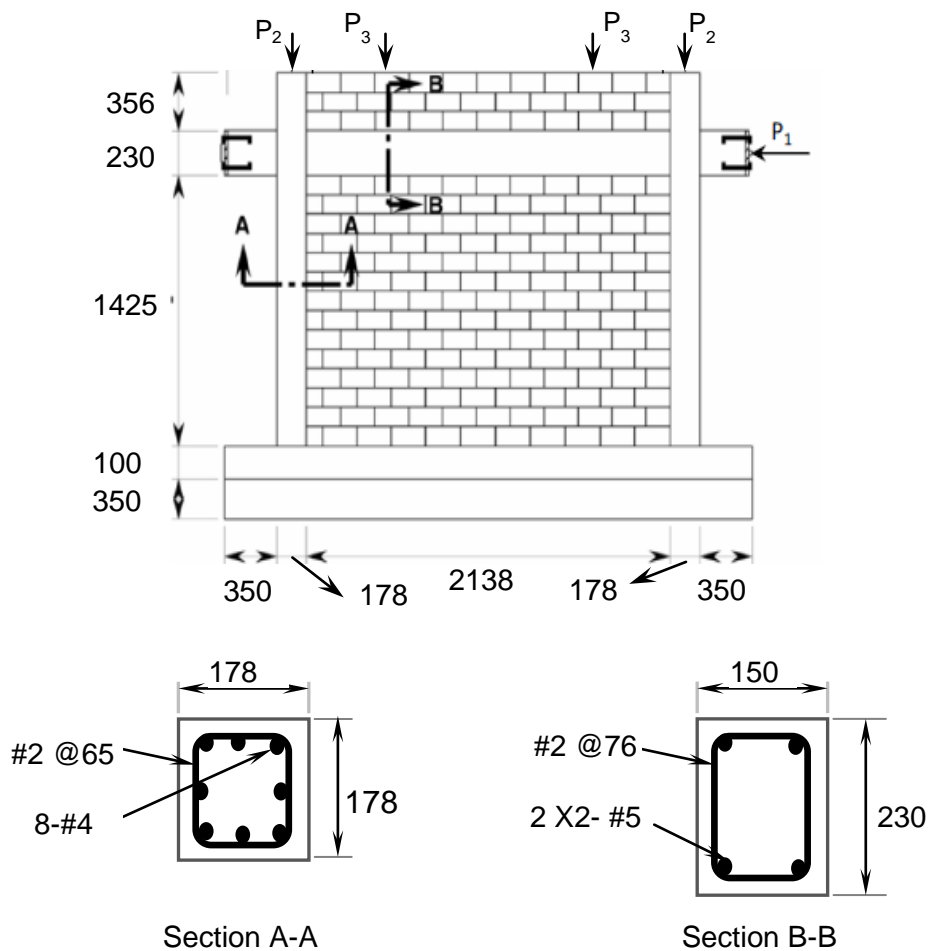
Figure 8.2Details of test specimen (Al-Chaar and Mehrabi, 2008)

First of all, Mehrabi's specimen's dimensions have been revised to fit in the parametric study and simplify the modelling work. In this section, the width of the beam is changed from 150mm to 178mm to make it the same size with the column, which is shown in Figure 8.3. All the rest are still the same with the original test set-up. Furthermore, the masonry infill in Mehrabi's experiments will be replaced with the masonry wall panel described in Chapter 3. The dimension of the brick is 215102.565mm. The thickness of the mortar in both bed-joints and head-joints in this specimen is 10mm. P2 and P3 in Figure 8.2 represent a constant vertical force during the test, and the value of P2 and P3 is 98kN and 49kN, respectively. The lateral load P1 is applied monotonically during the test. All the material properties of masonry infill have been characterized in Chapter 6 and will be applied in this chapter to simulate the newly designed infilled RC frame.
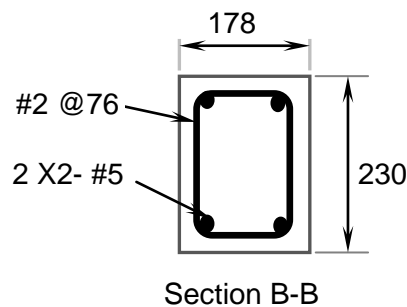
Section B-B

Figure 8.3New beam section for RC infilled frames

In this research, the study will be carried out on the influence of masonry infill, including single-leaf wall, collar-jointed wall and opening sizes, on the reinforced concrete frame structures. It should be noted that the study is only conducted numerically. The numerical specimens that have been investigated in the parametric study are explained and presented in detail as follows.

Firstly, a numerical simulation on bare frame is carried out. The geometry of bare frame is shown in Figure 8.4. Then the bare RC frame is infilled with single-leaf (shown in Figure 8.5) in two different types: (a) the infill being placed concentrically between columns (shown in Figure 8.6) and (b)

eccentrically (shown in Figure 8.7) respectively. After that, the one that the infill is placed eccentrically will be strengthened by building another wall parallel to the existing one and tie them together using 10mm thick collar joint. Therefore, it makes the infill wall into a double-leaf wall, which is shown in Figures 8.8 and 8.9. Also, the RC frame will be infilled with a masonry wall with an opening in order to determine the influence of the opening. The opening is located in the central area. The reason why the opening is located in the central area is because this research only investigates the influence of opening size, but not the opening location. The location of the opening towards the centre of the span, on the diagonal, resulted in further decrease of resistance, residual resistance, stiffness and larger amounts of loss of strength and energy due to loading. Therefore, the location factor has been excluded and the opening is only located in the central area in this research. There are four cases in terms of opening sizes, which are 9.7% (Figure 8.10), 17.5% (Figure 8.11), 27.4% (Figure 8.12) and 39.6% (Figure 8.13). All of the four cases will be strengthened using the collar joint technique as shown in Figure 8.8 and 8.9. For clarification and simplicity, a summary of the specimens are presented in Table 8.1.

Figure 8.4 Summary of designed specimens

Symbol	Description
BF	Bare frame, shown in Figure 8.4
SC	Single-leaf infill, concentrically, shown in Figures 8.5 and 8.6
SE	Single-leaf infill, eccentrically, shown in Figure8.7
DE	Double-leaf infill, eccentrically, shown in Figures 8.8 and 8.9
SO1	Single-leaf infill, 9.7% opening, shown in Figure 8.10
DO1	Double-leaf infill, 9.7% opening, shown in Figure 8.9
SO2	Single-leaf infill, 17.5% opening, shown in Figure 8.11
DO2	Double-leaf infill, 17.5% opening, shown in Figure 8.8
SO3	Single-leaf infill, 27.4% opening, shown in Figure 8.12
DO3	Double-leaf infill, 27.4% opening, shown in Figure 8.8
SO4	Single-leaf infill, 39.6% opening, shown in Figure 8.13
DO4	Double-leaf infill, 39.6% opening, shown in Figure 8.8
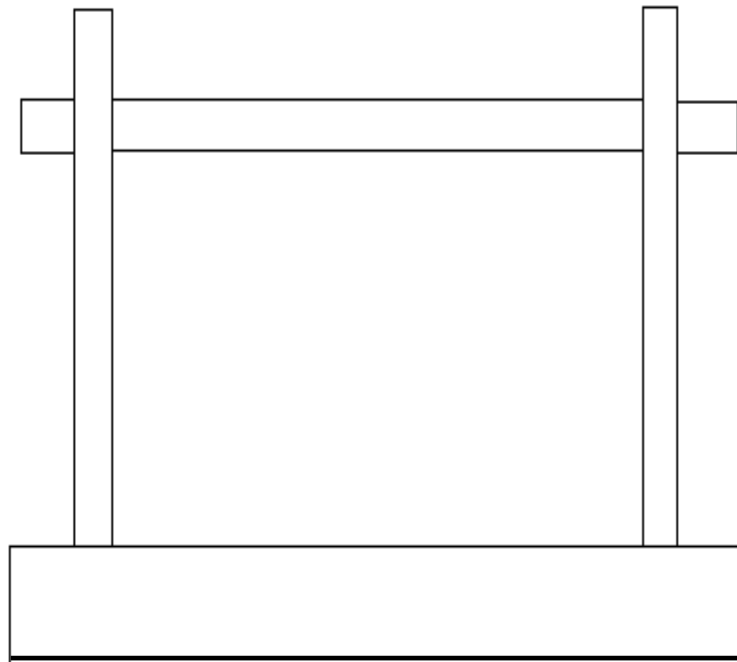
Figure 8.5 Bare frame (BF)
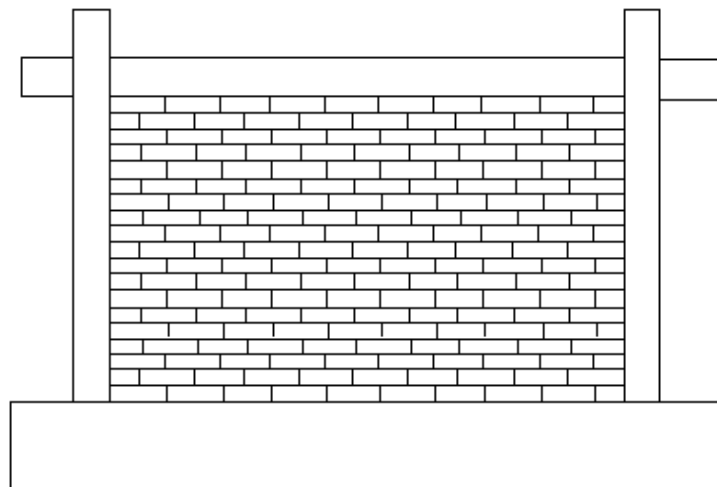
Figure 8.6 RC frame infilled with single-leaf wall concentrically (SC)
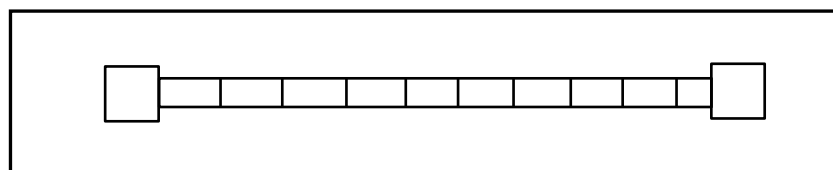
Figure 8.7 RC frame infilled with single-leaf wall concentrically (SC)
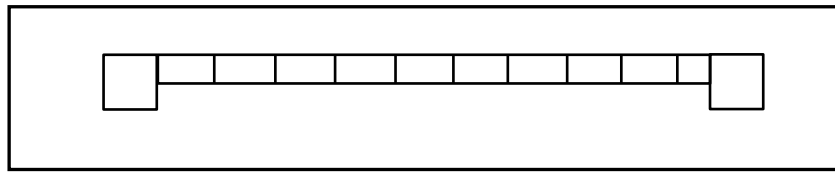
Figure 8.8 RC frame infilled with single-leaf wall eccentrically (SE)
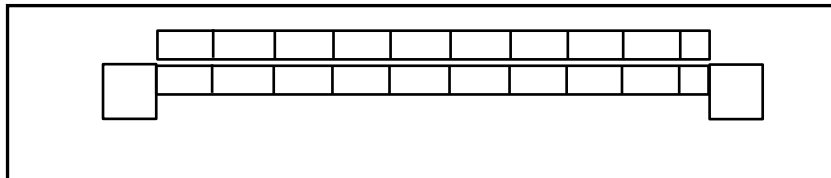
Figure 8.9 RC frame infilled with double-leaf wall from top side (DE)
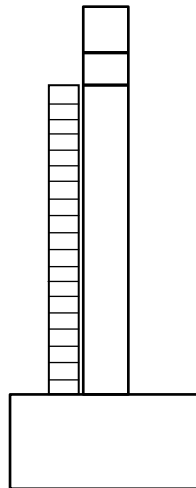
Figure 8.10 RC frame infilled with double-leaf wall from lateral side (DE)
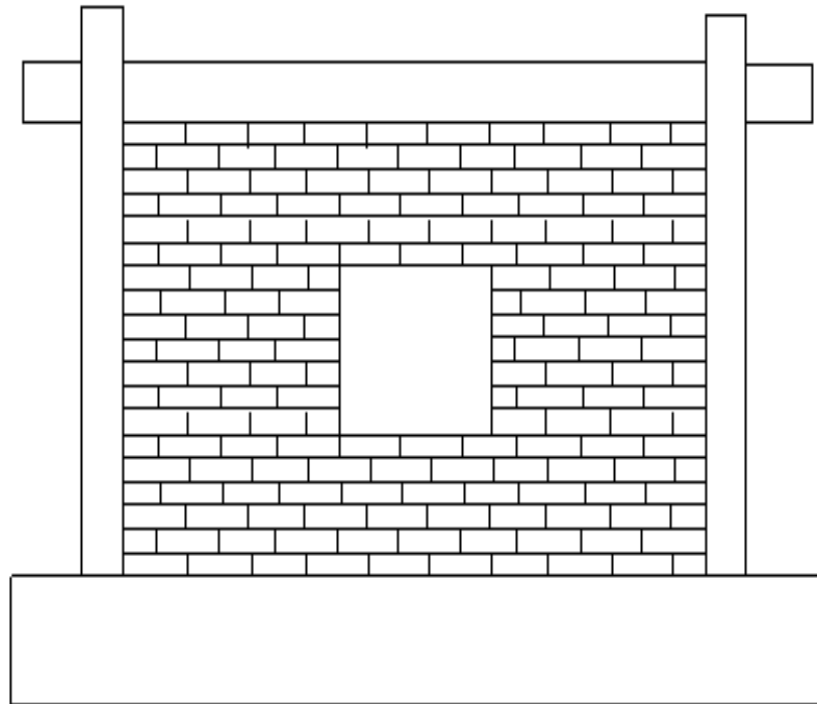
Figure 8.11 RC frame infilled with single-leaf wall with 9.7% opening (SO1)
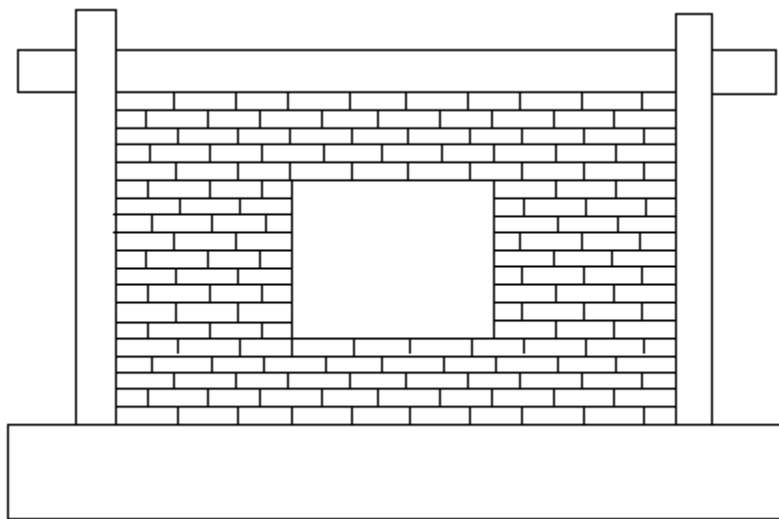
Figure 8.12RC frame infilled with single-leaf wall with 17.5% opening (SO2)
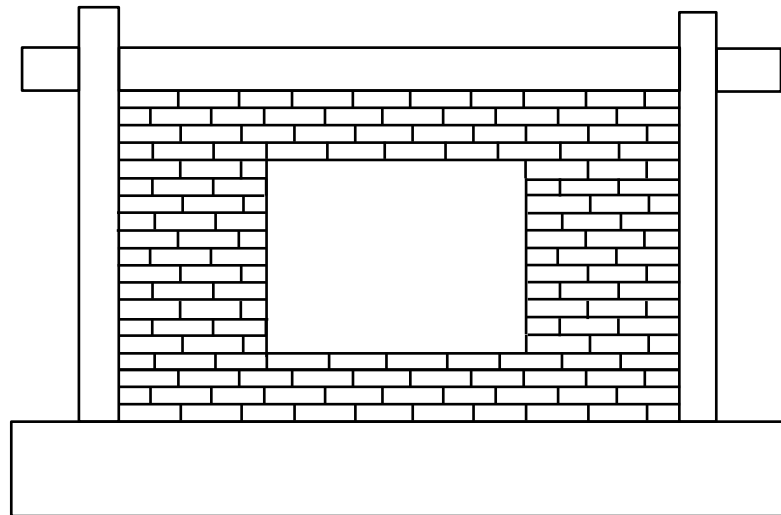
Figure 8.13 RC frame infilled with single-leaf wall with 27.4% opening (SO3)
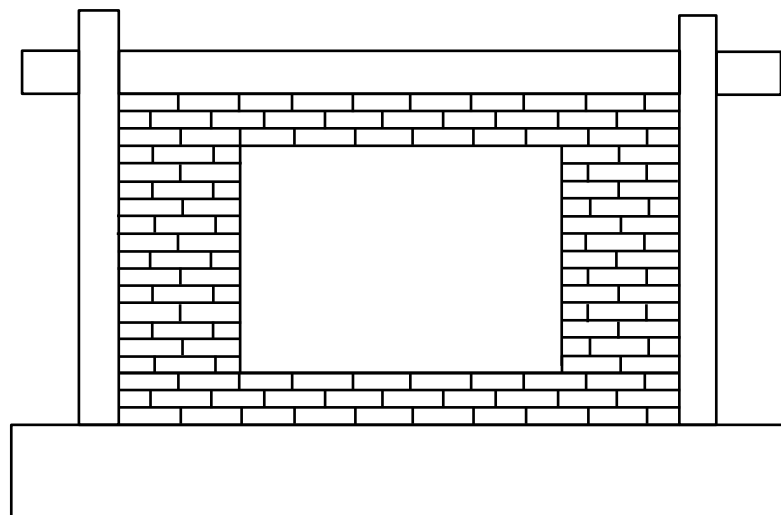
Figure 8.14 RC frame infilled with single-leaf wall with 39.6% opening (SO3)

8. 4 Numerical simulation

8.4.1 Numerical model

The surrounding frame (reinforced concrete) is modelled as a continuum model and assigned with the "total strain crack" material. "Total strain crack" material is an inherent material model in MIDAS FEA, which describes the

tensile and compressive behaviour of a material with a stress-strain relationship. For the infill wall, the simplified micro-scale model described in Chapter 5 is applied. In order to have a better understanding on the mechanical behaviour of infilled RC frame, the model will be simulated in 3D. The interface inelastic properties were simulated using a Mohr-Coulomb failure surface combined with a tension cut-off. It should be noted that the compression cape mode is not included in MIDAS FEA in 3D modelling. The vertical load is applied in the initial stage of the analysis and kept constant during the analysis. The base of the infilled RC frame is fixed in all directions.

8.4.2 Material property

The material properties of the surrounding RC frame and reinforcement applied in this model are taken directly from Mehrabi et al. (1996) and Al-Chaar and Mehrabi (2008). Material properties are shown in Tables 8.2 and 8.3.

Figure 8.15 Material property of reinforced concrete

Element	$E\ (N/mm^2)$	v	$f_t(N/mm^2)$	$G_f^I(N/mm)$	$f_c(N/mm^2)$	$G_c^{II}(N/mm)$
Reinforced concrete	24100	0.16	2.69	0.0158	27.6	19.26

Figure 8.16 Material property of reinforcements

Bar size	$E\ (N/mm^2)$	v	$f_y^1\ (N/mm^2)$	$f_u^2\ (N/mm^2)$
No. 2 (transverse)	210000	0.3	345	415
No. 4-5 (longitudinal)	210000	0.3	485	580

The Young's modulus of brick element is 19900 and the Poison's ratio is 0.15. The material properties of brick and brick-mortar interface have been characterized in Chapter 6. Therefore, the parameters will be assigned to the masonry infill directly here, which are listed in Table 8.4. However, the frame/infill interface is not known in this research. Therefore, it is estimated in this research. Usually the frame/infill interface is weaker than the brick-mortar interface (Sattar 2010). Therefore, in this research, the property of frame/infill interface will be estimated as 0.8 of the brick-mortar interface.

Figure 8.17 Material properties for interface elements

Parameter	Brick-mortar interface	Collar joint	Frame/infill interface	Pre-defined brick crack
Normal stiffness(N/mm^3)	11.7	11.7	9.4	1000
Shear stiffness(N/mm^3)	5.1	5.1	4.1	435
Tensile strength(N/mm^2)	0.235	0.235	0.188	2
Tensile fracture energy(N/mm)	0.0225	0.0225	0.0188	0.08
Cohesion(N/mm^2)	0.329	0.329	0.263	
Friction coefficient	0.92	0.92	0.92	
Dilatancy coefficient	0.52	0.52	0.52	
Shear fracture energy(N/mm)	0.225	0.225	0.18	

8. 5   Simulation results and comparisons

After assigning the parameters in the model, the simulation results can be obtained. The comparisons are displayed as following.

8.5.1 Comparison of bare and infilled RC frame
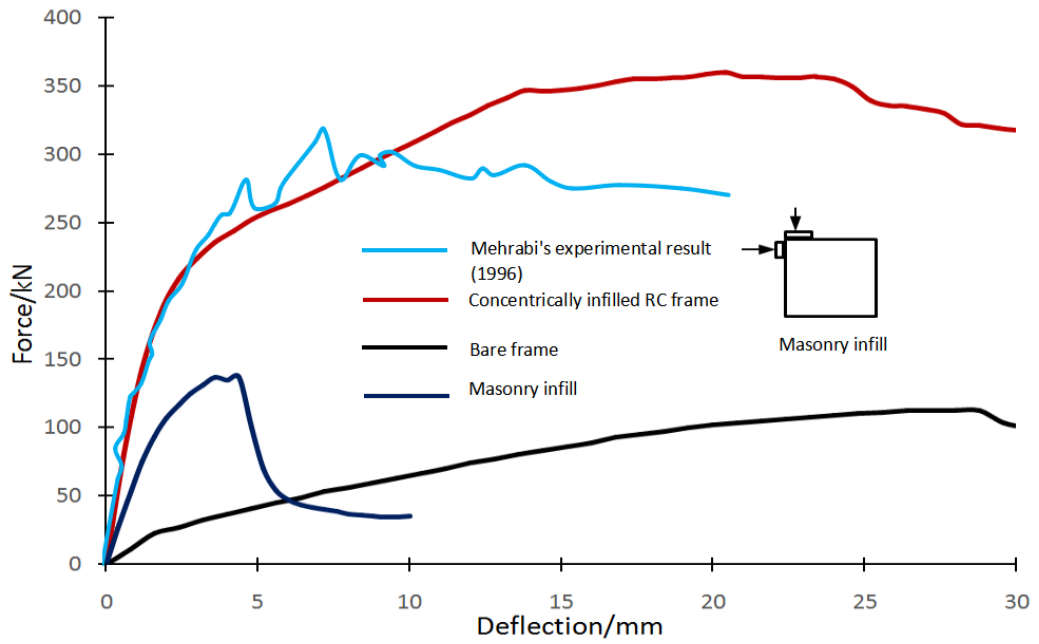
Figure 8.18 Load-deflection curve of BF and SC
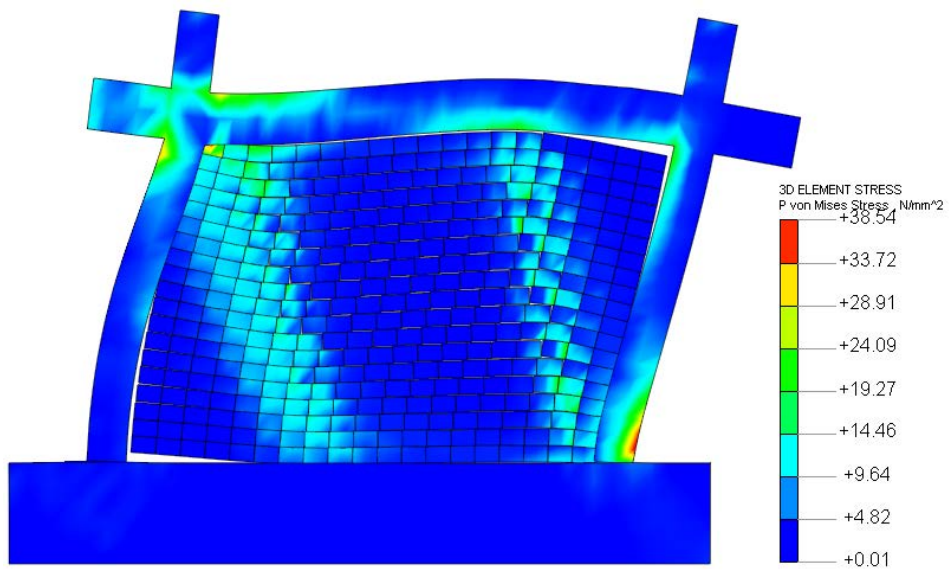
Figure 8.19 Deformation and stress contour of infilled RC frame at deflection of 10mm
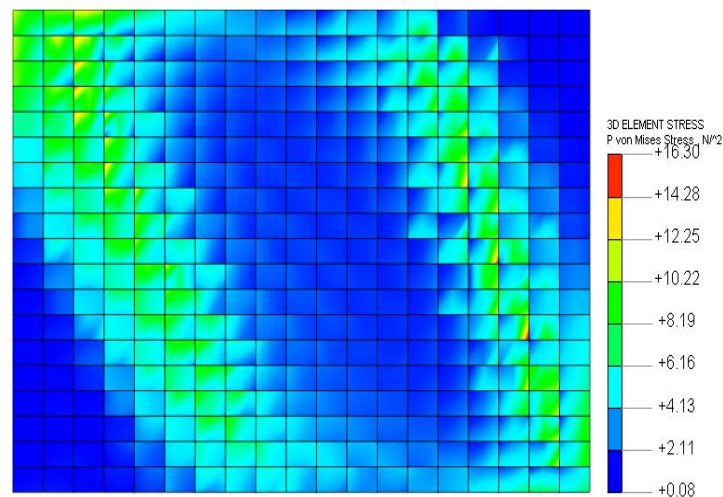
Figure 8.20 Von Mises stress distribution of the masonry infill
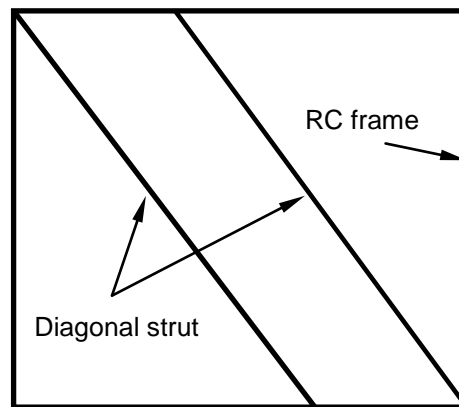
Figure 8.21 Simplified infilled RC frame

Figure 8.14 shows the load-deflection curves of the bare frame, masonry wall panel and masonry infilled RC frame under a combined quasi-static loading as well as the experimental result of Mehrabi's (1996) work. The figures demonstrate that the numerical result agrees with Mehrabi's (1996) experimental result in the beginning, however, it surpasses it at the deflection of 10mm. This is due to the reasons that the width of the beam used in this research is bigger than Mehrabi's. Besides, the masonry unit used in this research is much stiffer and stronger than the Mehrabi's. Therefore, the numerical specimen carries higher failure load. Furthermore, the figure demonstrates that the infilled RC frame has much higher stiffness and strength compared with the bare frame. Also, it overpasses the stiffness and strength sum of the bare frame and masonry wall panel, which has been

proven in the past researches (Mehrabi et al. 1996, Koutromanos 2011). In detail, the stiffness of the infilled RC frame is nearly 8 times more than the bare frame, as well as a 240% increase for the failure load. It has been proven by many researchers (Al-Chaar et al. 2002, Mehrabi et al. 1996, Stavridis and Shing, 2010, Sattar 2013) that masonry infill can have a big influence on the mechanical performance of an infilled RC frame structure. This improvement can help RC frame structure resist a larger lateral load during earthquakes.

Figure 8.15 illustrates the deformation and stress contour of the infilled RC frame at deflection of 10mm. This deformed shape illustrates the sliding in the bed joints at the mid height of the infill panel, as well as the diagonal cracking of the infill panel. The failure patterns of the masonry infill mainly have three main types: a) diagonal cracking, b) mortar joint sliding and separation, and c) corner crushing, and joint sliding and separation is the governing failure mechanism for this infilled RC frame. It should be noted that the masonry infill acts more or less like the masonry wall tested in the laboratory, i.e., the top-left corner has nearly reached its compressive strength, which signals crushing at the loaded corners under higher lateral displacements. These results agreed well with the experimental analytical results by Mehrabi et al (1994). Around the unloaded corner, the masonry infill is detached from the surrounding frame. Furthermore, there are some diagonal cracks and mortar sliding occurred along the diagonal area. These findings were also found in plain masonry wall panel presented in Chapter 4. Therefore, it could be assumed that it is possible to simplify the lateral loaded masonry infill wall as bare masonry wall panel during the experimental work. However, there is one thing that should be noted. The aspect ratio of the experimental infill is 1.08, while the aspect ratio for the masonry infill in infilled RC frame is 0.7. Therefore, further investigation on the aspect ratio should be conducted.

Figure 8.16 shows the stress distribution of the masonry infill at a deflection of 10mm. It can be seen that there are two diagonal struts (higher

compressive stress compared with surrounding area) formed in the masonry infill, which is simplified and illustrated in Figure 8.17. The load was passed along these two diagonal struts, and this is the reason why the diagonal cracking occurred along the diagonal struts (Figure 8.15). This loading system of infilled RC frame can also be found in other researches (El-Dakhakhni et al. 2003, Crisafulli et al. 2000). Some other researchers have proposed one diagonal strut (Zarnic and Tomazevic 1986) or multi diagonal struts (Chrysotomou et al. 2002) theory depending on the aspect ratio, to simplify the masonry infill. Therefore, if the width of the diagonal strut is known, the modelling of infilled RC frame can be simplified. By this method, a large amount of time can be saved in the modelling a whole infilled RC frame structure. In this research, the width of the diagonal strut can be calculated by counting the grid. As displayed in Figure 8.16, the total number of the diagonal grid is 9.5 while the number of the strut grid is 3 to 4. Therefore, the width of diagonal strut is $\frac{3\sim4}{9.4} = 0.32\sim0.42$, which agrees with the research of Holmes (1961) that the strut width is taken roughly as 1/3 of the diagonal length.

8.5.2   Comparison of concentrically and eccentrically infilled RC frame (SC and SE)

Figure 8.18 shows the comparison of the concentrically infilled frame and eccentrically infilled frame in terms of load-deflection relationship. The figure clearly illustrates that the initial stiffness of the composite structure does not change due to only minor cracks occurring. However, after the big cracks appeared and the load has re-distributed among the structure, both the stiffness and failure load of the whole structure will be decreased slightly if the infill is eccentrically located between the columns. The structure behaves nearly linearly from beginning in both cases, as there is no big crack occurring in both surrounding frame and infill. This linear behaviour stops when the structure reached around 230kN. At this stage, the stiffness of the

structure started to decline due to the occurrence of big cracks on the infill. However, the stiffness reduction of eccentrically infilled RC frame is larger than the concentrically infilled one due to the torsion in the eccentrically infilled RC frame. The stress will be redistributed among the infill after the occurrence of cracks. The structure can still carry more load after the load redistribution among the infill. The lateral load will stop increasing when it reaches its failure load. When the torsion in the eccentrically infilled RC frame is large enough, it can cause the infill fail out-of-plane. Therefore, if torsion existed in a structure, the failure is a combination of in-plane and out-of-plane failures.

Figure 8.19 represents the deformation of the eccentrically infilled RC frame. The cracking patterns are very similar with the concentrically infilled one. It can be seen that the in-plane failure (mortar sliding and separation) dominates the failure modes. In this case, it is very hard to tell the out-of-plane failure. It is because the out-of-plane failure appeared as the de-bonding of mortar joints and brick units, which can also be found in in-plane failures (Figure 8.15).
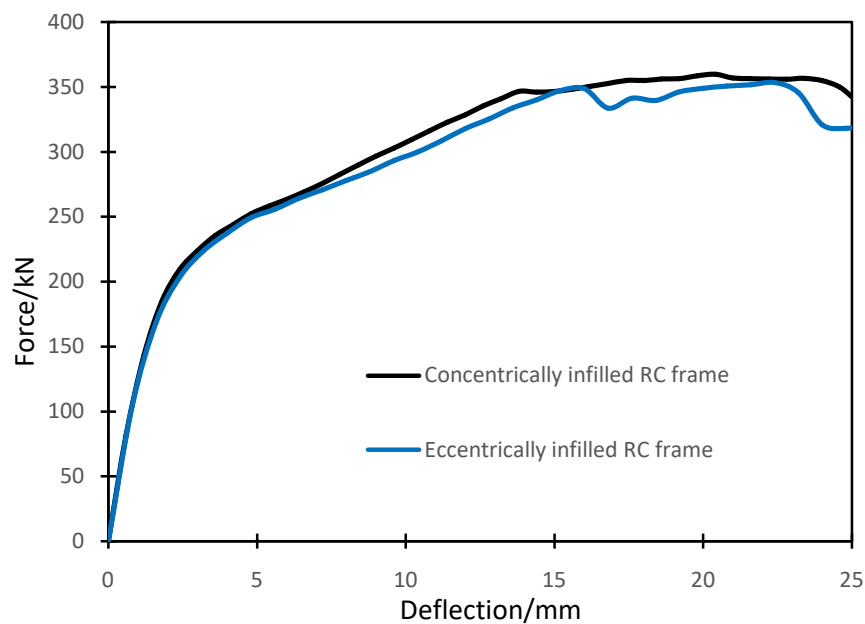
Figure 8.22 Load-deflection curve of specimen SC and SE
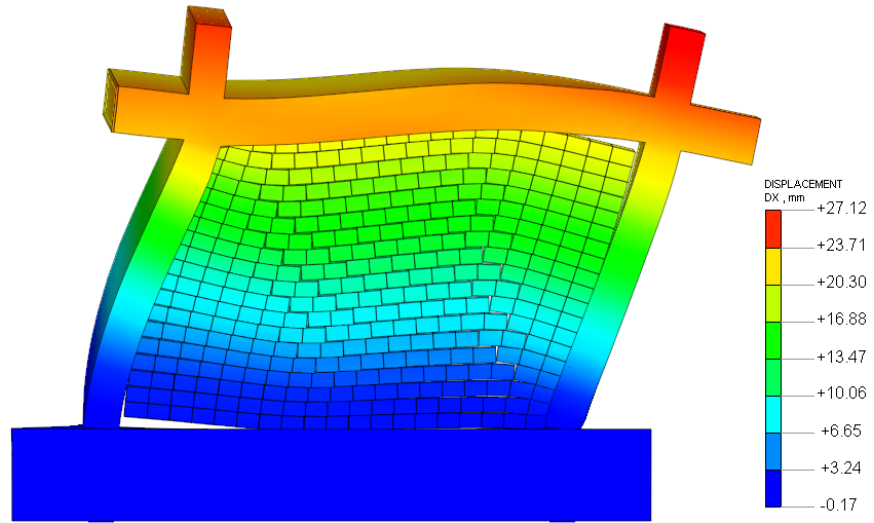
Figure 8.23 Deformed shape of eccentrically infilled RC frame at deflection of 25mm

8.5.3 Comparison of RC frame infilled with single- and double-leaf masonry wall
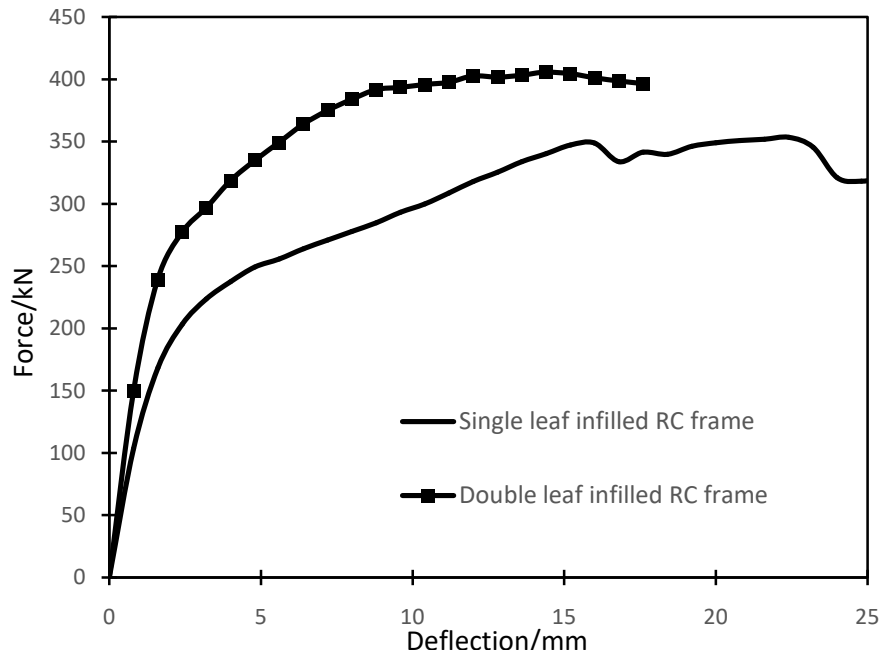
Figure 8.24Load-deflection curve of specimen SE and DE

216
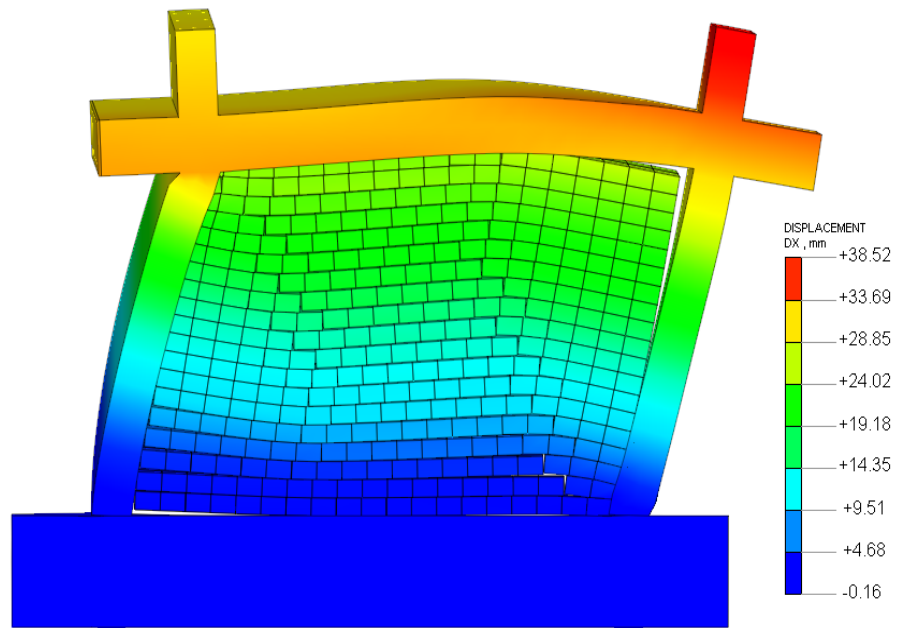
Figure 8.25 Deformed shape of collar jointed infilled RC frame at deflection of 30mm
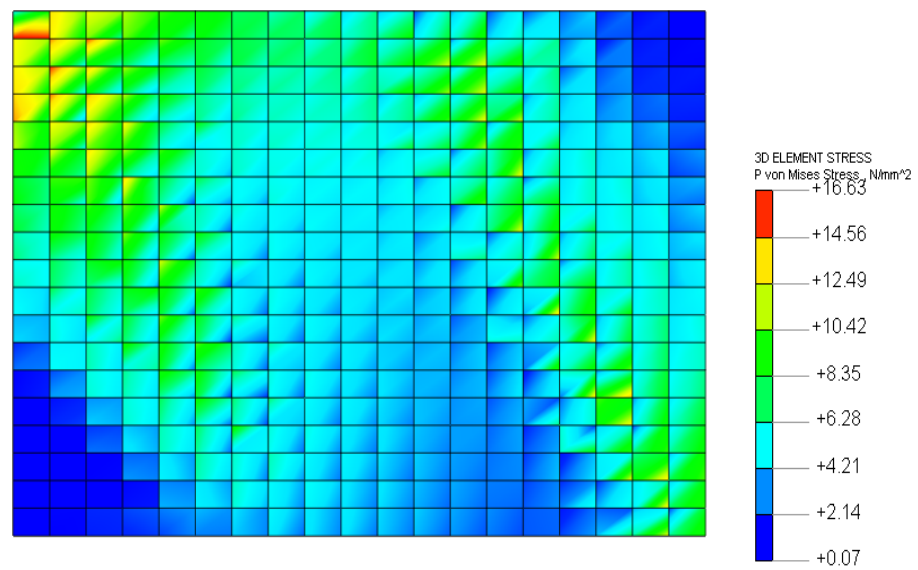
Figure 8.26 Stress distribution on the front side
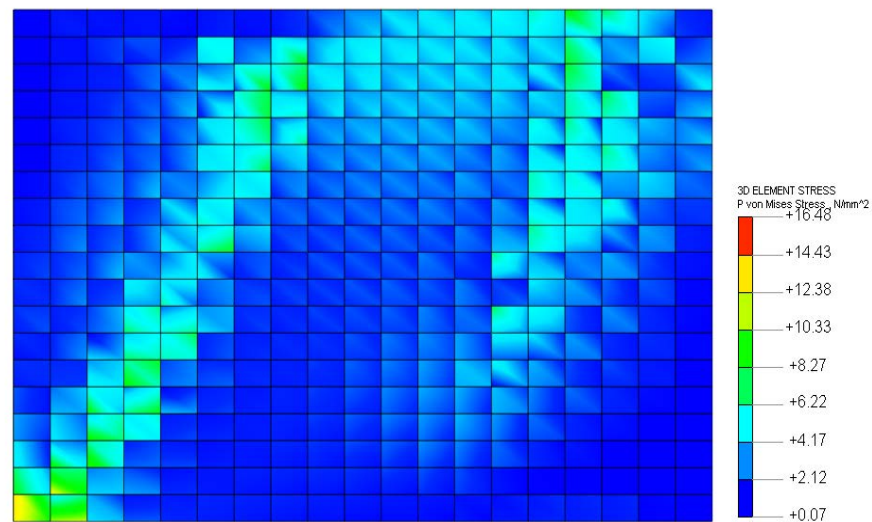
Figure 8.27 Stress distribution on the back side

Figure 8.20 represents the load-deflection curves of the single- and double-leaf infilled RC frames. The figure demonstrates that the double-leaf infilled method can postpone the failure of crack occurrence. For the single-leaf masonry wall infilled frame, the big crack occurred when the lateral load reached about 230kN, however, for double-leaf infilled frame, big cracks appeared only when the lateral load reached about 290kN. Furthermore, the double-leaf infilled method can increase the stiffness, by approximately 1.4 times of its initial stiffness. After big cracks appeared in both cases, both structures can keep carrying more loads until both reached their failure load stage. The failure load of the double-leaf masonry wall infilled structure is about 20% higher than the single-leaf masonry wall infilled structure. Therefore, it can be summarised that the second leaf (collar jointed system) can improve the stiffness and failure load of the single eccentrically infilled frame to some degree. Figure 8.21 shows the deformed shape of RC frame infilled with double-leaf masonry wall. It shows that the failure patterns have more diagonal cracks compared with the single-leaf masonry wall infilled RC frame, where appeared along the two diagonal struts area.

It can also be seen that there are less sliding failure cracks or mortar joints and brick units de-bonding cracks, which can be seen in Figure 8.19. This

finding means that the out-of-plane failure has been reduced because the collar joint strengthening technique has increased the out-of-plane thickness, therefore reducing out-of-plane failure. Figures 8.22 and 23 illustrate that the stress distribution among two leaves are almost the same, which means that the collar joint improves the integrity of masonry infill and makes the two leaves work as a single-leaf wall. Compared with Figure 8.16, Figure 8.22 displays a less remarkable diagonal-strut model. This is because the lateral load has been spread more evenly among the whole wall. Compared with Figure 8.22, Figure 8.23 shows a less strong but more average stress distribution, which means the external load has been flowed to the second leaf via the collar joint, but the load was reduced and spread over among the second leaf.

8.5.4 Influence of opening size on infilled RC frame
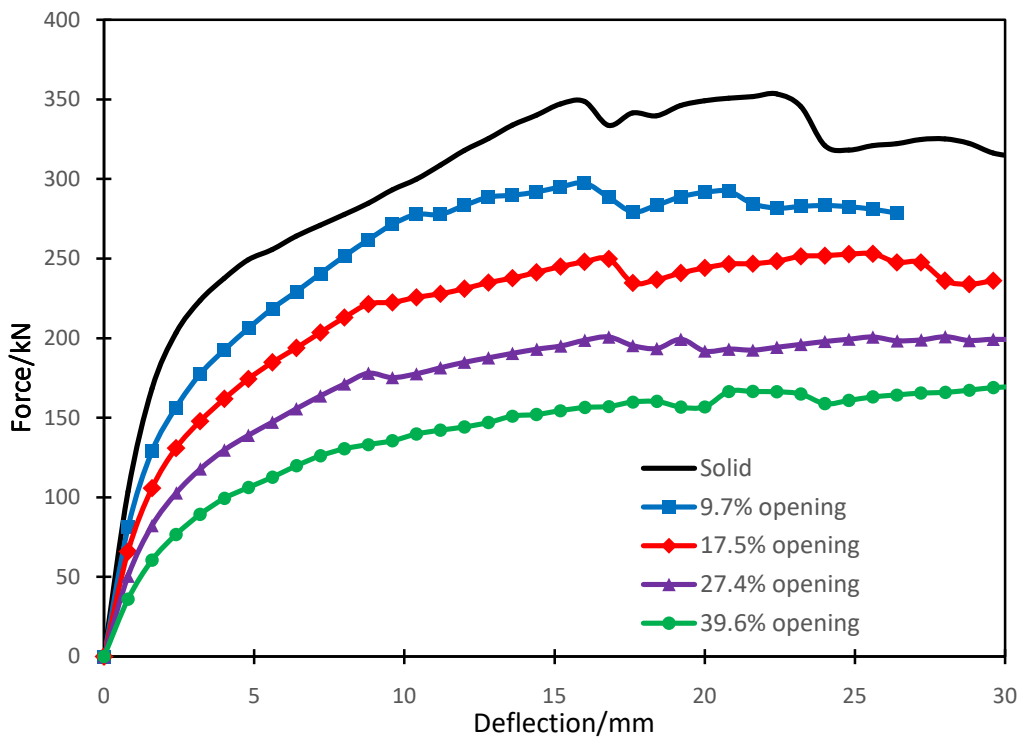
Figure 8.28 Load-deflection curves of infilled RC frame with/without openings
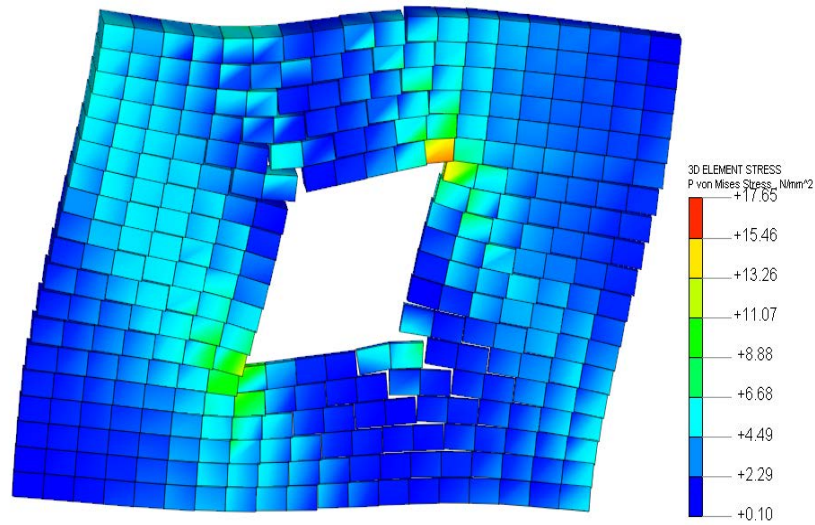
Figure 8.29 Stress distribution of specimen with 9.7% opening
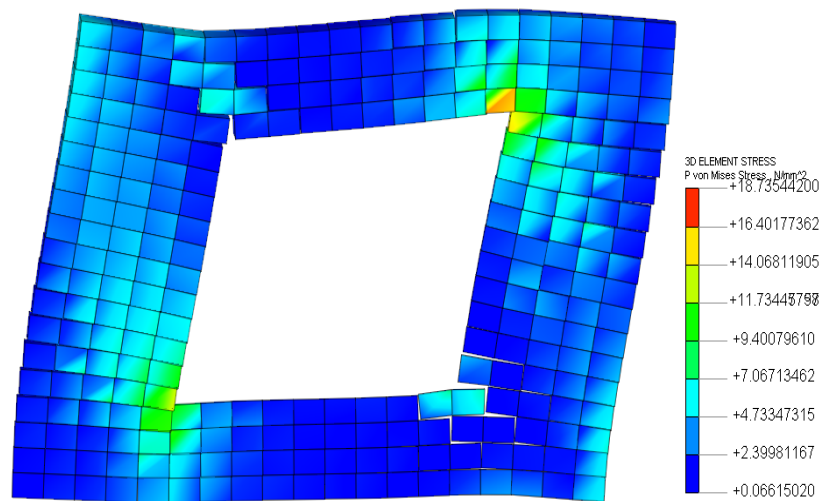
Figure 8.30 Stress distribution of specimen with 27.4% opening

Figure 8.24 illustrates the load-deflection relationships of RC frames infilled with masonry infill contains opening with different sizes. Based on the figure, it can be revealed that if the masonry infill has an opening, the stiffness will be reduced as well as the maximum lateral load. The degree of reduction depends on the opening size. The ratio of the reduction to the opening size is not known yet as more specimens should be carried out in order to obtain the relationship. However, it is clearly shown that the bigger opening size, the larger reduction of stiffness and maximum lateral load. Similarly, Surendran and Kaushik (2012) presented that the presence of openings significantly reduced the initial lateral stiffness of the infilled frames.

However, in case of two similar rectangular frames with equal areas of openings, the frame having larger width of opening exhibits more initial lateral stiffness. Figure 8.25 shows the stress distribution of the masonry infill with 9.7% opening. It can be seen that two-diagonal-strut model has not been destroyed. This is because the opening locates in the central area of the masonry wall and it does not interrupt the two-diagonal-strut model, which is the reason why smaller opening size can carry more lateral load. In the case of small opening, the lateral load from the top beam can still pass from the two diagonal struts to the base. Figure 8.26 demonstrates the stress distribution of masonry infill with 27.4% opening. It clearly shows that the two-diagonal-strut model has been destroyed. Therefore, with bigger opening size, the two-diagonal strut model will be broken and the lateral loading carrying capacity will be decreased.

8.5.5 Collar joint retrofitting on infilled RC frame with openings
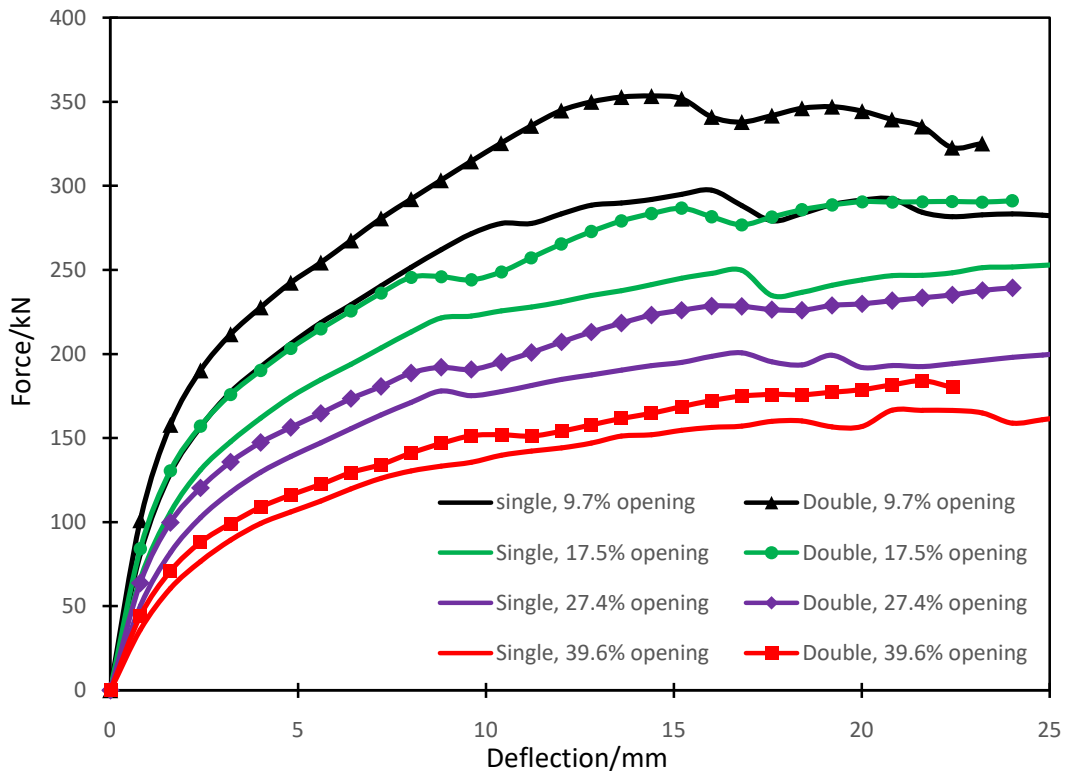
Figure 8.31 Load-deflection curves of strengthened/unstrengthened infilled RC frame with/without openings

221

Figure 8.27 compares the load-deflection relationships of the single-leaf and double-leaf masonry wall infilled RC frame with different opening sizes. Obviously, it is seen that the collar joint technique can improve the stiffness and strength of an infilled RC frame with opening. However, the improvement varies, which depends on the opening size. For the 9.7% opening, the improvement of the strength is 55kN or 18%, while for the opening size of 17.5%, 27.4% and 39.6%, the strength improvement is around 50kN (20.8%), 40kN (22%) and 25kN (16%). Compared with the infilled RC frame with solid infill, it can be concluded that improvement varies depending on the opening size. The relationship between the opening size and improvement by using collar jointed technique is displayed in Figure 8.28. It can be seen that the improvement increases gradually up until it reached its maximum improvement. After passing the maximum improvement, the improvement will decrease with the increase of opening size. However, it should be noted that more specimens with different opening sizes should be carried out in order to obtain a more accurate curve.
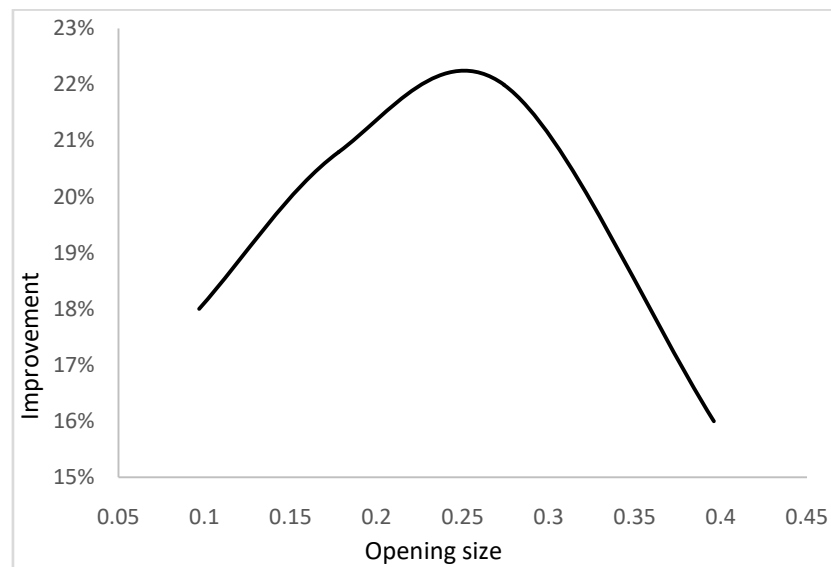
Figure 8.32 The relationship between opening size and improvement

8. 6 Discussion

In this chapter, the strengthening/retrofitting approach using the collar joint technique has been extended to the masonry infilled RC frames. The numerical results showed that this approach could have a positive influence in enhancing the composite structure. Though the influence is not remarkable, this approach can still be applied in practice. In some countries, the collar joint system has been implemented in order to provide some certain functions (like waterproof, fireproof etc.). Therefore, this research proves that this system can be beneficial to the existing composite structures. In this research, the diagonal-strut model has been found on the masonry infill. However, this approach hasn't been studied thoroughly here in this research as the aim of this research is to obtain a detailed study on the composite structure. Nevertheless, this approach can be applied in a more complex structure to simplify the numerical model.

It should be noted that the collar jointed masonry wall may have some disadvantages to the original structure. Though the masonry infill could improve the strength and stiffness of the composite structure, it adds mass to the original structure as well. The added stiffness decreases the natural period of the structure, which may result in higher seismic loads. Furthermore, the added mass may cause larger seismic action to the composite structure and may cause more severe damage as well. Therefore, the collar jointed technique needs to be conducted dynamically in future research in order to obtain its influence on the seismic behaviour of the composite structure.

In this chapter, the masonry infill with opening has been studied and the results agreed with the literature review. However, the relationship between the opening size and strength/stiffness reduction has not been obtained yet. According to the literature review, the strength/stiffness reduction is dependent on the opening shape as well as the location. Therefore, in order to obtain a more detailed and accurate reduction ratio, more specimens with

different types of openings as well as the locations, should be carried out. Moreover, the collar jointed technique has also been applied on the masonry infill with opening. The results demonstrate that this simple strengthening approach could improve the mechanical behaviour of the composite structure to some degree. A relationship between opening size and improvement has been obtained.

8. 7 Conclusions

In this research, a numerical study on the performance of an RC frame infilled with single-leaf and collar jointed masonry walls (with/without openings), has been carried out. The infilled RC frame in this research is newly designed with the surrounding RC frame taken from Mehrabi's (1996) experimental specimens and the masonry infill taken from the experimental specimens described in Chapter 3. The material parameters of RC frame are directly taken from Mehrabi's works and the parameters of masonry infill are taken from the calibration results in Chapter 6. The newly designed structures are simulated in MIDAS FEA. It should be noted that the seismic performance of this composite structure is not conducted here, which will be studied in further research.

According to the above analysis, some findings and conclusions can be made:

- This research confirmed that the masonry infill can significantly improve the stiffness and maximum load of the bare RC frame. Therefore, the masonry infill should be taken into account in designing a masonry infilled RC frame structure or it should be assured that the masonry infill and the surrounding RC frame has no interaction.

- The failure patterns of the masonry infill in the composite structure mainly have three types: a) diagonal cracking, b) mortar joint sliding,

and c) corner crush, which have some similarities with the bare masonry wall panel.

- The failure patterns are the same with those found on bare masonry wall panel. These findings can prove that the restriction conditions on masonry wall panel, which was described in Chapter 3, can approximately represent the real restriction provided by surrounding RC frame in reality. Therefore, the performance of masonry infill could be obtained from the bare masonry wall panel test.

- The masonry infill can be simplified as a two-diagonal-strut model. However, a one or multi diagonal strut model can be used depending on the aspect ratio of masonry wall.

- The collar joint technique can improve the stiffness and failure load of the composite structure to some degree. For the eccentrically infilled RC frame, the collar joint technique can reduce the out-of-plane failure. Furthermore, the collar joint technique can improve the integrity of the eccentrically infilled frame to some degree and make the two leaves work as a whole panel. Therefore, collar joint techniques used as strengthening/retrofitting approach on infilled RC frame is appropriate.

- Openings in the masonry infill can decrease the stiffness and strength of the infilled RC frame structures remarkably. The bigger the opening, the greater the reduction of stiffness and strength. Furthermore, the location of the opening is also critical as the opening may break the strut-model in masonry infill, thus reducing stiffness and strength remarkably.

- Collar joint technique can help to improve the mechanical behaviour of infilled RC frame with an opening. However, the significance of the

improvement depends on the opening size, and the relationship is shown in Figure 8.28. In reality, the collar jointed technique is quite commonly used in the masonry infill, therefore, this research result assures the safety of using this construction system.

Chapter 9 Conclusions, limitations and recommendations

This thesis deals with the analysis of unreinforced masonry walls strengthened using the collar jointed technique. The principal aims are to identify the effectiveness of the proposed strengthening approach and to develop a reliable computational model that can help to understand the mechanical behaviour of a masonry wall subjected to combined static loadings. In addition, the application of the collar joint technique has been extended to masonry infill panels found in RC frame structures in order to assess the effect on the performance of the RC frame, as well as to find out the mechanical behaviour of masonry wall infills constrained by RC frames. The conclusions, limitations as well as possible recommendations for future work are presented in this Chapter.

9. 1 Conclusions

9.1.1 Primary conclusions

In this thesis, the proposed method of enhancing masonry wall panels using the collar jointed technique as a retrofitting/strengthening approach has been investigated experimentally and numerically. The experiments were carried out in the laboratory, while for the numerical work, a simplified micro-scale finite element model was developed to model the masonry elements. Moreover, the collar jointed technique has also been extended to masonry infill panels found in RC frame structures. According to the research results, the primary conclusions are:

1. Both the experimental and numerical results indicate that the collar joint technique is beneficial to the masonry structure under combined quasi-static loading as it can improve the stiffness and lateral resistance of the structure. The collar joint technique increased the lateral resistance by about 50% on the pre-damaged masonry walls while it increased the stiffness about 100% on the post-damaged masonry walls. Furthermore, the ductility of the post-damaged masonry wall was improved remarkably. The result assures that this strengthening/retrofitting approach is effective in improving the performance of masonry wall panels. For the pre-damaged approach, it could be applied in the designing and constructing stage. For the existed masonry structures with collar jointed wall system, it assures the safety of the usage. However, for the post-damaged type, the pre-surface treatment may be needed in order to improve the retrofitting effectiveness.

2. Collar jointed infill panels have been incorporated within an RC frame and the results showed that this method could provide some benefits to the composite structure (whether as solid masonry infill or as masonry infill with an opening). The increase of lateral resistance is approximately increased by 20% for all cases. However, for a particular masonry infill with an opening, there is a maximum increase for a certain opening size. When the opening is smaller or bigger than this certain size, the increase of the collar joint technique will be decreased. This finding helps the engineers and builders in deciding the use of collar joint technique in the non-seismic area, in order to improve the mechanical behaviour of the composite structure. For the collar jointed walls used as partitions in the composite structures, this result confirms the safety of its usage.

3. A simplified micro-scale model was developed based on the generated data from the experimental results. The mechanical behaviour of single- and double-leaf (collar jointed) masonry walls has been investigated using the developed method, and the simulation results agreed well with the experimental results. Specifically, the load-transfer in collar jointed

228

masonry walls has been addressed, which contributes to the understanding of the mechanical behaviour of the collar jointed masonry wall. In a typical collar-jointed masonry wall, the lateral load was mainly passed to the base via the diagonal strut in the first leaf. However, the collar joint transferred the load from the first leaf and spread the shear load evenly among the second leaf. As the numerical results agreed well with the experiments, therefore, this method can be used by other researchers in numerically investigating the performance of masonry wall panels.

4. Compared with the review summarised in Table 2.2, Chapter 2, the assessment score of this collar-jointed retrofitting approach in terms of improvement, economy, sustainability and buildability is 5, 8, 8, and 9, respectively, which makes the total score of 30. This approach is therefore the most beneficial strengthening approach overall. This result proves that the proposed approach in this research is a cost-effective and practical strengthening/retrofitting method, which provides a potential choice for the engineers and researchers, especially in the developing countries.

5. The strengthening effects of the pre-damaged and post damaged masonry walls are different; the strengthening of pre-damaged wall type is more efficient. The pre-damaged type could increase the lateral resistance about 50% while the post-damaged type could only restore the initial strength. This is due to the combination of the collar joint in the post-damaged type is poor. The first leaf was built earlier while the collar joint was constructed at the same time with the second leaf. Therefore, the bond between the first leaf and the collar joint was much weaker (because of the curing effect) than the bond between the second leaf and the collar joint. Therefore, in order to improve the retrofitting effectiveness, some pre-surface treatment may need to be carried out prior to the retrofitting work. Further work is required to see how to

improve the method of retrofitting in post damaged walls (see Recommendations).

9.1.2 Secondary conclusions

In relation to the Objectives:

1. The review in Chapter 2 demonstrated that the mechanical behaviour of masonry walls is a complex issue, especially double- or multi-leaf masonry walls. This research confirmed the complexity of masonry, especially for the collar jointed masonry wall. The mechanical behaviour of a masonry wall could be taken as linearly elastic under small lateral load. However, for the collar-jointed masonry wall, the stresses in different leaves are totally different. The load was passed to the base via diagonal strut in the first leaf while the load was spread evenly among the second leaf.

2. Chapter 2 assessed the advantages and disadvantages of the existing approaches to strengthen and retrofit masonry structures and concluded that there was no best approach. The selection of a retrofit method should require consideration of all of the following aspects; technical, economic and social.

3. In this research, a new strengthening approach (e.g. a collar-joint) for single-leaf masonry walls was proposed. The reason for this proposed method was that the collar jointed technique is quite a common/established construction method. Though the improvement of the collar jointed strengthening/retrofitting technique is not very remarkable (around 50% for the pre-damaged masonry wall panels while approximate 20% for the masonry infilled RC frame), it has been shown to be easy to be implemented and so ideal for the householders in the developing countries. For those structures which already incorporate

collar-jointed systems, the research confirms the expected performance of this technique.

4. A review on the existing modelling approaches has been presented and compared. In this research, the simplified micro-scale finite element modelling was preferred. This approach is able to catch all the failure modes of the masonry wall panels without consuming too much computational time.

5. In terms of the failure mechanisms, the experimental studies on single-leaf unreinforced masonry walls have shown that cracks are more likely to occur along the brick-mortar interfaces. Usually, the failure is represented by de-bonding of the bricks from the mortar. It should be noted that the failure pattern is significantly dependent on the dimensions of the specimen, loading pattern and boundary conditions. In this research, the experimental specimens (including single- and double-leaf masonry panels) have their own unique (dimension, boundary condition and loading pattern). Therefore, the failure pattern has its own unique characteristics. However, this result can be referred in other research if the similar experiments were carried out. In this research, the results in Chapter 4 showed that there are 3 failure patterns for a single-leaf wall: i) diagonal cracking, ii) corner crushing and iii) sliding; this is in agreement with the literature (Lourenco and Rots 1997, Campbell Barrza 2012). However, the failure modes of the double-leaf masonry wall panels differ from those of single-leaf wall panels. For the double-leaf masonry wall panel, the failure pattern was characterized by diagonal cracking. In terms of the failure process, pre- and post-damaged walls behaved differently. For the case of a pre-damaged wall, there were three notable features of behaviour, namely: i) initial flexural cracking in the bed joints of the walls; followed by, ii) propagation of stepped shear cracks; with increasing load leading to, iii) complete collapse. For the post-damaged masonry wall panel, there were four notable features of behaviour, namely: i) initial flexural crack; followed by ii) formation of diagonal

stepped cracks through the diagonal area, with increasing load leading to iii) detachment of the collar joint from the wall; and iv) collapse as a result of shear failure. In the literature review, the failure of multi-leaf masonry wall was mainly characterized by the crushing of the inner core and out-of-plane failure of external leaves. It should be noted that this difference might be due to the loading patterns and boundary conditions and the type of masonry unit and mortar.

6. For this investigation, the most efficient FE Model was found to be a simplified micro-scale model, wherein bricks are modelled as separate blocks behaving in a linear elastic manner while the mortar joints are represented by zero thickness interfaces behaving in an elastic-perfectly plastic manner. For the brick, material parameters of Young's modulus () and Poison's ratio () are required. While the zero thickness interface is based upon elastic normal () and shear () stiffness, cohesive (), tensile (), frictional (Φ), dilatancy (Ψ), mode I fracture energy (), mode II fracture energy (), compressive () and compressive fracture energy. From a sensitivity analysis, predicted failure was largely independent of the brick properties but very dependent on the joint interface parameters.

7. The sensitivity study showed that different parameters of the interface affect the mechanical behaviour of masonry wall at different stages. According to the results, only normal/shear stiffness and tensile strength of the interface have a significant influence on the first stage (elastic stage). At this stage, the masonry wall behaves approximately in a linear elastic manner. For the second stage (re-distribution stage), the load was re-distributed through the wall and continued to carry more load. Normal/shear stiffness, tensile strength, coefficient of friction angle, coefficient of dilatancy angle, Mode I fracture energy and Mode II fracture energy play an important role. For the third stage (failure stage), all the parameters, i.e. normal/shear stiffness, tensile strength, coefficient of friction angle, coefficient of dilatancy angle, Mode I fracture energy, Mode II fracture energy compressive strength and compressive fracture

energy have a significant influence on the mechanical behaviour of the masonry walls.

8. Following the materials' parameters' calibration, the characterized parameters were assigned to the single-leaf Wall 3 and to the double-leaf Wall 4 and Wall 7 so as to predict the structural response. The predicted results were compared with those obtained from the experimental tests carried out in the laboratory and good correlation was achieved. The model could capture all the failure patterns found in the experiments, both in the single-leaf and the double-leaf masonry wall panels. For the double-leaf wall panels, the model could capture the trend, the maximum load and deflection.

9. By modelling the behaviour of a RC frame containing collar-jointed masonry infills, it can be seen that the masonry has a large influence on the composite behaviour of the structure, particularly when the masonry contains openings. The opening on the masonry infill would jeopardise the loading path system (diagonal strut model), therefore resulting in reducing the lateral resistance. Moreover, the collar jointed technique appears to improve the stiffness and failure load of the infilled RC frame, no matter whether it is solid or with an opening as the lateral resistance has been improved by approximate by 20% in all cases. Finally, the restrained masonry infill wall within the RC frame behaved similarly to that of the masonry wall tested in the laboratory. This suggests that the boundary conditions imposed in the experiments successfully represented those conditions present in a real frame.

9. 2   Limitations of this research

Both experimental and analytical methods were used to evaluate the mechanical performance of a masonry wall under combined quasi-static lateral loading. However, there are still some issues that are not covered in

this thesis. The limitations in this research regarding to the experimental and computational work are listed as following:

1. In this project, only monotonic loading was considered. As most walls are strengthened against earthquake loads, future research needs to take into account cyclic loading. Furthermore, dynamic analysis should be considered when investigating the influence of the collar jointed masonry wall on the structural period of the composite structure.

2. In terms of the experimental tests, only one type of brick and mortar was used in this research. Furthermore, as masonry is a complex composite material, more walls need to be tested to increase the size of the data sets.

3. In this research, the material calibration work is "tuned" manually, which is cumbersome and time consuming. In future research, other approaches in calibrating material parameters should be applied as well.

9. 3   Recommendations for future work

Regarding further research on unreinforced single-leaf masonry wall as well as collar jointed masonry walls, and the computational modelling of masonry structures, the following recommendations are given:

- It is advisable to do more experiments regarding the material properties of masonry. Experimental data are scarce and it is desirable to expand the experimental data, particularly with respects to brick and mortar types (it is expected that failure mechanisms will also be dependent on masonry element properties).

- Data collection: the results of the experiments would be more reliable if more than one LVDT could be used to measure displacement during the tests. DEMEC gauges were used to measure strain during the tests, and the tests had to be paused in order to record the DEMEC gauge readings. If an electronic measurement system could be used to measure the strain change then more accurate and reliable data would be recorded.

- Enhancing the collar-joint: For future work, steel ties/anchors could be used to enhance the shear capacity of the joint. Also, for the retrofitted masonry wall, more preparation could be performed to help key in the collar joint to the existing leaf (i.e. partially grind out the mortar joints); this would be expected to drastically improve the post damaged wall's behaviour.

- The collar joint was fully infilled in this research. However, in practice, different percentages of the collar joint infill would be likely occurred and so the effect of a partially infilled collar joint needs to be determined.

- This research only considered in-plane failure. Out-of-plane failure can be taken into account in the future work.

References

Abdel-Hafez, L. M., Abouelezz, A. E. Y. and Elzefeary, F. F. (2015) 'Behavior of masonry strengthened infilled reinforced concrete frames under in-plane load', *HBRC Journal,* 11.2, 213-223.

Abdou, L., Ami, S. R., Meftah, F. and Mebarki, A. (2006) 'Experimental investigations of the joint-mortar behaviour', *Mechanics Research Communications,* 33(3), 370-384.

Abrams, D. P. and Lynch, J. M. (2001) 'Flexural behaviour of retrofitted masonry piers,' in *KEERC-MAE Joint Seminar on Risk Mitigation for regions of Moderate Seismicity*, Illinois, USA,

Abrams, D. P. and Shah, N. (1992) '*Cyclic load testing of unreinforced masonry walls'*, ILLINOIS UNIV AT URBANA ADVANCED CONSTRUCTION TECHNOLOGY CENTER.

Al-Chaar, G. and Mehrabi, A. (2008) '*Constitutive models for nonlinear finite element analysis of masonry prisms and infill walls'*, US Army Corps of Engineering.

Al-Chaar, G. K. (2002) '*Evaluating strength and stiffness of unreinforced masonry infill structures'*, ERDC.CERL TR-02-1. Champaign, IL: Engineer Research and Development Center-Construction Engineering Research Laboratory.

Al-Chaar, G. K., Issa, M. and Sweeney, S. (2002) 'Behavior of masonry-infilled non-ductile reinforced concrete concrete frames', *Journal of Structural Engineering*, 1055-1063.

Alcaino, P. and Santa-Maria, H. (2008) 'Experimental response of externally retrofitted masonry walls subjected to shear loading', *Journal of composites for Construction ASCE,* 12 (5), 489-98.

Ali, S., Moore, I. D. and Page, A. W. (1987) 'Substructuring technique in nonlinear analysis of brick masonry subjected to concentrated load', *Computers & structures,* 27(3), 417-425.

Almeida, J. C., Lourenco, P. B. and Barros, J. O. (2002) '*Characterization of brick and brick-mortar interface under uniaxial tension',* 7th international seminar on structural masonry for developing countries. Brazil: 67-76.

Anand, S. C. and Yalamanchili, K. K. (1996) 'Three-dimensional failure analysis of composite masonry walls', *Journal of Structural Engineering-Asce,* 122(9), 1031-1039.

Anderson, C. and Held, L. C. (1986) 'The effect of sand grading on mortar properties and tensile bond strength of brickwork specimens', *Proceedings of the Brick Masonry Society,* 1, 1-6.

Attard, M. M., Nappi, A. and Tin-Loi, F. (2007) 'Modelling fracture in masonry', *Journal of structural Engineering, ASCE,* 133(10), 1385-1392.

Azevedo, J. and Sincraian, G. (2001) '*Modelling the seismic behaviour of monumental masonry structures',* Proceedings of the international congress archi 2000,UNESCO, Bethlehem, Palestine.

Beattoe, G., Molyneaux, T. C. K., Gilbert, M. and Burnett, S. (2001) '*Masonry shear strength under impact loading',* In proceeding of 9th Canadian Masonry Symposum, New Brunswick, Canada.

Bhattacharya, S., Nayak, S. and Dutta, S. C. (2014) 'A critical review of retrofitting methods for unreinforced masonry structures', *International Journal of Disaster Risk Reduction,* 7, 51-67.

Binda, L., Pina-Henriques, J., Anzani, A., Fontana, A. and Lourenco, P. B. (2006) 'A contribution for the understanding of load-transfer mechanisms in multi-leaf masonry walls: Testing and modelling', *Engineering Structures,* 28(8), 1132-1148.

Brooks, J. J. (2014) '*Concrete and masonry movement',* Oxford, UK:Butterworth Heinemann Publictations.

British Standards Institution. (1976) BS 1199 and 1200. 'Specification for building sands from natural source', London, British Standards Institution.

British Standards Institution. (1985) BS 3921. 'Specification for clay bricks', London, British Standards Institution.

British Standards Institution. (1998) BS 4551-1. 'Methods of testing mortars, screeds and plasters, *Part 1. Physical testing',* London, British Standards Institution.

British Standards Institution. (1999) BS EN 1015-11. 'Methods of test for mortar for masonry, *Part 1: Determination of flexural and compressive strength of hardened mortar',* London, British Standards Institution.

British Standards Institution. (2000) BS 410-2. 'Test sieves-Technical requirements and testing, *Part 2: Test sieves of perforated metal plate',* London, British Standards Institution.

British Standards Institution. (2005) BS 5628-1. 'Code of practice for the use of masonry, *Part 1: structural use of unreinforced masonry',* London, British Standards Institution.

British Standards Institution. (2010) BS EN 998-2. 'Specification for mortar for masonry, *Part 2: Masonry mortar',* London, British Standards Institution

British Standards Institution. (2011a) BS EN 772-1. 'Cememnt Part 1: Composition, specifications and conformity criteria for common cements', London, British Standards Institution.

British Standards Institution. (2011b) BS 197-1. 'Methods of test for masonry units, *Part 1: Determination of compressive strength',* London, British Standards Institution.

British Standards Institution. (2015) BS 459-1. 'Building lime Part 1: Definitions, specifications and conformity criteria', London, British Standards Institution.

Burgoyne C.J., (2004) 'Does FRP have an econmic fugure?', 4th conference on advanced composite materials in bridges and structures, Calgary, Alberta, July 2004.

Campbell Barraz, J. A. (2012) '*Numerical model for nonlinear analysis of masonry walls',* PhD thesis.

Chaimoon, K. (2007) '*Numerical simulation of fracture in unreinforced masonry',* unpublished thesis The University of New South Wales, Sydney, Australia.

Chaimoon, K. and Attard, M. M. (2007) 'Modeling of unreinforced masonry walls under shear and compression', *Engineering Structures,* 29(9), 2056-2068.

Chrysostomou, C. Z., Gergely, P. and Abel, J. F. (2002) 'A six-strut model for nonlinear dynamic analysis of steel infilled frames', *International Journal of Structural Stability and Dynamics,* 2.03(335-353).

Chuxian, S., Guiqiu, L. and Wenchao, W. (1997) '*The design of brick masonry structure with concrete column',* 11th international brick and block masonry conference, Shanghai, China: 626-633.

Crisafulli, F. (1997) '*Seismic behaviour of reinforced concrete structures with masonry infills',* PhD thesis, University of Canterbury.

Crisafulli, F., Carr, A. and Park, R. (2000) 'Analytical modelling of infilled frame structures: a general review', *Bulletin-New Zealand Society for Earthquake Engineering,* 33.1, 30-47.

Crisafulli, F., Carr, A. and Park, R. (2005) 'Experimental response of framed masonry structures designed with new reinforcing details' Bulletin of the New Zealand society for earthquake engineering, Vol. 38, No.1, 19-32.

Cundall, P. A. (1971) 'A computer model for simulating prgressive large scale movements in blocky rock systems ', in *Proceedings of the symposium of the international society of rock mechanics*, Nancy, France,

Dhanasekar, M. (1985) '*The performance of brick masonry subjected to in-plane loading*', PhD thesis, University of Newcastle.

Dialer, C. (1990) '*Fracture and deformation behaviour of stress, biaxial tests on scale model masonry*', PhD thesis, Technical University of Munich, Germany.

Dolatshahi, K. M. and Aref, A. J. (2011) 'Two-dimensional computational framework of meso-scale rigid and line interface elements for masonry structures', *Engineering Structures,* 33(12), 3657-3667.

Dowling, D., Samali, B. and Li, J. (2005) 'An improved means of reinforcing adobe walls-external vertical reinforcement', in *Sismo Adobe*, PUCP, Lima, Peru, May 16-19th,

Ehsani, M., Saadatmanesh, H. and Velazquez-Dimas, J. (1999) 'Behavior of retrofitted URM walls under simulated earthquake loading', *Journal of Composites for Construction,* 3 (3)(134-42).

El-Dakhakhni, W., Elgaaly, M. and Hamid, A. (2003) 'Three-strut model for concrete masonry-infilled steel frames', *Journal of Structural Engineering,* 129(2), 177-185.

ElGawady, M., Lestuzzi, P. and Badoux, M. (2006) '*Retrofitting of masonry walls using shotcrete',* 13th international brick and block masonry conference, Vlo. 10 No. 10, New Zealand.

ElGawady, M. A., Lestuzzi, P. and Badoux, M. (2004a) 'a review of conventional seismic retrofitting techniques for URM', in *13th International brick and block masonry conference*, Amsterdam,

ElGawady, M. A., Lestuzzi, P. and Badoux, M. (2004b) 'A review of retrofitting of unreinforced masonry walls using composits', in *4th International Conference on Advanced Composite Materials in Bridges and Structures*, Calgary, Alberta, Cananda, July 20-23, 2004,

Eurocode 6. (1996) 'Design of masonry structures-Part 1-1: General-Rules for reinforced and unreinforced masonry, including lateral loading'. London.

Eurocode 8. (1996) 'Design provisions for earthquake resistance of structure. London'.

Fardis, M. N., Bousias, S. N., Franchioni, G. and Panagiotakos, T. B. (1999) 'Seismic response and design of RC structurs with plan-eccentric masonry infills', *Journal of Earthquake Engineering and Structural Dynimicas,* 28(173-191).

Ferguson, W. (2002) '*Collar-jointed walls: an assessment of their performance and buildability',* Proceedings of the British Masonry Society.

Forth, J. P. (2009) '*Movement in masonry: ICE manual of construction materials',* Thomas Telford. 431-442.

Forth, J. P., Brooks, J. J. and Tapsir, S. H. (2000) 'The effect of unit water absorption on long-term movements of masonry', *Cement and Concrete Composites,* 22.4, 273-280.

Garofano, A. (2011) 'Structural behaviour of masonry walls stregthened with mortar layers reinforced with FRP grids', Master's thesis.

Ghaboussi, J. and Barbosa, R. (1990) 'Three-dimensional discrete element method for granular materials ', *International journal of Numerical and Analytical Methods in Geomechanics,* 14.7, 451-472.

Ghazali, M. Z. and Riddington, J. R. (1988) 'Simple test method for masonry shear strength ', *Proceedings of the institution of civil engineers,* 85.3, 567-574.

Giordana, A., Mele, E. and Luca, A. (2002) 'Modelling of historical masonry structures: Comparison of different approaches through a case study', *Engineering Structures,* 24(8), 1057-1069.

Groot, C. (1993) '*Effects of water on mortar-brick bond',* PhD thesis Delft University of Technology, Delft.

Hamid, A., Mahmoud, A. and Abo El Maged, S. (1994) 'Strengthening and repair of unreinforced masonry structures: stage-of-the-art', in *10th Internation Brick and Block Masonry Conference*, Calgary, Canada, 485-497.

Harries, K. A. and Sharma, B. (2016) '*Nonconventional and vernacular construction materials: characterisation, properties and applications',* Woodhead Publishing.

Heaton, T., Sammon, C., Ault, J., Black, L. and Forth, J. P. (2014) 'Masonry units bound with waste vegetable oil-Chemical analysis and evaluation of engineering properties', *Construction and Building materials,* 64, 460-472.

Hendry, A. W. (1998) '*Sructural masonry',* 2nd Edition ed*.,* Palgrave Macmillan, London, UK.

Heyman, J. (1998) '*Structural Analysis: A historical approach',* University Press, Cambridge, UK.

Kanyeto, O. J. (2006) '*Investigation of the behaviour of laterally loaded thin-jointed concrete-block masonry panels'*, PhD thesis, Kingston University London, Kingston Upon Thames.

Kaushik, H., Rai, D. and Jain, S. (2007) 'Stress-strain characteristics of clay brick masonry under uniaxial compression', *Journal of Materials in Civil Engineering,* 19.9, 728-739.

Kaushik, H. B., Rai, D. C. and Jain, S. K. (2007) 'Stress-strain characteristics of clay brick masonry under uniaxial compression', *Journal of Materials in Civil Engineering,* 19(9), 728-739.

Koutromanos, I. (2011) '*Numerical analysis of masonry-infilled reinforced concrete frames subjected to seismic loads and experimental evaluation of retrofit techniques'*, PhD thesis, University of California, San Diego.

Krauth, T., Ruth, W. T. and Vannoy, D. W. (2001) '*Investigation and repair of an improperly constructed masonry barrier wall system',* Forensic Engineering: the investigatio of failure: proceedings of the second international conference on forensic engineering organized by the institution of civil engineering, London, UK:Thomas Telford.

Lawrence, S. J., Sugo, H. O. and Page, A. W. (2008) 'Masonry bond strength and the effects of supplementary cementitious materials', *Australian Journal of Structural Engineering,* 8 (2), 101-115.

Lemos, J. (2007) 'Discrete element modelling of masonry structures', *international Journal of Architecture Heritage,* 1, 190-213.

Lenczner, D. (1990) 'Review on creep and stress relaxation in brick masonry ', *Structural Engineering,* 2, 161-168.

Lotif, H. R. (1992) '*Finite element analysis of fracture of concrete and masonry structures'*, PhD thesis, University of Colorado at Boulder.

Lotif, H. R. and Shing, P. B. (1994) 'Interface model applied to fracture of masonry structures', *Journal of Structural Engineering,* 120.1, 63-80.

Lourenco, P. B. (1998b) 'Senstivity analysis of masonry structures', The 8th Canadian Masonry Symposium, Jasper, Canada: 563-574.

Lourenco, P. B. (2002) 'Computations of historical masonry constructions', Progress in Structural Engineering and Materials, 4 (3), 301-19.

Lourenco, P. B. and Pina-Henriques, J. (2006) 'Validation of analytical and continuum numerical methods for estimating the compressive strength of masonry', Computers and Structures, 84.29, 1977-1989.

Lourenco, P. B. (1996) 'Comuptational strategies for masonry structures', PhD thesis, Delft University of Technology.

Lourenco, P. B. and Rots, J. G. (1997) 'Multisurface interface model for analysis of masonry structures', Journal of Engineering Mechanics-Asce, 123(7), 660-668.

Mahmood, H. and Ingham, J. (2011) 'Diagonal compression testing of FRP-Retrofitted unreinforced clay brick masonry wallettes', Journal of composites for Construction ASCE, 15 (5), 810-20.

Mainstone, R. J. (1971) 'On the stiffness and strengths of infilled frames', Proceedings of the Institution of Civil Engineers, 57-90.

Marquis, E. L. and Borchelt, G. (1986) Bond strength comprarison of laboratory and field tests, the 4th Canadian Masonry Symposium, Federation New Brunswick: 94-204.

Matthys, H. and Noland, L. (1989) Proceedings of an international seminar on evaluation, strengthening and retrofitting masonry buildings, TMS, Colorado, USA.

Mayorca, P. and Meguro, K. (2004) 'Proposal of an efficient technique for retrofitting unreinforced masonry dwellings', in 13th World Conference on Earthquake Engineering,, No. 2431.

Mehrabi, A. (1994) Behaviour of masonry-infilled reinforced concrete frames subjected to lateral loading, PhD thesis, University of Colorado-Boulder.

Mehrabi, A. B. and Shing, P. B. (1997) 'Finite element modelling of masonry-infilled RC frames', Journal of Structural Engineering, 123, 604-613.

Mehrabi, A. B., Shing, P. B., Schuller, M. P. and Noland, J. L. (1994) 'Performance of masonry0infilled R/C frames under in-plane lateral loads', Report No. CU.SR-94/6, University of Colorado at Boulder.

Mehrabi, A. B., Shing, P. B., Schuller, M. P. and Noland, J. L. (1996) 'Experimental evaluation of masonry-infilled RC frames', *Journal of Structural Engineering-Asce,* 122(3), 228-237.

Melbourne, C. and Tomor, A. K. (2005) *Effect of weak/deteriorated masonry on the performance of arch bridges (Arch tests R-S).* , Test Report, University of Salford, Salford, UK.

MIDAS (2013) Nonlinear FE analysis software, MIDAS Information Technology Co. CSP.

Mortar Industry Association (2013) 'Learning text part 5: Brick and block production', Mortar Industry Assoication.

Mirza, S. A., Phipps, M. E. and Bell, A. J. (2002) '*The performance of collar jointed masonry in compression',* Proceedings of the British Masonry Society.

Mosalam, K., Glascoe, L. and Bernier, J. (2009) 'Mechanical properties of unreinforced brick masonry section-1', *Documented to US Department of Energy by Lawrence Livermore National Laboratory.*

Oliveira, D. V. C. (2003) '*Experimental and numerical analysis of blocky masonry structures under cyclic loading'* PhD thesis, University of Minho, Portugal.

Page, A. W. (1978) 'Finite-element model for masonry ', *Journal of structure Division, ASCE,* 104 (8), 1267-85.

Papas, A. W. (2012) '*Calibration of the numerical material behaviour of multi-leaf stone masonry walls based on experimental results'*, PhD thesis, University of Padova.

Pel, L., Kopinga, K. and Brocken, H. (1995) '*Moisture transport in prous building materials'*, PhD thesis, Technische Universiteit Eindhoven.

Peraza, D. (2009) 'Special problems with composite multiwythe masonry walls', *Foresnsic Engineering*, 66-73.

Pina-Henriques, J., Lourenco, P. B., Binda, L. and Anzani, A. (2004) *Testing and modelling of multiple-leaf masonry walls under shear and compression,* translated by Leiden (NL): Balkema: 299-310.

Pradhan, P. M., Pradhan, P. L. and Maskey, R. K. (2012) 'A review on partial infilled frames under lateral loads', *Kathmandu University Journal of Science, Engineering and Technology,* 8.1, 142-152.

Rai, D. and Goel, S. (1996) 'Seismic strengthening of unreinforced masonry piers with steel elements', *Earthquake Spectrume,* 12, 845-862.

Raijmakers, T. and Vermeltfoort, A. T. H. (1992) '*Deformation controlled tests in masonry shear walls*', Report B-92-1156, TNO-BOUW, Delft, The Nehterlands.

Ramalho, M. A., Taliercio, A., Anzani, A., Binda, L. and Papa, E. (2005) 'Experimental and numerical study of multi-leaf masonry walls', *Transactions on the built environment*, 333-342.

Ramalho, M. A., Taliercio, A., Anzani, A., Binda, L. and Papa, E. (2008) 'A numerical model for the description of the nonlinear behaviour of multi-leaf masonry walls', *Advances in Engineering Software,* 39(4), 249-257.

RILEM TC-50 FMC Recommendation (1985) '*Determination of the fracture energy of mortar and concrete by means of three-point bend tests on notched beams*', Materials and Structures, 18(106). 285-290.

Roca, P., González, J. L., Oñate, E. and Lourenço, P. B. (1998) 'Experimental and numerical issues in the modelling of the mechanical behaviour of masonry', *Structural Analysis of Historical Constructions II. CIMNE, Barcelona*.

Rots, J. G. (1991) 'Numerical simulation of cracking in masonry', *HERON,* 36(2), 49-63.

Rots, J. G. (1997) '*Structural masonry: An experimental/numerical basis for practical design rules',* The Netherlands:A.A. Balkema Publishers.

Sahlin, S. (1971) '*Structural masonry',* Premtoce-Hall, Englewood Cliffs, NJ.

Sarangapani, G., Venkatarama, R. B. V. and Jagadish, K. S. (2005) 'Brick-mortar bond and masonry compressive strength', *Journal of Materials in Civil Engineering,* 17(2), 229-237.

Sarhosis, V. (2012) '*Computational modelling of low bond strength masonry*', PhD thesis, The University of Leeds.

Sarhosis, V., Garity, S. W. and Sheng, Y. (2015) 'Influence of brick-mortar interface on the mechanical behaivour of low bond strength masonry brickwork lintels ', *Engineering Structures,* 88, 1-11.

Sarhosis, V. and Sheng, Y. (2014) 'Identification of material parameters for low bond strength masorny', *Engineering Structures,* 60, 100-10.

Sathiparan, N., Mayorca, P., Nesheli, K. N., Guragain, R. and Meguro, K. (2005) 'Experimental study on in-plane and out-of-plane behaviour of masonry wallettes retrofitted by PP-band meshes', *生産研究,* 57(6), 530-533.

Sattar, S. (2013) '*Influence of masonry infill walls and other building characteristics on seismic collapse of concrete frame buildigs'*, PhD thesis, University of Colorado

Saw, C. B. (1974) 'Linear elastic finite element analysis of masonry walls on beams', *Building Science,* 9(4), 299-307.

Schubert, P. (1988) '*The influence of mortar on the strength of masonry',* the 8th international brick and block masonry conference, 162-174.

Schwegler, G. (1994) 'Masonry construction strengthened with fiber composites in seismically endangered zones', in *the 1oth European Conference on Earthquake Engineering*, Vienna, Austria,

Stavridis, A. (2009) *Analytical and experimental study of seismic performance of reinforced concrete frames infilled with maosnry walls*, PhD thesis, University of California San Diego.

Stavridis, A. and Shing, P. B. (2008) '*Calibration of a numerical model for masonry infilled RC frames',* The 14th world conference on earthquake engineering, Beijing, China.

Stavridis, A. and Shing, P. B. (2010) 'Finite-element modelling of nonlinear behaviour of masonry-infilled RC frames', *Journal of Structural Engineering,* 136, 285-296.

Surendran, S. and Kaushik, H. B. (2012) 'Masonry infill RC frames with openings: review of in-plane lateral load behaviour and modeling approaches', *The open construction and building technology journal,* Suppl 1-M9, 126-154.

Taghdi, M. (2000) '*Seismic retrofit of low-rise masonry and concrete walls by steel strips'*, PhD thesis, University of Ottawa, Ottawa, Canada.

Tarque, N. (2011) '*Numerical modelling of the seismic behaviour of adobe buildings'*, PhD thesis, Universitá degli Studi di Pavia, Istituto Universitario di Studi Superiori, Pavia, Italy.

Teng, J. G., Chen, J. F., Smith, S. T. and Lam, L. (2003) 'Behaviour and strength of FRP-strengthened RC structures: a state-of-the-art review', *Proceedings of the institution of civil engineers-structures and buildings,* 156(1), 51-62.

Tetley, R. and Madabhushi, G. (2007) 'Vulnerability of adobe buildings under earthquake loading', in *Fourth Conference Earthquake Geotechnical Engineering*, Thessaloniki, Greece,

Tomaževič, M. and Klemenc, I. (1997) 'Seismic behaviour of confined masonry walls', *Earthquake Engineering and Structural Dynamics,* 26.10, 1059-1071.

Triantafillou, T. C. (1998) 'Strengthening of masonry structures using Epoxy-bonded FRP laminates', *Journal of Composites for Construction*, 96-104.

Turer, A., Korkmaz, S. Z. and Korkmaz, H. H. (2007a) 'Performance improvement studies of masonry houses using elastic post-tensioning straps', *Earthquake Engineering and Structural Dynamics,* 36, 683-705.

Turer, A., Korkmaz, S. Z. and Korkmaz, H. H. (2007b) 'Performance improvement studies of masonry houses using elastic post-tensioning straps', *Earth Engineering and Structural Dynamics,* 36.5, 683-705.

Tzamtzis, A. D. and Asteris, P. G. (2003) 'Finite element analysis of masonry structures: Part I: Review of previous work', in *9th North American masonry conference*,

Valluzzi, M. R., Tinazzi, D. and Modena, C. (2002) 'Shear behaviour of masonry panels strengthened by FRP laminates', *Construction and Building materials,* 16.7, 409-416.

Van der Pluijm, R. (1992b) 'Material properties of masonry and its components under tension and shear', in *6th Canadian masonry symposium*, Saskatchewan Canada, 675-686.

Van der Pluijm, R. (1993) '*Shear behaviour of bed joints',* the 6th North American Masonry Conference, Drexel University, Philadelphia, Pennsylvania, USA: 125-136.

Van der Pluijm, R. (1997) 'Non-linear behaviour of masonry under tension', *HERON-ENGLISH EDITION,* 42, 25-54.

Van der Pluijm, R. (1999) '*Out-of-plane bending of masonry behaviour and strength'*, PhD thesis, Eindhoven University of Technology, The Netherlands.

Van der Pluijm, R., Rutten, H. and Ceelen, M. (2000) '*Shear behaviour of bed joints',* 12th Int. Brick/Block Masonry Conf. Proc. 1849-1862.

Van Noort, J. R. (2012) '*Computational modelling of masonry structures'*, PhD thesis, Delft Unviersity of Technology.

Van Zijl, G. P. A. G. (2004) 'Modelling Masonry Shear-Compression: Role of Dilatancy Highlighted', *Journal of Engineering Mechanics,* 130.11, 1289-1296.

Van Zijl, G. P. A. G. (2004) 'Modelling masonry shear-compression: role of dilatancy highlighted', *Journal of Engineering Mechanics,* 130, 1289-1296.

Vermeltfoort, A. and Raijmakers, T. (1993) '*Shear tests on masonry walls',*6th North American Masonry Conference, 1183-93.

Vermeltfoort, A. T. H. (2005) '*Brick-mortar interaction in masonry under compression'*, PhD thesis, Technische Universiteit Eindhoven.

Vermeltfoort, A. T. H., Martens, D. E. W. and Van Zijl, G. P. G. (2007) 'Brick mortar interface effects on masonry under compression', *Canadian Journal of Civil Engineering,* 24 (1), 1475-1485.

Vintzileou, E. (2007) 'Grouting of three-leaf masonry: experimental results and prediction of mechanical properties', *Evoluzione nella sperimentazione per le costruzioni, Cipro. Cerca con Google.*

Vintzileou, E. and Miltiadou-Fezans, A. (2008) 'Mechanical properties of three-leaf stone masonry grouted with ternary or hydraulic lime-based grouts', *Engineering Structures,* 30, 2265-2276.

Vintzileou, E. and Tassios, T. P. (1995) 'Three-leaf stone masonry strengthened by injecting cement grouts', *Journal of Structural Engineering,* 121.5, 848-856.

Wang, J., Heath, A. and Walker, P. (2013) 'Experimental investigation of brickwork behaviour under shear, compression and flexure', *Construction and Building materials,* 48, 448-456.

Wijanto, L. S. (2007) '*Seismic Assessment of Unreinforced Masonry Walls'*, PhD thesis, University of Canterbur, New Zealand.

Zarnic, R. and Tomazevic, M. (1984) 'The behaviour of masonry infilled reinforced concrete frames subjected to cyclic lateral loading.', in *In: Proceedings of ninth world conference on earthquake engineering*, San Francisco, USA, 863-870.

Zhuge, Y. (2008) 'Distinct element modelling of unreinforced masonry wall under seismic loads with and without cable retrofitting', *Transactions of Tianjin University,* 14(1), 471-475.

Zhuge, Y., Jin, F. and Hunt, S. (2004) 'The prediction of damage to maosnry houses caused by foundation movements', *Advances in Structural Engineering,* 7(1), 81-93.

Zucchini, A. and Lourenco, P. B. (2006) 'Mechanics of masonry in compression: Results from a homogenisation approach', *Computers and Structures,* 85(3), 193-204.